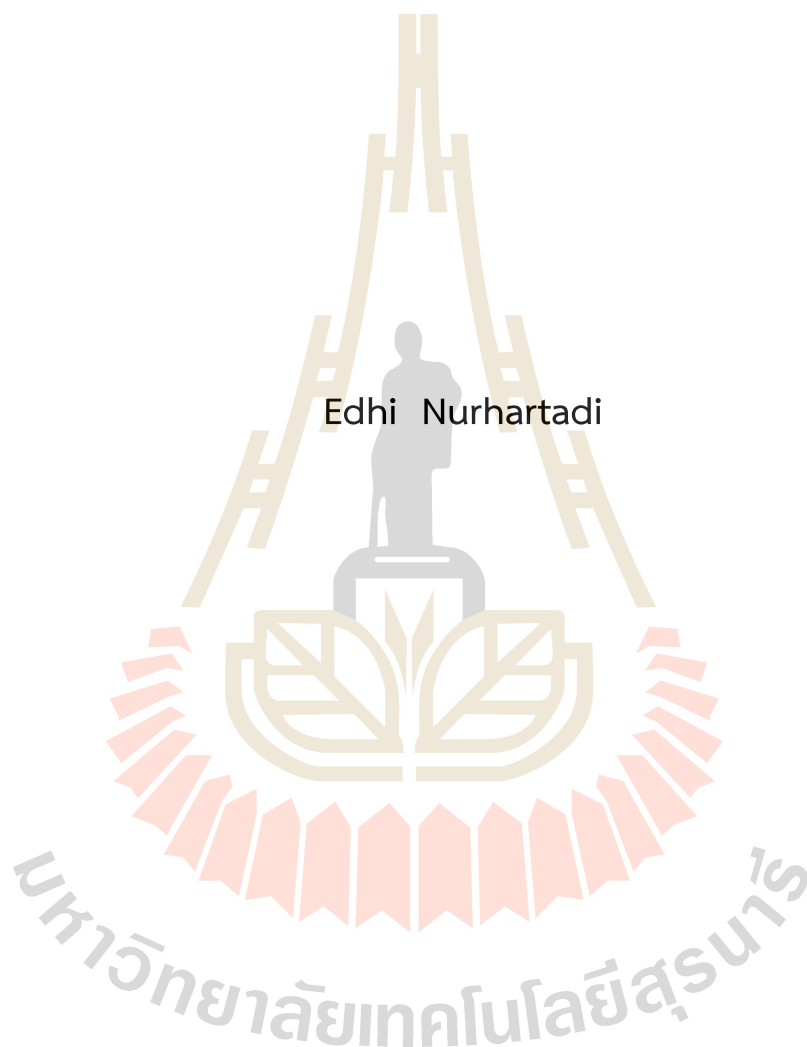


PURIFICATION AND CHARACTERIZATION OF ANTIMICROBIAL
PEPTIDES FROM CORN GLUTEN MEAL HYDROLYSATES



Edhi Nurhartadi

A Thesis Submitted in Partial Fulfillment of the Requirements for the
Degree of Doctor of Philosophy in Food Technology
Suranaree University of Technology
Academic Year 2024

การทำบริสุทธิ์และแสดงลักษณะของเพปไทด์ด้านแบคทีเรียที่ได้จาก
การไฮโดรไลสจากกากโปรตีนข้าวโพด



เอ็ดดี้ นูร์ฮาร์ทาดิ

วิทยานิพนธ์นี้เป็นส่วนหนึ่งของการศึกษาตามหลักสูตรปริญญาวิทยาศาสตรดุษฎีบัณฑิต
สาขาวิชาเทคโนโลยีอาหาร
มหาวิทยาลัยเทคโนโลยีสุรนารี
ปีการศึกษา 2567

PURIFICATION AND CHARACTERIZATION OF ANTIMICROBIAL PEPTIDES FROM CORN GLUTEN MEAL HYDROLYSATES

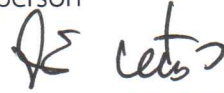
Suranaree University of Technology has approved this thesis submitted in partial fulfillment of the requirements for the Degree of Doctor of Philosophy.

Thesis Examining Committee



(Assoc. Prof. Dr. Si Hong Park)

Chairperson



(Assoc. Prof. Dr. Jirawat Yongsawatdigul)

Member (Thesis Advisor)



(Assoc. Prof. Dr. Ratchadaporn Oonsivilai)

Member



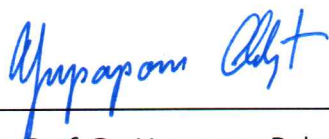
(Assist. Prof. Dr. Watsana Penkhruue)

Member



(Dr. Kanjana Thumanu)

Member



(Assoc. Prof. Dr. Yupaporn Ruksakulpiwat)

Vice Rector for Academic Affairs and
Quality Assurance



(Prof. Dr. Neung Teaumroong)

Dean of Institute of Agricultural
Technology

เอ็ดดี้ นูร์ฮาร์ทาดี้ : การทำบริสุทธิ์และแสดงลักษณะของเพปไทด์ต้านแบคทีเรียที่ได้จาก
ไฮโดรไลเสทจากโปรตีนข้าวโพด (PURIFICATION AND CHARACTERIZATION OF
ANTIMICROBIAL PEPTIDES FROM CORN GLUTEN MEAL HYDROLYSATES) อาจารย์
ที่ปรึกษา : รองศาสตราจารย์ ดร.จิรวุฒน์ ยงสวัสดิกุล, 158 หน้า

คำสำคัญ : เพปไทด์ต้านแบคทีเรีย/จากโปรตีนข้าวโพด/กลไกการออกฤทธิ์/การทำให้บริสุทธิ์

จากโปรตีนข้าวโพดเป็นผลผลิตพลอยได้ที่มีโปรตีนสูงจากกระบวนการแปรรูปแป้งข้าวโพด เพปไทด์ที่มีฤทธิ์ต้านแบคทีเรียที่ได้จากไฮโดรไลเสทจากโปรตีนข้าวโพดยังไม่มีการศึกษาอย่างแพร่หลาย งานวิจัยนี้มีวัตถุประสงค์เพื่อผลิตเพปไทด์จากไฮโดรไลเสทจากโปรตีนข้าวโพด (Corn gluten meal hydrolysate; CGMH) ที่มีฤทธิ์ต้านแบคทีเรีย นอกจากนี้เพื่อแยก ระบุ และศึกษาคุณลักษณะของเพปไทด์ต้านแบคทีเรียจาก CGMH และอธิบายกลไกการต้านแบคทีเรีย รวมถึงศึกษาการปรับเปลี่ยนโครงสร้างของเพปไทด์เพื่อเพิ่มสมบัติต้านแบคทีเรีย

เพปไทด์จากที่แยกส่วน P1 จาก CGMH ที่ย่อยด้วยเพปซิน 4% และผ่านการแยกด้วยโครมาโทกราฟีขนาดกลาง แสดงฤทธิ์ต้านแบคทีเรียสูงสุด โดยแสดงค่าความเข้มข้นต่ำสุดที่สามารถยับยั้ง (Minimum inhibitory concentration; MIC) ต่อ *Staphylococcus aureus* ATCC 29213 ที่ 1 มิลลิโมลาร์ แฟรคชัน (Fraction) P1 ทำลายความสมบูรณ์ของเยื่อหุ้มเซลล์ เมื่อวิเคราะห์ด้วยเทคนิคกล้องคอนโฟคอล (Confocal laser scanning microscopy; CLSM) ภาพถ่ายจากกล้องจุลทรรศน์อิเล็กตรอนแบบส่องกราด (Scanning electron microscopy; SEM) และเทคนิคจุลทรรศน์อิเล็กตรอนแบบส่องผ่าน (Transmission electron microscopy; TEM) แสดงถึงพื้นผิวเซลล์ที่ถูกทำลายและการร่วออกของของเหลวภายในเซลล์หลังจากทดสอบกับแฟรคชัน P1 การทดสอบด้วยเทคนิคฟูเรียร์ทรานซฟอร์หมอินฟราเรดสเปกโทรสโกปี (Synchrotron radiation-Fourier transmission infrared microspectroscopy; SR-FTIR) พบว่าแฟรคชัน P1 ก่อให้เกิดการเปลี่ยนแปลงของกรดนิวคลีอิก โปรตีน และกรดไขมันภายในเยื่อหุ้มเซลล์ แฟรคชัน P1 มีผลต่อการย่อยสลายเม็ดเลือดแดงต่ำ ผลการทดสอบเพปไทด์ในตัวอย่างนมที่ผ่านกระบวนการให้ความร้อนสูงในระยะเวลาสั้น (Ultra-High Temperature; UHT) พบว่าสามารถยับยั้ง *S. aureus* ที่ถ่ายลงในตัวอย่างที่ความเข้มข้น 8 มิลลิโมลาร์ เพปไทด์ชนิดใหม่ 11 ท่อนที่ระบุจากแฟรคชัน P1 อาจมีผลต่อฤทธิ์การต้านแบคทีเรีย

เพปไทด์ EAGGGEDDKKKVE (EE13) มีประจุสุทธิลบที่ได้จากการทำบริสุทธิ์แฟรคชัน P1 แสดงฤทธิ์การต้าน *S. aureus* ที่ค่า MIC 4 มิลลิโมลาร์ โดยเพปไทด์ EE13 ทำลายเยื่อหุ้มเซลล์ที่ความเข้มข้น $1 \times \text{MIC}$ เมื่อวิเคราะห์ด้วย CLSM การศึกษา SEM บ่งชี้ถึงรูปพรรณสัณฐานของเซลล์ที่เปลี่ยนไป ผลการศึกษา SR-FTIR บ่งชี้การเปลี่ยนแปลงโครงสร้างของกรดนิวคลีอิก โปรตีน และกรดไขมันของ *S. aureus* การศึกษาการจำลองการจับเชิงโมเลกุล (Molecular docking) แสดงให้เห็นว่าเพปไทด์ EE13 สามารถจับเอนไซม์ทรานส์ไกลโคซิเลส (Transglycosylase) บนเยื่อหุ้มเซลล์ ซึ่งเป็นเอนไซม์ที่เกี่ยวข้องกับการสังเคราะห์เพปทิโดไกลแคน (Peptidoglycan) การทดสอบความเป็นพิษต่อ

เซลล์เม็ดเลือดแดงแสดงให้เห็นว่า เพปไทด์ EE13 มีค่าการย่อยสลายเม็ดเลือดแดงต่ำที่ความเข้มข้นต่ำกว่า 8 มิลลิโมลาร์ การทดสอบผลเสริมฤทธิ์แสดงให้เห็นว่าการบ่มเซลล์ที่อุณหภูมิ 50 องศาเซลเซียส เป็นเวลา 10 นาที ตามด้วยการเติมเพปไทด์ EE13 ที่ความเข้มข้น 2.0 มิลลิโมลาร์ ก่อให้เกิดการทำลายเยื่อหุ้มเซลล์ของ *S. aureus*

การปรับเปลี่ยนโครงสร้างของเพปไทด์ PTGAKVTKAAKKA (PA13) เป็น RLLRKVTKLWKKF (RF135) ทำให้ค่า MIC ต่อ *Salmonella* Typhimurium TISTR 292 เท่ากับ 4 ไมโครโมลาร์ เพปไทด์ RF135 ที่ความเข้มข้น $1 \times \text{MIC}$ ทำให้เยื่อหุ้มเซลล์เสียหาย ส่งผลต่อการเรืองแสงของโพรพิเดียมไอโอดัดเพิ่มขึ้น และเกิดการรั่วไหลของกรดนิวคลีอิก ซึ่งแสดงจากการเพิ่มขึ้นของค่าการดูดกลืนแสงที่ 260 นาโนเมตร ผลการทดสอบ SEM แสดงให้เห็นว่าเพปไทด์ RF135 ทำให้เกิดการเปลี่ยนแปลงทางสัณฐานวิทยาของเซลล์ เช่น การเกิดรอยย่น รูขรุขระ ใหญ่บนเยื่อหุ้มเซลล์ ผิวเซลล์มีลักษณะขรุขระ และรูปร่างเซลล์ที่ไม่สม่ำเสมอมากขึ้น จนนำไปสู่การแตกสลายของเซลล์ การเปลี่ยนแปลงที่พบจาก TEM คือปริมาณไฮโดรพลาสมิกที่เข้มข้นขึ้นและเยื่อหุ้มเซลล์ที่เสียหาย ผลของเพปไทด์ RF135 ที่ความเข้มข้น $1 \times \text{MIC}$ ทำให้เกิดการเปลี่ยนแปลงสารประกอบต่างๆ ภายในเซลล์ รวมถึงกรดไขมัน โปรตีน และกรดนิวคลีอิก เมื่อวิเคราะห์ด้วย SR-FTIR จากการวิเคราะห์การจับเชิงโมเลกุลพบว่า เพปไทด์ RF135 สามารถจับกับเอนไซม์ เออาร์เอ็นดี ดีฟอร์มมีเลส (ArnD deformylase) ซึ่งเป็นเอนไซม์ที่เกี่ยวข้องกับกระบวนการสังเคราะห์เยื่อหุ้มด้านนอกของ *S. Typhimurium* การทดสอบการย่อยสลายต่อเซลล์เม็ดเลือดแดง พบว่า เพปไทด์ RF135 แสดงค่าการย่อยสลายต่ำกว่าร้อยละ 10 ที่ความเข้มข้น 512 ไมโครโมลาร์

ผลการวิจัยนี้แสดงให้เห็นว่าเพปไทด์ที่ได้จากการทำบริสุทธิ์ เพปไทด์สังเคราะห์ และเพปไทด์ที่ถูกปรับเปลี่ยนโครงสร้าง ที่ได้จาก CGMH ทำลายเยื่อหุ้มเซลล์ในแบคทีเรียแกรมบวกและแกรมลบ ข้อค้นพบนี้บ่งชี้ว่าเพปไทด์ด้านแบคทีเรียจาก CGMH มีศักยภาพที่จะพัฒนาเพื่อประยุกต์ในอุตสาหกรรมอาหารและยา

สาขาวิชาเทคโนโลยีอาหาร
ปีการศึกษา 2567

ลายมือชื่อนักศึกษา
ลายมือชื่ออาจารย์ที่ปรึกษา.....

EDHI NURHARTADI: PURIFICATION AND CHARACTERIZATION OF ANTIMICROBIAL PEPTIDES FROM CORN GLUTEN MEAL HYDROLYSATES

THESIS ADVISOR: ASSOC. PROF. DR. JIRAWAT YONGSAWATDIGUL, 158 PP.

Keywords: ANTIBACTERIAL PEPTIDES/CORN GLUTEN MEAL/MECHANISM OF ACTION/PURIFICATION

Corn gluten meal (CGM) is a high-protein byproduct from corn starch processing. The research on peptides with antimicrobial activity derived from CGM hydrolysis with enzymes is still rarely investigated. The current research objectives were to produce peptides from corn gluten meal hydrolysate (CGMH) with antibacterial activity. In addition, to isolate, identify, and characterize antibacterial peptides derived from pepsin-hydrolyzed CGM. Mechanisms underlying their antibacterial action were elucidated. Furthermore, structure modification of peptide was performed to enhance its antibacterial properties.

The P1 fraction isolated from the CGMH by 4% pepsin by preparative chromatography indicated the most potent antibacterial activity. The minimum inhibitory concentration (MIC) value of the P1 fraction was 1 mM toward *Staphylococcus aureus* ATCC 29213. The P1 fraction caused disruption of the membrane integrity of *S. aureus*, as observed by confocal laser scanning microscopy (CLSM). The images of scanning electron microscopy (SEM) and transmission electron microscopy (TEM) showed cell surface damages and cytoplasmic leakages on *S. aureus* after exposure with the P1 fraction. Synchrotron radiation-Fourier transmission infrared (SR-FTIR) microspectroscopy demonstrated that the P1 fraction caused changes in nucleic acids, proteins, and fatty acids in the cell membrane. The P1 exhibited relatively low hemolytic. In the challenge test on the commercial ultra-high temperature milk inoculated with *S. aureus*, the P1 fraction was found to suppress *S. aureus* growth at 8 mM. Eleven novel peptides from the P1 that might have contributed to its antibacterial activity were identified.

The EAGGGEDDKKKVE (EE13) was an anionic peptide identified from the P1 fraction that showed the most potent antimicrobial activity with MIC at 4.0 mM against *S. aureus*. EE13 significantly disrupted the membrane integrity of *S. aureus* at 1×MIC, as observed by CLSM. SEM revealed that EE13 at 1×MIC caused morphological alterations of *S. aureus* cells. SR-FTIR spectroscopy indicated that EE13 induced alterations in nucleic acids, proteins, and fatty acids of *S. aureus*. Molecular docking studies showed

that EE13 exhibited a strong binding affinity for membrane-bound transglycosylase, an enzymes associated with peptidoglycan synthesis in *S. aureus*. The hemolytic test indicated that EE13 had low hemolytic activity below 8 mM. The synergistic effect was shown by treating cells at 50 °C for 10 min followed by 2.0 mM EE13, which induced membrane damage of *S aureus*.

The structural modification of the peptide PTGAKVTKAAKKA (PA13) to RLLRKVTKLWKKF (RF135) showed the most potent antibacterial activity with a MIC value of 4.0 μM against *Salmonella* Typhimurium TISTR 292. The RF135 caused membrane damage at 1xMIC, resulting in increased red fluorescence intensity of propidium iodide. The RF135 at 1xMIC induced nucleic acid release, as evidenced by an increase in OD₂₆₀ values. SEM demonstrated morphological alterations in *S. Typhimurium* cells triggered by RF135, such as deeper craters, enlarged pores in the envelope, rough surface, and an increasingly irregular cell shape that led to cell lysis. The ultrastructure of *S. Typhimurium* was altered after being induced with RF135, as observed with TEM, including concentrated cytoplasmic content and cell membrane damage. The effect of RF135 at 1xMIC on the intracellular biomolecules of *S. Typhimurium* cells led to changes in fatty acids, proteins, and nucleic acids as monitored by SR-FTIR spectroscopy. Molecular docking analysis revealed that RF135 strongly bound with ArnD deformylase, an enzyme associated with the outer membrane of *S. Typhimurium*. The hemolysis assay showed the safety of the RF135 with hemolysis activity below 10% at a concentration below 512 μM .

The results demonstrated that the peptide fraction, the synthetic peptide, and the modified peptide derived from CGMH employed a membrane-damaging mechanism on the tested Gram-positive and Gram-negative bacteria. The research findings suggest that antibacterial peptides obtained from CGMH could potentially be developed for applications in the food and pharmaceutical industries.

School of Food Technology
Academic Year 2024

Student's Signature
Advisor's Signature

ACKNOWLEDGEMENTS

I want to thank all people who provided motivation and assistance throughout my PhD journey. One Research One Grant of SUT was greatly appreciated.

I would sincerely like to thank my thesis advisor, Assoc. Prof. Dr. Jirawat Yongsawatdigul and co-advisor Asst. Prof. Dr. Sureelak Rodtong, thank you for your consistent support and advisory role during the research. Their involvement was essential in facilitating my academic success.

I want to thank the chairperson of my defense committee, Assoc. Prof. Dr. Si Hong Park from the Department of Food Science and Technology, Oregon State University, USA, and committee member Assoc. Prof. Dr. Ratchadaporn Oonsivilai, the Head of the School of Food Technology, Institute of Agricultural Technology, Suranaree University of Technology, Asst. Prof. Dr. Watsana Penkhruue from the School of Preclinical Sciences, Institute of Science, Suranaree University of Technology, and Dr. Kanjana Thumanu from the Synchrotron Light Research Institute (Public Organization), Thailand, for their valuable comments and advice on my thesis.

In addition, I want to express my gratitude to all of the lecturers at the School of Food Technology, SUT, who have helped me learn over the past four years and have enabled me to grow professionally. I am also really grateful to all Food Protein Research Laboratory group members for their insightful conversations and recommendations. Additional appreciation is also expressed to SUT and SLRI for laboratory facilities.

I want to thank Dr. Thippawan Pimchan and Dr. Tian Fu for sharing their knowledge of antimicrobial peptides.

My gratitude goes to the family of the Department of Food Science and Technology, Sebelas Maret University.

Last but not least, my gratitude to my family for their unwavering love, understanding, motivation, and support throughout my academic journey, inspiring me to complete my studies successfully.

Edhi Nurhartadi

CONTENTS

Page

ABSTRACT IN THAI	I
ABSTRACT IN ENGLISH	III
ACKNOWLEDGEMENTS	V
CONTENTS	VI
LIST OF TABLES	XIII
LIST OF FIGURES	XIV
LIST OF ABBREVIATIONS	XXI
CHAPTER	
I INTRODUCTION	1
1.1 Background and significance of the study.....	1
1.2 Research objectives	5
1.3 Research hypotheses	5
1.4 Scope of the study	5
1.5 Expected results.....	6
1.6 References	6
II LITERATURE REVIEWS	10
2.1 Food spoilage and foodborne illness.....	10
2.2 Protein hydrolysates.....	11
2.3 Antimicrobial peptides	14
2.4 AMPs from protein byproduct	15
2.5 Separation and purification of AMPs	17
2.5.1 Size-exclusion chromatography	17
2.5.2 Cation-exchange HPLC	17
2.5.3 Reverse phase-HPLC	17
2.6 AMPs mechanism of action	18
2.6.1 Membrane-active AMPs	19
2.6.1.1 Toroidal model	19
2.6.1.2 Aggregate channel model.....	19
2.6.1.3 Barrel-stave model	19

CONTENTS (Continued)

	Page
2.6.1.4 Carpet model	21
2.6.2 Intracellular-active AMPs	21
2.7 Detection of cell damage by AMPs	22
2.7.1 Membrane permeability	22
2.7.2 Cytoplasmic membrane depolarization.....	23
2.7.3 Intracellular component leakage	23
2.7.4 Microscopy.....	24
2.7.4.1 Confocal laser scanning microscopy (CLSM)	24
2.7.4.2 Scanning electron microscopy (SEM)	24
2.7.4.3 Transmission electron microscopy (TEM).....	25
2.7.4.4 Atomic force microscopy	25
2.7.5 Synchrotron radiation Fourier transmission infrared.....	25
2.8 AMPs design.....	27
2.8.1 Site-directed mutagenesis.....	27
2.8.2 <i>De novo</i> design.....	27
2.8.3 Synthetic libraries.....	27
2.8.4 Template-assisted methodologies.....	28
2.8.5 Mechanism-based strategies.....	28
2.9 Application of AMPs derived from protein hydrolysates in food product.....	28
2.10 Modification of AMPs.....	29
2.11 Endogenous plant AMPs.....	30
2.11.1 Thionins	30
2.11.2 Plant defensins	30
2.11.3 Hevein-like peptides.....	31
2.11.4 Knottin-type peptides	31
2.11.5 α -Hairpinin family	31
2.11.6 Lipid transfer proteins	31
2.11.7 Snakins	31
2.11.8 Cyclotide family.....	32
2.12 AMPs from corn gluten meal	32

CONTENTS (Continued)

	Page
2.13 References	33
III ANTIBACTERIAL ACTIVITY OF ENZYMATIC CORN GLUTEN MEAL HYDROLYSATE AND ABILITY TO INHIBIT <i>Staphylococcus aureus</i> IN ULTRA-HIGH-TEMPERATURE PROCESSED MILK.....	45
3.1 Abstract	45
3.2 Introduction.....	46
3.3 Materials and methods	47
3.3.1 Materials and chemicals	47
3.3.2 Bacterial strains	47
3.3.3 Preparation of corn gluten meal hydrolysate (CGMH).....	48
3.3.4 Fractionation of CGMH	48
3.3.5 Antimicrobial activity	48
3.3.5.1 Minimum inhibitory concentration (MIC).....	48
3.3.5.2 Minimum bactericidal concentration (MBC)	49
3.3.5.3 Bactericidal curve.....	49
3.3.6 Peptide identification.....	49
3.3.7 <i>In silico</i> characterization of peptides	50
3.3.8 Mode of action.....	50
3.3.8.1 Membrane integrity	50
3.3.8.2 Morphological changes.....	50
3.3.8.3 Intracellular changes	51
3.3.8.4 Alteration of intracellular components	51
3.3.9 Antimicrobial stability of the P1 fraction	52
3.3.9.1 Temperature	52
3.3.9.2 pH.....	52
3.3.10 Hemolysis activity.....	52
3.3.11 Inhibitory effect of the P1 fraction on <i>S. aureus</i> growth in milk.....	53
3.3.12 Statistical analysis.....	53
3.4 Results and discussion	53
3.4.1 Peptide fractionation	53

CONTENTS (Continued)

	Page
3.4.2 MIC and MBC	54
3.4.3 Bactericidal curve	55
3.4.4 Confocal laser scanning microscopy.....	56
3.4.5 SEM and TEM.....	57
3.4.6 SR-FTIR	59
3.4.7 Antimicrobial stability of P1	64
3.4.8 Hemolytic activity assay.....	64
3.4.9 Application in milk	65
3.4.10 Peptide identification.....	66
3.5 Conclusion.....	70
3.6 References	70
IV ANTIBACTERIAL ACTIVITY AND POTENTIAL APPLICATION OF A NOVEL ANIONIC ANTIBACTERIAL PEPTIDE DERIVED FROM CORN GLUTEN MEAL HYDROLYSATE	76
4.1 Abstract	76
4.2 Introduction.....	77
4.3 Materials and methods.....	78
4.3.1 Materials.....	78
4.3.2 Bacterial strain cultures	78
4.3.3 Peptide synthesis and <i>in silico</i> analysis	79
4.3.4 Antibacterial activity	79
4.3.4.1 Minimum inhibitory concentration (MIC).....	79
4.3.4.2 Bacterial-killing curve	79
4.3.5 The <i>in silico</i> peptide-membrane interaction.....	80
4.3.6 Antibacterial mechanism.....	80
4.3.6.1 Membrane integrity	80
4.3.6.2 Localization of EE13 in bacterial cell.....	81
4.3.6.3 Cell morphology	81
4.3.6.4 Changes of intracellular fingerprints.....	82
4.3.6.5 Molecular docking	82
4.3.7 Hemolysis activity.....	83

CONTENTS (Continued)

	Page
4.3.8 The effect of mild heat and peptide EE13 treatment on <i>S. aureus</i>	84
4.3.9 Statistical analysis.....	84
4.4 Results and discussion	84
4.4.1 Antibacterial activity of EE13	84
4.4.2 Characteristics of EE13	85
4.4.3 Peptide-bacterial membrane interaction model	87
4.4.4 Bacterial killing curve.....	88
4.4.5 Antibacterial mechanism.....	89
4.4.5.1 Membrane integrity	89
4.4.5.2 Cell morphology.....	90
4.4.5.3 SR-FTIR.....	91
4.4.5.4 Molecular docking	94
4.4.6 Hemolysis activity.....	97
4.4.7 The combined effect of mild heat and peptide EE13 treatment	98
4.4.7.1 The combined effect on membrane integrity	100
4.4.7.2 Localization of 5-carboxyfluorescein-EE13 in <i>S. aureus</i> cells	101
4.4.7.3 The combined effect on morphology changes of <i>S. aureus</i> cells	102
4.5 Conclusion.....	103
4.6 References.....	104
V MODIFICATION AND MECHANISM OF ACTION OF PEPTIDE DERIVED FROM CORN GLUTEN MEAL HYDROLYSATE	110
5.1 Abstract	110
5.2 Introduction.....	111
5.3 Materials and methods.....	112
5.3.1 Materials	112
5.3.2 Bacterial cultures.....	113
5.3.3 Peptide modification	113

CONTENTS (Continued)

	Page
5.3.4 Peptide synthesis.....	114
5.3.5 Peptide informatic analysis	114
5.3.6 Prediction and modeling of peptide-membrane interaction	114
5.3.7 Antibacterial activity	115
5.3.7.1 Minimum inhibitory concentration (MIC).....	115
5.3.7.2 Bacterial-killing curve	115
5.3.8 Antibacterial mechanism	116
5.3.8.1 Membrane integrity	116
5.3.8.2 FAM-labeled peptide localization.....	116
5.3.8.3 Nucleic acid leakage.....	117
5.3.8.4 Cell morphology changes	117
5.3.8.5 Ultrastructural alteration.....	117
5.3.8.6 Biochemical intracellular changes	118
5.3.9 Molecular docking	118
5.3.10 Hemolysis activity.....	119
5.3.11 Statistical analysis.....	120
5.1 Results and discussion	120
5.4.1 Peptide design and characterization.....	120
5.4.2 Prediction of antibacterial activity.....	123
5.4.3 Prediction of peptide-membrane interaction model.....	124
5.4.3.1 Prediction using PMIPred web server	124
5.4.3.2 Prediction using PPM 3.0 web server	127
5.4.4 Antibacterial activity	127
5.4.4.1 Minimum inhibitory concentration (MIC).....	127
5.4.4.2 Bacterial killing curve	128
5.4.5 Antibacterial mechanism	129
5.4.5.1 Membrane integrity	129
5.4.5.2 Labeled 5-FAM-RF135 localization	130
5.4.5.3 Nucleic acid leakage.....	131

CONTENTS (Continued)

	Page
5.4.5.4 Scanning electron microscopy (SEM)	132
5.4.5.5 Transmission electron microscopy (TEM).....	133
5.4.5.6 SR-FTIR.....	136
5.4.6 Molecular docking study.....	136
5.4.7 Hemolysis activity.....	140
5.2 Conclusion.....	141
5.3 References	141
VI SUMMARY	147
APPENDIX.....	149
BIOGRAPHY.....	158



LIST OF TABLES

Table	Page
2.1	Recent antibacterial peptides derived from agricultural-based protein byproducts with enzymatic hydrolysis 16
3.1	Minimum inhibitory concentration (MIC) and minimum bactericidal concentration (MBC) determination of P1, P2, and P6 against 4 pathogenic bacteria 55
3.2	Integration area ($\times 10^{-4}$) at various wavenumbers of secondary derivative spectra of <i>Staphylococcus aureus</i> ATCC 29213 exposed to the P1 fraction at 1 \times MIC with different exposure times..... 61
3.3	Identification of selected peptides from P1 fraction obtained from pepsin-hydrolyzed corn gluten meal..... 69
4.1	Minimum inhibitory concentration (MIC) of peptides obtained from CGMH on four different test bacteria..... 85
4.2	Characteristics of peptide EE13..... 86
4.3	Energy binding affinity (ΔG) and dissociation constant (Kd) of the interaction of EE13 with different receptors in <i>Staphylococcus aureus</i> 95
5.1	Physicochemical properties comparison between PA13 and RF135 peptides 121
5.2	Comparison classification prediction as antimicrobial peptides (AMPs) for the original and modified peptides using CAMPr3 and AntiBP3 124
5.3	The minimum inhibitory concentration (MIC) of PA13 and RF135 was calculated from the microbroth dilution assay (μM)..... 128
5.4	Predicted results of energy binding affinity (ΔG) and dissociation constant (Kd) on the interaction of modified peptide RF135 with several different receptors in <i>Salmonella</i> Typhimurium with the Prodigy server 137

LIST OF FIGURES

Figure		Page
2.1	Process for the production of protein hydrolysates	12
2.2	Properties of the bioactive peptides.....	13
2.3	Structure examples of four classes of AMPs.....	14
2.4	The structural features of the cell walls and membranes of Gram-positive and Gram-negative bacteria.....	18
2.5	Four mechanisms of action for AMPs (A) toroidal model (B) carpet model (C) barrel-stave model (D) aggregate channel model (E) DNA synthesis inhibited due to AMPs (F) Protein synthesis inhibited due to AMPs and (G) Chaperones assisted protein folding in interaction with AMPs	20
2.6	Mechanism of action of AMP with non-membrane permeabilizing	22
2.7	The major biochemical bands components of cells and tissues are displayed as lipids, proteins, nucleic acid (phospholipids), and carbohydrates in the spectral ranges from 3000-2800 cm^{-1} and 1800-800 cm^{-1}	26
3.1	(A) Chromatogram of CGMH peptide fractionation. (B) Antibacterial activity assay of six peptide fractions of CGMH towards <i>Staphylococcus aureus</i> ATCC 29213 and <i>Escherichia coli</i> TISTR 780 at a concentration of 2 mM. (C) Antibacterial activity of 3 selected peptide fractions of CGMH against the test bacteria at 2 mM	54
3.2	Bacterial killing curve of P1 against <i>Staphylococcus aureus</i> ATCC 29213 at various concentrations during 24 h incubation	56
3.3	Confocal laser scanning micrographs of <i>Staphylococcus aureus</i> ATCC 29213 exposed to the P1 and stained with SYTO-9 and propidium iodide (PI)	57
3.4	Scanning electron micrographs of (A) control <i>Staphylococcus aureus</i> ATCC 29213 without peptide; (B) <i>S. aureus</i> exposed with P1 at 1×MIC (1 mM); and (C) 4×MIC (4 mM)	58
3.5	Transmission electron micrograph of (A) <i>Staphylococcus aureus</i> ATCC 29213 without P-1, control; (B) <i>S. aureus</i> after exposure to the P1 at 1×MIC (1 mM) for 8 h; (C) at 4×MIC (4 mM) for 8 h	59

LIST OF FIGURES (Continued)

Figure	Page	
3.6	The original SR-FTIR spectra of <i>Staphylococcus aureus</i> ATCC 29213 exposed to P1 at 1xMIC in 0, 4, and 8 h for region 3800-900 cm ⁻¹ (A); The secondary derivative spectra of <i>S. aureus</i> exposed to P1 at 1xMIC in 0, 4, and 8 h for region 3000-2800 cm ⁻¹ (B); The secondary derivative spectra of <i>S. aureus</i> exposed to P1 at 1xMIC in 0, 4, and 8 h for region 1800-900 cm ⁻¹ (C) 60	60
3.7	2D-PCA score (A), loading plots PC-1 (B) and PC-2 (C) of spectra data for <i>Staphylococcus aureus</i> ATCC 29213 treated with P1 at 1xMIC for 0, 4, and 8 h..... 62	62
3.8	PCA analysis results (A) the 2D-PCA score and (B) loading plot of PC-1 from control <i>Staphylococcus aureus</i> ATCC 29213 cells and the cell treated with P1 at 1xMIC for 4 h at 37 °C; (C) the 2D-PCA score and (D) loading plot of PC-1 from control <i>S. aureus</i> cells and the cells treated with P1 at 1xMIC for 8 h at 37 °C..... 63	63
3.9	Effect of various temperatures (A) and pHs (B) on antibacterial activity of P1 at 1xMIC against <i>Staphylococcus aureus</i> ATCC 29213 64	64
3.10	The hemolytic activity of P1 fraction on human red blood cells 65	65
3.11	Antibacterial effect of the P1 against the <i>Staphylococcus aureus</i> ATCC 29213 growth inoculated in UHT milk at 37 °C for 24 h 66	66
4.1	The primary structure visualization of the peptide EAGGGEDDKKKVE (EE13) using the program PEPDRAW (http://pepdraw.com/) (A) 3D Molecular prediction of EAGGGEDDKKKVE (EE-13) obtained from Pepfold3 (https://bioserv.rpbs.univ-paris-diderot.fr/services/PEP-FOLD3/) (B) The helical wheel projection of EAGGGEDDKKKVE (EE-13) obtained from HeliQuest (http://heliquest.ipmc.cnrs.fr/cgi-bin/ComputParams.py). Blue for positively charged residues (Lys) and red for negatively charged residues (Glu and Asp). Yellow for hydrophobic residues (Val) and grey for the neutral residues (Gly and Ala). The arrow featured the helical hydrophobic moment (C) 86	86

LIST OF FIGURES (Continued)

Figure	Page
4.2	The prediction position of peptide EE13 on the non-binding → binding continuum. Predicted sensors of EE13 fall in the purple zone (A). The membrane-binding probability of peptide EE13 falls in the purple area using PMIPred server (B) 3D model interaction between peptide EE13 and membrane using PPM 3.0 server 87
4.3	Killing curve of <i>Staphylococcus aureus</i> ATCC 29213 against EAGGGEDDKKKVE (EE13) at 1/8×MIC, 1/4×MIC, 1/2×MIC, and 1×MIC incubated at 37 °C for 24 h..... 89
4.4	Confocal laser scanning micrographs of <i>Staphylococcus aureus</i> ATCC 29213 cells: (A-C) untreated cells (control), (D-F) cells exposed with EAGGGEDDKKKVE (EE13) at 1/2×MIC and (G-I) cells exposed with peptide at 1×MIC..... 90
4.5	Scanning electron micrographs of (A) control of <i>Staphylococcus aureus</i> ATCC 29213 cells (B) <i>S. aureus</i> cells treated with peptide EAGGGEDDKKKVE (EE13) at 1/2×MIC (2.0 mM) incubated at 37 °C for 4 h. (C) <i>S. aureus</i> cells treated with EE13 at 1×MIC (4.0 mM) incubated at 37 °C, for 4 h 91
4.6	FTIR spectra of <i>Staphylococcus aureus</i> ATCC 29213 in the absence and presence of 1/2×MIC EAGGGEDDKKKVE (EE13), incubated at 37 °C for 4 h (A), 2 nd derivative spectra of <i>S. aureus</i> control and subjected to EE13 at 1/2×MIC incubated at 37 °C for 4 h 3000-2800 cm ⁻¹ (B), 2 nd derivative spectra of <i>S. aureus</i> control and <i>S. aureus</i> exposed to EE13 at 1/2×MIC incubated at 37 °C for 4 h at region of 1800-900 cm ⁻¹ (C)..... 92
4.7	2D-PCA score plot (A) and loading plots (B) of whole spectrum data for <i>Staphylococcus aureus</i> ATCC 29213 treatment with EAGGGEDDKKKVE (EE13) at 1/2×MIC for 4 h..... 94
4.8	A docking illustration of the complex of membrane-bound transglycosylase (PDB ID3VMQ_B) and peptide EE13 (A) the binding site (B) the binding relationship between amino acid (C) interaction profile showed hydrogen bonds, salt bridges, and nonbonded interactions. The chain A is for EE13, and the chain B is for 3VMQ_B..... 96

LIST OF FIGURES (Continued)

Figure	Page	
4.9	A docking illustration of the complex of d-alanine-d-alanine ligase (PDB ID: 7U9K_B) and peptide EE13 (A) the binding site (B) the binding relationship between amino acids (C) interaction profile showed hydrogen bond and nonbonded interactions. The chain A is for EE13 and the chain B is 7U9K_B.....	97
4.10	The hemolytic activity of the EAGGGEDDKKKVE (EE13) on human red blood cells	98
4.11	Effect of combined mild heat treatment and the peptide EAGGGEDDKKKVE (EE13) on the growth of <i>Staphylococcus aureus</i> ATCC 29213 cells after 0, 4, and 8 h incubation time	100
4.12	CLSM images of <i>Staphylococcus aureus</i> ATCC 29213 (A) untreated cells (B) cells treated with mild heat temperature 50 °C for 10 min (C) cells treated with EE13 at 1/2×MIC (2.0 mM), and (D) cells treated with combined of mild heat temperature at 50 °C and EE13 at 1/2×MIC (2.0 mM) incubated 37 °C for 4 h.....	101
4.13	Localization of 5-carboxyfluorescein-EE13 in <i>Staphylococcus aureus</i> ATCC 29213 cells (A) untreated cells, (B) cells treated with 5-FAM-EE13 at 1/2×MIC (2.0 mM), and (C) cells treated with combined of mild heat treatment at 50 °C for 10 min and 5-FAM-EE13 at 1/2×MIC (2.0 mM) incubated 37 °C for 4 h.....	102
4.14	SEM images of <i>Staphylococcus aureus</i> ATCC 29213 cells subjected to various treatments: (A) Untreated cells (control), (B) cells treated with mild heat treatment at 50 °C for 10 min, (C) cells treated with EE13 at 1/2×MIC, and (D) cells treated with combined mild heat and followed by EE13 at 1/2×MIC treatment.....	103
5.1	Structural modification of PA13 to RF135 using NetWheels (http://lbqp.unb.br/NetWheels/).....	113
5.2	Schematic representation of the peptide (A) PA13, (B) RF135, using the program PepDraw (http://pepdraw.com/).....	122

LIST OF FIGURES (Continued)

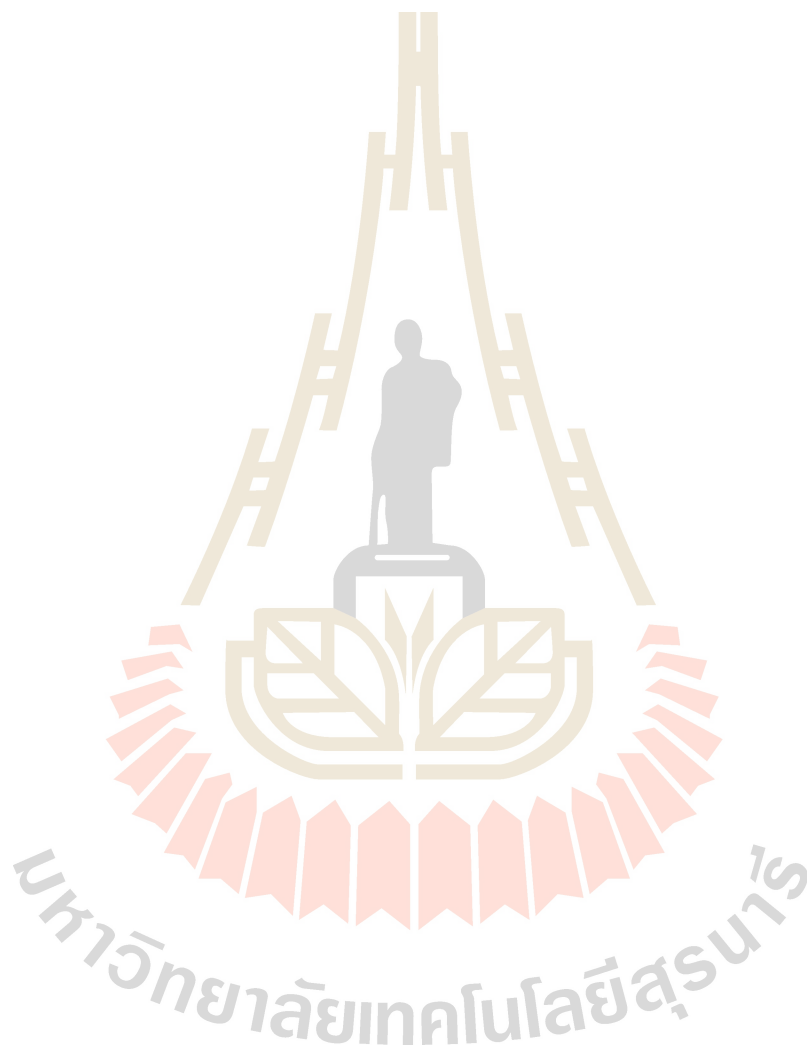
Figure	Page	
5.3	The 3D prediction structure of (A) PA13 and (B) RF135; the projection of the helical wheels (C) PA13 and (D) RF135. The images were compiled with http://heliquet.ipmc.cnrs.fr/cgi-bin/ComputParams.py . The hydrophobic moment and net charge are displayed. Residues with positive charged colored in blue; hydrophobic residues are colored yellow; uncharged residues colored in grey, green, and purple. The N and C terminal amino acids are marked by the small red letters. The arrow denotes the hydrophobic moment.....	123
5.4	Prediction of peptide (A) PA13 on the neutral membrane (e.g., 1-palmitoyl-2-oleoyl-sn-glycero-3-phosphocholine (POPC)) (B) RF135 on the neutral membrane (e.g., 1-palmitoyl-2-oleoyl-sn-glycero-3-phosphocholine (POPC)).....	125
5.5	Prediction of membrane-peptide interaction (A) PA13 on the negatively charged membrane (e.g. 1-palmitoyl-2-oleoyl-sn-glycero-3-phosphocholine/ palmitoyl-oleoylphosphatidylglycerol (POPC/POPG)) (B) RF135 on the negatively charged membrane (e.g. 1-palmitoyl-2-oleoyl-sn-glycero-3-phosphocholine/ palmitoyl-oleoylphosphatidyl-glycerol (POPC/POPG)).....	126
5.6	The 3D structure obtained from PEP-FOLD3 was utilized to model bacterial membrane interactions through a PPM 3.0 server: (A) PA13, (B) RF135	127
5.7	Bacterial-killing curve of untreated <i>Salmonella</i> Typhimurium TISTR 292 cells and cells treated with RF135 at 1/2×MIC, 1×MIC, 2×MIC, and 4×MIC during 24 h incubation	129
5.8	Confocal laser scanning micrographs of untreated <i>Salmonella</i> Typhimurium TISTR 292 (A), <i>S. Typhimurium</i> was exposed to the RF135 at 1/2×MIC (B), and <i>S. Typhimurium</i> exposed to RF135 at 1×MIC and stained with SYTO-9 and propidium iodide (PI)	130
5.9	Confocal laser scanning micrographs of untreated <i>Salmonella</i> Typhimurium TISTR 292 (A), <i>S. Typhimurium</i> was exposed to 5-FAM-RF135 at 1/2×MIC (B), and <i>S. Typhimurium</i> exposed to 5-FAM-RF135 at 1×MIC and stained with propidium iodide (PI)	131

LIST OF FIGURES (Continued)

Figure	Page
5.10 The leakage of nucleic acid from <i>Salmonella</i> Typhimurium TISTR 292 treated with RF135 at 1×MIC and 2×MIC compared to untreated cells incubated at 37 °C for 6 h	131
5.11 Scanning electron micrographs of (A) untreated <i>Salmonella</i> Typhimurium TISTR 292 cells (B) <i>S.</i> Typhimurium cells exposure with RF135 at 1/2×MIC and (C) cells treated with 1×MIC for 2 h	132
5.12 Transmission electron micrographs of (A) untreated <i>Salmonella</i> Typhimurium TISTR 292 cells (B) <i>S.</i> Typhimurium cells exposure with RF135 at 1×MIC and (C) 2×MIC for 2 h	133
5.13 The average of original SR-FTIR spectra of untreated <i>Salmonella</i> Typhimurium TISTR 292 cells and exposed to RF135 at 1×MIC at 37 °C for 2 h in the wavenumber range 3000-900 cm ⁻¹ (A); 2 nd derivative spectra of untreated <i>S.</i> Typhimurium cells and exposed to RF135 at 1×MIC at 37 °C for 2 h in the wavenumber range 3000-2800 cm ⁻¹ (B); 2 nd derivative spectra of untreated <i>S.</i> Typhimurium cells and exposed to RF135 at 1×MIC at 37 °C for 2 h in the wavenumber range 1800-900 cm ⁻¹ (C)	134
5.14 PCA analysis of SR-FTIR spectra of <i>Salmonella</i> Typhimurium TISTR 292 control and cells treated with RLLRKVTKLWKKF (RF135) incubated at 37 °C for 2 h. (A) 2D-PCA score plot; (B) PCA loading plot of PC-1	136
5.15 A docking illustration of the complex of 8T0J and peptide RF135 (A) the connection interface (B) the binding relationship of residues amino acid (C) interaction representation showed the existence of hydrogen bonds, salt bridges, and non-bonded interactions. The chain A is for RF135 and the chain B is for 8T0J	138
5.16 A docking illustration of the complex of 6T5X_B and peptide RF135 (A) the interface for binding (B) the binding interaction of residues amino acid (C) the visualization of interaction indicated the presence of hydrogen bonds, salt bridges, and non-bonded interactions. The chain A is for RF135 and the chain B is for 6T5X_B.	139

LIST OF FIGURES (Continued)

Figure	Page
5.17 The hemolytic activity of the peptide RF135 on human red blood cells.....	140



LIST OF ABBREVIATIONS

Å	=	Angstrom
ABP	=	Antibacterial peptide
Ala (A)	=	Alanine
AMP	=	Antimicrobial peptide
AMPs	=	Antimicrobial peptides
ANOVA	=	Analysis of variance
Arg (R)	=	Arginine
Asn (N)	=	Asparagine
Asp (D)	=	Aspartic acid
AOAC	=	Association of Official Analytical Chemists
ATCC	=	American Type Culture Collection
<i>B. cereus</i>	=	<i>Bacillus cereus</i>
BaF ₂	=	Barium difluoride
BLAST	=	Basic Local Alignment Search Tool
CAMP _{r3}	=	Collection of Anti-Microbial Peptides
CFU	=	Colony forming unit
CGM	=	Corn gluten meal
CGMH	=	Corn gluten meal hydrolysate
°C	=	Degree Celsius
CLSM	=	Confocal laser scanning microscopy
cm	=	Centimeter
Cys (C)	=	Cysteine
$\Delta\Delta F$	=	Relative curvature-sensing free energy
$\Delta\Delta F_{\text{adj}}$	=	Adjusted curvature-sensing free energy
$\Delta\Delta F_{L24}$	=	Length adjusted curvature-sensing free energy
ΔF_{sm}	=	Membrane-binding energy
ΔG	=	Free energy
Da	=	Dalton

LIST OF ABBREVIATIONS (Continued)

cm	=	Centimeter
Cys (C)	=	Cysteine
$\Delta\Delta F$	=	Relative curvature-sensing free energy
$\Delta\Delta F_{\text{adj}}$	=	Adjusted curvature-sensing free energy
$\Delta\Delta F_{L24}$	=	Length adjusted curvature-sensing free energy
ΔF_{sm}	=	Membrane-binding energy
ΔG	=	Free energy
Da	=	Dalton
DH	=	Degree of hydrolysis
DMST	=	Department of Medical Sciences Thailand
DNA	=	Deoxyribonucleic acid
<i>E. coli</i>	=	<i>Escherichia coli</i>
EBI	=	The European Bioinformatics Institute
EMBL	=	the European Molecular Biology Laboratory
EMSC	=	Extended Multiplicative Scatter Correction
FAM	=	Fluorescein amidites
FASTA	=	Fast adaptive shrinkage threshold algorithm
FE-SEM	=	Field emission scanning electron microscopy
FE-TEM	=	Field emission transmission electron microscopy
FPLC	=	Fast protein liquid chromatography
Glu (E)	=	Glutamic acid
Gln (Q)	=	Glutamine
Gly (G)	=	Glycine
GRAVY	=	Grand average of hydropathicity
h	=	Hour
H	=	Hydrophobicity
μH	=	Hydrophobic moment
hRBCs	=	Human red blood cells
His (H)	=	Histidine
Ile (I)	=	Isoleucine

LIST OF ABBREVIATIONS (Continued)

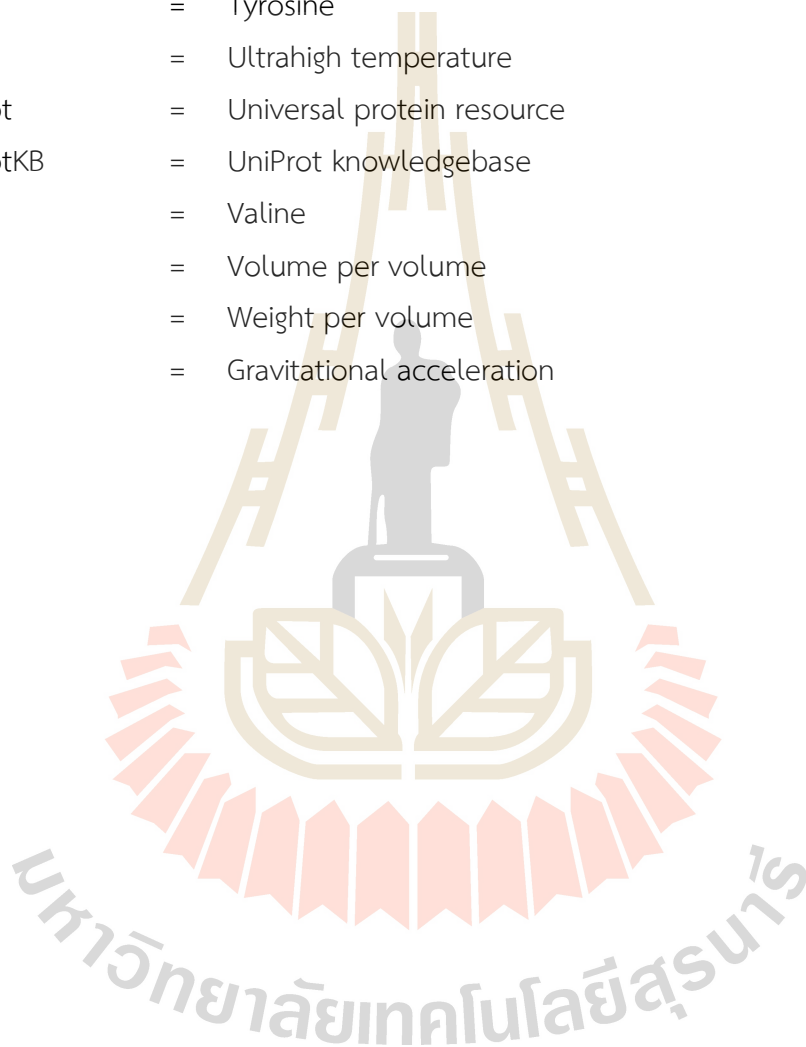
Gly (G)	=	Glycine
GRAVY	=	Grand average of hydropathicity
h	=	Hour
H	=	Hydrophobicity
μ H	=	Hydrophobic moment
hRBCs	=	Human red blood cells
His (H)	=	Histidine
Ile (I)	=	Isoleucine
kDa	=	kilo Dalton (10^3 Dalton)
Kd	=	Dissociation constant
keV	=	kilo electron Volt
LC-MS/MS	=	Liquid chromatography with tandem mass spectrometry
Leu (L)	=	Leucine
MBC	=	Minimum Bactericidal Concentration
Met (M)	=	Methionine
MHB	=	Mueller Hinton Broth
MIC	=	Minimum inhibitory concentration
MRSA	=	Methicillin-resistant <i>Staphylococcus aureus</i>
μ g	=	Microgram (10^{-6} gram)
μ L	=	Microliter (10^{-6} L)
μ M	=	Micromolar (10^{-6} mol L ⁻¹)
mg	=	Milligram (10^{-3} gram)
min	=	Minute
mL	=	Milliliter (10^{-3} L)
mM	=	Millimolar (10^{-3} mol L ⁻¹)
m/z	=	Mass per charge ratio
NaCl	=	Sodium chloride
NCBI	=	National Center for Biotechnology Information
nm	=	Nanometer
OD	=	Optical density

LIST OF ABBREVIATIONS (Continued)

OPM	=	Orientation of protein in membranes
PBS	=	Phosphate buffered saline
PCA	=	Plate count agar
PCA	=	Principal component analysis
PDB	=	Protein Data Bank
pH	=	Potential of hydrogen
pl	=	Isoelectric point
PI	=	Propidium iodide
P _m	=	Membrane-binding probability
PMIPred	=	Protein-Membrane Interaction prediction
POPC	=	1-palmitoyl-2-oleoyl-glycero-3-phosphocholine
POPG	=	Palmitoyl 2 Oleoyl Phosphatidyl Glycerol
Pro (P)	=	Proline
Prodigy	=	The protein energy binding prediction
RCSB	=	the Research Collaboratory for Structural Bioinformatics
RNA	=	Ribonucleic acid
RP-HPLC	=	Reversed-phase high-performance liquid chromatography
rpm	=	Revolutions per minute
s	=	Second
<i>S. aureus</i>	=	<i>Staphylococcus aureus</i>
SD	=	Standard deviation
SEC	=	Size exclusion chromatography
SEM	=	Scanning electron microscope
Ser (S)	=	Serine
SR-FTIR	=	Synchrotron radiation-based Fourier transform infrared
ssp.	=	Subspecies
<i>S. Typhimurium</i>	=	<i>Salmonella</i> Typhimurium
TEM	=	Transmission electron microscopes
Thr (T)	=	Threonine
TISTR	=	Thailand Institute of Scientific and Technological Research

LIST OF ABBREVIATIONS (Continued)

TNBS	=	2, 4, 6-trinitrobenzenesulfonic acid
Trp (W)	=	Tryptophan
TSA	=	Tryptic Soy Agar
TSB	=	Tryptic Soy Broth
Tyr (Y)	=	Tyrosine
UHT	=	Ultrahigh temperature
UniProt	=	Universal protein resource
UniProtKB	=	UniProt knowledgebase
Val (V)	=	Valine
v/v	=	Volume per volume
w/v	=	Weight per volume
xg	=	Gravitational acceleration



CHAPTER I

INTRODUCTION

1.1 Background and significance of the study

There is an increasing problem of antibiotic resistance in bacteria around the world. A significant contributing factor is the overuse of antibiotics. Antimicrobial resistance is characterized by three fundamental mechanisms: antibacterial drugs are degraded enzymatically, antimicrobial-targeted protein alteration, and the permeability of membranes to antibiotic changes (Dever & Dermody, 1991). As a consequence, the occurrence of exogenous resistance genes or chromosomal mutations can contribute to the growth of resistance in bacteria (Durão, Balbontín, & Gordo, 2018).

Antimicrobial materials (antibiotics, preservatives, heavy metals, disinfectants, and antiseptics) are used throughout the value chain of food production and manufacturing processes to increase productivity and efficiency. Unfortunately, food processing environments may be contaminated with antibiotic-resistant bacteria. This contamination occurs because bacteria are stressed by the overexpression of efflux pumps, which play an important role in removing antimicrobials from the cell (Oniciuc et al., 2019). As a result of this stress, antibiotic-resistant bacteria are produced, which can then spread to other food processing environments.

Food poisoning is typically caused by Gram-negative bacteria such as *Salmonella Typhimurium*, *Escherichia coli*, and *Pseudomonas aeruginosa*. In addition, foodborne illnesses and food spoilage caused by other Gram-positive bacteria like *Staphylococcus aureus* and *Bacillus cereus* have been reported due to chemical preservatives have historically been utilized. This method uses a molecular dynamic simulation approach to obtain atomic-level information by measuring the interaction between the designed AMPs and the target bacterial membrane. ed to prevent food spoilage and its etiological agent (Mostafa et al., 2018). For example, sodium benzoate and potassium sorbate are frequently utilized to inhibit the growth of foodborne pathogens. Sodium benzoate and potassium sorbate are weak acids, and their

antimicrobial activity is due to the increasing of protons and anions within the microbial cell, which interfere normal metabolism (Musyoka et al., 2018).

Even though chemical food preservatives can effectively reduce the growth of pathogens in foods, consumers remain concerned about the safety of foodstuffs (Chakchouk-Mtibaa et al., 2014). In recent years, a lot of research about the risks of chemical food preservatives has influenced the clean-labeling movement. Therefore, it is necessary to seek natural preservatives that could replace the usage of chemical preservatives in the food industry.

Food ingredients that have preservation effects can be found in bioactive peptides and protein hydrolysates that can be obtained by enzymatic hydrolysis of foods with high protein content. Many studies have demonstrated that antioxidant and antimicrobial properties can be discovered in proteins, protein hydrolysates, peptides, or amino acids (Gokoglu, 2019). For instance, soy protein, whey protein, milk protein, and gelatin-based materials containing natural antimicrobial compounds have been investigated for their potential as natural food packaging with antibacterial properties (Zhen et al., 2021).

Antimicrobial peptides (AMPs), discovered in a wide range of microorganisms, plants, and animals, serve as an essential part of the immune system by protecting the host from microbial pathogens (Seo, Won, Kim, Mishig-Ochir, & Lee, 2012). AMPs with a positively charged character work by interacting with the anionic membrane lipids of bacteria, making it impossible for them to develop resistance to AMPs (Fjell, Hiss, Hancock, & Schneider, 2012).

The prominent role of AMPs is to either eliminate or hinder the development of microorganisms at the molecular dimension. Typically, cationic AMP exert their effects through membrane structural disruption and pore formation, resulting in the degradation of the lipid bilayer in Gram-positive and Gram-negative bacteria and fungi cells. Therefore, regardless of their structure, AMPs can work over several cell targets and, in some cases, is recognized as a multitarget molecules since they can perform more than one role (Leite et al., 2019).

AMPs are a different biomolecular class in various microorganisms, plants, and animals. AMPs in plants can be narrowly classified into endogenous peptides, which exist in plant matrices, and peptides derived from plant proteomes through processing mechanisms such as enzymatic hydrolysis and fermentation (Chai, Tan, Ee, Xiao, & Wong, 2019).

Recent studies reported on the characterization of properties of plant protein hydrolysates. Raharjo, Utami, Fajr, Swasono, & Haryadi (2021) studied antibacterial peptides isolated from *Ricinus communis* seed protein hydrolyzed by trypsin. The hydrolysate exhibited high efficacy against *E. coli* and *S. aureus* bacteria. The antibacterial effect was marked by its ionic characteristics, and the secondary structure facilitates the perturbation of the bacterial cell membrane. Heat-pretreated cottonseed byproduct hydrolysate by Alcalase inhibited the development of *Colletotrichum gloeosporioides* and *S. aureus*. The antibacterial activity of hydrolyzed protein is determined by its interaction with the cell wall and membrane of the bacterial cell, and the characteristics of the peptide determine this interaction (de Oliveira Filho et al., 2021). Heymich et al. (2021) described chymotrypsin hydrolyzed legumin from chickpea (*Cicer arietum* L.), yielding AMPs with high activity for 16 bacterial species, which included pathogenic, spoilage, and two antibiotic-resistant bacteria. Cottonseed protein hydrolysates with Alcalase were used as a source of antibacterial peptides for food and feed industries (Song et al., 2020). AMPs were purified and characterized from alcalase-hydrolyzed cottonseed protein. The three isolated antibacterial peptides HRRRFSLY, KFMPT, and RRLFSDY caused *E. coli* membrane disintegration. These findings suggested that peptides that have antibacterial action and are derived from cottonseed protein could be a potential source for functional foods or related drugs (Kong et al., 2020). The microwave-assisted and enzymatic (Alcalase and Flavourzyme) hydrolysis of chia seed (*Salvia hispanica*) proteins was demonstrated to produce bioactive peptides that can potentially be used as antimicrobial agents to inhibit *E. coli*, *S. enterica*, and *L. monocytogenes* in food and medical purposes (Aguilar-Toalá, Deering, & Liceaga, 2020).

In the past few years, the investigation has proved that various low-value waste with protein sources like pig liver and blood from porcine industry residues (Borrajo et al., 2020; Jin, Choi, & Yim, 2020), dark tuna muscles (Bui et al., 2021), orange seed waste from orange juice industry (Mazloomi et al., 2020), rice bran (Zaky, Chen, Liu, Li, & Jia (2019), and industrial poultry waste (Teshnizi, Robotjazi, & Mosaabadi, 2020) could be utilized to generate functional and bioactive protein hydrolysates and peptides. Corn gluten meal (CGM) is a protein-rich byproduct that is currently underutilized.

CGM contains 62-71% protein, about 65% zein, 30% glutelin, and also between 21-26% carbohydrate, which 12-15% starch, and the rest 3-7% is fat and 1-2% is fiber (Zhu, He, & Hou, 2019). The most commonly available amino acids in CGM are Glu,

Leu, Pro, Ala, Phe, and Asp (Li, Guo, Hu, Xu, & Zhang, 2007). CGM is commonly used as animal feed due to its limited *in vivo* bioavailability. Alternatively, it is often disposed of due to its low water solubility and an imbalanced composition of amino acids (Li et al., 2019).

Most commercial zein is obtained from CGM as a coproduct of the corn wet milling process (Shukla & Cheryan, 2001). Zein is a category of alcohol-soluble proteins known as prolamins derived from the corn plant. Zein is immiscible in water because it has more than 50% hydrophobic amino acid residues on its surface. Zein is soluble in 55% to 90% of aqueous alcohol and precipitates readily as nanoparticles after combining with water at a total amount of alcohol that cannot dissolve zein. Zein has an isoelectric point of 6.8 (Bouman et al., 2016).

Numerous research have explored the antimicrobial activities of corn peptides to improve the potency of corn proteins (maize) through chemical extraction and gene-cloned methods. Huynh, Borgmeyer, & Zobel (1992) purified a 22 KDa antifungal protein from maize seed by ammonium sulphate precipitation and demonstrated its ability to inhibit two fungal pathogens, *Fusarium oxysporum* and *Alternaria solani*. Duvick, Rood, Rao, & Marshak (1992) reported peptide MBP-1 isolated by sulfuric acid extraction from maize kernel. MBP-1 was discovered to inhibit *E. coli* at a concentration of 3 $\mu\text{g}\cdot\text{mL}^{-1}$ and also prevent germinating spores and elongating hyphae in different pathogenic plant fungi for corn plants like *Fusarium moniliforme* Sheld. and *Fusarium graminearum*, and pathogenic bacteria of corn *Clavibacter michiganese* ssp. *nebraskense* at concentrations of 60 $\mu\text{g}\cdot\text{mL}^{-1}$ and 30 $\mu\text{g}\cdot\text{mL}^{-1}$, respectively. Kant et al. (2009) demonstrated that PDC1, a corn defensin peptide isolated and its recombinant clone in *E. coli* and *Pichia pastoris*, significantly inhibited *Fusarium graminearum* development at 50 $\mu\text{g}\cdot\text{mL}^{-1}$. Hassan, Qutb, & Dong (2021) described ZM-804 as a novel cationic AMPs isolated through the inbred line method on the *Zea mays* B73 cDNA library. This peptide exhibited robust antimicrobial activity and caused cell membrane disruption and damage to *Clavibacter michiganensis* subsp. *michiganensis* and *Pseudomonas syringae* pv. tomato at MIC of 8 μM and 4 μM , respectively. However, the research on corn peptides with antimicrobial properties derived from corn gluten meal (CGM) through enzymatic hydrolysis is still limited. Investigating the antimicrobial activity in CGM hydrolysate would increase its utilization and value.

1.2 Research objectives

1.2.1 To produce peptides possessing antibacterial properties from CGM hydrolysate (CGMH).

1.2.2 To isolate, identify and characterize antibacterial peptides derived from CGMH.

1.2.3 To define the mechanism of the antibacterial activities of the peptides obtained from the CGMH on the most sensitive bacteria.

1.2.4 To investigate the potential impact of the structural modification on the antibacterial properties of the peptide.

1.3 Research hypotheses

Peptides obtained from CGMH by Alcalase and pepsin can prevent the development of pathogenic bacteria. The peptides generated in CGMH can be used in food preservation. In addition, peptides derived from CGMH may displayed one mode of action in the inhibition of bacterial growth. Moreover, structural modification on peptides obtained from CGMH may enhance its antibacterial activity.

1.4 Scope of the study

Alcalase and pepsin were used to hydrolyze CGM enzymatically. The degree of hydrolysis was measured in CGMH. The CGMH was fractionated using preparative flash chromatography to prepare antimicrobial peptides. An assessment of the antibacterial activities generated by CGMH was evaluated. The antimicrobial ability of peptides derived from CGMH was evaluated by establishing the minimum inhibitory concentration (MIC) and the minimum bactericidal concentration (MBC). The peptide fraction of CGMH showing the most potent antimicrobial activity was selected for peptide identification using LC-MS/MS. Modes of action from antimicrobial peptides on the most sensitive bacterium were determined. Peptides fraction of CGMH was synthesized based on peptide sequence databases. The synthetic peptides were estimated for their antimicrobial activity. Modifications were developed to enhance the antimicrobial properties of the synthesized peptides based on the CGMH peptide sequence to enhance their antimicrobial properties. The application of peptide fraction with antimicrobial activity to food preservation was evaluated.

1.5 Expected results

Valorization of CGM through enzymatic hydrolysis technique could liberate peptides with antimicrobial activity. These peptides could be utilized as biological preservatives in food processing to extend shelf-life and overcome the utilization of chemical preservatives. Identifying peptides from CGM-derived antimicrobial hydrolysates would provide insights into the relationship between the activity and structure of antimicrobial peptides. The information would help create enzyme-aided techniques for antibacterial peptides from CGM. Observation of peptides applied to bacterial cells can be used to study the mechanism of action of antibacterial activity derived from CGMH. Peptide sequence modification may facilitate the discovery of novel peptides with better antibacterial action. The use of CGMH, which has antibacterial activities, may be beneficial for food preservation. This study would contribute to advancing knowledge and understandings regarding the added value of CGMH as an antimicrobial peptide source.

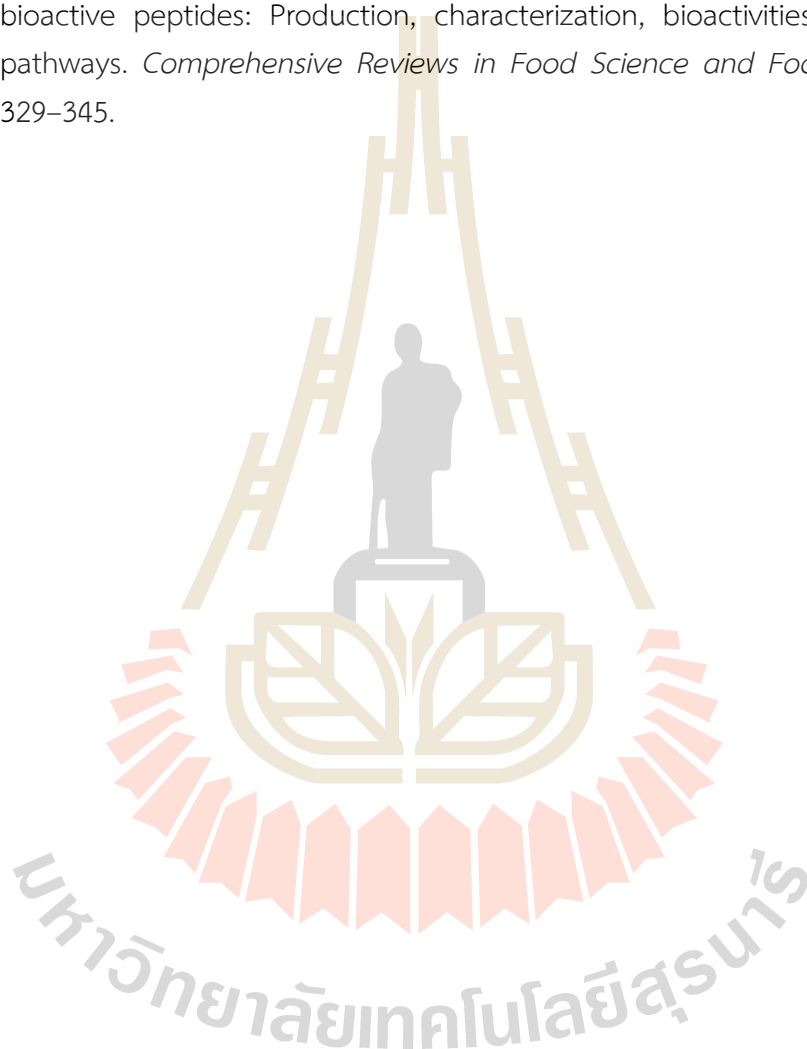
1.6 References

- Aguilar-Toalá, J. E., Deering, A. J., & Liceaga, A. M. (2020). New insights into the antimicrobial properties of hydrolysates and peptide fractions derived from chia seed (*Salvia hispanica* L.). *Probiotics and Antimicrobial Proteins*, *12*, 1571–1581.
- Borrajó, P., Pateiro, M., Gagaoua, M., Franco, D., Zhang, W., & Lorenzo, J. M. (2020). Evaluation of the antioxidant and antimicrobial activities of porcine liver protein hydrolysates obtained using alcalase, bromelain, and papain. *Applied Sciences*, *10*(7), 2290.
- Bouman, J., Belton, P., Venema, P., Van Der Linden, E., De Vries, R., & Qi, S. (2016). Controlled release from zein matrices: Interplay of drug hydrophobicity and pH. *Pharmaceutical Research*, *33*(3), 673–685.
- Bui, X. D., Vo, C. T., Bui, V. C., Pham, T. M., Bui, T. T. H., Nguyen-Sy, T., ... Show, P. L. (2021). Optimization of production parameters of fish protein hydrolysate from *Sarda Orientalis* black muscle (by-product) using protease enzyme. *Clean Technologies and Environmental Policy*, *23*, 31–40.
- Chai, T. T., Tan, Y. N., Ee, K. Y., Xiao, J., & Wong, F. C. (2019). Seeds, fermented foods, and agricultural by-products as sources of plant-derived antibacterial peptides. *Critical Reviews in Food Science and Nutrition*, *59*(sup1), S162–S177.
- Chakchouk-Mtibaa, A., Elleuch, L., Smaoui, S., Najah, S., Sellem, I., Mejdoub, H., ... Mellouli, L. (2014). Characterization of the bacteriocin BacJ1 and its effectiveness

- for the inactivation of *Salmonella typhimurium* during turkey escalope storage. *Food Chemistry*, *152*, 566–572.
- de Oliveira Filho, J. G., Rodrigues, J. M., Valadares, A. C. F., de Almeida, A. B., Valencia-Mejia, E., Fernandes, K. F., ... Dyszy, F. H. (2021). Bioactive properties of protein hydrolysate of cottonseed byproduct: antioxidant, antimicrobial, and angiotensin-converting enzyme (ACE) inhibitory activities. *Waste and Biomass Valorization*, *12*(3), 1395–1404.
- Dever, L. A., & Dermody, T. S. (1991). Mechanisms of bacterial multiresistance to antibiotics. *Archives of Internal Medicine*, *151*(5), 886–895.
- Durão, P., Balbontin, R., & Gordo, I. (2018). Evolutionary mechanisms shaping the maintenance of antibiotic resistance. *Trends in Microbiology*, *26*(8), 677–691.
- Duvick, J. P., Rood, T., Rao, A. G., & Marshak, D. R. (1992). Purification and characterization of a novel antimicrobial peptide from maize (*Zea mays* L.) kernels. *Journal of Biological Chemistry*, *267*(26), 18814–18820.
- Fjell, C. D., Hiss, J. A., Hancock, R. E. W., & Schneider, G. (2012). Designing antimicrobial peptides: Form follows function. *Nature Reviews Drug Discovery*, *11*(1), 37–51.
- Gokoglu, N. (2019). Novel natural food preservatives and applications in seafood preservation: A review. *Journal of the Science of Food and Agriculture*, *99*(5), 2068–2077.
- Hassan, M. F., Qutb, A. M., & Dong, W. (2021). Prediction and activity of a cationic α -helix antimicrobial peptide ZM-804 from maize. *International Journal of Molecular Sciences*, *22*(5), 2643.
- Heymich, M. L., Friedlein, U., Trollmann, M., Schwaiger, K., Böckmann, R. A., & Pischetsrieder, M. (2021). Generation of antimicrobial peptides Leg1 and Leg2 from chickpea storage protein, active against food spoilage bacteria and foodborne pathogens. *Food Chemistry*, *347*, 128917.
- Huynh, Q. K., Borgmeyer, J. R., & Zobel, J. F. (1992). Isolation and characterization of a 22 kDa protein with antifungal properties from maize seeds. *Biochemical and Biophysical Research Communications*, *182*(1), 1–5.
- Jin, S. K., Choi, J. S., & Yim, D. G. (2020). Hydrolysis conditions of porcine blood proteins and antimicrobial effects of their hydrolysates. *Food Science of Animal Resources*, *40*(2), 172–182.
- Kong, X., Song, W., Hua, Y., Li, X., Chen, Y., Zhang, C., & Chen, Y. (2020). Insights into the antibacterial activity of cottonseed protein-derived peptide against *Escherichia coli*. *Food and Function*, *11*(11), 10047–10057.
- Leite, M. L., Sampaio, K. B., Costa, F. F., Franco, O. L., Dias, S. C., & Da Cunha, N. B. (2019). Molecular farming of antimicrobial peptides: Available platforms and strategies

- for improving protein biosynthesis using modified virus vectors. *Anais Da Academia Brasileira de Ciencias*, 91, 1–23.
- Li, G., Liu, W., Wang, Y., Jia, F., Wang, Y., Ma, Y., ... Lu, J. (2019). Functions and applications of bioactive peptides from corn gluten meal. In F. Toldrá (Ed.), *Advances in Food and Nutrition Research* (Vol. 87, pp. 1–41). Amsterdam: Elsevier Inc.
- Li, H.-M., Guo, P., Hu, X., Xu, L., & Zhang, X.-Z. (2007). Preparation of corn (*Zea mays*) peptides and their protective effect against alcohol-induced acute hepatic injury in NH mice. *Biotechnology and Applied Biochemistry*, 47(3), 169.
- Mazloomi, S. N., Mora, L., Aristoy, M. C., Mahoonak, A. S., Ghorbani, M., Houshmand, G., & Toldrá, F. (2020). Impact of simulated gastrointestinal digestion on the biological activity of an alcalase hydrolysate of orange seed (*Siavaraze, Citrus sinensis*) by-products. *Foods*, 9(9), 1217.
- Mostafa, A. A., Al-Askar, A. A., Almaary, K. S., Dawoud, T. M., Sholkamy, E. N., & Bakri, M. M. (2018). Antimicrobial activity of some plant extracts against bacterial strains causing food poisoning diseases. *Saudi Journal of Biological Sciences*, 25(2), 361–366.
- Musyoka, J. N., Abong, G. O., Mbogo, D. M., Fuchs, R., Low, J., Heck, S., & Muzhingi, T. (2018). Effects of acidification and preservatives on microbial growth during storage of orange fleshed sweet potato puree. *International Journal of Food Science*, 2018, 8410747.
- Oniciuc, E. A., Likotrafti, E., Alvarez-Molina, A., Prieto, M., López, M., & Alvarez-Ordóñez, A. (2019). Food processing as a risk factor for antimicrobial resistance spread along the food chain. *Current Opinion in Food Science*, 30, 21–26.
- Raharjo, T., Utami, W., Fajr, A., Swasono, R., & Haryadi, W. (2021). Antibacterial peptides from tryptic hydrolysate of *Ricinus communis* seed protein fractionated using cation exchange chromatography. *Indonesian Journal of Pharmacy*, 32(1), 74–85.
- Seo, M. D., Won, H. S., Kim, J. H., Mishig-Ochir, T., & Lee, B. J. (2012). Antimicrobial peptides for therapeutic applications: A review. *Molecules*, 17(10), 12276–12286.
- Shukla, R., & Cheryan, M. (2001). Zein: The industrial protein from corn. *Industrial Crops and Products*, 13(3), 171–192.
- Song, W., Kong, X., Hua, Y., Chen, Y., Zhang, C., & Chen, Y. (2020). Identification of antibacterial peptides generated from enzymatic hydrolysis of cottonseed proteins. *LWT - Food Science and Technology*, 125, 109199.
- Teshnizi, Z. M., Robotjazi, S. M., & Mosaabadi, J. M. (2020). Optimization of the enzymatic hydrolysis of poultry slaughterhouse wastes using alcalase enzyme for the preparation of protein hydrolysates. *Applied Food Biotechnology*, 7(3), 153–160.

- Zaky, A. A., Chen, Z., Liu, Y., Li, S., & Jia, Y. (2019). Preparation and assessment of bioactive extracts having antioxidant activity from rice bran protein hydrolysates. *Journal of Food Measurement and Characterization*, *13*(4), 2542–2548. 9
- Zhen, N., Wang, X., Li, X., Xue, J., Zhao, Y., Wu, M., ... Zhang, H. (2021). Protein-based natural antibacterial materials and their applications in food preservation. *Microbial Biotechnology*, *15*(5), 1324–1338.
- Zhu, B., He, H., & Hou, T. (2019). A comprehensive review of corn protein-derived bioactive peptides: Production, characterization, bioactivities, and transport pathways. *Comprehensive Reviews in Food Science and Food Safety*, *18*(1), 329–345.



CHAPTER II

LITERATURE REVIEWS

2.1 Food spoilage and foodborne illness

Over 600 million infections and 420,000 deaths occur yearly from contaminated foodstuffs with fundamental causes of microbiological contamination (World Health Organization (WHO), 2022). The worldwide loss of 25% of produced food is responsible for food spoilage due to microbial contamination, resulting in high economic and environmental costs to producers. Bacteria such as *Escherichia coli*, *Salmonella* spp., and *Staphylococcus aureus* are not only the cause of food spoilage but also foodborne pathogens with significant public health and productivity implications (Elisseeva et al., 2020).

The spoilage of foodstuffs may lead to substantial financial losses for the food industry. At the same time, it significantly causes global food waste, which is estimated to contribute nearly one-third of the foodstuffs generated in distribution and consumption (Gustavsson, Cederberg, Sonesson, Otterdijk, & Meybeck, 2011). The process that makes food unacceptable to consumers is known as food spoilage. Microbial spoilage is the number one leading cause of food spoilage (Gram et al., 2002). Food spoilage is any change that causes food product quality to deteriorate, such as texture softening, color-changing, and growth of microorganisms. It is a complicated mechanism for various reasons, broadly categorized as chemical, physical, or biological factors (Kaczmarek, Avery, & Singleton, 2019).

Several factors cause microbial invasion of food. The first factor is the environmental conditions like soil, air, and water because many of the initial bacteria in the food raw materials accumulate in the microorganism reservoir. Second, pathogenic microorganisms can contaminate food by breathing and excreting parasites in humans, animals, and plants, leading to food poisoning and even human and animal diseases (Zhang et al., 2021). In particular, bacterial infection in most food poisoning cases was associated with Gram-negative bacteria, including *Escherichia coli*, *Salmonella* Typhimurium, and *Pseudomonas aeruginosa*. Additional Gram-positive

bacteria species, like *Staphylococcus aureus* and *Bacillus cereus*, were also found to be causal to food spoilage or foodborne diseases (Mostafa et al., 2018). There are two basics of foodborne illness; foodborne infections and foodborne intoxications. A foodborne infection develops as a result of pathogen consumption, colonization, and subsequent proliferation within the human host. In contrast, foodborne intoxication arises when a pathogen generates a toxin that is subsequently consumed by the human host (Bintsis, 2017).

In the food industries, many microbes such as *Listeria monocytogenes*, *Escherichia coli* O157:H7, *Salmonella* spp., *Campylobacter jejuni*, *Pseudomonas* spp., *Staphylococcus* spp., and *Bacillus cereus* are an actual problem. The existence of harmful bacteria in food production caused biofilm formation that may contribute to disease transmission, deterioration of food, a reduced interval between cleanups, lower thermal efficiency, or even blocking of machines; at least metal corrosion in pipelines and tanks leading to metal loss; and non-starter bacterial product contamination (Cappitelli, Polo, & Villa, 2014). Even though chemical food preservatives can effectively control the growth of pathogenic bacteria in food, consumers are still concerned about several safety issues (Chakchouk-Mtibaa et al., 2014).

The emergence of multiple resistance and co-resistance in microorganisms, especially bacteria, might be driven by the continuous use of antibiotics, biocides, chemical preservatives, and metals in the food production chain (Romero, Grande Burgos, Pérez-Pulido, Gálvez, & Lucas, 2017). In addition, the abuse of antimicrobial substances has been implicated in developing the growing antimicrobial resistance of foodborne microorganisms. Moreover, the excessive use of antimicrobial food preservatives can be associated with the imbalance of the intestinal bacteria in the gut, potentially leading to the development of pathogenic bacteria that are harmful to health. Therefore, managing antimicrobial resistance and seeking alternatives to overcome these problems is important by using nature-based antimicrobials such as probiotics, bacteriophages or antimicrobial peptides.

2.2 Protein hydrolysates

Protein hydrolysates are produced by the chemical or biological degradation of proteins into peptides with an average of 2-20 amino acid units that typically exhibit bioactive peptides. However, this can be different in some cases depending on the protein source (Shahidi & Ambigaipalan, 2018). The most notable changes affecting

functionality are a decrease in peptide chain molecular weight and a rise in polar groups ($-\text{NH}_4^+$, $-\text{COO}^-$), increasing hydrophilicity, and transforming molecular configuration. The peptide bonds may be cleaved with acids, alkalis, or enzymes. Although acid/alkali hydrolysis is less costly, controlling is hard to monitor and results in lower nutritional quality and functionality (Sinha, Radha, Prakash, & Kaul, 2007). Enzymatic hydrolysis is the most widely used of several methods because it is a relatively mild process and gives high-quality products (Kose & Oncel, 2015).

Food-derived bioactive peptides vary significantly in structure and mode of action. The enzymatic hydrolysis of various protein substrates with corresponding amino acid structures and sequences, using proteases of different specificities, produces a diverse spectrum of hydrolysates. Various bioactivities were reported in protein hydrolysates and biopeptides, which contained complex mixtures of peptides with different lengths and amino acid sequences (Nasri, 2017). The majority of identified peptides come from costly protein matrixes. (e.g., food). In the majority of instances, this makes their application unsuitable. Techniques with no detrimental environmental consequences (green processes) have recently risen to prominence because they plan to substitute non-renewable energy with agricultural waste. Agro-industrial waste is a protein-rich medium that has become a viable substitute for extracting bioactive compounds, mainly from protein hydrolysates (Lemes et al., 2016). The hydrolysis production processes are summarized in Figure 2.1.

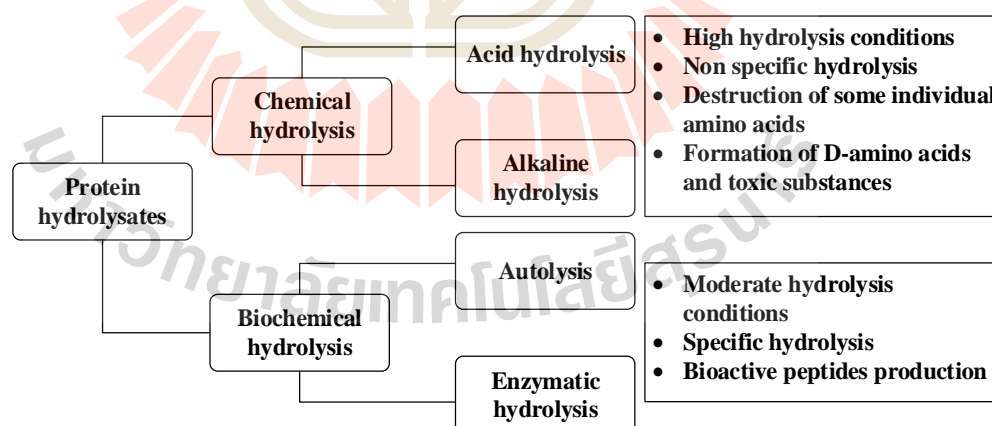


Figure 2.1 Process for the production of protein hydrolysates (Source: Zamora-Sillero, Gharsallaoui, & Prentice, 2018)

Bioactive peptides are approximately 2-30 amino acid residues that are not active in the native protein sequence and which, in addition to their nutritional

advantage, have beneficial effects on body systems after release (Korhonen & Pihlanto, 2006).

The bioactive peptides are functional chemical compounds formed by amino acid residues bound together by covalent bonds. Food-derived bioactive peptides are becoming increasingly valuable due to their essential properties, particularly high affinity, and quality of specificity, to play an important function in human health by promoting the digestion, hormone, cardiovascular, and immunity systems. They are often referred to as potential biological active regulators because they tend to reduce the likelihood of oxidation and microbial spoilage of foods (Kaur et al., 2020).

Proteolytic enzymes can generate biogenic or bioactive peptides in protein precursors through digestion (gastric digestion), food handling (maturing, fermentation, cooking), storage, or *in vitro* hydrolysis (Carrasco-Castilla, Hernández-Álvarez, Jiménez-Martínez, Gutiérrez-López, & Dávila-Ortiz, 2012).

Bioactive peptides are naturally occurring compounds in foods or proteins that are not active in their parent molecules. Yet, they can become involved and move to the active site after hydrolysis. Bioactive peptides may also be chemically produced and further characterized. The peptides have multiple functions, such as antihypertensive, antioxidant, antimicrobial, anticoagulant, and chelating activities (Figure 2.2). They also act as food flavorings and enzyme inhibitors associated with pathogenic bacteria growth. Many bioactive peptides from various sources have been reported in the scientific literature, with many databases detailing peptide composition, origin, and properties (Jakubczyk, Karas, Rybczynska-Tkaczyk, Zielinska, & Zielinski, 2020).

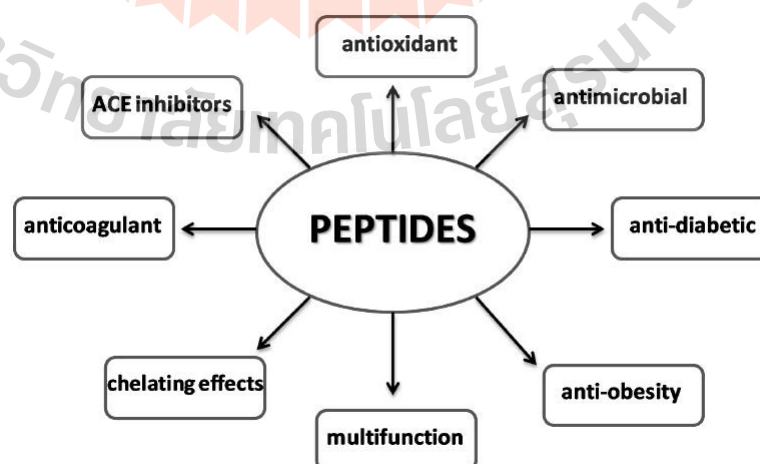


Figure 2.2 Properties of the bioactive peptides (Source: Jakubczyk et al., 2020)

Bioactive peptides could be manufactured by enzymatic hydrolysis or microbial fermentation of food proteins. However, because of residual organic solvents or hazardous product additives, enzymatic hydrolysis is more favorable in the food and pharmaceutical industries (Kim & Wijesekara, 2010).

2.3 Antimicrobial peptides

Antimicrobial peptides (AMPs) are a small group of proteins that possess antibacterial, antiviral, and antifungal characteristics. AMPs are recognized as "host-defense peptides" and are widely distributed in the systemic defenses and barriers of eukaryotic multicellular organisms (Lazzaro, Zasloff, & Rolff, 2020). AMPs inhibit or kill bacterial growth by disrupting the bacterial membrane, altering metabolism, or interfering with cytoplasmic components (Esmailpour, Ehsani, Aminlari, Shekarforoush, Hoseini, 2016).

AMPs are categorized into four groups depending on the secondary structures and physicochemical properties: linear, often α -helical peptides; β -sheet peptides with at least two disulfide bonds; extended linear peptides with Trp, Pro, and His residues; and loop (cyclic) peptides formed by a disulfide bridge (Hancock, 1997; Haney, Mansour, & Hancock, 2017). Figure 2.3 shows examples of the structures of AMPs.

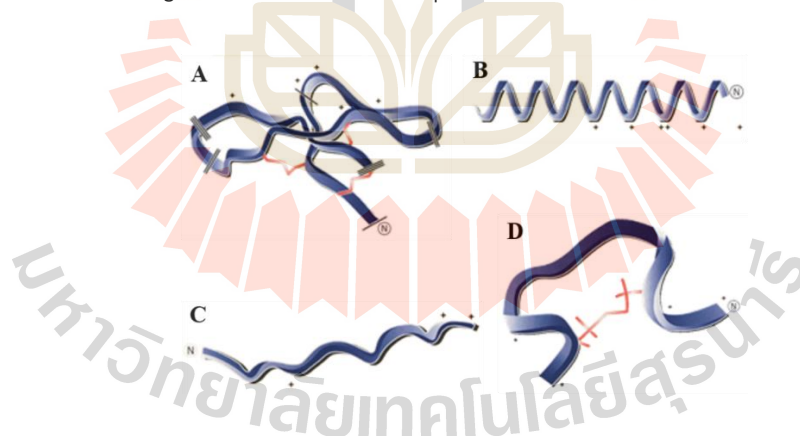


Figure 2.3 Structure examples of four classes of AMPs (Source: Hancock, 1997) (A) β -stranded of human defensin-1, (B) α -helical of cecropin-melittin hybrid, (C) extended coil of indolicidin, (D) loop of bactenecin. Structure "backbones" indicated by positive charges (+), amino termini (N), and disulfide bridges shown in (A) and (B). In (D), it has three β -strands; their start and stop positions are marked by the pairs of one, two, or three lines on the structure.

In water, α -helical AMPs for instance magainin (frog's skin gland), cecropin (cecropia moth), pexiganan (frog's skin), and temporin (frog's skin gland) have random structures with no rigidity. Still, in a hydrophobic membrane context, they follow amphipathic helices and undergo conformational changes. β -sheet peptides, like defensins and protegrins, have a more ordered structure with rigidity determined by the intramolecular disulfide bonds. In the opposite, extended peptides like indolicidin or loop peptides for example microcin are found to be relatively less structured (Oyston, Fox, Richards, & Clark, 2009). The most studied of these four classes is α -helical peptides since most AMPs discovered in nature take on an α -helical conformation.

AMPs molecules are characterized as small, positively charged, amphipathic molecules that can be synthesized in various possible structures. Despite their structural diversity, the majority of AMPs function by interfering with the cellular surface of bacteria, accompanied by a disruption of the cellular integrity. Bacteria frequently encounter AMPs in their natural environment and have developed resistance mechanisms (Andersson, Hughes, & Kubicek-Sutherland, 2016). Therefore, most of the resistance mechanisms of bacteria work by reducing the number of AMPs that come into contact with the surface of the bacterial cell. AMPs resistance strategies may include peptide entrapment or sequestering, proteolysis-based AMPs degradation, aggressive transfer of AMPs out of the cell, and structural changes to the cellular surface to eliminate AMPs interference. Many of these defense processes are activated in the presence of AMPs, which can help bacteria detect and respond to the impact of AMPs. The absence of this resistance mechanism impairs the ability of bacteria to establish themselves in plant or animal hosts and reduces the level of virulence of many pathogenic bacteria. Resistance mechanisms can develop in a lineage of bacteria or be passed on genetically from other AMP-resistant species. (Nawrocki, Crispell, & McBride, 2014).

2.4 AMPs from protein byproduct

The food industry is one of the most significant industries in the world. Large amounts of waste products are produced annually by the food industry. Food waste includes a significant amount of organic matter. Food byproducts are becoming a more common term for food waste. Protein byproducts from the food industry, derived from plant and animal food waste, have great potential as a source of value-added products (Yu & Brooks, 2016).

Protein byproducts are transformable into health-promoting bioactive peptides that can be used to develop functional foods and nutraceuticals (Yongsawatdigul & Hamzeh, 2021). Bioactive peptides can be synthesized by enzymatic hydrolysis and fermentation technology (Daliri, Oh, & Lee, 2017). Bioactive peptides can be used as natural alternatives to antibiotics and preservatives due to their ability to inhibit the growth of some microorganisms and, therefore, are recognized as antimicrobial peptides (Rivero-Pino, Leon, Millan-Linares, & Montserrat-de la Paz, 2023). Table 2.1 summarizes examples of protein-enriched agricultural byproducts, making them ideal for developing antibacterial peptides.

Table 2.1 Recent antibacterial peptides derived from agricultural-based protein byproducts with enzymatic hydrolysis

Sample	Hydrolysate production	Peptide sequence	MIC /IC ₅₀	Reference
Castor beans	Hydrolysis by trypsin	EESETVGQR, GQSTGTGQQR, and LDALEPDNR	nd	Raharjo, Utami, Fajr, Swasono, & Haryadi, (2021)
Cottonseed	Hydrolysis by alcalase	KDFPGRR, LGLRSGIILCNV, and DENFRKF	nd	Song et al. (2020);
Cottonseed	Hydrolysis by alcalase	HHRRFSLY KFMPT RRLFSDY	IC ₅₀ = 0.264 mg.mL ⁻¹ IC ₅₀ = 1.203 mg.mL ⁻¹ IC ₅₀ = 0.582 mg.mL ⁻¹	Kong et al. (2020)
Jatropha curcas meal	Hydrolysis by protamex	CAILTHKR	MIC=29-68 µg.mL ⁻¹ (<i>Escherichia coli</i> , <i>Shigella. dysenteriae</i> , <i>Pseudomonas aeruginosa</i> , <i>Staphylococcus aureus</i> , <i>Bacillus. subtilis</i> , <i>Streptococcus pneumoniae</i>)	Xiao & Zhang, (2012)
Rice bran	Hydrolysis by bromelain	KVDHFPL	MIC=0.25 µg.mL ⁻¹ (planktonic cells <i>Listeria monocytogenes</i>)	Pu & Tang (2017)
Rice bran	Hydrolysis by pepsin	LRRHASEGGHGPHW EKLLGKQDKGVIIRA SSFSKGVQRAAF	IC ₅₀ = 289 µM (<i>Candida albicans</i>) IC ₅₀ =75.6 µM (<i>Porphyromonas gingivalis</i>) IC ₅₀ =78.5 µM (<i>Porphyromonas gingivalis</i>)	Taniguchi et al. (2017)

nd: not determined MIC/IC₅₀

The antimicrobial properties of peptides derived from corn gluten meal hydrolysis have not been specifically investigated. Previous studies on corn peptides

have primarily focused on the antioxidant activity of the peptides, with some mentioning potential antimicrobial activity but without detailed analysis. Therefore, further research is necessary to gain a comprehensive understanding of the antibacterial activity of corn peptides.

2.5 Separation and purification of AMPs

Mant et al. (2007) stated that high-performance liquid chromatography (HPLC) has proven extremely versatile over the past 25 years for isolating and purifying peptides of varying sources, quantity, and complexity. AMPs are defined by their net charge, hydrophobicity, amino acid composition, and length (Decker, Mechesso, & Wang, 2022). Therefore, it is important to fully understand the biochemical properties of AMPs so that efficient purification can be achieved. Several methods and advancements in the separation and purification of AMPs from protein hydrolysates, such as size-exclusion chromatography (SEC), cation-exchange HPLC, and reverse phase-HPLC, or a combination of RP-HPLC - cation-exchange HPLC (Adoui et al., 2013; Selsted, 1997).

2.5.1 Size-exclusion chromatography

Size-exclusion chromatography (SEC) is a separation method in which molecules are sieved on the basis of their size. Abdel-Hamid, Goda, De Gobba, Jenssen, & Osman (2016) used SEC with a Sepadhex G-25 ultrafine resin column for antibacterial peptide fractionation from camel whey papain hydrolysate.

2.5.2 Cation-exchange HPLC

Cation-exchange chromatography separates molecules based on their surface charge using a negatively charged ion exchange resin designed to attract positively charged molecules. Generally, AMPs are known to be cationic peptides therefore, cation exchange chromatography may be a more convenient separation method. Ahmed, Raharjo, Swasono, & Raharjo (2022) employed cation exchange chromatography for the purification of an antibacterial peptide from tryptic hydrolysate of snake venom with a linear elution pH buffer gradient (4-8).

2.5.3 Reverse phase-HPLC

The principle of separation in reversed-phase chromatography is based on the reversible adsorption or desorption of solute molecules with different degrees of hydrophobicity on a hydrophobic stationary phase. Peptides were separated

on a hydrophobic stationary phase and were eluted with an increasing gradient of organic solvent concentration (Henzel & Stults, 2001). The application of RP-HPLC is very extensive in the purification of AMPs. Krishnamoorthy, Adhikari, & Anaikutti (2023) examined the purification of peptide derivatives of cathelicidin LL-37 by RP-HPLC. They reported that RP-HPLC is a convenient technique to purify peptides with the same net charge but with different hydrophobicity caused by the hydrophobic environment of the column matrix.

2.6 AMPs mechanism of action

The classification of bacteria into Gram-positive and Gram-negative was determined by major cellular variations (Figure 2.4). Both groups of bacteria have an analogous inner membrane or cytoplasmic membrane, but the outer membranes of the cells are entirely different from each other. Gram-positive bacteria feature a peptidoglycan layer that is both cross-linked and enriched with negatively charged teichoic acid, resulting in a durable matrix that maintains the structural integrity of the bacterial cells neighbouring the cytoplasmic membrane. Gram-negative bacteria have a thinner, less cross-linked peptidoglycan layer but they have an outer membrane beyond the peptidoglycan layer. The inner membrane is composed of phospholipids. In contrast, the outer layer is predominantly a coating of lipopolysaccharide (LPS) molecules covered with many phosphate groups with negatively charged divalent cations (e.g., Ca^{2+} and Mg^{2+}), leading to an electrostatic network (Li et al., 2017).

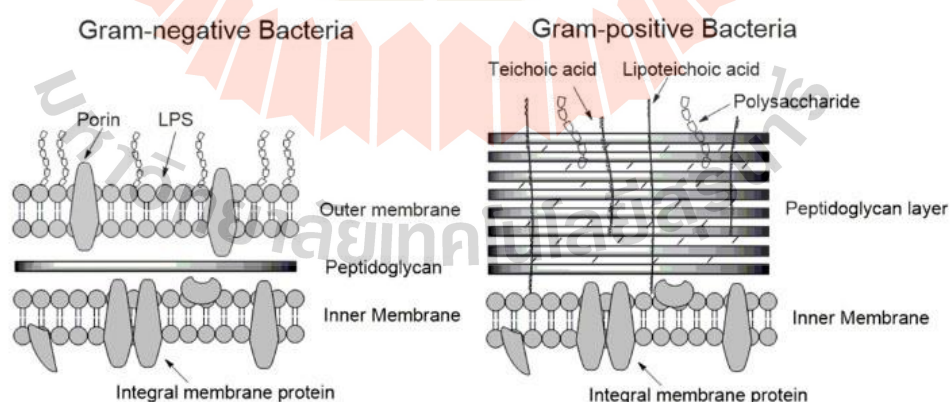


Figure 2.4 The structural features of the cell walls and membranes of Gram-positive and Gram-negative bacteria (Source: Li et al., 2017).

The lipid layer of bacterial membranes is one target of AMPs. AMPs may cause an increasing leakage rate of the internal aqueous content of liposomes. Furthermore, AMPs are predominantly cationic, and their specificity for bacterial membranes can be attributed to their interaction with anionic phospholipids (Epanand & Vogel, 1999)

There are two types of AMPs, namely membrane-active AMPs and intracellular-active AMPs. Membrane-active AMPs are reported to adhere to target organisms on the membrane lipids and create pores of trans-membrane. On the contrary, intracellular active AMPs interacts with intracellular targets, including DNA, RNA, and proteins, which leads to death of the cell (Xiao et al., 2015).

2.6.1 Membrane-active AMPs

The mechanisms by which AMPs disrupt the membrane of bacterial cells are complex and controversial. Electrostatic activity is how antimicrobial peptides interact with membranes. AMPs have a permeable effect on the membrane. Figure 2.5 displays the four most recognized models, which include the toroidal pore, barrel-stave, carpet, and aggregate model (Cruz, Ortiz, Guzmán, Fernández-Lafuente, & Torres, 2014).

2.6.1.1 Toroidal model

The toroidal model describes the bacterial membrane interaction with peptide as follows, once in contact with the lipid bilayer, peptides are vertically inserted into the cell membrane, where hydrophobic peptide residues interact with the hydrophobic membrane surface, generating a pore. The pores grow larger and larger as the peptides curve inward into the membrane, causing irrecoverable membrane disruptions (Sengupta, Leontiadou, Mark, & Marrink, 2008).

2.6.1.2 Aggregate channel model

In the aggregate channel model, peptides attach a lipid bilayer to the head of a phospholipid group and are randomly combined with lipids in the membrane. Peptides and lipids are aggregated like micelles and are without any specific inclination. These aggregates provide routes for ion release across the membrane and cover a wide range of membrane surfaces (Sato & Feix, 2006).

2.6.1.3 Barrel-stave model

In the barrel-stave model, when AMPs are bound to the outer membrane of bacteria, it emphasizes the surface electrostatic feature. Following the linking, α -helical or β -sheet amphipathic peptides align on the membrane's surface to

form a stave in a process known as a 'barrel-shaped cluster.' These AMPs are vertically integrated into the toroidal membrane model. The progressive reconstruction of peptide monomers enhances channels or pores, gradually liberating cellular material from bacteria (Wimley, 2010).

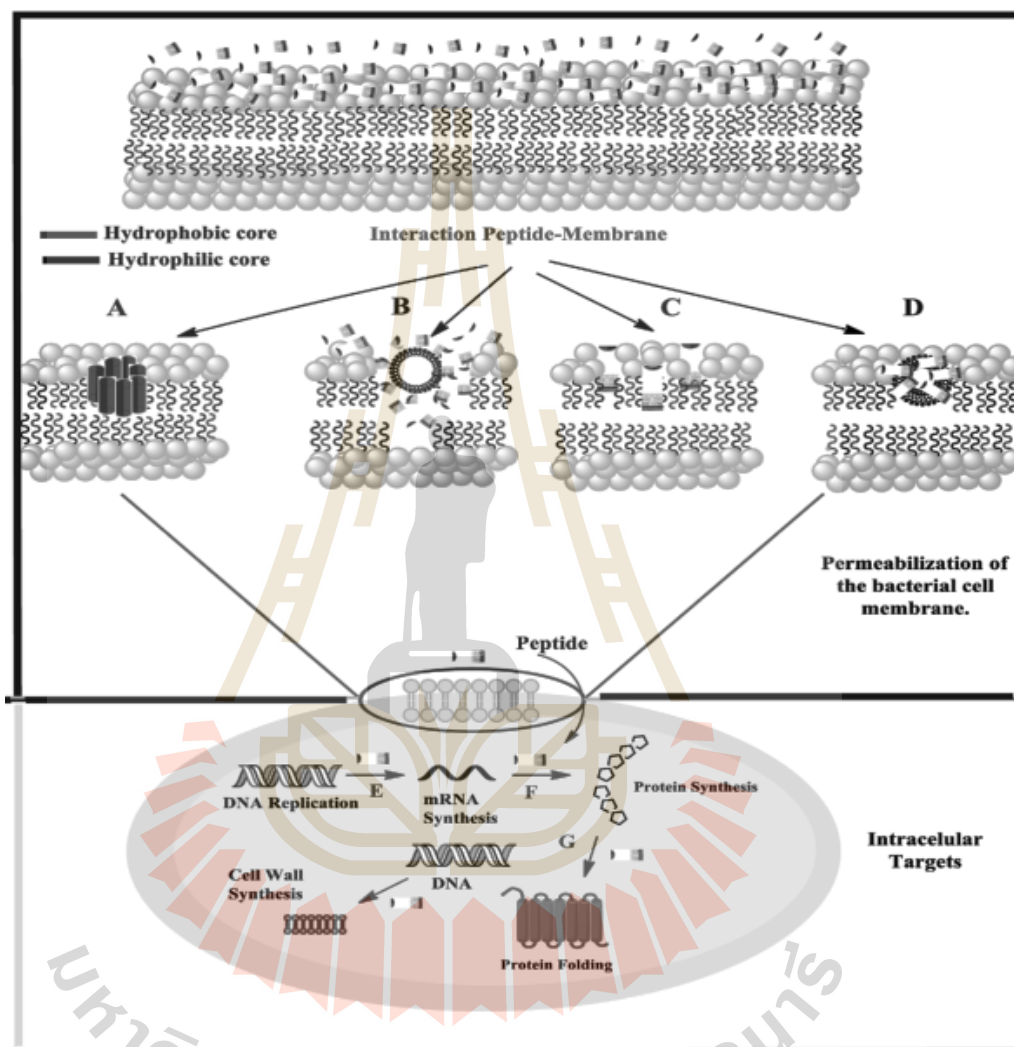


Figure 2.5 Four mechanisms of action for AMPs (A) toroidal model (B) carpet model (C) barrel-stave model (D) aggregate channel model (E) DNA synthesis inhibited due to AMPs (F) Protein synthesis inhibited due to AMPs and (G) Chaperones assisted protein folding in interaction with AMPs (Source: Cruz et al., 2014).

2.6.1.4 Carpet model

In the carpet model, the peptide electrostatically binds to the cell membrane and orients itself in a parallel to the membrane surface, surrounding it like a carpet. Peptide micelles compounded by membrane components serve as a detergent, disrupting lipid bilayer formation. Consequently, rapid bacterial lysis is caused by the creation of wormholes around the membrane. Regardless of the action process, AMPs destroy bacteria directly by breaching the bacterial membrane or individually or synergistically disrupting intracellular targets with the membrane disruption (Mudhakar & Harashima, 2009).

Once inside the cell, AMPs exhibit various properties, including inhibiting DNA, mRNA, and protein synthesis, cell wall synthesis, immobilizing and inactivating immune cells, and inactivating enzymes (Cruz et al., 2014; Xiao et al., 2015).

2.6.2 Intracellular-active AMPs

Many AMPs lack the capacity to enter bacterial cell membranes, and this mode of action is referred to as a non-membrane permeabilizing process. Numerous AMPs attach to intracellular targets such as cell walls and nucleic acids, causing protein modification pathways to become disrupted. AMPs interact with the peptidoglycan substrate or lipopolysaccharides, resulting in the creation of pores. Some bacteriocins may interact with lipid II (a precursor for bacterial cell wall biosynthesis), inhibiting cell wall formation, causing transmembrane processes, and affecting the efflux pump, leading to a leakage of ions (Figure 2.6). Several researchers studied how a few AMPs penetrate the cell without disrupting the cell membrane or cell wall and target nucleic acids such as DNA and RNA. Specific AMPs block DNA synthesis and do not activate the membrane's septum. It also influences enzyme activity during replication and protein synthesis. The translation and transcription mechanism is often interrupted by AMPs. The protein modification mechanism is also influenced by AMPs (Rai, Pandit, Gaikwad, & Kövics, 2016).

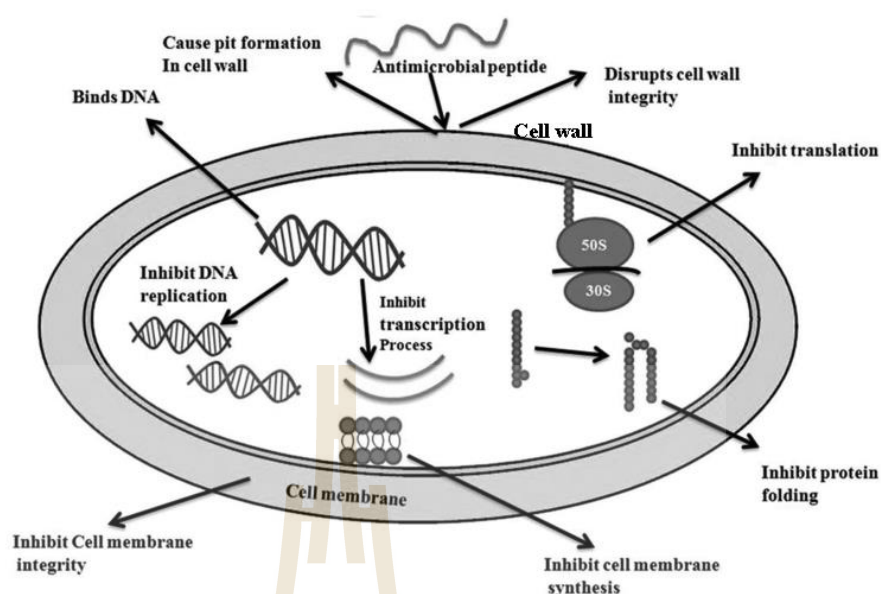


Figure 2.6 Mechanism of action of AMP with non-membrane permeabilizing
(Source: Rai et al., 2016)

2.7 Detection of cell damage by AMPs

2.7.1 Membrane permeability

The consequence of AMPs on bacterial membrane integrity can be quantified using a microtiter plate with added membrane dyes and fluorescence observed in a spectrophotometer. For example, the action of AMPs might lead to the permeabilization of the outer membrane of Gram-negative bacteria by adding N-phenyl-1-naphthylamine, NPN. If AMPs disrupt the outer membrane, NPN will penetrate inside the membrane, showing increased fluorescence intensity. An effect that the addition of AMPs to bacterial suspension with NPN can be viewed in a 96-well microplate through a fluorescence spectrophotometer. Holdbrook et al. (2018) showed that in bacterial cells with NPN the membrane permeabilization rose in a continuous manner as the concentration of AMPs increased.

AMPs can be assayed for their membrane disruption using Sytox Green, a nucleic-acid-staining dye that only penetrates disrupted membranes. Ouardien et al. (2018) found that AMPs induced cell membrane permeabilization as indicated by Sytox Green penetration into the cell. PI constitutes another fluorescent dye which could be applied to demonstrate the membrane permeabilization on the bacterial cell caused by AMPs. PI, however, cannot pass through the intact cell membrane. When the

integrity of the cell membrane is compromised, the dye enters the cell and intercalates into nucleic acids. Pandit et al. (2020) demonstrated membrane permeabilization of *Pseudomonas aeruginosa* and *Candida albicans* by AMP22 and AMP24 peptides, as indicated by increased fluorescence intensity of PI as peptide concentration increased.

The use of PI to determine pore formation on bacterial cell membranes can also be combined with SYTO-9. Live and dead Gram-positive and Gram-negative bacterial cells can be stained with SYTO-9 stain. Both stain PI and SYTO-9 bind to DNA. However, only SYTO-9 will penetrate the healthy membranes, leading to green fluorescent cells. If AMPs cause the membrane to be perforated and the pores formed are large enough, PI can enter, resulting in red-fluorescent cells (Schäfer & Wenzel, 2020).

2.7.2 Cytoplasmic membrane depolarization

The bacterial cell membrane and wall have a negative charge due to phospholipids, lipopolysaccharides, and teichoic acids in the cell wall and outer membrane. Therefore, some cationic AMPs can kill bacteria by depolarizing the bacterial membrane. The effect of AMPs in depolarizing the bacterial cell membrane can be analyzed with diSC₃₋₅ (3,3'-Dipropylthiadicarbocyanine iodide), a cationic, membrane-permeable fluorescent dye. This specific dye functions as a potentiometric sensor and gathers within polarized cells. Rajasekaran, Kim, & Shin (2017) reported that the increase of fluorescence diSC₃₋₅ in the medium was caused by the peptide activity that created pores or disruption on the *S. aureus* cell membrane.

2.7.3 Intracellular component leakage

Further evidence is provided by detecting which compounds leak out of the bacterial cell due to membrane leakage caused by AMPs, such as reducing sugar, ions, ATP, or DNA/RNA (Raheem & Straus, 2019). Examples of this type of test are that bacterial cells leak out reducing sugar, which was tested using a DNS colorimetric reaction (Zhang, Zhang, & Xu, 2020). The leak of calcium ions from bacteria cells was assessed using atomic absorption spectrometry (Zhang et al., 2021). Intracellular ATP leak out of the bacterial cells can be determined by means of the ATP detection kit (Wan et al., 2023). DNA/RNA leakage from bacterial cells can be evaluated using a spectrophotometer at 260 nm (Shwaiki, Arendt, & Lynch, 2020).

2.7.4 Microscopy

2.7.4.1 Confocal laser scanning microscopy (CLSM)

Confocal Laser Scanning Microscopy (CLSM) is a form of fluorescence microscopy. Fluorescence microscopy uses laser light to cause samples with special dye to fluoresce, creating a 2D micrograph. The procedure is essentially based on a focused laser beam scanning of an object point by point, therefore allowing the 3D reconstruction of the 2D micrograph (Elliott, 2020). Ciociola et al. (2018) also reported that CLSM can be used to observe the internalization of mammalian proline-rich peptide labeled with 5-carboxyfluorescein inside cells of *E. coli* and *P. aeruginosa*. Wang, Xu, & Hu (2022) used CLSM to prove the permeability of antimicrobial peptide HJH-3 through bacterial cell membrane binding to bacterial DNA using propidium iodide and Hoechst 33528 stain.

2.7.4.2 Scanning electron microscopy (SEM)

Scanning electron microscopy (SEM) has become one of the most important tools developed for the characterization of microstructure, morphology, and even chemical composition (Akhtar, Khan, Khan, & Asiri, 2018). SEM basically consists of an electron source, an electromagnetic lens utilized to focus electrons, an electron detector, a sample chamber, a computer, and a screen for visualizing images. In scanning electron microscopy, the mentioned sequence is followed: an electron source, an electromagnetic lens for electron focusing, electron detector, sample chamber, computer, and visualization screen (Singh, 2016). The most important steps in the preparation of bacterial cells are fixation, dehydration, and drying. Besides, coating of specimens with a conducting film by sputtering is usually carried out in order to ensure the conductivity of the surface being investigated, hence to avoid image distortion due to electron charging effects (Czerwińska-Gtówka & Krukiewicz, 2021).

Many researchers have used SEM to investigate the mechanism of action of antimicrobial peptides. According to Zhou et al. (2022), the new peptide LL-1 exerts its bactericidal effects through changing the surface morphology of *E. coli*, which was characterized by the presence of roughness, blurred outlines, and reduced cell adhesion as observed via SEM. Kim, Jeong, Cho, Lee, & Kim (2018) said that SEM could visualize the effect of LPcin-YK3 peptide, a shorter analog peptide from bovine lactophorin, on *S. aureus* morphology, resulting in an enlarged, deformed, and roughened surface. According to Rani, Arora, Majhi, Mishra, & Mallajosyula (2022),

through SEM observation, human defensin analogs can cause morphological abnormalities on the surface of *E. coli* cells, leading to cell lysis.

2.7.4.3 Transmission electron microscopy (TEM)

Transmission electron microscopy (TEM) is a powerful tool to analyze bacterial cells with respect to their morphology and ultrastructure. TEM involves the transmission of an electron beam through an ultra-thin specimen, which interacts with electrons as they pass through. Images from TEM are produced by the interaction of electrons transmitted through the specimen (Mishra & Chauhan, 2016). In TEM, the sample must be prepared on a TEM grid and positioned at the center of the microscope's specialized chamber. It is used in the study of both internal structure and external surface (Tizro, Choi, & Khanlou, 2019). TEM has been one of the various methods employed by a large number of researchers in the study of mode of action for AMPs. Hartmann et al. (2010) reported that the TEM images of the treated cells of *E. coli* and *S. aureus* with supra-MICs of both cationic peptides, gramicidin S and peptidyl-glycylleucine-carboxamide, disrupt the polar regions and leakage into the periplasmic space takes place. Zhou et al. (2022) found that LL-1 caused significant deformation, cell swelling, reduction in intracellular electron density, lysis of the cytoplasm, and cell membrane damage in *E. coli*, as observed by TEM.

2.7.4.4 Atomic force microscopy

Atomic force microscopy (AFM) operates on the principle of scanning a surface with a nanometer-sharp tip mounted on a flexible cantilever, using the distance-dependent tip-sample interaction forces to detect the proximity of the surface and build an image as the tip follows the surface contours (Hammond, Ryadnov, & Hoogenboom, 2021). Swana, Nagarajan, & Camesano (2021) visually analyzed pore formation on a supported phosphatidylcholine lipid bilayer induced with alamethicin using atomic force microscopy (AFM).

2.7.5 Synchrotron radiation Fourier transmission infrared

Spectroscopy-based methods for microbial identification and detection deliver high benefits due to their high level of sensitivity, fast response, cost-effectiveness, and convenience of use (Huleihel, Pavlov, & Erukhimovitch, 2009). Fourier transform infrared (FTIR) spectroscopy is a useful analytical tool to characterize the biochemical composition of microorganisms and to study the molecular basis of their adaptation responses to stress conditions (Alvarez-Ordóñez, Mouwen, López, & Prieto,

2011). The 4000-400 cm^{-1} region, which corresponds to the mid-infrared region of the electromagnetic spectrum, is commonly used in FTIR spectra for bacterial detection (Novais, Freitas, Rodrigues, & Peixe, 2019). Synchrotron radiation Fourier transform infrared (SR-FTIR) combines unprecedented brightness, power, focus ability, polarization, and synchronization tunability with the established analytical approach of conventional FTIR (Stem, 2008).

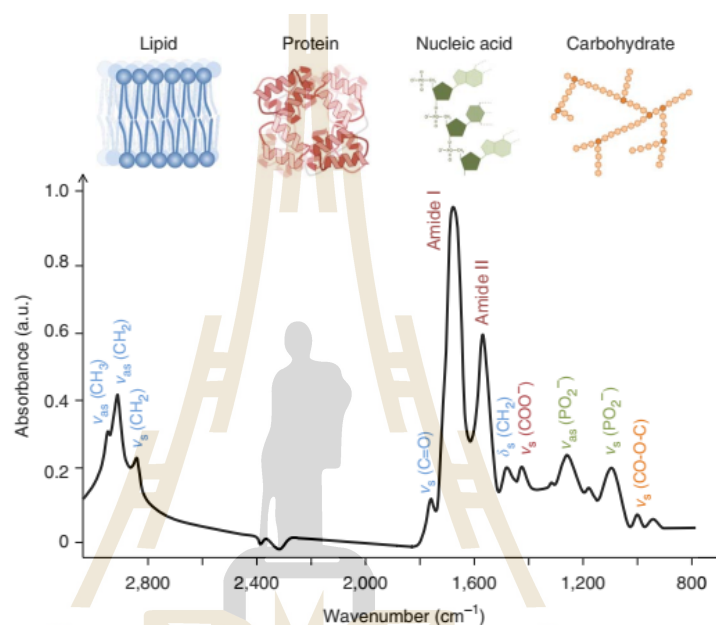


Figure 2.7 The major biochemical bands components of cells and tissues are displayed as lipids, proteins, nucleic acid (phospholipids), and carbohydrates in the spectral ranges from 3000-2800 cm^{-1} and 1800-800 cm^{-1} (Source: Baker et al., 2014)

Furthermore, Alvarez-Ordóñez et al. (2011) classified the mid-IR spectrum (4000-400 cm^{-1}) into five spectral areas that are commonly used, namely: 1) 3000-2800 cm^{-1} are for a functional group of membrane fatty acids and by some amino acid side-chain vibrations dominated by the C-H stretching vibrations of $-\text{CH}_3$ and $>\text{CH}_2$ functional group; 2) 1800-1500 cm^{-1} for amide I and amide II groups belong to proteins and peptides; 3) 1500-1200 cm^{-1} for proteins, fatty acids, and phosphate-carrying compounds due to the $>\text{CH}_2$ and $-\text{CH}_3$ bending modes; 4) 1200-900 cm^{-1} for the symmetric stretching vibration of PO_2^- groups in nucleic acids and to C-O-C and C-O-P stretching correspond to carbohydrates and polysaccharides in the cell wall and also

the influence of nucleic acids; 5) 900-700 cm^{-1} for the true fingerprint region and holds specific, weak spectral from aromatic ring vibrations of aromatic amino acids (Tyr, Trp, Phe) and nucleotides. Figure 2.7 shows a typical biological IR spectrum based on molecular assignments.

Zoumpopoulou, Papadimitriou, Polissiou, Tarantilis, & Tsakalidou (2010) reported the ability of FTIR spectroscopy to detect changes in the fatty acids of the cell membrane and the polysaccharides of the cell wall of *S. Typhimurium* in response to lactobacilli-derived antibacterial compounds. Sun et al. (2023) also reported FTIR spectroscopy can trace modification on fingerprint, polysaccharide, protein, amide, and fatty acid of *S. aureus* caused by antibacterial peptide of *Moringa oleifera* seeds.

2.8 AMPs design

The development of novel AMPs requires consideration of five essential factors: chain length, secondary structure, net charge, hydrophobicity, and amphiphilicity (Huan et al., 2020). According to Torres, Sothiselvam, Lu, & de la Fuente-Nunez (2019), five basic methods can be utilized in designing AMPs: site-directed mutagenesis, computational (*de novo*) design approaches, synthetic libraries, template-assisted methodologies, and mechanism-based strategies.

2.8.1 Site-directed mutagenesis

In this method, natural AMPs are redesigned by adding, deleting, or substituting one or more peptide residues. Huan, Kong, Mou, & Yi (2015) demonstrated that replacing neutral/acidic amino acid residues with Arg or Lys in native porcine β -defensin (pBD2) may enhance antimicrobial activity.

2.8.2 *De novo* design

In this method, the amphipathic structure of AMPs is prioritized, which is correlated with the physicochemical properties of the antimicrobial activity. Vishnepolsky et al. (2019) developed a tool to design a novel short peptide (13aa) with antibacterial activity and a high therapeutic index against Gram-negative bacteria.

2.8.3 Synthetic libraries

This method is based on recognizing the characteristics of peptides in the AMPs library, which is then used to design peptides with broad-spectrum antibacterial activity. Ross et al. (2020) redesigned the peptide enterocin AS-48 based on a scaffold-minimal peptide library and obtained several peptide homologs with high antimicrobial activity and no toxicity to eukaryotic cells.

2.8.4 Template-assisted methodologies

This method is performed by comparing and extracting important peptide patterns from native peptides based on their residues, such as charge, hydrophobicity, etc. Pane et al. (2018) used a computational platform to design novel peptides derived from the N and C terminals of pepsin A, which showed broad antimicrobial activity against foodborne pathogens and showed no toxicity.

2.8.5 Mechanism-based strategies

This method uses a molecular dynamic simulation approach to obtain atomic-level information by measuring the interfacing between the designed AMPs and the target bacterial membrane. Mirnejad, Fasihi-Ramandi, Behmard, Najafi, & Moghaddam (2023) studied the interaction of a novel short AMPs cecropin-melittin (CM11) with Gram-positive and Gram-negative membrane models using a series of molecular dynamics simulations. They discovered that the novel peptide interacted more strongly with Gram-positive than Gram-negative membranes.

2.9 Application of AMPs derived from protein hydrolysates in food product

AMPs are a type of short peptide found throughout species that play a vital role in the immunological systems of various organisms (Huan, Kong, Mou, & Yi, 2020). In food preservation, AMPs are practical and viable alternatives to chemical preservatives. One fact is that nisin, a 34-amino-acid antimicrobial peptide generated by *Lactococcus lactis*, has been established to be generally recognized as safe (GRAS), effective, and consistent food preserving and has been applied for multiple decades in more than 50 countries (Gharsallaoui, Oulahal, Joly, & Degraeve, 2016). Enzymatic hydrolysis of food proteins could be used to synthesize antimicrobial peptides *in vitro*. Peptide antimicrobial activity, and hence the protein hydrolysates they contain, highly depends on amino acid profile, conformation, peptide size, and sequencing (Pane et al., 2017).

Several recent studies on the characterization and application of AMPs from protein hydrolysates for alternative food preservation applications have been carried out by several researchers. Protein hydrolysates made from *Anguilla* byproducts using Savinase® (PHAB-s) have a higher protein content than those made using Protamex® (PHAB-p). It was found to have the most potent inhibition against seven different bacteria. Both peptide administrations as preservatives on minced meat for 11 days in cold storage decreased microbiological development. At the same concentration, their

readings were much more significant than BHT. The PHAB-s significantly inhibited microbial growth in the meat while stored at 4 °C, specifically at a concentration of 1% (w/w) (Bougatef et al., 2020).

Elbarbary, Ejima, & Sato (2019) reported the digestion of cheese whey using porcine pepsin, calf, and fungal rennets. The *E. coli* number in milk stored at 4 °C reduced mildly (0.6 log) after 168 h in control samples (without hydrolysate). Pepsin or calf rennet hydrolysate at a concentration of 3,000 $\mu\text{g}\cdot\text{mL}^{-1}$ has no inhibitory effect on *E. coli* growth. However, following 168 h of refrigeration, hydrolysates at 5,000 and 6,000 $\mu\text{g}\cdot\text{mL}^{-1}$ could diminish the bacterial number by around 2 log. Upon 24 h of incubation at room temperature, depending on the quantity of pepsin or calf rennet hydrolysate, the number of bacteria in all samples multiplied by almost a hundredfold. However, at a concentration of 6,000 $\mu\text{g}\cdot\text{mL}^{-1}$, the bacterial population in both hydrolysates was tenfold lower than in control samples.

Przybylski, Firdaous, Châtaigné, Dhulster, & Nedjar (2016) explained the major component of bovine hemoglobin (BH) or bovine cruor, a slaughterhouse byproduct, is hemoglobin, a significant antimicrobial peptide source. Pepsin from porcine gastric mucosa (0.1 M; pH 3.5) was used to digest the BH at 23 °C. At pH 7.0, the pepsin digestion produced α -137–141 hemoglobin fragment (Thr-Ser-Lys-Tyr-Arg), a short (653 Da) hydrophilic peptide with two positive charges. The α -137–141 had remarkable antimicrobial effects on beef kept at 4 °C, primarily used at a concentration of 0.5% (w/w). The most significant impact was on coliform proliferation. Furthermore, the effect of this peptide was equivalent to that of BHT. This research demonstrated that α -137–141 has the capability to be used as a meat preservative.

2.10 Modification of AMPs

The modifications to the AMPs sequence can enhance antimicrobial activity either by introducing a specific amino acid or by altering the sequence to increase the ability of the AMPs to interact and cause disruption of the bacterial cell membrane (Zhang et al., 2022). This technique can be accomplished by incorporating hydrophobic and basic amino acids, which are generally known to have improved antimicrobial activity (Matthyssen et al., 2022). In addition, Zhang et al. (2021) described the introduction of D-amino acids can increase the stability of the peptide against proteolytic enzymes without affecting its antimicrobial activity. Furthermore, the design of ultrashort cationic lipopeptides rich in arginine (Arg), cyclic peptides, and self-

assembling peptides can also improve the activity of antimicrobial peptides (Zhang et al., 2022).

Generally, AMPs are composed of hydrophobic amino acids, cationic (positively charged) and amphiphilic (both hydrophilic and hydrophobic) properties. These properties influence the presence of hydrophobic groups and the distribution of hydrophobic and hydrophilic regions within AMPs (Lei et al., 2019). Studies demonstrated hydrophobicity is essential for AMPs to interact with bacterial membranes and exhibit antimicrobial activity. However, increased hydrophobicity by AMPs modification can lead to potentially higher hemolytic activity (Lyu, Yang, Lei, & Zhao, 2023). Conversely, the association of hydrophobicity and hemolysis is not always straightforward, as research done by Edwards et al. (2016) showed that AMPs with higher hydrophobicity do not always exhibit hemolysis. Therefore, understanding and predicting the hemolytic activity in AMPs is crucial to ensure their safety and efficacy as potential antimicrobial agents.

2.11 Endogenous plant AMPs

Plants naturally produce antimicrobial peptide or endogenous AMPs that is used as an innate immune system that functions to defend themselves from various pathogens such as bacteria, fungi, and viruses (Campos, De Souza, De Oliveira, Dias, & Franco, 2018). In addition, AMPs in plants are also used for the growth and development factors of the plant itself (Berrocal-Lobo et al., 2002). The endogenous AMPs of plant can be classified as follows:

2.11.1 Thionins

Thionins are belong to plant AMPs that consist of 45-50 amino acids. They rich of cysteine residues, that contributing on the structure stability and function. In addition, they can be divided into α/β -thionins and γ -thionins. They play important role in the plant defense system against pathogens. They exhibit antimicrobial activity against bacteria, fungi, and protozoa (Dang & Van Damme, 2015; Taveira et al., 2016).

2.11.2 Plant defensins

Plant defensins consist of 45-54 amino acids and feature a unique folding pattern stabilized by disulfide bonds fored between cysteine residues. This structure help to keep the functionality under different environment conditions. The plant defensins are classified into class I defensins and class II defensins. For class I

defensins are primarily involved in antimicrobial activity against pathogen like fungi. Meanwhile, class II defensins besides antimicrobial activity, may play roles as growth and development factors in pathogen defense (Sher Khan et al., 2019; Stotz, Thomson, & Wang, 2009).

2.11.3 Hevein-like peptides

Hevein-like peptides are a group of cysteine-rich, chitin-binding peptides found in plants. It was characterized by the ability on fungal growth inhibition. They were classified based on the number of cysteine residues into 6C-, 8C-, and 10C-hevein-like peptides (Wong et al., 2017).

2.11.4 Knottin-type peptides

Knottin-type peptides, also known as inhibitor cysteine knot (ICK) peptides, found in various plants. They contain 30-50 amino acids. Due to biological multifunction such as protease inhibitors, antimicrobial activity, and ion channel modulation, it can be found as traditional and herbal supplements in global cuisines (Attah et al., 2022).

2.11.5 α -Hairpinin family

The α -hairpinin family is a small group of short, cysteine-rich peptides primarily found in plants. Many α -hairpinins exhibit significant antifungal and antibacterial activities, make them important components of plant innate immunity. Due to their stability and diverse biological activities, α -hairpinins have potential applications in biotechnology and medicine for developing new antimicrobial agents and therapeutic peptides (Slavokhotova & Rogozhin, 2020).

2.11.6 Lipid transfer proteins

Lipid transfer proteins are a group of small cationic peptides with Cys-Cys bonds pattern, highly-conserved proteins found in plants that facilitate the lipids movements between cell membranes. In addition, many LTPs exhibit antimicrobial properties, being pathogenesis-related proteins for pathogen defense. It consists of about 7-9 kDa and divided into LTP1s (9 kDa) and LTP2s (7 kDa) (Cândido et al., 2014).

2.11.7 Snakins

Snakins have smaller sizes, about 7 kDa, and positively charged Cys-rich peptides. It has some motifs similar to hemotoxic and disintegrin-like snake venom. Snakins have a play role in controlling fungal and bacteria (Iqbal & Khan, 2023).

2.11.8 Cyclotide family

Cyclotide typically consists of 28-37 amino acids and is distinguished by a head-to-tail cyclized backbone and knotted arrangement of three disulfide bonds forming cyclic cystine knot motif. Their primary biological functions as plant defense mechanisms against pests and pathogens. Cyclotides are being explored for drug design and therapeutic applications (Gould & Camarero, 2017; Pelegriani, Quirino, & Franco, 2007).

2.12 AMPs from corn gluten meal

Corn gluten meal (CGM) is a wet milling byproduct of corn starch with a protein content of 600-710 g.kg⁻¹. Zein and glutelin are the CGM main protein fractions, accounting for 680 and 280 g.kg⁻¹ of total protein weight, respectively (Zhou et al., 2013). CGM is rarely found in human food and is often sold as a feedstock or discarded (Li, Han, & Chen, 2008). Because of their compositions and shapes, CGM proteins with a high number cannot be consumed. This matter represented a significant lack of protein supplies that could have been used to address the global protein scarcity exacerbated by rising population growth and improved economies (He et al., 2018).

Bioactive peptides generated from CGM hydrolysate have been well documented in recent years for their antioxidant, ACE inhibitory, ROS scavenging, anti-proliferative, antihypertensive, and anti-inflammatory characteristics (Liang, Chalamaiah, Ren, Ma, & Wu, 2018; Liu, Fang, Feng, Li, & Gu, 2020; Liu et al., 2020; Wang et al., 2016). However, several studies have described these antimicrobial peptide properties, which are remarkable in preventing foodborne disease and spoilage. Application of chemical hydrolysis and gene protein expression from maize proteins has been reported to produce antifungal and antibacterial peptides (Al Kashgry et al., 2020; Duvick, Rood, Rao, & Marshak, 1992; Hassan, Outb, & Dong, 2021; Kant, Liu, & Pauls, 2009). Duvick et al. (1992) reported that the chemical hydrolysis-isolated peptide MBP-1 from maize had shown antimicrobial activity as it inhibited the germination of fungi and the growth of bacteria. On the contrary, Al Kashgry et al. (2020) expressed that AMPs expressed through heterologous expression of maize defensin gene MzDef in *E. coli* demonstrate potential antifungal and antibacterial activities. According to Kant et al. (2009) reported the gene encoding the plant defensin corn 1 (Pdc1) has already been transformed into several expression systems, including into the eukaryote (*P. pastoris*) and the prokaryote (*E. coli*). The results revealed that *F. graminearum* is sensitive to the maize defensin

PDC1 peptide. Hassan et al. (2021) reported the discovery of a novel cationic AMPs, termed ZM-804 peptide, originating from *Z. mays* L. The inbred line B73 cDNA library was suggested as a valuable source of innovative cationic AMPs with noteworthy predictive values. The most remarkable thing was that the ZM-804 peptide showed potent antibacterial activity, which also provided a new hope for alternative tools to treat plant diseases. However, up to now, peptides derived from the CGM hydrolysate have not been reported showing antimicrobial properties. Thus, CGM hydrolysate is also a potential source of AMPs.

2.13 References

- Abdel-Hamid, M., Goda, H. A., De Gobba, C., Jenssen, H., & Osman, A. (2016). Antibacterial activity of papain hydrolysed camel whey and its fractions. *International Dairy Journal*, *61*, 91–98.
- Adoui, F., Boughera, F., Chataigne, G., Chihib, N., Hameur, H. El, Dhulster, P., & Zidoune, M. N. (2013). A simple method to separate the antimicrobial peptides from complex peptic casein hydrolysate and identification of a novel antibacterial domains within the sequence of bovine α s-casein. *International Review of Chemical Engineering*, *5*(2), 179–187.
- Ahmed, N., Raharjo, S., Swasono, R. T., & Raharjo, T. J. (2022). The antibacterial peptides (AMPs) originated from tryptic hydrolysis of *Naja sumatrana* venom fractionated using cation exchange chromatography. *Rasayan Journal of Chemistry*, *15*(4), 2642–2653.
- Akhtar, K., Khan, S. A., Khan, S. B., & Asiri, A. M. (2018). Scanning electron microscopy: Principle and applications in nanomaterials characterization. In Sharma, S. K. (Ed.). *Handbook of Materials Characterization* (pp. 113–145). New York: Springer International Publishing.
- Al Kashgry, N. A. T., Abulreesh, H. H., El-Sheikh, I. A., Almaroai, Y. A., Salem, R., Mohamed, I., ... Mohamed, M. S. M. (2020). Utilization of a recombinant defensin from maize (*Zea mays* L.) as a potential antimicrobial peptide. *AMB Express*, *10*(1), 208.
- Alvarez-Ordóñez, A., Mouwen, D. J. M., López, M., & Prieto, M. (2011). Fourier transform infrared spectroscopy as a tool to characterize molecular composition and stress response in foodborne pathogenic bacteria. *Journal of Microbiological Methods*, *84*(3), 369–378.
- Andersson, D. I., Hughes, D., & Kubicek-Sutherland, J. Z. (2016). Mechanisms and consequences of bacterial resistance to antimicrobial peptides. *Drug Resistance Updates*, *26*, 43–57.

- Attah, F. A., Lawal, B. A., Yusuf, A. B., Adedeji, O. J., Folahan, J. T., Akhigbe, K. O., ... Chamcheu, J. C. (2022). Nutritional and pharmaceutical applications of under-explored knottin peptide-rich phytomedicines. *Plants*, *11*(23), 3271.
- Baker, M. J., Trevisan, J., Bassan, P., Bhargava, R., Butler, H. J., Dorling, K. M., ... Martin, F. L. (2014). Using Fourier transform IR spectroscopy to analyze biological materials. *Nature Protocols*, *9*(8), 1771–1791.
- Berrocal-Lobo, M., Segura, A., Moreno, M., López, G., García-Olmedo, F., & Molina, A. (2002). Snakin-2, an antimicrobial peptide from potato whose gene is locally induced by wounding and responds to pathogen infection. *Plant Physiology*, *128*(3), 951–961.
- Bintsis, T. (2017). Foodborne pathogens. *AIMS Microbiology*, *3*(3), 529–563.
- Bougatef, H., Krichen, F., Kobbi, S., Martinez-Alvarez, O., Nedjar, N., Bougatef, A., & Sila, A. (2020). Physicochemical and biological properties of eel by-products protein hydrolysates: Potential application to meat product preservation. *Waste and Biomass Valorization*, *11*(3), 931–942.
- Campos, M. L., De Souza, C. M., De Oliveira, K. B. S., Dias, S. C., & Franco, O. L. (2018). The role of antimicrobial peptides in plant immunity. *Journal of Experimental Botany*, *69*(21), 4997–5011.
- Cappitelli, F., Polo, A., & Villa, F. (2014). Biofilm formation in food processing environments is still poorly understood and controlled. *Food Engineering Reviews*, *6*(1–2), 29–42.
- Carrasco-Castilla, J., Hernández-Álvarez, A. J., Jiménez-Martínez, C., Gutiérrez-López, G. F., & Dávila-Ortiz, G. (2012). Use of proteomics and peptidomics methods in food bioactive peptide science and engineering. *Food Engineering Reviews*, *4*(4), 224–243.
- Chakchouk-Mtibaa, A., Elleuch, L., Smaoui, S., Najah, S., Sellem, I., Mejdoub, H., ... Mellouli, L. (2014). Characterization of the bacteriocin BacJ1 and its effectiveness for the inactivation of *Salmonella typhimurium* during turkey escalope storage. *Food Chemistry*, *152*, 566–572.
- Ciociola, T., Giovati, L., Giovannelli, A., Conti, S., Castagnola, M., & Vitali, A. (2018). The activity of a mammalian proline-rich peptide against Gram-negative bacteria, including drug-resistant strains, relies on a nonmembranolytic mode of action. *Infection and Drug Resistance*, *11*, 969–979.
- Cruz, J., Ortiz, C., Guzmán, F., Fernández-Lafuente, R., & Torres, R. (2014). Antimicrobial peptides: Promising compounds against pathogenic microorganisms. *Current Medicinal Chemistry*, *21*(20), 2299–2321.
- Czerwińska-Główka, D., & Krukiewicz, K. (2021). Guidelines for a morphometric analysis

- of prokaryotic and eukaryotic cells by scanning electron microscopy. *Cells*, *10*(12), 3304.
- Daliri, E. B. M., Oh, D. H., & Lee, B. H. (2017). Bioactive peptides. *Foods*, *6*(5), 1–21.
- Dang, L., & Van Damme, E. J. M. (2015). Toxic proteins in plants. *Phytochemistry*, *117*(1), 51–64.
- De Souza Cândido, E., E Silva Cardoso, M. H., Sousa, D. A., Viana, J. C., De Oliveira-Júnior, N. G., Miranda, V., & Franco, O. L. (2014). The use of versatile plant antimicrobial peptides in agribusiness and human health. *Peptides*, *55*, 65–78.
- Decker, A. P., Mechesso, A. F., & Wang, G. (2022). Expanding the landscape of amino acid-rich antimicrobial peptides: Definition, deployment in nature, implications for peptide design and therapeutic potential. *International Journal of Molecular Sciences*, *23*(21), 12874.
- Duvick, J. P., Rood, T., Rao, A. G., & Marshak, D. R. (1992). Purification and characterization of a novel antimicrobial peptide from maize (*Zea mays* L.) kernels. *Journal of Biological Chemistry*, *267*(26), 18814–18820.
- Edwards, I. A., Elliott, A. G., Kavanagh, A. M., Zuegg, J., Blaskovich, M. A. T., & Cooper, M. A. (2016). Contribution of amphipathicity and hydrophobicity to the antimicrobial activity and cytotoxicity of β -hairpin peptides. *ACS Infectious Diseases*, *2*(6), 442–450.
- Elbarbary, H. A., Ejima, A., & Sato, K. (2019). Generation of antibacterial peptides from crude cheese whey using pepsin and rennet enzymes at various pH conditions. *Journal of the Science of Food and Agriculture*, *99*(2), 555–563.
- Elisseeva, S., Kelly, C., Cruz-Romero, M., Zhdanov, A. V., Kerry, J. P., & Papkovsky, D. B. (2020). The use of optical oxygen sensing and respirometry to quantify the effects of antimicrobials on common food spoilage bacteria and food samples. *Sensors and Actuators, B: Chemical*, *322*, 128572.
- Elliott, A. D. (2020). Confocal microscopy: Principles and modern practices. *Current Protocols in Cytometry*, *92*(1), 139–148.
- Epand, R. M., & Vogel, H. J. (1999). Diversity of antimicrobial peptides and their mechanisms of action. *Biochimica et Biophysica Acta - Biomembranes*, *1462*(1–2), 11–28.
- Esmailpour, M., Ehsani, M. R., Aminlari, M., Shekarforoush, S., & Hoseini, E. (2016). Antimicrobial activity of peptides derived from enzymatic hydrolysis of goat milk caseins. *Comparative Clinical Pathology*, *25*(3), 599–605.
- Gharsallaoui, A., Oulahal, N., Joly, C., & Degraeve, P. (2016). Nisin as a food preservative: Part 1: Physicochemical properties, antimicrobial activity, and main uses. *Critical Reviews in Food Science and Nutrition*, *56*(8), 1262–1274.

- Gould, A., & Camarero, J. A. (2017). Cyclotides: Overview and biotechnological applications. *Chembiochem*, 18(14), 1350–1363.
- Gram, L., Ravn, L., Rasch, M., Bruhn, J. B., Christensen, A. B., & Givskov, M. (2002). Food spoilage - Interactions between food spoilage bacteria. *International Journal of Food Microbiology*, 78(1–2), 79–97.
- Gustavsson, J., Cederberg, C., Sonesson, U., Otterdijk, R. van, & Meybeck, A. (2011). Global food losses and food waste. In *Food Loss and Food Waste: Causes and Solutions*. Rome: Food and Agriculture Organization.
- Hammond, K., Ryadnov, M. G., & Hoogenboom, B. W. (2021). Atomic force microscopy to elucidate how peptides disrupt membranes. *BBA - Biomembranes*, 1863(1), 183447.
- Hancock, R. E. W. (1997). Peptide antibiotics. *Lancet*, 349(9049), 418–422.
- Haney, E. F., Mansour, S. C., & Hancock, R. E. W. (2017). Antimicrobial peptides: An introduction. *Methods in Molecular Biology*, 1548, 3–22.
- Hartmann, M., Berditsch, M., Hawecker, J., Ardakani, M. F., Gerthsen, D., & Ulrich, A. S. (2010). Damage of the bacterial cell envelope by antimicrobial peptides gramicidin S and PGLa as revealed by transmission and scanning electron microscopy. *Antimicrobial Agents and Chemotherapy*, 54(8), 3132–3142.
- Hassan, M. F., Qutb, A. M., & Dong, W. (2021). Prediction and activity of a cationic α -helix antimicrobial peptide ZM-804 from maize. *International Journal of Molecular Sciences*, 22(5), 2643.
- He, Y. Q., Ma, C. Y., Pan, Y., Yin, L. J., Zhou, J., Duan, Y., .. Ma, H. (2018). Bioavailability of corn gluten meal hydrolysates and their effects on the immune system. *Czech Journal of Food Sciences*, 36(1), 1–7.
- Henzel, W. J., & Stults, J. T. (2001). Reversed-phase isolation of peptides. In *Current Protocols in Protein Science* (Vol. 24, Issue 1, pp. 1–16). Hoboken, NJ: John Wiley & Sons, Inc.
- Holdbrook, D. A., Singh, S., Choong, Y. K., Petrlova, J., Malmsten, M., Bond, P. J., ... Saravanan, R. (2018). Influence of pH on the activity of thrombin-derived antimicrobial peptides. *Biochimica et Biophysica Acta - Biomembranes*, 1860(11), 2374–2384.
- Huan, Y., Kong, Q., Mou, H., & Yi, H. (2020). Antimicrobial peptides: Classification, design, application and research progress in multiple fields. *Frontiers in Microbiology*, 11, 582779.
- Huang, X. X., Gao, C. Y., Zhao, Q. J., & Li, C. L. (2015). Antimicrobial characterization of site-directed mutagenesis of porcine beta defensin 2. *PLoS ONE*, 10(2), 9–10.
- Huleihel, M., Pavlov, V., & Erukhimovitch, V. (2009). The use of FTIR microscopy for the

- evaluation of anti-bacterial agents activity. *Journal of Photochemistry and Photobiology B: Biology*, 96(1), 17–23.
- Iqbal, A., & Khan, R. S. (2023). Snakins: Antimicrobial potential and prospects of genetic engineering for enhanced disease resistance in plants. *Molecular Biology Reports*, 50(10), 8683–8690.
- Jakubczyk, A., Karas, M., Rybczynska-Tkaczyk, K., Zielinska, E., & Zielinski, D. (2020). Current trends of bioactive peptides - New sources and therapeutic effect. *Foods*, 9(7), 846.
- Kaczmarek, M., Avery, S. V., & Singleton, I. (2019). Microbes associated with fresh produce: Sources, types and methods to reduce spoilage and contamination. In *Advances in Applied Microbiology* (Vol. 107, pp. 29–82). Amsterdam: Elsevier Inc.
- Kant, P., Liu, W. Z., & Pauls, K. P. (2009). PDC1, a corn defensin peptide expressed in *Escherichia coli* and *Pichia pastoris* inhibits growth of *Fusarium graminearum*. *Peptides*, 30(9), 1593–1599.
- Kaur, H., Afsar, M., Devgon, I., Khan, M. A., Jangra, S., Kaur, L., & Kumar, A. (2020). Bioactive peptides: Emerging tool to fight diseases. *European Journal of Molecular and Clinical Medicine*, 7(7), 4277–4293.
- Kim, J. S., Jeong, J. H., Cho, J. H., Lee, D. H., & Kim, Y. (2018). Antimicrobial activity of antimicrobial peptide LPcin-YK3 derived from bovine lactophorin. *Journal of Microbiology and Biotechnology*, 28(8), 1299–1309.
- Kim, S. K., & Wijesekara, I. (2010). Development and biological activities of marine-derived bioactive peptides: A review. *Journal of Functional Foods*, 2(1), 1–9.
- Kong, X., Song, W., Hua, Y., Li, X., Chen, Y., Zhang, C., & Chen, Y. (2020). Insights into the antibacterial activity of cottonseed protein-derived peptide against *Escherichia coli*. *Food and Function*, 11(11), 10047–10057. c
- Korhonen, H., & Pihlanto, A. (2006). Bioactive peptides: Production and functionality. *International Dairy Journal*, 16(9), 945–960.
- Kose, A., & Oncel, S. S. (2015). Properties of microalgal enzymatic protein hydrolysates: Biochemical composition, protein distribution and FTIR characteristics. *Biotechnology Reports*, 6, 137–143.
- Krishnamoorthy, R., Adhikari, P., & Anaikutti, P. (2023). Design, synthesis, and characterization of non-hemolytic antimicrobial peptides related to human cathelicidin LL-37. *RSC Advances*, 13(23), 15594–15605.
- Lazzaro, B. P., Zasloff, M., & Rolff, J. (2020). Antimicrobial peptides: Application informed by evolution. *Science*, 368(6490), eaau5480.
- Lei, J., Sun, L. C., Huang, S., Zhu, C., Li, P., He, J., ... He, Q. Y. (2019). The antimicrobial

- peptides and their potential clinical applications. *American Journal of Translational Research*, *11*(7), 3919–3931.
- Lemes, A. C., Sala, L., Ores, J. D. C., Braga, A. R. C., Egea, M. B., & Fernandes, K. F. (2016). A review of the latest advances in encrypted bioactive peptides from protein-rich waste. *International Journal of Molecular Sciences*, *17*(6), 950.
- Li, J., Koh, J. J., Liu, S., Lakshminarayanan, R., Verma, C. S., & Beuerman, R. W. (2017). Membrane active antimicrobial peptides: Translating mechanistic insights to design. *Frontiers in Neuroscience*, *11*, 73.
- Li, X., Han, L., & Chen, L. (2008). In vitro antioxidant activity of protein hydrolysates prepared from corn gluten meal. *Journal of the Science of Food and Agriculture*, *88*, 1660–1666.
- Liang, Q., Chalamaiah, M., Ren, X., Ma, H., & Wu, J. (2018). Identification of new anti-inflammatory peptides from zein hydrolysate after simulated gastrointestinal digestion and transport in Caco-2 cells. *Journal of Agricultural and Food Chemistry*, *66*(5), 1114–1120.
- Liu, W. Y., Fang, L., Feng, X. W., Li, G. M., & Gu, R. Z. (2020). In vitro antioxidant and angiotensin I-converting enzyme inhibitory properties of peptides derived from corn gluten meal. *European Food Research and Technology*, *246*, 2017–2027.
- Liu, X. L., Song, C. L., Chen, J. P., Liu, X., Ren, J., & Zheng, X. Q. (2020). Preparation and evaluation of new glycopeptides obtained by proteolysis from corn gluten meal followed by transglutaminase-induced glycosylation with glucosamine. *Foods*, *9*(5), 555.
- Lyu, Z., Yang, P., Lei, J., & Zhao, J. (2023). Biological function of antimicrobial peptides on suppressing pathogens and improving host immunity. *Antibiotics*, *12*(6), 1037.
- Mant, C. T., Chen, Y., Yan, Z., Popa, T. V., Kovacs, J. M., Mills, J. B., ... Hodges, R. S. (2007). HPLC analysis and purification of peptides. In Fields, G. (Ed.). *Methods in molecular biology (Clifton, N.J.)* (Vol. 386, pp. 3–55). New Jersey: Humana Press Inc.
- Matthyssen, T., Li, W., Holden, J. A., Lenzo, J. C., Hadjigol, S., & O'Brien-Simpson, N. M. (2022). The potential of modified and multimeric antimicrobial peptide materials as superbug killers. *Frontiers in Chemistry*, *9*, 795433.
- Mirnejad, R., Fasihi-Ramandi, M., Behmard, E., Najafi, A., & Moghaddam, M. M. (2023). Interaction of antibacterial CM11 peptide with the gram-positive and gram-negative bacterial membrane models: a molecular dynamics simulations study. *Chemical Papers*, *77*(7), 3727–3735.
- Mishra, M., & Chauhan, P. (2016). Applications of microscopy in bacteriology. *Microscopy Research*, *04*(01), 1–9.

- Mostafa, A. A., Al-Askar, A. A., Almaary, K. S., Dawoud, T. M., Sholkamy, E. N., & Bakri, M. M. (2018). Antimicrobial activity of some plant extracts against bacterial strains causing food poisoning diseases. *Saudi Journal of Biological Sciences*, *25*(2), 361–366.
- Mudhakar, D., & Harashima, H. (2009). Learning from the viral journey: How to enter cells and how to overcome intracellular barriers to reach the nucleus. *AAPS Journal*, *11*(1), 65–77.
- Nasri, M. (2017). Protein hydrolysates and biopeptides: Production, biological activities, and applications in foods and health benefits. A review. *Advances in Food and Nutrition Research*, *81*, 109–159.
- Nawrocki, K. L., Crispell, E. K., & McBride, S. M. (2014). Antimicrobial peptide resistance mechanisms of gram-positive bacteria. *Antibiotics*, *3*(4), 461–492.
- Novais, Â., Freitas, A. R., Rodrigues, C., & Peixe, L. (2019). Fourier transform infrared spectroscopy: Unlocking fundamentals and prospects for bacterial strain typing. *European Journal of Clinical Microbiology and Infectious Diseases*, *38*(3), 427–448.
- Omardien, S., Drijfhout, J. W., van Veen, H., Schachtschabel, S., Riool, M., Hamoen, L. W., ... Zaat, S. A. J. (2018). Synthetic antimicrobial peptides delocalize membrane bound proteins thereby inducing a cell envelope stress response. *Biochimica et Biophysica Acta - Biomembranes*, *1860*(11), 2416–2427.
- Oyston, P. C. F., Fox, M. A., Richards, S. J., & Clark, G. C. (2009). Novel peptide therapeutics for treatment of infections. *Journal of Medical Microbiology*, *58*(8), 977–987.
- Pandit, G., Biswas, K., Ghosh, S., Debnath, S., Bidkar, A. P., Satpati, P., ... Chatterjee, S. (2020). Rationally designed antimicrobial peptides: Insight into the mechanism of eleven residue peptides against microbial infections. *Biochimica et Biophysica Acta - Biomembranes*, *1862*(4), 183177.
- Pane, K., Cafaro, V., Avitabile, A., Torres, M. D. T., Vollaro, A., De Gregorio, E., ... Notomista, E. (2018). Identification of novel cryptic multifunctional antimicrobial peptides from the human stomach enabled by a computational-experimental platform. *ACS Synthetic Biology*, *7*(9), 2105–2115.
- Pane, K., Durante, L., Crescenzi, O., Cafaro, V., Pizzo, E., Varcamonti, M., ... Notomista, E. (2017). Antimicrobial potency of cationic antimicrobial peptides can be predicted from their amino acid composition: Application to the detection of “cryptic” antimicrobial peptides. *Journal of Theoretical Biology*, *419*, 254–265.
- Pelegriani, P. B., Quirino, B. F., & Franco, O. L. (2007). Plant cyclotides: An unusual class of defense compounds. *Peptides*, *28*(7), 1475–1481.

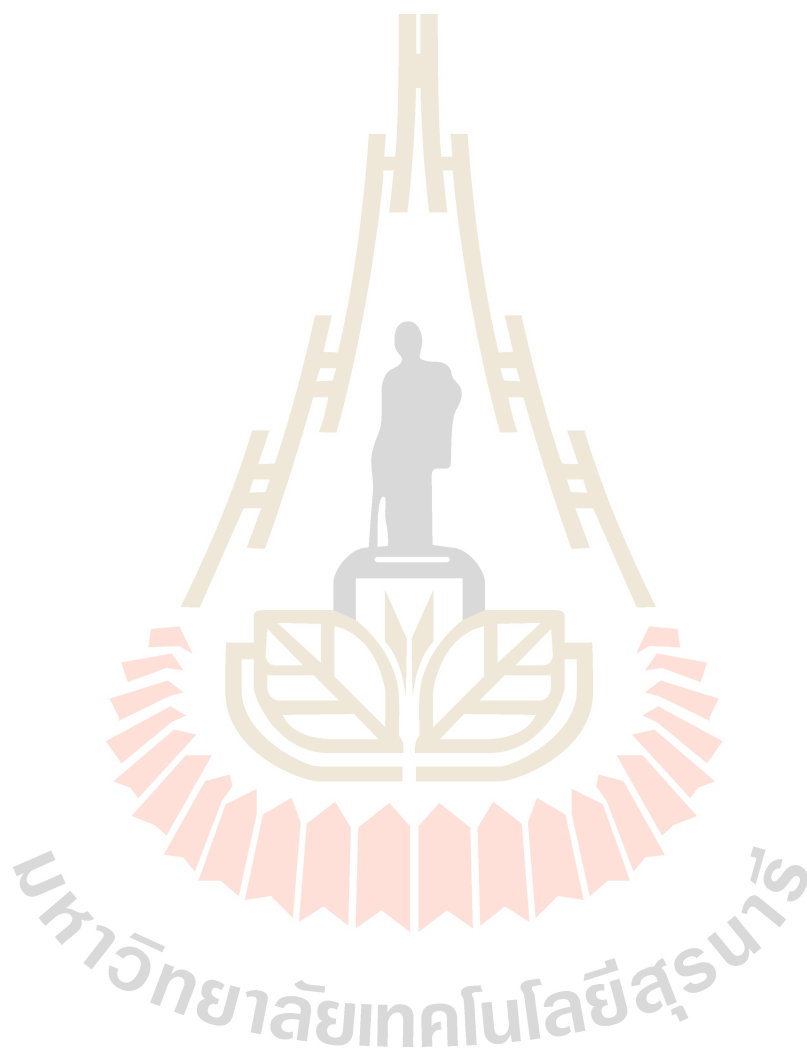
- Przybylski, R., Firdaous, L., Châtaigné, G., Dhulster, P., & Nedjar, N. (2016). Production of an antimicrobial peptide derived from slaughterhouse by-product and its potential application on meat as preservative. *Food Chemistry*, *211*, 306–313.
- Pu, C., & Tang, W. (2017). The antibacterial and antibiofilm efficacies of a liposomal peptide originating from rice bran protein against *Listeria monocytogenes*. *Food and Function*, *8*(11), 4159–4169.
- Raharjo, T., Utami, W., Fajr, A., Swasono, R., & Haryadi, W. (2021). Antibacterial peptides from tryptic hydrolysate of *Ricinus communis* seed protein fractionated using cation exchange chromatography. *Indonesian Journal of Pharmacy*, *32*(1), 74–85.
- Raheem, N., & Straus, S. K. (2019). Mechanisms of action for antimicrobial peptides with antibacterial and antibiofilm functions. *Frontiers in Microbiology*, *10*, 2866.
- Rai, M., Pandit, R., Gaikwad, S., & Kövics, G. (2016). Antimicrobial peptides as natural bio-preservative to enhance the shelf-life of food. *Journal of Food Science and Technology*, *53*(9), 3381–3394.
- Rajasekaran, G., Kim, E. Y., & Shin, S. Y. (2017). LL-37-derived membrane-active FK-13 analogs possessing cell selectivity, anti-biofilm activity and synergy with chloramphenicol and anti-inflammatory activity. *Biochimica et Biophysica Acta*, *1859*(5), 722–733.
- Rani, L., Arora, A., Majhi, S., Mishra, A., & Mallajosyula, S. S. (2022). Experimental and simulation studies reveal mechanism of action of human defensin derivatives. *Biochimica et Biophysica Acta - Biomembranes*, *1864*(2), 183824.
- Rivero-Pino, F., Leon, M. J., Millan-Linares, M. C., & Montserrat-de la Paz, S. (2023). Antimicrobial plant-derived peptides obtained by enzymatic hydrolysis and fermentation as components to improve current food systems. *Trends in Food Science and Technology*, *135*, 32–42.
- Romero, J. L., Grande Burgos, M. J., Pérez-Pulido, R., Gálvez, A., & Lucas, R. (2017). Resistance to antibiotics, biocides, preservatives and metals in bacteria isolated from seafoods: Co-selection of strains resistant or tolerant to different classes of compounds. *Frontiers in Microbiology*, *8*, 1650.
- Ross, J. N., Fields, F. R., Kalwajtys, V. R., Gonzalez, A. J., O'Connor, S., Zhang, A., ... Lee, S. W. (2020). Synthetic peptide libraries designed from a minimal alpha-helical domain of AS-48-bacteriocin homologs exhibit potent antibacterial activity. *Frontiers in Microbiology*, *11*, 589666.
- Sato, H., & Feix, J. B. (2006). Peptide-membrane interactions and mechanisms of membrane destruction by amphipathic α -helical antimicrobial peptides. *Biochimica et Biophysica Acta - Biomembranes*, *1758*(9), 1245–1256.

- Schäfer, A. B., & Wenzel, M. (2020). A how-to guide for mode of action analysis of antimicrobial peptides. *Frontiers in Cellular and Infection Microbiology*, *10*, 540898.
- Selsted, M. E. (1997). HPLC methods for purification of antimicrobial peptides. In Shafer, W. M. (Ed.). *Methods in molecular biology (Clifton, N.J.)* (Vol. 78, pp. 17–33). New Jersey: Humana Press Inc.
- Sengupta, D., Leontiadou, H., Mark, A. E., & Marrink, S. J. (2008). Toroidal pores formed by antimicrobial peptides show significant disorder. *Biochimica et Biophysica Acta - Biomembranes*, *1778*(10), 2308–2317.
- Shahidi, F., & Ambigaipalan, P. (2018). Bioactives from seafood processing by-products. In *Encyclopedia of Food Chemistry*. Amsterdam: Elsevier Inc.
- Sher Khan, R., Iqbal, A., Malak, R., Shehryar, K., Attia, S., Ahmed, T., ... Mii, M. (2019). Plant defensins: Types, mechanism of action and prospects of genetic engineering for enhanced disease resistance in plants. *3 Biotech*, *9*(5), 1–12.
- Shwaiki, L. N., Arendt, E. K., & Lynch, K. M. (2020). Study on the characterisation and application of synthetic peptide Snakin-1 derived from potato tubers – Action against food spoilage yeast. *Food Control*, *118*, 107362.
- Singh, A. K. (2016). Experimental methodologies for the characterization of nanoparticles. In *Engineered Nanoparticles* (pp. 125–170). Amsterdam: Elsevier Inc.
- Sinha, R., Radha, C., Prakash, J., & Kaul, P. (2007). Whey protein hydrolysate: Functional properties, nutritional quality and utilization in beverage formulation. *Food Chemistry*, *101*(4), 1484–1491.
- Slavokhotova, A. A., & Rogozhin, E. A. (2020). Defense peptides from the α -hairpinin family are components of plant innate immunity. *Frontiers in Plant Science*, *11*, 465.
- Song, W., Kong, X., Hua, Y., Chen, Y., Zhang, C., & Chen, Y. (2020). Identification of antibacterial peptides generated from enzymatic hydrolysis of cottonseed proteins. *LWT - Food Science and Technology*, *125*, 109199.
- Stem, M. R. (2008). Understanding why researchers should use synchrotron-enhanced FTIR instead of traditional FTIR. *Journal of Chemical Education*, *85*(7), 983–989.
- Stotz, H. U., Thomson, J. G., & Wang, Y. (2009). Plant defensins: Defense, development and application. *Plant Signaling & Behavior*, *4*(11), 1010–1012.
- Sun, A., Huang, Z., He, L., Dong, W., Tian, Y., Huang, A., & Wang, X. (2023). Metabolomic analyses reveal the antibacterial properties of a novel antimicrobial peptide MOp3 from *Moringa oleifera* seeds against *Staphylococcus aureus* and its application in the infecting pasteurized milk. *Food Control*, *150*, 109779.

- Swana, K. W., Nagarajan, R., & Camesano, T. A. (2021). Atomic force microscopy to characterize antimicrobial peptide-induced defects in model supported lipid bilayers. *Microorganisms*, *9*(9), 1975.
- Taniguchi, M., Kameda, M., Namae, T., Ochiai, A., Saitoh, E., & Tanaka, T. (2017). Identification and characterization of multifunctional cationic peptides derived from peptic hydrolysates of rice bran protein. *Journal of Functional Foods*, *34*, 287–296.
- Taveira, G. B., Carvalho, A. O., Rodrigues, R., Trindade, F. G., Da Cunha, M., & Gomes, V. M. (2016). Thionin-like peptide from *Capsicum annuum* fruits: Mechanism of action and synergism with fluconazole against *Candida* species. *BMC Microbiology*, *16*, 12.
- Tizro, P., Choi, C., & Khanlou, N. (2019). Sample preparation for transmission electron microscopy. *Methods in Molecular Biology*, *1897*, 417–424.
- Torres, M. D. T., Sothiselvam, S., Lu, T. K., & de la Fuente-Nunez, C. (2019). Peptide design principles for antimicrobial applications. *Journal of Molecular Biology*, *431*(18), 3547–3567.
- Vishnepolsky, B., Zaalishvili, G., Karapetian, M., Nasrashvili, T., Kuljanishvili, N., Gabrielian, A., ... Pirtskhalava, M. (2019). De novo design and in vitro testing of antimicrobial peptides against gram-negative bacteria. *Pharmaceuticals*, *12*(2), 82.
- Wan, Y., Wang, X., Yang, L., Li, Q., Zheng, X., Bai, T., & Wang, X. (2023). Antibacterial activity of juglone revealed in a wound model of *Staphylococcus aureus* infection. *International Journal of Molecular Sciences*, *24*(4), 3931.
- Wang, L., Ding, L., Yu, Z., Zhang, T., Ma, S., & Liu, J. (2016). Intracellular ROS scavenging and antioxidant enzyme regulating capacities of corn gluten meal-derived antioxidant peptides in HepG2 cells. *Food Research International*, *90*, 33–41.
- Wang, Q., Xu, Y., & Hu, J. (2022). Intracellular mechanism of antimicrobial peptide HJH-3 against *Salmonella pullorum*. *RSC Advances*, *12*(23), 14485–14491.
- Wimley, W. (2010). Describing the mechanism of antimicrobial peptide action with the interfacial activity model. *ASC Chemical Biology*, *5*(10), 905–917.
- Wong, K. H., Tan, W. L., Kini, S. G., Xiao, T., Serra, A., Sze, S. K., & Tam, J. P. (2017). Vaccatides: Antifungal glutamine-rich hevein-like peptides from *Vaccaria hispanica*. *Frontiers in Plant Science*, *8*, 1100.
- World Health Organization (WHO). (2022). *Food safety-in fact*. Retrieved from <https://www.who.int/news-room/fact-sheets/detail/food-safety>
- Xiao, H., Shao, F., Wu, M., Ren, W., Xiong, X., Tan, B., & Yin, Y. (2015). The application of antimicrobial peptides as growth and health promoters for swine. *Journal of Animal Science and Biotechnology*, *6*, 19.

- Xiao, J., & Zhang, H. (2012). An *Escherichia coli* cell membrane chromatography-offline LC-TOF-MS method for screening and identifying antimicrobial peptides from *Jatropha curcas* meal protein isolate hydrolysates. *Journal of Biomolecular Screening*, 17(6), 752–760.
- Yongsawatdigul, J., & Hamzeh, A. (2021). Bioactive peptides from agriculture and food industry co-products: Peptide structure and health benefits. In Barros, A. N., & Gouvinhas, I. (Eds.). *Innovation in the Food Sector through the Valorization of Food and Agro-Food By-Products*. London: IntechOpen Ltd.
- Yu, L. J., & Brooks, M. S. L. (2016). Food industry protein by-products and their applications. In Dhillon, G. S. (Ed.). *Protein Byproducts: Transformation from Environmental Burden Into Value-Added Products* (Vol. 2012, pp. 121–133). Amsterdam: Elsevier Inc.
- Zamora-Sillero, J., Gharsallaoui, A., & Prentice, C. (2018). Peptides from fish by-product protein hydrolysates and its functional properties: An overview. *Marine Biotechnology*, 20(2), 118–130.
- Zhang, J., Zhang, J., Wang, Y., Zhang, X., Nie, T., & Liu, Y. (2022). Strategies to improve the activity and biocompatibility: Modification of peptide antibiotics. *Foodborne Pathogens and Disease*, 19(6), 376–385.
- Zhang, L. L., Zhang, L. F., & Xu, J. G. (2020). Chemical composition, antibacterial activity and action mechanism of different extracts from hawthorn (*Crataegus pinnatifida* Bge.). *Scientific Reports*, 10(1), 1–13.
- Zhang, Q. Y., Yan, Z. B., Meng, Y. M., Hong, X. Y., Shao, G., Ma, J. J., ... Fu, C. Y. (2021). Antimicrobial peptides: Mechanism of action, activity and clinical potential. *Military Medical Research*, 8(1), 1–25.
- Zhang, R., Fan, X., Jiang, X., Zou, M., Xiao, H., & Wu, G. (2021). Multiple mechanisms of the synthesized antimicrobial peptide TS against Gram-negative bacteria for high efficacy antibacterial action in vivo. *Molecules*, 26(1), 60.
- Zhang, X., Liu, X., Yang, C., Xi, T., Zhao, J., Liu, L., & Yang, K. (2021). New strategy to delay food spoilage: Application of new food contact material with antibacterial function. *Journal of Materials Science and Technology*, 70, 59–66.
- Zhou, C., Ma, H., Ding, Q., Lin, L., Yu, X., Luo, L., ... Yagoub, A. E. G. A. (2013). Ultrasonic pretreatment of corn gluten meal proteins and neutrase: Effect on protein conformation and preparation of ACE (angiotensin converting enzyme) inhibitory peptides. *Food and Bioproducts Processing*, 91(4), 665–671.
- Zhou, L., Lian, K., Wang, M., Jing, X., Zhang, Y., & Cao, J. (2022). The antimicrobial effect of a novel peptide LL-1 on *Escherichia coli* by increasing membrane permeability. *BMC Microbiology*, 22, 220.

Zoumpopoulou, G., Papadimitriou, K., Polissiou, M. G., Tarantilis, P. A., & Tsakalidou, E. (2010). Detection of changes in the cellular composition of *Salmonella enterica* serovar Typhimurium in the presence of antimicrobial compound(s) of *Lactobacillus* strains using Fourier transform infrared spectroscopy. *International Journal of Food Microbiology*, 144(1), 202–207.



CHAPTER III

ANTIBACTERIAL ACTIVITY OF ENZYMATIC CORN GLUTEN MEAL HYDROLYSATE AND ABILITY TO INHIBIT *Staphylococcus aureus* IN ULTRA-HIGH TEMPERATURE PROCESSED MILK

3.1 Abstract

The aim of this work was to determine the antibacterial properties and mode of activity of isolated corn gluten meal (CGM) hydrolysate fractions. The P1 fraction from reverse-phase liquid chromatography separation of pepsin-hydrolyzed CGM presented the most potent antibacterial activity with minimum inhibitory concentration (MIC) of 1 mM and 4 mM minimum bactericidal concentration (MBC) against *Staphylococcus aureus* ATCC 29213. The kinetics of P1 antibacterial activity revealed a bacteriostatic effect at 1×MIC and 2×MIC for 8 h, but a bactericidal effect at 4×MIC. The P1 fraction at 1×MIC and 4×MIC disrupted the membrane integrity of *S. aureus* after 8 h exposure as observed by confocal laser scanning microscopy. Scanning electron microscopy and transmission electron microscopy indicated cell surface damage and cytoplasmic leakage in *S. aureus* after being exposed to the P1 fraction. Synchrotron radiation-Fourier transmission infrared (SR-FTIR) microspectroscopy revealed changes in nucleic acid, protein, and fatty acid compositions of *S. aureus* cell membrane after 8 h exposure to P1 at 1×MIC. The antibacterial activity of P1 exhibited stability within the range of pH 4.5-6.5 and temperatures of 40-100 °C. The P1 exhibited relatively low hemolytic activity up to 8 mM. The P1 fraction at 8 mM suppressed the growth of *S. aureus* during a challenge test on commercial ultra-high temperature milk inoculated with *S. aureus* ATCC 29213. Eleven novel hydrophilic peptides (6 cationic and 5 anionic) were identified and are suggested to contribute to the observed antibacterial activity of the P1 fraction. We conclude that the pepsin-hydrolyzed CGM peptide fraction showed potential to be utilized as a novel antimicrobial agent for the control of *S. aureus* in foods.

Keywords: Antibacterial peptide; corn gluten meal; protein hydrolysate; *Staphylococcus aureus*; mode of action

3.2 Introduction

Infection of foodborne pathogenic bacteria is one of the leading causes of severe and fatal illnesses globally (Fung, Wang, & Menon, 2018). The food industry has increasingly relied on chemical preservatives, including nitrites, sulfur dioxide, benzoate, and sorbate, among others to enhance the shelf life of food products. Some food preservatives may negatively affect human health, including headaches, palpitations, allergic reactions, asthma, and even cancer (Vally & Misso, 2012; Walczak-Nowicka & Herbet, 2022). In response to the growing demand for “more natural” food preservatives, an increasing number of natural compounds exhibiting antimicrobial properties from several sources have been sought (Lee and Paik, 2016).

Natural antimicrobial agents are found in plants, animals, and microorganisms (Quinto et al., 2019). Bioactive peptides obtained from plant or animal proteins by enzymatic hydrolysis and fermentation can act as antimicrobial agents (Corrêa, de Melo Nazareth, Rocha, & Luciano, 2023). Antimicrobial peptides (AMPs) can be a promising food preservative with numerous advantages, including minimizing the use of synthetic food preservatives, preventing food spoilage, and creating nutritional supplements with health benefits (Ahmed and Hammami, 2019). The Antimicrobial Peptide Database has identified 3,940 peptides, including 3,146 natural AMPs (<https://aps.unmc.edu>).

Corn gluten meal (CGM) is a by-product of corn starch wet milling process, which still comprises 67-71% protein in dry matter. Zein and glutelin are the major proteins, constituting approximately 65% and 30%, respectively (Hardwick & Glatz, 1989; Kim, Whang, Kim, Koh, & Suh, 2004), but the hydrophobic properties of CGM proteins make them insoluble. Consequently, CGM is generally utilized for animal feed or discarded. Enzymatic hydrolysis of CGM yielded peptides with various bioactive properties, including antioxidant, anti-inflammatory, angiotensin-converting enzyme-inhibitory, antihypertensive, hepatoprotective, and dipeptidyl peptidase IV-inhibitory activities (Chanajon, Noisa, & Yongsawatdigul, 2022; Chanajon, Girgih, Oluwagunwa, Aluko, & Yongsawatdigul, 2024; Kopparapu, Duan, Huang, & Katrolia, 2022; Wongngam, Hamzeh, Tian, Roytrakul, & Yongsawatdigul, 2023). Antifungal and antibacterial peptides from maize peptides prepared from chemical hydrolysis and recombinant defensin from maize have also been reported (Al Kashgry et al., 2020; Duvick, Rood, Rao, & Marshak, 1992; Kant, Liu, & Pauls, 2009). Duvick et al. (1992) reported that maize peptide MBP-1 prepared by sulfuric acid hydrolysis inhibited fungal germination (*Fusarium graminearum*, *F. moniliforme*) at 60 µg.mL⁻¹ and bacterial growth (*Clavibacter*

michiganese ssp *nebraskense*) at 30 $\mu\text{g}\cdot\text{mL}^{-1}$. Meanwhile, Al Kashgry et al. (2020) reported that the antimicrobial peptide MzDef was produced by heterologous expression in *E. coli* and inhibited the growth of fungi (*Rhizoctonia solani*, *Fusarium verticillioides*, and *Aspergillus niger*), *Escherichia coli* and *Bacillus cereus* at 3.2 μM .

Numerous studies have demonstrated that enzymatic hydrolysis of food proteins produced potent AMPs and evaluated their activity on food samples contaminated with pathogenic bacteria. Protein and lipid contents in food matrices can affect the antimicrobial activity, hence the need for purer products such the isolated peptide fractions. However, the use of corn peptides with antimicrobial properties derived from enzymatic hydrolysis of CGM is underexploited. Therefore, the current study aimed to produce a CGM hydrolysate and identify the active antibacterial peptide fractions. In addition, the mode of action of the most active peptide fraction was further investigated. Additionally, the impact of food processing factors such as temperature and pH on antibacterial activity and its safety were studied. The efficacy of the peptide fraction on bacterial control was evaluated using the commercial ultra-high temperature (UHT) milk inoculated with *Staphylococcus aureus* ATCC 29213 as a model. Finally, the plausible antimicrobial peptide sequences were identified.

3.3 Materials and methods

3.3.1 Materials and chemicals

CGM was provided by Friendship Corn Starch Industry (Samutprakarn, Thailand). Pepsin derived from porcine stomach mucosa ($400 \text{ U}\cdot\text{mg}^{-1}$), 2,4,6-trinitrobenzene sulfonic acid (TNBS), trifluoroacetic acid (TFA), and propidium iodide (PI) were obtained from Sigma-Aldrich™ (St. Louis, MO, USA). SYTO9 stain was purchased from Thermo Fischer Scientific (Waltham, MA, USA). Tryptic soy broth (TSB), Mueller-Hinton broth (MHB), microbiological agar, and plate count agar (PCA) were purchased from HiMedia™ (Mumbai, India). Glutaraldehyde and OsO_4 were obtained from Electron Microscopy Sciences (Hatfield, PA, USA). Unless otherwise specified, all chemicals utilized were of analytical grade.

3.3.2 Bacterial strains

Four Gram- positive bacteria, *S. aureus* ATCC 29213, *Listeria monocytogenes* DMST 17303, *Bacillus cereus* DMST 5040, and methicillin-resistant *S. aureus* DMST 20652, and two Gram-negative bacteria, *E. coli* TISTR 780 and *Salmonella* Typhimurium TISTR 292 were employed. Bacteria were grown in TSB at 37 °C for 18-24

h, which were then streaked onto tryptic soy agar (TSA) and incubated at 37 °C for 18-24 h to obtain a pure single colony.

3.3.3 Preparation of corn gluten meal hydrolysate (CGMH)

A 5% (w/v) aqueous CGM mixture was prepared and hydrolyzed with pepsin at 4:100 enzyme:substrate ratio, pH 2.0, and 37 °C, for 6 h in a shaking water bath. Pepsin activity was terminated by heating the reaction mixture at 95 °C for 10 min, cooled to room temperature, centrifuged (10,000 ×g at 4 °C for 10 min), and the supernatant was stored at -20 °C as the CGM hydrolysate (CGMH). Peptide content in the supernatant was estimated by the TNBS method (Adler-Nissen, 1979) with L-leucine as a standard.

3.3.4 Fractionation of CGMH

Briefly, the CGMH supernatant was passed through a 0.45-µm PVDF syringe filter (Vertipure™, Vertical Chromatography, Nonthaburi, Thailand). A 2 mL aliquot of the filtrate was then fractionated using preparative reverse-phase chromatography (Interchim PuriFlash 5.250, Interchim S.A, Montluçon, Allier France) equipped with C18-AQ Flash Column (15 µm, 30×250 mm, Interchim Puriflash PF-15C18AQ-F0012). Mobile phase A (0.05% TFA in deionized water) and mobile phase B (0.05% TFA in acetonitrile) were used for peptide elution. The flow rate was set at 15.0 mL.min⁻¹, and eluted peptides were detected at 214 nm. Fractions were collected, lyophilized, kept at -20 °C, and tested for antibacterial activity.

3.3.5 Antimicrobial activity

3.3.5.1 Minimum inhibitory concentration (MIC)

CGMH peptide fractions were tested for antibacterial activity using broth microdilution technique as described by Hou et al. (2011) with slight modifications. All bacterial cultures were streaked on TSA and incubated for 24 h at 37 °C. The colony suspension made in sterile 0.85% NaCl solution was adjusted to a 0.5 McFarland (OD₆₀₀=0.085-0.100). Subsequently, after a 10-fold dilution with a final concentration of approximately 1×10⁵ CFU.mL⁻¹, 50 µL of Mueller Hinton Broth containing bacteria were added with 50 µL of peptides in a 96-well microplate. Kanamycin of 0.01 mg.mL⁻¹ was used separately as a positive control. The MIC was determined as peptide fraction with the lowest concentration that exhibited inhibition on the tested bacteria as assessed by the turbidity at 600 nm (OD₆₀₀) using a Varioskan™ LUX multimode microplate reader (Thermo Fisher Scientific Inc.).

3.3.5.2 Minimum bactericidal concentration (MBC)

MBC was estimated by taking an aliquot (100 μL) of the wells without visible microbial growth and enumerating in a plate count agar (PCA) for 18 h at 37 °C. The lowest concentration of peptide that killed more than 99.9% of the cells compared to the untreated sample was considered as MBC value. Triplicate tests were conducted.

3.3.5.3 Bactericidal curve

Briefly, *S. aureus* cells in 0.85% NaCl was added to MHB to contain a final cell count of approximately 1×10^5 CFU mL^{-1} . The P1 fraction at 1xMIC, 2xMIC, and 4xMIC were then introduced to the bacterial suspension and incubated at 37 °C. Cell viability was assessed for various time intervals of 0, 1, 2, 3, 4, 6, 8, 19, and 24 h using a drop plate technique on Plate Count Agar (PCA) in triplicates. The plates were incubated at 37 °C for 18-24 h. Overall the P1 fraction exhibited the highest antibacterial activity and was used for further tests as described below.

3.3.6 Peptide identification

Amino acid sequencing of the P1 peptide fraction was performed using an Easy-nLC 1200 system paired with a Q Exactive™ Hybrid Quadrupole-Orbitrap™ Mass Spectrometer (Thermo Fisher Scientific) that contain an ESI nanospray source. The peptide fraction (5 μL) was separated by reverse-phase chromatography on a 150 $\mu\text{m} \times 15$ cm nanocolumn packed with a ReproSil-Pur C18-AQ resin (1.9 μm , 100 Å, Dr. Maisch GmbH, Germany) and eluted using linear gradient consisting of mobile phase A (0.1% formic acid in water) and mobile phase B (20% 0.1% formic acid in 80% acetonitrile). The flow rate was set at 0.6 $\mu\text{L} \cdot \text{min}^{-1}$ and LC linear gradient was carried out as follows: 2 min 4-8% B, 43 min 8-28% B, 10 min 28-40% B, 1 min 40-95% B, and 10 min 95-95% B. Mass spectrometry conditions were as follows: 2.2 kV spray voltage, 270 °C capillary temperature, scan range of 300 to 1,800 Da, and 70000 full scan resolution at 400 m/z. Spectra of peptides were analyzed by PEAKS Studio 10.0 software (Bioinformatics Solutions Inc, Waterloo, ON, Canada). Peptides with *de novo* scores above 70% were synthesized. Furthermore, peptide sequences were examined for compatibility on the NCBI Protein BLAST with a database of maize (*Zea mays* L.) taxid 4577 (<http://blast.ncbi.nlm.nih.gov/>) (Altschul et al., 1997; Madden, 2002). The selected peptides were synthesized by solid-phase peptide synthesis (GL Biochem, Shanghai, Ltd., China), with purity of 95-98%.

3.3.7 *In silico* characterization of peptides

Molecular weight, hydrophobicity, and net charge of peptides identified to be present in the P1 fraction were determined with peptide2.0 (<https://www.peptide2.com>). The grand average of the hydropathicity (GRAVY) index was estimated according to ProtParam (<https://www.expasy.org/>). The secondary structures of peptides were predicted using SOPMA (self-optimized prediction method with alignment) at the Network Protein Sequence Analysis (https://npsa-prabi.ibcp.fr/cgi-bin/secpred_mlr.pl/) (Combet, Blanchet, Geourjon, & Deléage, 2000). The peptides were predicted as antimicrobial peptides using the Collection of Anti-Microbial Peptide (CAMP) server (<http://www.camp3.bicnirrh.res.in/>).

3.3.8 Mode of action

3.3.8.1 Membrane integrity

The membrane integrity alteration in the *S. aureus* cells caused by peptide was evaluated using the confocal laser scanning microscope (CLSM) method described by de Almeida et al. (2019) with minor modifications. The mid-logarithmic *S. aureus* cells in TSB were centrifuged at 5,000 ×g for 5 min, rinsed twice with 10 mM PBS, and resuspended in 10 mM PBS to attain OD₆₀₀ of 0.2-0.3. Cells were subsequently exposed to the peptide fraction at 1×MIC and 4×MIC for 8 h at 37 °C. The control was prepared without peptides. After incubation, the peptide-treated cells and the control were rinsed twice with 10 mM PBS and resuspended in 10 mM PBS. PI at 10 µg.mL⁻¹ and SYTO9 at 2.5 µg.mL⁻¹ were added and incubated in the dark at 4 °C for 30 min. Subsequently, cells were collected and rinsed using 10 mM PBS. Finally, 10 µL bacterial cells were embedded on a glass slide and observed under the CLSM (Nikon 90i, Nikon, Tokyo, Japan).

3.3.8.2 Morphological changes

Scanning electron microscopy (SEM) was used to evaluate *S. aureus* morphological changes induced by the P1 peptides as described by Zhu et al. (2014). *S. aureus* was induced with the P1 fraction at 1×MIC and 4×MIC and incubated at 37 °C for 8 h. Cells without peptides were also prepared. Subsequently, cell pellets were collected and rinsed twice with 10 mM PBS. Cells were then fixed with 2.5% (v/v) glutaraldehyde and left at 4 °C for 24 h, continued by 1% OsO₄ (w/v) fixation for 2 h, followed by rinsing twice in distilled water. Subsequently, cells were dehydrated in a graded acetone series (20, 40, 60, 80, and 100%) for 15 min. Finally, specimens were

spotted on conductive aluminum tape, then put into an SEM sample stub, applied dual carbon and ultrathin gold coating, and observed with an FE-SEM (Auriga-Carl Zeiss, Oberkochen, Germany) at 2-2.5 keV electron energy.

3.3.8.3 Intracellular changes

Transmission electron microscopy (TEM) specimens were prepared after the dehydration step as mentioned above in section 2.8.2, and the specimens infiltrated with epoxy resin in graded acetone (1:3, 1:1, and 3:1) (Zhu et al., 2014). The specimens with 100% epoxy resin were polymerized at 60 °C for 24 h. Specimens were ultrathin sectioned to a 70-90 nm thickness using an ultramicrotome with a diamond knife. Samples were post-stained with 2% (w/v) uranyl acetate and 0.25% (w/v) lead citrate within each staining of 15 min at room temperature. Images were observed with a TEM (Tecnai G2 20, FEI, Hillsboro, OR, USA) with 120 keV electron energy.

3.3.8.4 Alteration of intracellular components

Synchrotron radiation-based Fourier transform infrared (SR-FTIR) spectromicroscopy was used to evaluate the intracellular modifications in *S. aureus* caused by the P1 peptide fraction as described by Naksang et al. (2020) with slight modifications. *S. aureus* cells were seeded in TSB, kept at 37 °C, added with P1 fraction at 1×MIC, and incubated at 37 °C for 0, 4, and 8 h. Five µL of bacterial cells were centrifuged at 5,000 ×g for 5 min. Pellets were rinsed twice using sterile 0.85% NaCl and washed thrice with sterile distilled water. One µL of culture suspension was spotted on a barium fluoride (BaF₂) window and dehydrated for 30 min. SR-FTIR experiment was conducted in Beamline 4.1 of the Synchrotron Light Research Institute (Nakhon Ratchasima, Thailand) with a Vertex-70 spectrometer (Bruker Optics, Ettlingen, Germany) and a Hyperion-2000 microscope (Bruker Optics). Spectra were generated in the 4,000-800 cm⁻¹ range. Measurement of the transmission mode was undertaken in mapping mode with a 10×10 µm² aperture size, 6 cm⁻¹ spectral resolution, and 64 co-added scans. Spectra were analyzed using OPUS version 7.5 software (Bruker Optics). Spectra were smoothed by the Savitzky-Golay algorithm with 3 polynomial order and 17 smoothing points, which were subsequently analyzed for second-order derivatives and principal component analysis (PCA) using Unscramble X 10.4 (Camo Analytics, Oslo, Norway).

3.3.9 Antimicrobial stability of the P1 fraction

3.3.9.1 Temperature

Thermal stability was conducted by heating the P1 fraction at 40, 60, 80, and 100 °C for 1 h. The unheated sample was used as a control. After heating, the P1 fraction was immediately cooled and antibacterial activity against *S. aureus* was conducted as described above in section 3.3.5.1.

3.3.9.2 pH

The influence of pH on antibacterial activity was examined by incubating the peptide fraction at pH 4.5, 5.5, and 6.5 overnight (Wang et al., 2019). Peptide in deionized water was used as a control. The antibacterial activity was tested in a 96-well microtiter plate according to the protocol described above in section 3.3.5.1.

3.3.10 Hemolysis activity

Hemolytic capacity of the P1 fraction was determined using the method of Wang et al. (2015) with some modifications. The experiment was conducted following ethical guidelines approved by the Human Research Ethics Committee of Suranaree University of Technology (EC-64-32). In brief, 1 mL of fresh human red blood cells (hRBCs) was collected from a healthy volunteer in a polycarbonate tube in the presence of heparin. The acquired hRBCs were centrifuged at 1,000 xg for 5 min at 4 °C and subsequently rinsed thrice in PBS buffer (pH 7.2), followed by diluting to 1% (v/v) with PBS buffer. Subsequently, 50 µL of the hRBCs suspension was mixed with 50 µL of fraction in PBS buffer (pH 7.2) at varying concentrations and incubated at 37 °C for 1 h. After centrifugation at 1,000 xg for 5 min at 4 °C, the supernatant was transferred to a fresh 96-well microtiter plate, and hemoglobin acquisition was determined at 570 nm (OD₅₇₀) using a microplate reader (Spectrostar® Nano, BMG Labtech, Ortenberg, Germany). Negative and positive controls were PBS buffer and 1% Triton X-100, respectively. The percentage for hemolysis was calculated based on the following equation:

$$\text{Hemolysis (\%)} = \frac{(\text{OD}_{570} \text{ the treated sample} - \text{OD}_{570} \text{ the negative control})}{(\text{OD}_{570} \text{ the positive sample} - \text{OD}_{570} \text{ the negative control})} \times 100\%$$

3.3.11 Inhibitory effect of the P1 fraction on *S. aureus* growth in milk

Inhibitory activity of the P1 fraction was evaluated in UHT processed milk inoculated with *S. aureus*. Peptides at different concentrations of 1, 2, 4, and 8 mM were added to the sterilized milk (Nongpho Ratchaburi Dairy Co Ltd, Ratchaburi, Thailand) inoculated with 10^2 - 10^3 CFU.mL⁻¹ *S. aureus* and incubated at 37 °C for 24 h. Samples with 0.01 mg.mL⁻¹ kanamycin and without P1 were used as positive and negative controls, respectively. Enumeration was carried out using a spot plate technique on PCA and incubated at 37 °C for 24 h, in triplicate.

3.3.12 Statistical analysis

All tests were conducted at least 3 independent biological replicates. Results were presented as mean \pm SD. Statistical analysis was carried out using GraphPad Prism version 8 (GraphPad Software, La Jolla, CA, USA).

3.4 Results and discussion

3.4.1 Peptide fractionation

Six fractions of CGMH were obtained from the C18AQ flash column chromatography separation (Figure 3.1A). All six fractions demonstrated antibacterial properties towards *S. aureus*, and only P2 showed low inhibition against *E. coli* at 2 mM L-leucine equivalent (Figure 3.1B). The results showed that CGMH contained peptides exhibiting antibacterial activity. Fractions P1, P2, and P6 were selected for further evaluation on other bacteria at 2 mM. Fractions P3, P4, and P5, were disregarded due to their limited peptide yield and lower antibacterial activity (Figures 3.1A, B). The results revealed that the P1 fraction possessed the most potent antibacterial activity against *S. aureus*, *B. cereus*, methicillin-resistant *S. aureus*, and *S. Typhimurium* (Figure 3.1C). This indicates that the P1 fraction has potent antibacterial activity against both Gram-positive and Gram-negative bacteria when compared to the other two fractions. Kang, Yi, Lee, & Oh (2006) also reported that the permeate fraction of pepsin-hydrolyzed zein separated using an ultrafiltration membrane with a molecular weight cut-off 3,000 Da showed antibacterial activity against *S. aureus* and *B. subtilis* with MIC value of 2.5 mg.mL⁻¹.

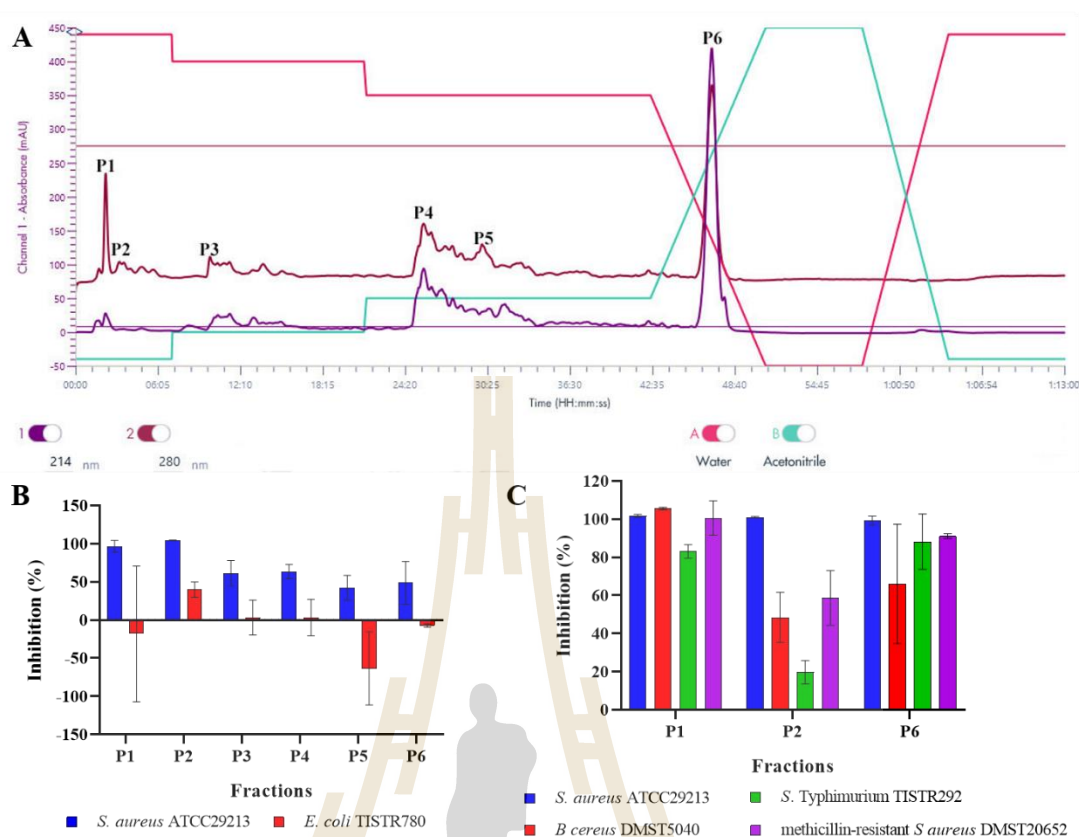


Figure 3.1 (A) Chromatogram of CGMH peptide fractionation. (B) Antibacterial activity assay of six peptide fractions of CGMH towards *Staphylococcus aureus* ATCC 29213 and *Escherichia coli* TISTR 780 at a concentration of 2 mM. (C) Antibacterial activity of 3 selected peptide fractions of CGMH against the test bacteria at 2 mM. Data are given as mean \pm SD ($n = 3$).

3.4.2 MIC and MBC

MIC values of the P1 fraction were 1 - 2 mM for all test bacteria (Table 3.1), showing that the peptides have antibacterial activity against both Gram-positive and Gram-negative bacteria. The MBC values of the P1 were calculated to be 4 to 8 mM (Table 3.1). The MBC results indicate a bactericidal effect with no more than two dilutions above MIC values. The capability of antibacterial peptides to penetrate the bacterial membrane depends on several characteristics, including the composition of amino acids, amphiphilicity, cationic character, and molecular size (Chai, Tan, Ee, Xiao, & Wong, 2019). However, the majority of AMPs are composed of oligopeptides containing 5 to 100 positively charged amino acids, typically 2 to 11 residues in addition to predominantly hydrophobic residues (Hafeez, Jiang, Bergen, & Zhu, 2021).

Table 3.1 Minimum inhibitory concentration (MIC) and minimum bactericidal concentration (MBC) determination of P1, P2, and P6 against 4 pathogenic bacteria.

Bacteria	Minimum inhibitory concentration (mM)			Minimum bactericidal concentration (mM)		
	P1	P2	P6	P1	P2	P6
<i>Staphylococcus aureus</i> ATCC 29213	1	2	4	4	>8	8
<i>Bacillus cereus</i> DMST 5040	2	4	8	8	>8	>8
<i>Salmonella</i> Typhimurium TISTR 292	2	ND	4	8	ND	>8
Methicillin-resistant <i>S. aureus</i> DMST 20652	2	4	8	8	>8	>8

ND is defined as not determined.

Zhou, Han, Koyama, & Ishizaki (2023) also reported that the fraction obtained from reverse-phase chromatography of kuruma shrimp head protein hydrolyzed by papain showed a high potent antibacterial efficacy against 4 foodborne pathogens, including *Staphylococcus aureus*, *Micrococcus luteus*, *E. coli*, and *Shewanella putrafaciens* with a MIC at a range of 5-16.67 mg.mL⁻¹. Moreover, Pezeshk, Ojagh, Rezaei, & Shabanpour (2019) reported that hydrolysis of yellowfin tuna viscera protein with Protamex produced a peptide fraction with strong antibacterial activity towards *E. coli*, *Pseudomonas aeruginosa*, *Staphylococcus aureus*, and *Listeria monocytogenes* at MIC of 0.5 mg.mL⁻¹. These studies along with our results demonstrate that peptides in protein hydrolysates from various food sources have antibacterial activities.

3.4.3 Bactericidal curve

The antibacterial activities of P1 were dose- and time-dependent (Figure 3.2). In the absence of P1, *S. aureus* showed a typical growth curve, reaching cell counts of 9.1 log CFU.mL⁻¹ after 24-h incubation. When cells were exposed to the P1 fraction at 1×MIC and 2×MIC, cell viability decreased by 4.6 log CFU.mL⁻¹ after 8-h exposure and gradually increased afterwards and reached 7.7 log CFU.mL⁻¹ and 5.9 log

CFU.mL⁻¹ respectively, after 24 h. At 4×MIC of P1, *S. aureus* growth was reduced by 1 log at 6-h exposure and drastically decreased afterwards, and cell viability was undetected at 18 h. Our results indicate that the P1 acted as a bactericidal agent at 4 mM as no viable cells were observed.

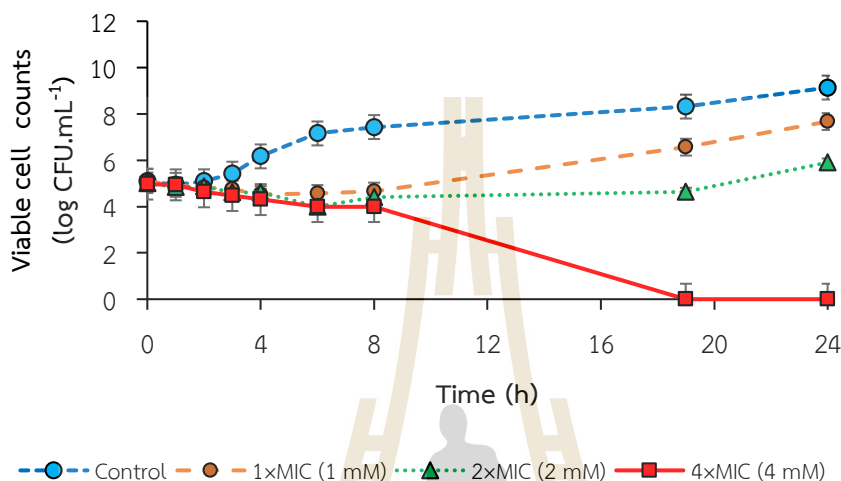


Figure 3.2 Bacterial killing curve of P1 against *Staphylococcus aureus* ATCC 29213 at various concentrations during 24 h incubation. Data are given as mean \pm SD ($n=3$).

3.4.4 Confocal laser scanning microscopy

SYTO-9 is a cell-permeable fluorescent dye that binds to nucleic acids, leading to green fluorescence that can be observed for both live and dead cells (Stiefel, Schmidt-Emrich, Maniura-Weber, & Ren, 2015). In contrast, PI is not cell-permeable and only interacts with nucleic acids in dead cells with membrane disruption. The control (no peptide) showed green fluorescence after staining with SYTO-9, and no red fluorescence of PI was observed, indicating live cells with membrane integrity (Figures 3.3A-C).

In contrast, after exposure to the P1 fraction at 1×MIC and 4×MIC for 8 h, red fluorescence was observed, which increased with higher concentrations (Figures 3.3D-I). These results indicate that treatment with the P1 fraction induced damages to the cell envelopes of *S. aureus*. In addition, some cells exhibited only SYTO-9 fluorescence, suggesting that live cells remained in the presence of the P1 at both 1×MIC and 4×MIC (Figures 3.3D-F). Our results confirmed that the P1 peptides increased membrane permeability and disrupted membrane integrity of bacteria cells.

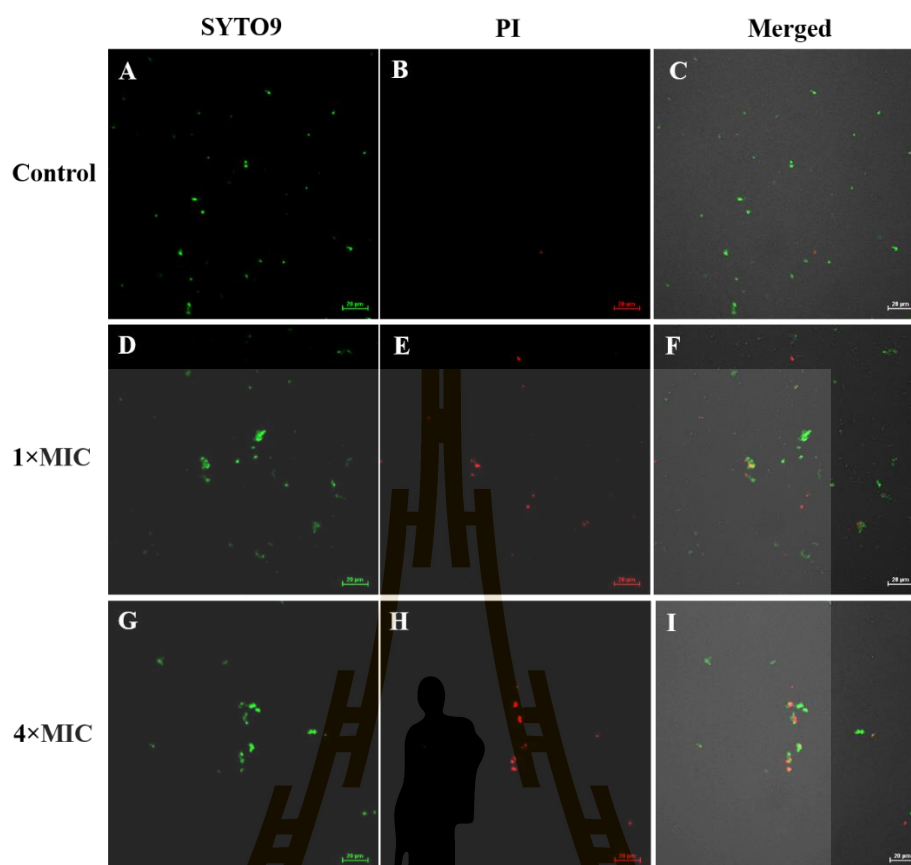


Figure 3.3 Confocal laser scanning micrographs of *Staphylococcus aureus* ATCC 29213 exposed to the P1 and stained with SYTO-9 and propidium iodide (PI). Scale bar is 20 μm .

3.4.5 SEM and TEM

The control without the P1 fraction exhibited intact cells with spherical shape and smooth surfaces in grape-like clusters (Figure 3.4A). After the P1 treatment at 1xMIC, cells appeared slightly collapsed, and several pores were noticed on cell surfaces (Figure 3.4B). At 4xMIC, a deep crater and pores were observed with irregularly spherical appearance (Figure 3.4C). These findings demonstrate that P1 peptides caused significant damages to the *S. aureus* cells.

Hartmann et al. (2010) reported that cationic AMPs, such as gramicidin S and peptidyl-glycylleucine-carboxamide, induced changes in *S. aureus* morphology, including pore formation and lysis. In addition, Zhao et al. (2022) reported morphological changes in the cell membrane of *S. aureus* after exposure to Mop2, a peptide derived from *Moringa oleifera* seeds hydrolysates. Our results suggest that the P1 fraction from CGMH caused morphological changes in *S. aureus*.

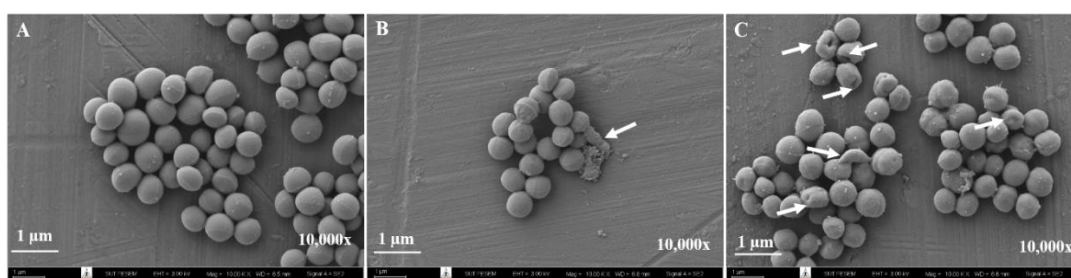


Figure 3.4 Scanning electron micrographs of (A) control *Staphylococcus aureus* ATCC 29213 without peptide; (B) *S. aureus* exposed with P1 at 1xMIC (1 mM); and (C) 4xMIC (4 mM). Scale bars represent 1 µm. Images were taken at 10,000x magnification. White arrows indicate morphological alterations.

TEM microscopy of *S. aureus* induced by the P1 at 1xMIC and 4xMIC exhibited changes in the cell envelope (Figure 3.5). The cell membrane of the control (Figure 3.5A) was intact and visible as a line of electron-dense materials. Cells were rounded with well-defined membranes and intact cell walls. Cells exposed to the P1 at 1xMIC (Figure 3.5B) presented altered outer membranes, mesosome-like structure, disrupted septum, and decreased electron density. After exposure to 4xMIC, the *S. aureus* exhibited severely altered outer cell membranes, resulting in cytoplasm leakage and cell lysis (Figure 3.5C). Hartmann et al. (2010) described the effects of peptidyl-glycylleucine-carboxamide and gramicidin S interacting with the lipid bilayer of *S. aureus*, leading to envelope breakdown and membrane permeability as well as the formation of blisters, protruding bubbles, membrane stacks, mesosomes, deep craters, and cell rupture. Grigor'eva et al. (2020) evaluated *S. aureus* cells exposed to two synthetic cationic peptides, KFFKFFKFFK or RRRRRRRRRFFF, which resulted in the loss of cytoplasmic structure, forming mesosome-derived multimembrane structures, and thin cell walls.

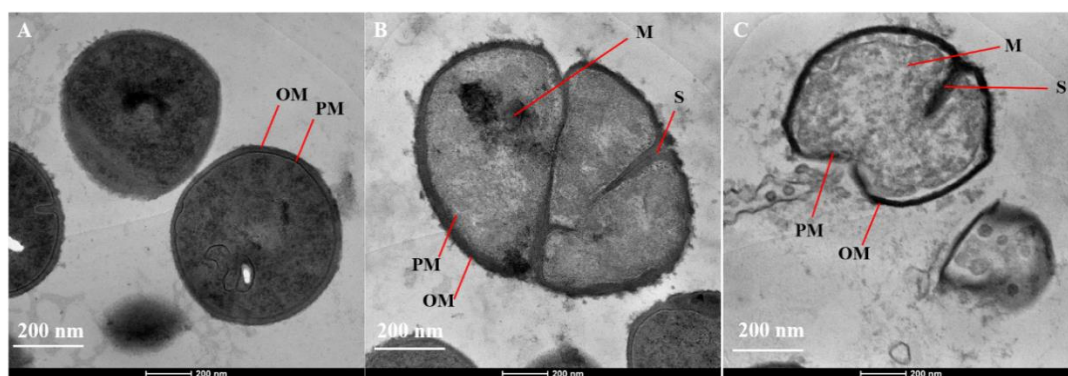


Figure 3.5 Transmission electron micrograph of (A) *Staphylococcus aureus* ATCC 29213 without P-1, control; (B) *S. aureus* after exposure to the P1 at 1×MIC (1 mM) for 8 h; (C) at 4×MIC (4 mM) for 8 h. M = Mesosomes, S = Septum, PM = Plasma membrane, and OM = Outer membrane. Scale bars represent 200 nm.

3.4.6 SR-FTIR

SR-FTIR spectra of *S. aureus* ATCC 29213 cells exposed to the P1 at 1×MIC for various times are shown in Figure 3.6A. The FTIR spectra showed the modifications in cellular compositions in *S. aureus* as indicated in the intensity of the spectral signals at the major peaks at 3297, 2963, 2925, 2854, 1747, 1654, 1546, 1454, 1398, 1238, 1083, and 964 cm^{-1} . FTIR spectra of bacterial cells can be categorized as region I for fatty acids (3100-2800 cm^{-1}), region II for amide groups of proteins and peptides (1800-1500 cm^{-1}), region III for mixed functional groups of fatty acids, proteins, and phosphate carrier molecules (1500-1200 cm^{-1}), and the region IV designated for nucleic acids, DNA, and RNA (1200-900 cm^{-1}) (Lasch & Naumann 2015). All regions exhibited strong SR-FTIR absorption, revealing the main functional groups of cellular components of *S. aureus* (Figure 3.6A). The native spectra pattern is aligned with the previous reports of Wongthong et al. (2020). Secondary derivatives of spectra, which exhibited significant modifications of fatty acids, were observed at 2963 and 2925 cm^{-1} after the P1 exposure (Figure 3.6B). Shifts of bands 1654 and 1546 cm^{-1} in the amide I region and amide II region of proteins were also evident in the P1-treated samples (Figure 3.6C). In addition, the peak shifts at 1454 and 1398 cm^{-1} bands representing the asymmetric methyl deformation and CH_3 symmetric deformation were noted. Moreover, changes at 1238 cm^{-1} , corresponding to the phosphate group (P=O) asymmetric stretching of phosphodiester in phospholipids and RNA (Davis & Mauer, 2010), and at 1083 cm^{-1} corresponding to a symmetric phosphate stretching in DNA,

RNA, and phospholipids (Yu & Irudayaraj, 2005) were evident after prolonged exposure to the P1 peptides.

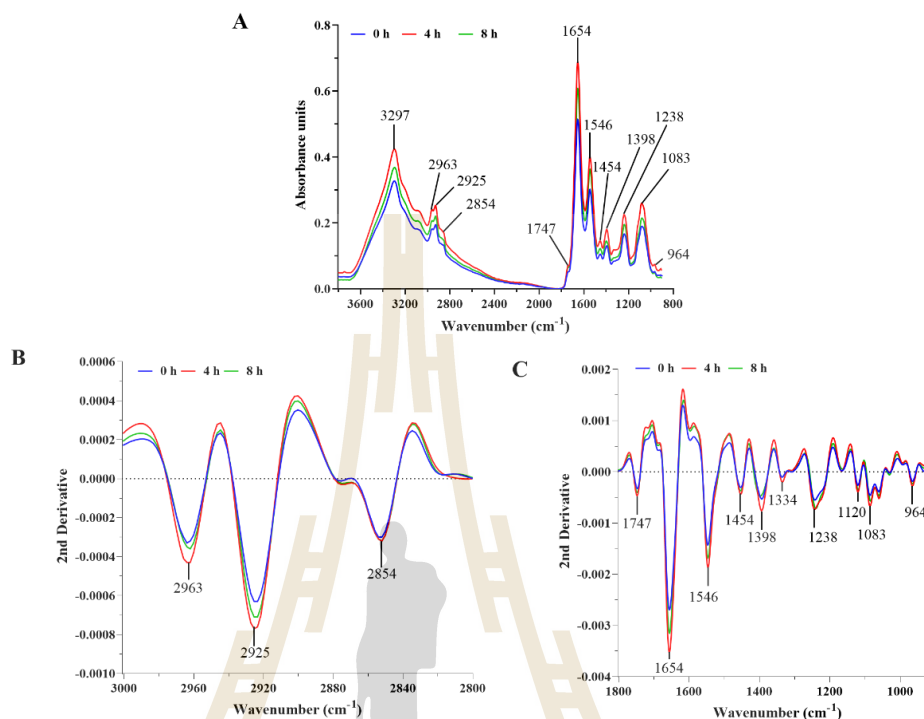


Figure 3.6 The original SR-FTIR spectra of *Staphylococcus aureus* ATCC 29213 exposed to P1 at 1xMIC in 0, 4, and 8 h for region 3800-900 cm^{-1} (A); The secondary derivative spectra of *S. aureus* exposed to P1 at 1xMIC in 0, 4, and 8 h for region 3000-2800 cm^{-1} (B); The secondary derivative spectra of *S. aureus* exposed to P1 at 1xMIC in 0, 4, and 8 h for region 1800-900 cm^{-1} (C). Three replicates of measurements were averaged.

Table 3.2 shows changes in the integral area of the wavenumbers related to potential biomolecules in *S. aureus* cells induced by the P1 fraction at 1xMIC for 0, 4, and 8 h. Integral areas at wavenumbers of 2963, 2925, 1454, and 1398 cm^{-1} , which are related to the symmetric and asymmetric vibrations of CH groups in fatty acids, increased after exposing to the P1 peptides, suggesting disruption of the cell membrane of *S. aureus*. In addition, an increase in the spectra of amide I at 1654 cm^{-1} and amide II at 1546 cm^{-1} , related to C=O vibration stretching, C-N vibration stretching, and N-H vibration bending of protein, was also observed. Furthermore, changes in nucleic acids at 1238 and 1083 cm^{-1} corresponding to asymmetric stretching of PO_2^- and stretching of PO_2^- were notable. Therefore, these findings describe the significant

alterations in the cell membrane, proteins, and nucleic acids after P1 treatment at 1×MIC for 4 h.

Table 3.2 Integration area ($\times 10^{-4}$) at various wavenumbers of secondary derivative spectra of *Staphylococcus aureus* ATCC 29213 exposed to the P1 fraction at 1×MIC with different exposure times.

Wave number (cm^{-1})	The biochemical component assignment	Exposure time (h)		
		0	4	8
2963	Fatty acids	46.67 ^a	66.67 ^b	50.00 ^a
2925	Fatty acids	103.33 ^a	130.00 ^b	120.00 ^{ab}
2854	Fatty acids	36.67 ^a	36.67 ^a	36.67 ^a
1747	Lipid esters	46.67 ^a	66.67 ^b	60.00 ^b
1654	Amide I (Proteinaceous compounds)	713.33 ^a	926.67 ^b	803.33 ^a
1546	Amide II (Proteinaceous compounds)	326.67 ^a	436.67 ^b	380.00 ^{ab}
1454	The cell membrane (lipids, proteins)	66.67 ^a	93.33 ^b	80.00 ^c
1398	The cell membrane (amino acids, fatty acids)	123.33 ^a	180.00 ^b	100.00 ^c
1238	Phosphodiester in nucleic acid	136.67	250.00	240.00
1120	Phosphodiester in nucleic acid	60.00	36.67	30.00
1083	DNA and RNA, phospholipids	100.00	180.00	193.33
964	DNA and RNA, phospholipids	20.00	30.00	30.00

The different letters in the same row indicate significant differences ($p < 0.05$)

Principal component analysis (PCA) rationalized the multivariate dataset and distinguished within the control and treated cells. The two-dimensional PCA score plot (Figure 3.7A) demonstrated that spectra of *S. aureus* cells administered with P1 at 1×MIC for 0, 4, and 8 h are clearly separated within PC1 (40%) and PC2 (15%). The PCA reading on the PC1 axis revealed that 0 h and 4 h treatments were well segregated from the 8 h treatment. The 8 h treatment was associated with the PC1 loading plot of wavenumbers 2954, 1730, 1625, 1523, 1415, 1238, and 950 cm^{-1} , which indicated a modification of fatty acids, proteins, and nucleic acids in the *S. aureus* cells treated with the P1 peptides for 8 h (Figure 3.7B). The 8 h treatment was found to be associated with the highest positive value of PC1 loading in the protein region at 1625 cm^{-1} and nucleic acids at 1238 cm^{-1} , in contrast to the 0 and 4 h treatments which correlated with high negative values of PC1 loading at 1392 cm^{-1} (fatty acids), 1255 cm^{-1}

¹ (proteins), and 1097 cm^{-1} (nucleic acids) (Figure 3.7B). These results implied significant changes of intracellular proteins and nucleic acids upon prolonged treatment with the P1 peptides. The PCA reading over the PC2 axis indicated that the control was separated from the 4-h and 8-h treated groups. The control (0 h) group is predominantly associated with the high positive value of PC2 loading at 2919 cm^{-1} (fatty acids), 1733 and 1650 cm^{-1} (proteins), and 1018 and 933 cm^{-1} (nucleic acids). In contrast, the 4-h and 8-h treated groups were correlated with the highest negative value of PC2 loading in the protein region at 1625 cm^{-1} and nucleic acids at 1087 cm^{-1} (Figure 3.7C), which showed an alteration of intracellular proteins and nucleic acids of *S. aureus* cells treated with the P1 fraction.

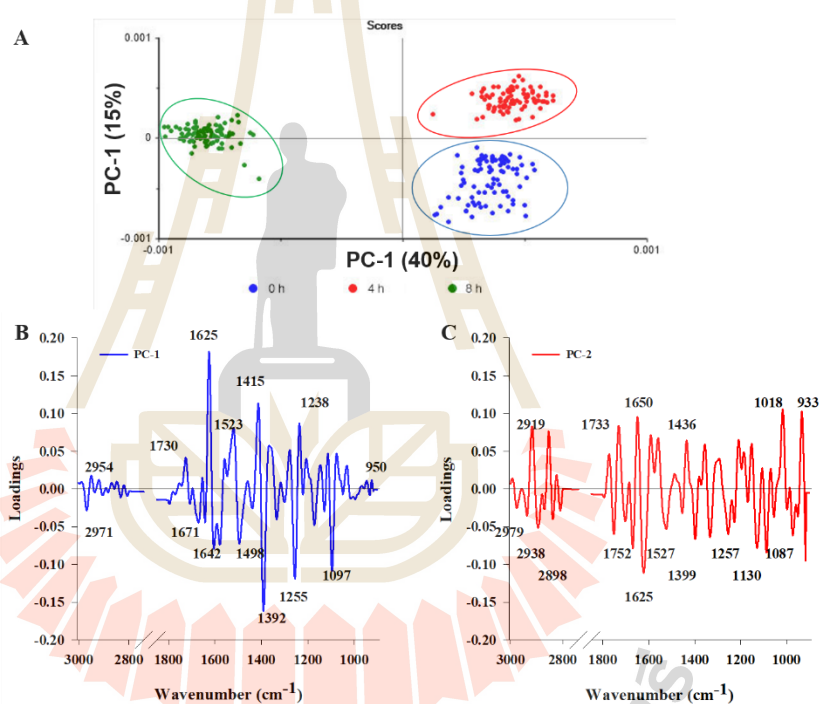


Figure 3.7 2D-PCA score (A), loading plots PC-1 (B) and PC-2 (C) of spectra data for *Staphylococcus aureus* ATCC 29213 treated with P1 at 1xMIC for 0, 4, and 8 h

The following analyses assessed the PCA between *S. aureus* control and cells treated with P1 at 1xMIC incubated at 4 and 8 h, as shown in Figure 3.8. The biplot-PCA score on 4 h incubation (Figure 3.8A) shows that the control cells and cells treated with P1 1xMIC are distinctively distinguished with PC1 46% and PC2 9%. The treatment effect of P1 at 1xMIC against cells for 4 h in the negative of PC1 in the 2D-PCA score corresponded with the positive loading plot PC1 at wavenumbers 2938, 1627,

1392, 1255, 1126 and 973 cm^{-1} (Figure 3.8B). This result suggested alterations in the fatty acid, proteins and nucleic acid in the cell membrane of *S. aureus* treated with P1 at 1xMIC for 4 h.

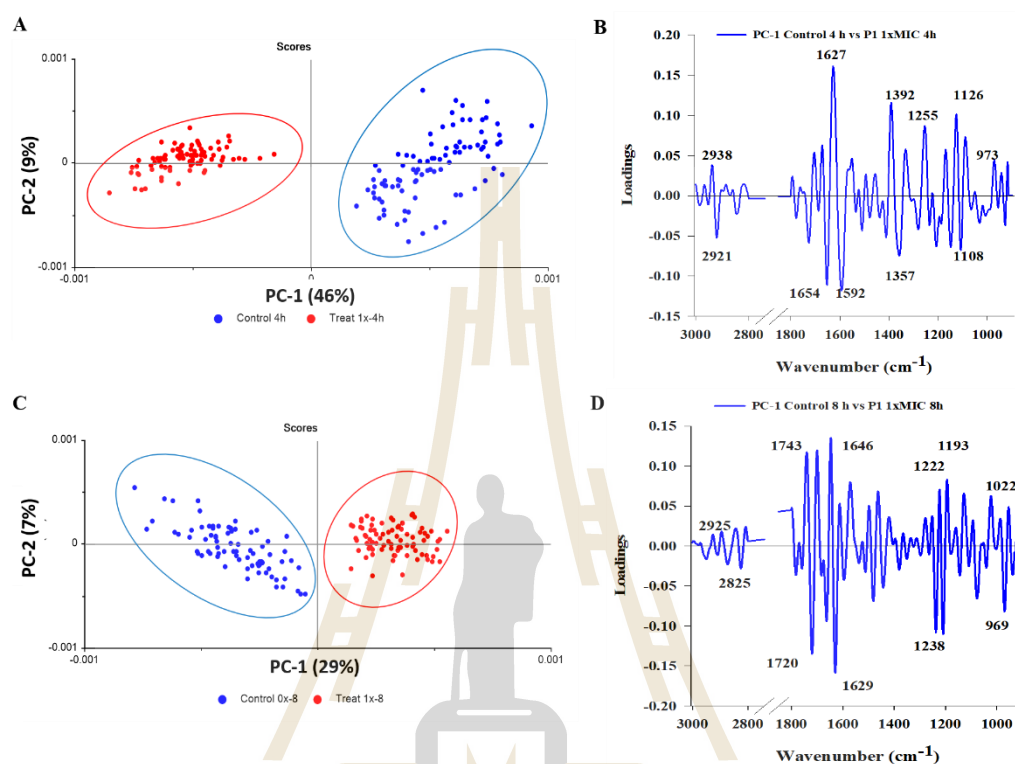


Figure 3.8 PCA analysis results (A) the 2D-PCA score and (B) loading plot of PC-1 from control *Staphylococcus aureus* ATCC 29213 cells and the cells treated with P1 at 1xMIC for 4 h at 37 °C; (C) the 2D-PCA score and (D) loading plot of PC-1 from control *S. aureus* cells and the cells treated with P1 at 1xMIC for 8 h at 37 °C.

Furthermore, the 2D-PCA score of control cells and cells infected with P1 at 1xMIC for 8 h showed good separation with PC1 29% and PC2 7% (Figure 3.8C). The impact of P1 treatment at 1xMIC for 8 h on cells in positive PC1 on the biplot PCA score corresponds to the negative loading plot of PC1 at wavenumbers 2825, 1720, 1629, 1238, and 969 cm^{-1} (Figure 3.8D). These results demonstrated that there were changes in the fatty acids, proteins, and nucleic acids in the cell membrane of *S. aureus* cells induced with P1 at 1xMIC for 8 h.

3.4.7 Antimicrobial stability of P1

The P1 fraction sustained its antibacterial action even after incubation at 40-100 °C for 1 h (Figure 3.8A). Heating at 100 °C for 1 h resulted in a slight decrease in antimicrobial activity but comparable to the control ($p > 0.05$). These results indicate that antimicrobial activity of the P1 fraction showed stability at high temperatures, thus, could be applied in thermally processed food products. Baidara et al. (2016) reported that penisin, a peptide isolated from *Paenibacillus* sp., maintained its antimicrobial action when heated to 100 °C for 30 min but diminished at 121 °C. Antibacterial peptides derived from cottonseed protein also possessed thermal stability in a wide range of 4-120 °C (Song et al., 2020).

The P1 fraction displayed antibacterial activity at a pH range of 4.5-6.5 (Figure 3.8B). When pH changes, charges of peptides would be modified in conjunction with conformation. Beaulieu et al. (2010) showed that the antibacterial activity of the peptide fraction isolated from snow crab by-products remained stable at pH 5-9. In addition, Song et al. (2020) revealed the stability of antibacterial peptides derived from cottonseed protein at pH 3-9.

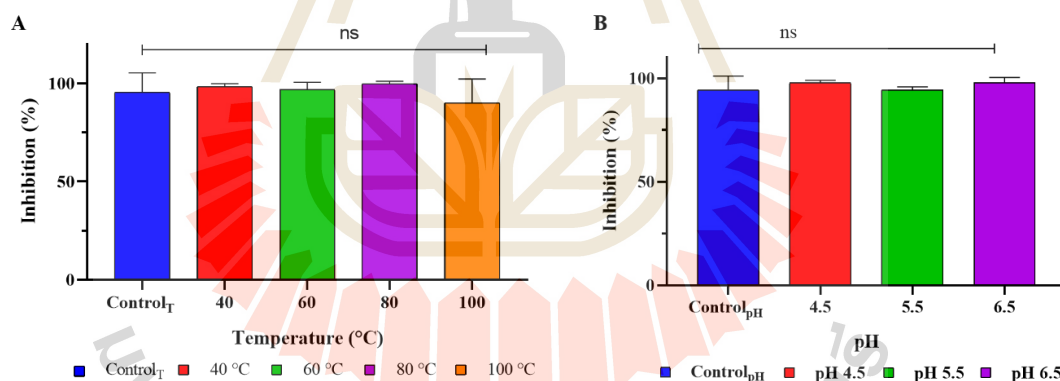


Figure 3.9 Effect of various temperatures (A) and pHs (B) on antibacterial activity of P1 at 1×MIC against *Staphylococcus aureus* ATCC 29231; control_T = no heat treatment; control_{pH} = peptide in DI water.

3.4.8 Hemolysis activity assay

The P1 fraction induced hemolysis in a dose-dependent manner up to 8 mM (Figure 3.9). The highest hemolysis of 5.2% was found at 8 mM, equivalent to 8×MIC. This result indicated that the P1 fraction exhibited low hemolytic activity at 1 and 4 mM, which were MIC and MBC values. It should be mentioned that the hemolysis rate at 8 mM was still lower than 10%. Hemolysis rates >10% can potentially cause red

blood cell lysis, which indicates toxicity (Greber, Dawgul, Kamysz, & Sawicki, 2017). Therefore, the low hemolysis rate primarily suggested that the P1 fraction could be considered safe for food applications. Hu et al. (2016) studied an antibacterial peptide from chicken hemoglobin hydrolyzed with papain and found no hemolytic up to 0.36 mg.mL^{-1} . Furthermore, Ghanbari & Ebrahimpour (2018) reported that an antibacterial peptide derived from bromelain hydrolysate of sea cucumber with MIC of 3.1 mg.mL^{-1} had no hemolytic activity at 6.2 mg.mL^{-1} .

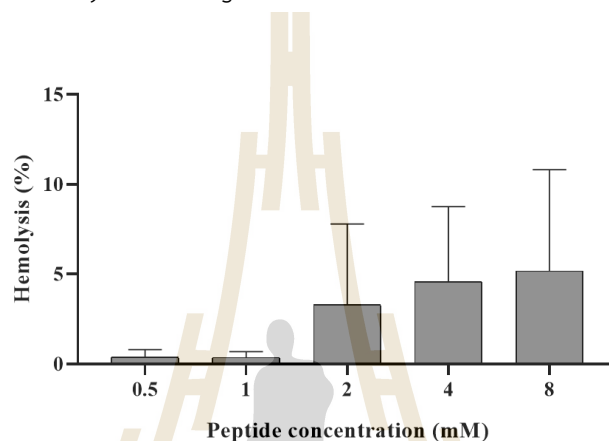


Figure 3.10 The hemolytic activity of P1 fraction on human red blood cells. Data are given as mean \pm SD ($n = 3$).

3.4.9 Application in milk

Antimicrobial activity of the P1 fraction in food was demonstrated using a commercial UHT milk inoculated with *S. aureus* ATCC 29213 as a model. Enterotoxigenic *S. aureus* may be found in milk and dairy products (Deddefo, Mamo, Leta, & Amenu, 2022). The control (no peptide) exhibited an increase in cell counts from 3.6 to $10.5 \text{ log CFU.mL}^{-1}$ within 24 h (Figure 3.10). Addition of the P1 fraction at 1-4xMIC inhibited *S. aureus* growth only in the first 2 h, and an increase in cell numbers to 8-9 log CFU.mL^{-1} was observed after 12 h. In contrast, the P1 fraction at 8xMIC (8 mM) stabilized the number of cells ($3 \text{ log CFU.mL}^{-1}$) up to 12 h and gradually decreased to undetectable at 24 h. The effective concentration of 8 mM in milk is higher than the MBC determined in the MHB broth, which was found to be 4 mM (Table 3.1). The decline in antibacterial activity may be due to interactions of peptides and milk proteins, fats, or carbohydrates (Wang, Dekker, Heising, Zhao, & Fogliano, 2023). These results are in agreement with the study of Pu & Tang (2017a) who reported the inhibition of *S. aureus* ATCC 25923 in pasteurized whole milk by GLSRLFTALK, an antibacterial

peptide derived from anchovy cooking wastewater protein with MIC at $16 \mu\text{g}\cdot\text{mL}^{-1}$. Moreover, Yang et al. (2020) also reported a peptide FTKPGVCPRRRWGAG derived from *Larimichthys crocea* whey acidic protein inhibited and reduced *S. aureus* ATCC 27217 growth in sterilized milk at $31.2 \mu\text{g}\cdot\text{mL}^{-1}$, while the MIC was $15.6 \mu\text{g}\cdot\text{mL}^{-1}$. These results showed feasibility of the use of P1 peptides derived from CGMH as “natural” antibacterial agents in foods.

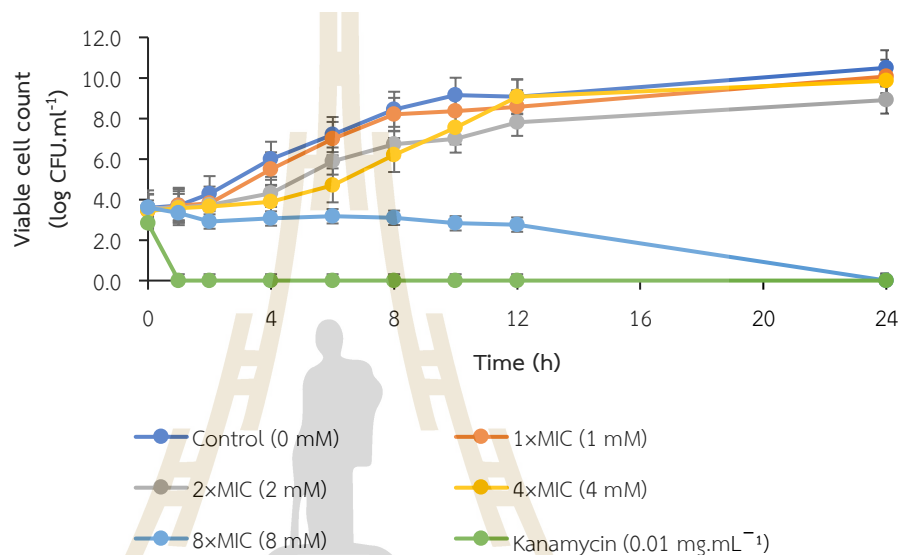


Figure 3.11 Antibacterial effect of the P1 against the *Staphylococcus aureus* ATCC 29213 growth inoculated in UHT milk at 37 °C for 24 h. Each data point was given as mean \pm SD ($n=3$).

3.4.10 Peptide identification

Eleven peptides were identified and showed similarities to the amino sequences of corn (Table 3.3). All identified peptides exhibited molecular mass ranging from 915 to 1894 Da. Seven cationic peptides containing Lys (K), Arg (R), and His (H) exhibited a net charge of +2 to +4. Four anionic peptides containing Glu (E), Asp (D), and Gln (Q) had a net charge of -3 to -1. Wang (2022) explained that peptides in the Antimicrobial Peptide Database were recognized as 88% cationic, 6% neutral, and 6% anionic AMPs. A cationic AMP increases membrane permeability and facilitates the release of cellular contents by electrostatically binding to negatively charged bacterial membranes (Zhang et al., 2021). In contrast, anionic AMP interacts with bacteria by attaching to metal ions and establishing cationic salt links with their negatively charged membranes (Harris, Dennison, & Phoenix, 2009). Furthermore, Almarwani, Phambu, Hamada, & Sunda-Meya (2020) observed that the complex of Zn ions with anionic

antibacterial peptides interacted with negatively charged phospholipids, causing membrane disruption in the membrane model. Therefore, it can be suggested that the presence of cationic and anionic peptides may have synergistically contributed to the observed antibacterial activity of the P1 fraction.

The hydrophobicity of 11 peptides varied from 0 to 50%. The cationic peptides such as PTGAKVTKAAKKA, PTGAKVTKAAKA, LKNGKKVE, APRPSSPHKA, PEPSKSAPAPKKLSSL, KQQAAPPPKAKQ, and PTGAKKGGKHLKQ possessed hydrophobicity ranging from 25 to 50%. Whereas the anionic peptides like EAGGGEDDKKKVE, KQVHPDTE, ERSNSSSGSGEQKEDQKE, and EGVEEEQGGGGGQKSATA exhibited hydrophobicity varying from 0 to 25%. Hydrophobicity properties of peptides are essential for permeabilizing bacterial membranes (Edwards et al., 2016). The ability of water-soluble AMPs to penetrate the membrane lipid bilayer is determined by their hydrophobicity (Kumar, Kizhakkedathu, & Straus, 2018). In addition, Chen et al. (2007) found that peptides have optimal antimicrobial activity when they reach a certain hydrophobicity threshold. Our results indicate that 11 peptides exhibited varying hydrophobicity, which may contribute to the antibacterial activity of the P1 fraction.

The grand average of hydropathicity index (GRAVY) represents peptide hydrophobicity by summing up all of the amino acid hydropathy values and dividing by the amino acid sequence length (Kyte & Doolittle, 1982). A positive GRAVY value indicates hydrophobic nature, and a negative value suggests hydrophilic characteristics. The calculated GRAVY value ranged from -2.606 to -0.308, indicating hydrophilic nature. As displayed in Table 3.3, peptides EAGGGEDDKKKVE, KQVHPDTE, LKNGKKVE, APRPSSPHKA, ERSNSSSGSGEQKEDQKE, KQQAAPPPKAKQ, EGVEEEQGGGGGQKSATA and PTGAKKGGKHLKQ possessed negative GRAVY values, indicating high hydrophilic character (Sahay, Piprodhe, & Pise, 2020). These positively charged peptides are likely to interact strongly with bacterial membranes. In addition, AMPs with enhanced activity has higher amphiphilic and hydrophobic properties with a positive GRAVY value (Xie et al., 2019). Therefore, peptides PTGAKVTKAAKKA with a positive net charge, hydrophobicity more than 25%, and a high negative GRAVY value might contribute to the antibacterial ability of the P1 fraction. These results suggest that the P1 fraction contained various peptides with potential characteristics of AMPs.

The secondary structure of peptides plays an important role in the interactions with bacterial cell membranes (Liang, Zhang, Yuan, Bao, & Xiong, 2020). Most peptides exhibited random coil structures (Table 3.3). Only 2 peptides,

ERSNSSGSGEQKEDQKE and EGVEEEQGGGGGQKSATA, exhibited both α -helix and random coil structure. Cardoso et al. (2021) reported that a peptide with a random coil structure transformed into α -helical conformation when interacting with lipid membranes. This structure modification is generally known as a coil-to-helix transition (Makhlynets & Caputo, 2021).

The peptide identification (Table 3.3) indicates that the 11 peptides in the P1 fraction of CGMH have distinct structural properties. These peptides are suggested to synergistically contribute to anti-staphylococci activity of the P1 fraction. Therefore, further testing is needed to determine the most potent antibacterial peptide(s) in the P1 fraction.

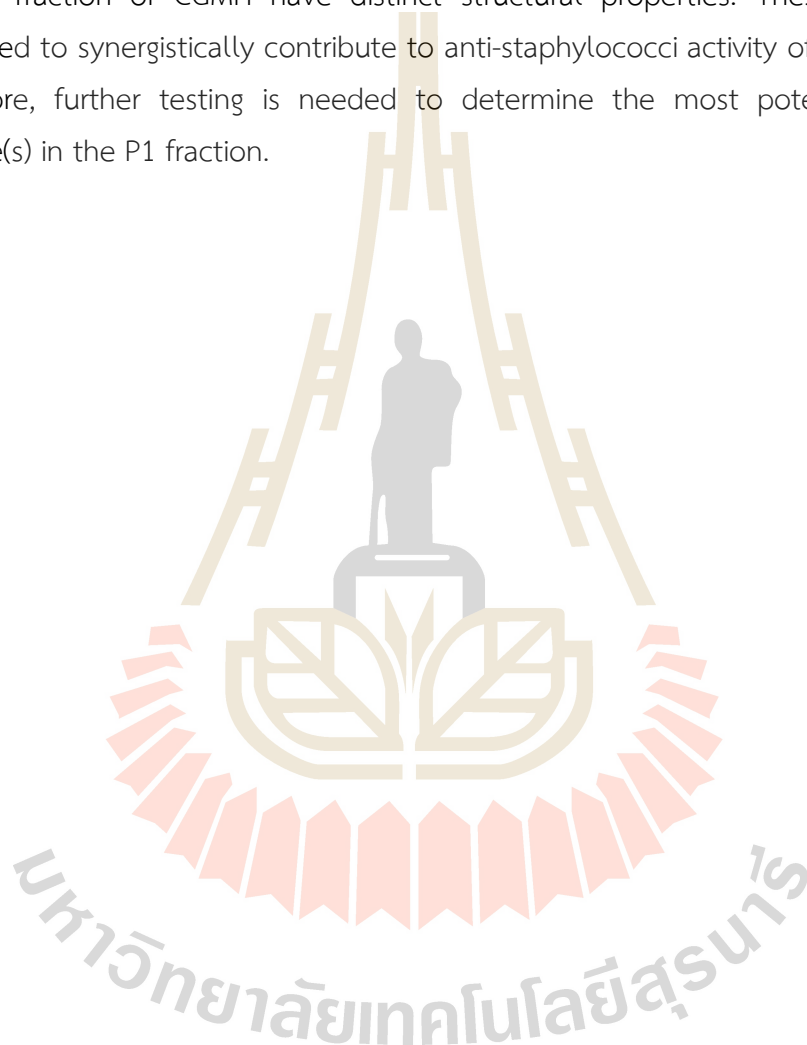


Table 3.3 Identification of selected peptides from P1 fraction obtained from pepsin-hydrolyzed corn gluten meal.

Amino acid sequence	Parent protein	Database	<i>de novo</i> score	Molecular weight (Da) ^a	Net charge ^a	Hydrophobicity (%) ^a	GRAVY index ^b	Secondary structure ^c
EAGGGEDDKKKVE	Adenine nucleotide transporter BT1	UniProtKB id: P29518	98	1361.41	-2	15.38	-1.877	Random coil (100%)
PTGAKVTKAAKKA	Elongation factor 1- α	UniProtKB id: Q41803	98	1270.52	+4	46.15	-0.585	Random coil (100%)
PTGAKVTKAAKA	Elongation factor 1- α	UniProtKB id: Q41803	98	1142.35	+3	50	-0.308	Random coil (100%)
KQVHPDTE	Histone H2B.5	UniProtKB id: P54348	95	953.017	-1	25	-1.963	Random coil (100%)
LKNGKKVE	Eukaryotic translation initiation factor 5A	UniProtKB id: P80639	94	915.09	+2	25	-1.388	Random coil (100%)
APRPSSPHKA	40S ribosomal protein S4	UniProtKB id: O22424	89	1047.179	+2	50	-1.440	Random coil (100%)
PEPSKSAPAPKKLSSL	Histone deacetylase HDT3	UniProtKB id: Q9M4U4	86	1636.899	+2	50	-0.850	Random coil (100%)
ERSNSSSGEGQKEDQKE	Homeotic protein knotted-1	UniProtKB id: P24345	85	1894.878	-2	0	-2.606	α -Helix (11.76%) Random coil (88.24%)
KQQAAPPKAKQ	GRF-Interacting factor 10	UniProtKB id: A5HEG9	84	1291.506	+3	50	-1.800	Random coil (100%)
EGVEEEQGGGGQKSATA	Albumin b-32	UniProtKB id: P10593	81	1690.697	-3	16.67	-1.167	α -Helix (22.22%) Extended strand (16.67%) Random coil (61.11%)
PTGAKKGKHLKQ	Histone H1	UniProtKB id: P23444	79	1292.532	+4	25	-1.650	Random coil (100%)

^aMolecular weight, net charge, and hydrophobicity were calculated with peptide2.0 (<https://www.peptide2.com/>)

^bGRAVY (grand average of hydropathicity) index was generated with the ProtParam utility provided at the Expert Protein Analysis System (ExPASy) Server (<https://web.expasy.org/protparam/>). It represents the degree of peptide solubility: positive GRAVY (hydrophobic) and negative GRAVY (hydrophilic);

^cThe values determined according to an analysis of the network protein sequences (<https://npsa-prabi.ibcp.fr/>) using SOPMA (secondary structure consensus prediction)

3.5 Conclusion

This is the first study demonstrating that the P1 peptide fraction derived from CGMH exhibited the most potent antibacterial activity against *S. aureus* ATCC 29213. The P1 killed *S. aureus* ATCC 29213 within 8 h at 4×MIC. Moreover, it caused membrane disintegration and perturbation of the outer membrane as well as intracellular components, including fatty acids, proteins, and nucleic acids of *S. aureus* ATCC 29213. Antibacterial activity remained even exposing to 100 °C for 1 h. The P1 also suppressed the growth of *S. aureus* ATCC 29213 inoculated in the commercial UHT milk. Eleven potential antimicrobial peptides were identified with cationic and anionic characteristics. The P1 fraction from CGMH could be potential antimicrobial agent for controlling *S. aureus* in foods.

3.6 References

- Adler-Nissen, J. (1979). Determination of the degree of hydrolysis of food protein hydrolysates by trinitrobenzenesulfonic acid. *Journal of Agricultural and Food Chemistry*, 27(6), 1256–1262.
- Ahmed, T. A. E., & Hammami, R. (2018). Recent insights into structure–function relationships of antimicrobial peptides. *Journal of Food Biochemistry*, 43, e12546.
- Al Kashgry, N. A. T., Abulreesh, H. H., El-Sheikh, I. A., Almaroai, Y. A., Salem, R., Mohamed, I., ... Mohamed, M. S. M. (2020). Utilization of a recombinant defensin from maize (*Zea mays* L.) as a potential antimicrobial peptide. *AMB Express*, 10(1), 208.
- Almarwani, B., Phambu, N., Hamada, Y. Z., & Sunda-Meya, A. (2020). Interactions of an anionic antimicrobial peptide with zinc(II): Application to bacterial mimetic membranes. *Langmuir*, 36(48), 14554–14562.
- Altschul, S. F., Madden, T. L., Schäffer, A. A., Zhang, J., Zhang, Z., Miller, W., & Lipman, D. J. (1997). Gapped BLAST and PSI-BLAST: A new generation of protein database search programs. *Nucleic Acids Research*, 25(17), 3389–3402.
- Baindara, P., Chaudhry, V., Mittal, G., Liao, L. M., Matos, C. O., Khatri, N., ... Korpole, S. (2016). Characterization of the antimicrobial peptide penisin, a class Ia novel lantibiotic from *Paenibacillus* sp. strain A3. *Antimicrobial Agents and Chemotherapy*, 60(1), 580–591.
- Beaulieu, L., Thibodeau, J., Desbiens, M., Saint-Louis, R., Zatylny-Gaudin, C., & Thibault, S. (2010). Evidence of antibacterial activities in peptide fractions originating from snow crab (*Chionoecetes opilio*) by-products. *Probiotics and Antimicrobial Proteins*, 2, 197–209.

- Cardoso, P., Glossop, H., Meikle, T. G., Aburto-Medina, A., Conn, C. E., Sarojini, V., & Valery, C. (2021). Molecular engineering of antimicrobial peptides: microbial targets, peptide motifs and translation opportunities. *Biophysical Reviews*, *13*(1), 35–69.
- Chai, T. T., Tan, Y. N., Ee, K. Y., Xiao, J., & Wong, F. C. (2019). Seeds, fermented foods, and agricultural by-products as sources of plant-derived antibacterial peptides. *Critical Reviews in Food Science and Nutrition*, *59*(sup1), S162–S177.
- Chanajon, P., Girgih, A. T., Oluwagunwa, O. A., Aluko, R. E., & Yongsawatdigul, J. (2024). Long-term intake of corn gluten meal protein hydrolysate attenuated hypertension development and modulated associated plasma metabolite levels in spontaneously hypertensive rats. *Journal of Functional Foods*, *117*, 106231.
- Chanajon, P., Noisa, P., & Yongsawatdigul, J. (2022). Prolyl oligopeptidase inhibition and cellular antioxidant activities of a corn gluten meal hydrolysate. *Cereal Chemistry*, *99*(6), 1183–1195.
- Chen, Y., Guarnieri, M. T., Vasil, A. I., Vasil, M. L., Mant, C. T., & Hodges, R. S. (2007). Role of peptide hydrophobicity in the mechanism of action of α -helical antimicrobial peptides. *Antimicrobial Agents and Chemotherapy*, *51*(4), 1398–1406.
- Combet, C., Blanchet, C., Geourjon, C., & Deléage, G. (2000). NPS@: Network protein sequence analysis. *Trends in Biochemical Sciences*, *25*(3), 147–150.
- Corrêa, J. A. F., de Melo Nazareth, T., Rocha, G. F. da, & Luciano, F. B. (2023). Bioactive antimicrobial peptides from food proteins: Perspectives and challenges for controlling foodborne pathogens. *Pathogens*, *12*(3), 477.
- Davis, R., & Mauer, L. (2010). Fourier transform infrared (FT-IR) spectroscopy: A rapid tool for detection and analysis of foodborne pathogenic bacteria. In Méndez-Vilas, A. (Ed.). *Current Research, Technology and Education Topics in Applied Microbiology and Microbial Biotechnology* (pp. 1582–1594). Badajoz: Formatex Research Center.
- de Almeida, N. R., Han, Y., Perez, J., Kirkpatrick, S., Wang, Y., & Sheridan, M. C. (2019). Design, synthesis, and nanostructure-dependent antibacterial activity of cationic peptide amphiphiles. *ACS Applied Materials and Interfaces*, *11*(3), 2790–2801.
- Deddefo, A., Mamo, G., Leta, S., & Amenu, K. (2022). Prevalence and molecular characteristics of *Staphylococcus aureus* in raw milk and milk products in Ethiopia: a systematic review and meta-analysis. *International Journal of Food Contamination*, *9*, 8.
- Duvick, J. P., Rood, T., Rao, A. G., & Marshak, D. R. (1992). Purification and characterization of a novel antimicrobial peptide from maize (*Zea mays* L.) kernels. *Journal of*

- Biological Chemistry*, 267(26), 18814–18820.
- Edwards, I. A., Elliott, A. G., Kavanagh, A. M., Zuegg, J., Blaskovich, M. A. T., & Cooper, M. A. (2016). Contribution of amphipathicity and hydrophobicity to the antimicrobial activity and cytotoxicity of β -hairpin peptides. *ACS Infectious Diseases*, 2(6), 442–450.
- Fung, F., Wang, H. S., & Menon, S. (2018). Food safety in the 21st century. *Biomedical Journal*, 41(2), 88–95.
- Ghanbari, R., & Ebrahimpour, A. (2018). Separation and identification of bromelain-generated antibacterial peptides from *Actinopyga lecanora*. *Food Science and Biotechnology*, 27(2), 591–598.
- Greber, K. E., Dawgul, M., Kamysz, W., & Sawicki, W. (2017). Cationic net charge and counter ion type as antimicrobial activity determinant factors of short lipopeptides. *Frontiers in Microbiology*, 8, 123.
- Grigor'eva, A., Bardasheva, A., Tupitsyna, A., Amirkhanov, N., Tikunova, N., Pyshnyi, D., & Ryabchikova, E. (2020). Changes in the ultrastructure of *Staphylococcus aureus* treated with cationic peptides and chlorhexidine. *Microorganisms*, 8(12), 1–19.
- Hafeez, A. B., Jiang, X., Bergen, P. J., & Zhu, Y. (2021). Antimicrobial peptides: An update on classifications and databases. *International Journal of Molecular Sciences*, 22, 11691.
- Hardwick, J. E., & Glatz, C. E. (1989). Enzymatic hydrolysis of corn gluten meal. *Journal of Agricultural and Food Chemistry*, 37(4), 1188–1192.
- Harris, F., Dennison, S., & Phoenix, D. (2009). Anionic antimicrobial peptides from eukaryotic organisms. *Current Protein & Peptide Science*, 10(6), 585–606.
- Hartmann, M., Berditsch, M., Hawecker, J., Ardakani, M. F., Gerthsen, D., & Ulrich, A. S. (2010). Damage of the bacterial cell envelope by antimicrobial peptides gramicidin S and PGLa as revealed by transmission and scanning electron microscopy. *Antimicrobial Agents and Chemotherapy*, 54(8), 3132–3142.
- Hou, Z., Lu, J., Fang, C., Zhou, Y., Bai, H., Zhang, X., ... Luo, X. (2011). Underlying mechanism of in vivo and in vitro activity of C-terminal-amidated thanatin against clinical isolates of extended-spectrum β -lactamase-producing *Escherichia coli*. *The Journal of Infectious Diseases*, 211, 273–282.
- Hu, F., Wu, Q., Song, S., She, R., Zhao, Y., Yang, Y., .. Shi, R. (2016). Antimicrobial activity and safety evaluation of peptides isolated from the hemoglobin of chickens. *BMC Microbiology*, 16, 287.
- Kang, Y.-Ju., Yi, S.-D., Lee, G.-H., & Oh, M.-J. (2006). Antibacterial activity of zein hydrolysate with pepsin. *Journal of Korean Society of Food Science and Nutrition*, 35(2), 127–131.

- Kant, P., Liu, W. Z., & Pauls, K. P. (2009). PDC1, a corn defensin peptide expressed in *Escherichia coli* and *Pichia pastoris* inhibits growth of *Fusarium graminearum*. *Peptides*, *30*(9), 1593–1599.
- Kerenga, B. K., McKenna, J. A., Harvey, P. J., Quimbar, P., Garcia-Ceron, D., Lay, F. T., ... & Bleackley, M. R. (2019). Salt-tolerant antifungal and antibacterial activities of the corn defensin ZmD32. *Frontiers in Microbiology*, *10*, 795.
- Kim, J. M., Whang, J. H., Kim, K. M., Koh, J. H., & Suh, H. J. (2004). Preparation of corn gluten hydrolysate with angiotensin I converting enzyme inhibitory activity and its solubility and moisture sorption. *Process Biochemistry*, *39*(8), 989–994.
- Kopparapu, N. K., Duan, Y., Huang, L., & Katrolia, P. (2022). Review on utilisation of corn gluten meal, a by-product from corn starch industry for production of value-added products. *International Journal of Food Science and Technology*, *57*(9), 5592–5599.
- Kumar, P., Kizhakkedathu, J. N., & Straus, S. K. (2018). Antimicrobial peptides: Diversity, mechanism of action and strategies to improve the activity and biocompatibility in vivo. *Biomolecules*, *8*(1), 4.
- Kyte, J., & Doolittle, R. F. (1982). A simple method for displaying the hydropathic character of a protein. *Journal of Molecular Biology*, *157*(1), 105–132.
- Lasch, P., & Naumann, D. (2015). Infrared spectroscopy in microbiology. In *Encyclopedia of Analytical Chemistry* (pp. 1–32). Hoboken, NJ: John Wiley & Sons, Inc.
- Lee, N. K., & Paik, H. D. (2016). Status, antimicrobial mechanism, and regulation of natural preservatives in livestock food systems. *Korean Journal for Food Science of Animal Resources*, *36*(4), 547–557.
- Liang, Y., Zhang, X., Yuan, Y., Bao, Y., & Xiong, M. (2020). Role and modulation of the secondary structure of antimicrobial peptides to improve selectivity. *Biomaterials Science*, *8*(24), 6858–6866.
- Madden, T. (2002). The BLAST sequence analysis tool. In M. J & O. J (Eds.), *The NCBI Handbook* (Issue Md, pp. 1–15). National Center for Biotechnology Information (US). Retrieved from <https://www.ncbi.nlm.nih.gov/books/NBK21097/>
- Makhlynets, O. V., & Caputo, G. A. (2021). Characteristics and therapeutic applications of antimicrobial peptides. *Biophysics Reviews*, *2*(1), 011301.
- Naksang, P., Tongchitpakdee, S., Thumanu, K., Oruna-Concha, M. J., Niranjana, K., & Rachtanapun, C. (2020). Assessment of antimicrobial activity, mode of action and volatile compounds of *Etilingera pavieana* essential oil. *Molecules*, *25*(14), 3245.
- Pezeshk, S., Ojagh, S. M., Rezaei, M., & Shabanpour, B. (2019). Fractionation of protein hydrolysates of fish waste using membrane ultrafiltration: investigation of

- antibacterial and antioxidant activities. *Probiotics and Antimicrobial Proteins*, 11(3), 1015–1022.
- Pu, C., & Tang, W. (2017). Affinity and selectivity of anchovy antibacterial peptide for *Staphylococcus aureus* cell membrane lipid and its application in whole milk. *Food Control*, 72, 153–163.
- Quinto, E. J., Caro, I., Villalobos-Delgado, L. H., Mateo, J., De-Mateo-silleras, B., & Redondo-Del-río, M. P. (2019). Food safety through natural antimicrobials. *Antibiotics*, 8(4), 1–30.
- Sahay, A., Piprodhe, A., & Pise, M. (2020). In silico analysis and homology modeling of strictosidine synthase involved in alkaloid biosynthesis in *Catharanthus roseus*. *Journal of Genetic Engineering and Biotechnology*, 18, 44.
- Song, W., Kong, X., Hua, Y., Chen, Y., Zhang, C., & Chen, Y. (2020). Identification of antibacterial peptides generated from enzymatic hydrolysis of cottonseed proteins. *LWT - Food Science and Technology*, 125, 109199.
- Stiefel, P., Schmidt-Emrich, S., Maniura-Weber, K., & Ren, Q. (2015). Critical aspects of using bacterial cell viability assays with the fluorophores SYTO9 and propidium iodide. *BMC Microbiology*, 15(1), 1–9.
- Vally, H., & Misso, N. L. A. (2012). Adverse reactions to the sulphite additives. *Gastroenterology and Hepatology from Bed to Bench*, 5(1), 16–23.
- Walczak-Nowicka, E. J., & Herbet, M. (2022). Sodium benzoate—Harmfulness and potential use in therapies for disorders related to the nervous system: A review. *Nutrients*, 14(7), 1497.
- Wang, G. (2022). Unifying the classification of antimicrobial peptides in the antimicrobial peptide database. *Methods in Enzymology*, 663(402), 1–18.
- Wang, J., Chou, S., Xu, L., Zhu, X., Dong, N., Shan, A., & Chen, Z. (2015). High specific selectivity and membrane-active mechanism of the synthetic centrosymmetric α -helical peptides with Gly-Gly pairs. *Scientific Reports*, 5, 15963.
- Wang, L., Dekker, M., Heising, J., Zhao, L., & Fogliano, V. (2023). Food matrix design can influence the antimicrobial activity in the food systems: A narrative review. *Critical Reviews in Food Science and Nutrition*, 8, 1–27.
- Wang, M., Lin, J., Sun, Q., Zheng, K., Ma, Y., & Wang, J. (2019). Design, expression, and characterization of a novel cecropin A-derived peptide with high antibacterial activity. *Applied Microbiology and Biotechnology*, 103(4), 1765–1775.
- Wongngam, W., Hamzeh, A., Tian, F., Roytrakul, S., & Yongsawatdigul, J. (2023). Purification and molecular docking of angiotensin converting enzyme-inhibitory peptides derived from corn gluten meal hydrolysate and from in silico gastrointestinal digestion. *Process Biochemistry*, 129, 113–120.

- Wongthong, S., Tippayawat, P., Wongwattanukul, M., Pong-ngern, P., Wonglakorn, L., Chanawong, A., Heraud, P., & Lulitanond, A. (2020). Attenuated total reflection: Fourier transform infrared spectroscopy for detection of heterogeneous vancomycin—intermediate *Staphylococcus aureus*. *World Journal of Microbiology and Biotechnology*, *36*(2), 1–12.
- Xie, Z., Wei, H., Meng, J., Cheng, T., Song, Y., Wang, M., & Zhang, Y. (2019). The analogs of temporin-GHa exhibit a broader spectrum of antimicrobial activity and a stronger antibiofilm potential against *Staphylococcus aureus*. *Molecules*, *24*(22), 4173.
- Yang, S., Li, J., Aweya, J. J., Yuan, Z., Weng, W., Zhang, Y., & Liu, G. M. (2020). Antimicrobial mechanism of *Larimichthys crocea* whey acidic protein-derived peptide (LCWAP) against *Staphylococcus aureus* and its application in milk. *International Journal of Food Microbiology*, *335*, 108891.
- Yu, C., & Irudayaraj, J. (2005). Spectroscopic characterization of microorganisms by Fourier transform infrared microspectroscopy. *Biopolymers*, *77*(6), 368–377.
- Zhang, Q. Y., Yan, Z. Bin, Meng, Y. M., Hong, X. Y., Shao, G., Ma, J. J., Cheng, X. R., Liu, J., Kang, J., & Fu, C. Y. (2021). Antimicrobial peptides: Mechanism of action, activity and clinical potential. *Military Medical Research*, *8*(1), 1–25.
- Zhao, Q., He, L., Wang, X., Ding, X., Li, L., Tian, Y., & Huang, A. (2022). Characterization of a novel antimicrobial peptide isolated from *Moringa oleifera* seed protein hydrolysates and its membrane damaging effects on *Staphylococcus aureus*. *Journal of Agricultural and Food Chemistry*, *70*(20), 6123–6133.
- Zhou, J., Han, Q., Koyama, T., & Ishizaki, S. (2023). Preparation, purification and characterization of antibacterial and ACE inhibitory peptides from head protein hydrolysate of kuruma shrimp, *Marsupenaeus japonicus*. *Molecules*, *28*(2), 894.
- Zhu, X., Dong, N., Wang, Z., Ma, Z., Zhang, L., Ma, Q., & Shan, A. (2014). Design of imperfectly amphipathic α -helical antimicrobial peptides with enhanced cell selectivity. *Acta Biomaterialia*, *10*(1), 244–257.

CHAPTER IV

ANTIBACTERIAL ACTIVITY AND POTENTIAL APPLICATION OF A NOVEL ANIONIC ANTIBACTERIAL PEPTIDE DERIVED FROM CORN GLUTEN MEAL HYDROLYSATE

4.1 Abstract

The current study aims to investigate the antibacterial activity of a novel anionic antibacterial peptide derived from pepsin-hydrolyzed corn gluten meal (CGM) and elucidate its mechanism of inhibition towards *Staphylococcus aureus* ATCC 29213. In addition, the combined effect of peptide and mild heat treatment at 50 °C for 10 min was described against *Staphylococcus aureus* ATCC 29213. After a series of chromatographic separation and *de novo* peptide sequencing, an anionic novel peptide of EAGGGEDDKKKVE (EE13) was identified to exhibit the most potent antibacterial activity with minimum inhibitory concentration (MIC) at 4.0 mM against *Staphylococcus aureus* ATCC 29213, *Bacillus cereus* DMST 5040, and *Salmonella* Typhimurium TISTR 292. The killing curve of *S. aureus* ATCC 29213 revealed that EE13 at 1/2×MIC showed a bacteriostatic effect for 4 h, while complete inhibition was observed at 1×MIC after 4 h. The EE13 significantly disrupted the membrane integrity of *S. aureus* at 1×MIC as observed by an increase in fluorescence of propidium iodide. Scanning electron microscopy (SEM) revealed that EE13 caused pore formation, dent cells, cell collapse, and lysis. Synchrotron radiation-based Fourier transform infrared (SR-FTIR) microspectroscopy indicated that EE13 at 1/2×MIC led to modifications in the nucleic acids, proteins, and fatty acids after 4-h exposure. Molecular docking revealed that EE13 exhibited strong binding affinity towards membrane-bound transglycosylase, enzymes associated with peptidoglycan synthesis. In addition, EE13 showed low hemolytic activity below 8.0 mM. When the mild heat treatment of 50 °C for 10 min was applied prior to the application of 1/2×MIC EE13, severe cell membrane damage was observed. These findings suggested that EE13, derived from CGM hydrolysate, was an anionic peptide that might potentially be applied as an antimicrobial agent in food.

Keywords: Anionic antibacterial peptide, antibacterial activity, corn gluten meal hydrolysate, hydrolysis, mechanism, mild heat treatment

4.2 Introduction

Chemical preservatives with antimicrobial activity are typically employed to inhibit the growth of spoilage and pathogenic microorganisms in food, including sodium benzoate and potassium sorbate (López-Malo, Barreto-Valdivieso, Palou, & Martín, 2007). However, these chemical preservatives in food may be associated with certain health risks, including skin allergies, oxidative stress, cancer development, genotoxicity, mutagenicity, and DNA-damaging activity (Lima, de Carvalho, Vieira, Moreira, & Conte-Junior, 2021). In addition, the misuse of chemical preservatives in the food industry can lead to the development of antimicrobial resistance (AMR) in foodborne microorganisms. Therefore, the quest of natural antimicrobial agents to reduce the use of chemical preservatives is a valuable and important endeavor.

Antimicrobial peptides (AMPs) is a natural host defense against pathogenic microorganisms (Ma, Guo, Fu, & Jin, 2020). AMPs exhibited different mechanisms of action compared to antibiotics. The first mechanism of action of AMPs is the perturbation of the cell membrane, which subsequently leads to lysis and cell death. In addition, AMPs inhibit intracellular functions by binding to nucleic acids or proteins (Benfield & Henriques, 2020).

Enzymatic hydrolysis of food proteins is an effective method that can efficiently generate a wide range of bioactive peptides including antioxidant, antihypertensive, immunomodulatory, and antimicrobial effects (Akbarian, Khani, Eghbalpour, & Uversky, 2022). From our previous study, corn gluten meal (CGM) hydrolyzed by pepsin produced a peptide fraction capable of inhibiting *S. aureus* ATCC 29213 growth with a membranolytic mechanism. In the CGMH peptide fraction, 11 peptides have been identified, consisting of 6 cationic peptides and 5 anionic peptides (Nurhartadi et al., 2024).

Cationic AMPs (CAMPs) have been widely studied as they can interact electrostatically with the negatively charges of the cell membrane, such as phospholipids in teichoic acid of Gram-positive bacteria and lipopolysaccharides of Gram-negative bacteria (Bechinger & Gorr, 2017; Straus & Hancock, 2006). Anionic AMPs (AAMPs) are the second group of AMPs that have a net charge from -1 to -8. AAMPs are recognized for their high contents of glutamic and aspartic acids. AAMPs are predominantly peptide fragments derived from proteolysis, while some are small

molecules encoded by genes (Dennison, Harris, Mura, & Phoenix, 2018). AAMPs are considered underexplored as compared to cationic counterparts.

Mild heat treatment is a physical technique typically administered by immersion in water at 30-60 °C for 10-20 min. This condition has the potential to cause damage to cellular structure and function (Giaccone et al., 2016). During mild heat treatment, bacteria can undergo sub-lethal injuries, particularly when the treatment is not intense enough to cause cell death (Wuytack et al., 2003). In addition, McMahon, Xu, Moore, Blair, & McDowell (2007) mentioned that sublethal heat stress can increase the permeability of bacterial cell membranes, thereby making them more susceptible to the effects of antimicrobial agents. The combined effect of mild heat with an AMP has not been investigated.

This study aimed to characterize synthetic AAMP derived from pepsin-hydrolyzed corn gluten meal (CGM) and to elucidate the mechanism of action of synthetic AAMP derivate corn gluten meal hydrolysate. In addition, the combined effect of the CGM AAMP with mild heat treatment on *Staphylococcus aureus* ATCC 29213, which was found to be the most sensitive to EE13, was systematically investigated.

4.3 Materials and methods

4.3.1 Materials

Trypticase soy broth (TSB), Mueller-Hinton broth (MHB), microbiological agar, and plate count agar (PCA) were purchased from HiMedia™ (Mumbai, India). Propidium iodide and SYTO-9 were obtained from ThermoFisher Scientific™ (Waltham, MA, USA). Glutaraldehyde and osmium tetroxide were procured from Electron Microscopy Sciences (Hatfield, PA, USA). Unless otherwise specified, all chemicals utilized were of analytical grade.

4.3.2 Bacterial strain cultures

Gram-positive bacteria, namely *Staphylococcus aureus* ATCC 29213, *Bacillus cereus* DMST 5040, *Listeria monocytogenes* DMST 17303, methicillin-resistant *S. aureus* DMST 20652, and two Gram-negative bacteria of *Escherichia coli* TISTR 780, *Salmonella* Typhimurium TISTR 292 were used as test organisms. All bacteria were cultured in trypticase soy broth (TSB) incubated at 37 °C for 24 h and subsequently streaked on tryptic soy agar (TSA) and incubated at 37 °C for 18-24 h.

4.3.3 Peptide synthesis and *in silico* analysis

The peptide EE13 (EAGGGEDDKKKVE) and the conjugated peptide 5-carboxyfluorescein-EE13 (5-FAM-EE13) were chemically synthesized using the Fmoc solid-phase peptide synthesis (SPPS) method by GL Biochem (Shanghai, China). Peptide purity of >95% was determined by reversed-phase high-performance liquid chromatography (RP-HPLC) and was confirmed by mass spectrometry (MS). The peptides were dissolved in deionized water and stored at -20 °C until use.

The molecular weight, isoelectric point, instability index, aliphatic index, and GRAVY index of the peptide were calculated using the ExPASy ProtParam Tools (<https://web.expasy.org/protparam/>) (Gasteiger et al., 2005). The net charge, hydrophobicity, and hydrophobic moment were generated using the HeliQuest server (<https://heliquest.ipmc.cnrs.fr/cgi-bin/ComputParams.py>) (Gautier, Douguet, Antony, & Drin, 2008). The 3D structures of the peptide were drawn using the PEP-FOLD3 (<https://bioserv.rpbs.univ-paris-diderot.fr/services/PEP-FOLD3>) (Lamiable et al., 2016). The molecular structure predictions were drawn with the PepDraw (<https://pepdraw.com/>).

4.3.4 Antibacterial activity

4.3.4.1 Minimum inhibitory concentration (MIC)

The antibacterial activity of synthetic peptide was tested using the broth microdilution technique in a 96-well microtiter plate according to Wiegand, Hilpert, & Hancock (2008) with slight modifications. Each bacterium was cultured on TSA and incubated at 37 °C for 24 h. Three to five single colonies from the plate were transferred into sterile 0.85% NaCl and then adjusted to a 0.5 McFarland scale ($OD_{600} \approx 0.085-0.100$). Subsequently, a 10-fold dilution series with sterile 0.85% NaCl was performed to reach the final concentration of approximately 5×10^5 CFU·mL⁻¹ in MHB, then 50 µL of diluted cell suspension were added with 50 µL of peptide in a 96-well microplate. Kanamycin of 10.0 ppm was used as a positive control to inhibit bacterial growth. The minimum inhibitory concentration (MIC) of the peptide was determined by assessing the turbidity at 600 nm (OD_{600}) using a microplate reader (Spectrostar® Nano, BMG Labtech, Ortenberg, Germany).

4.3.4.2 Bacterial-killing curve

The bacterial-killing curve of EE13 was evaluated on *Staphylococcus aureus* ATCC 29213, which was determined to be the most sensitive

bacterium tested. A mid-log phase of the bacterium was cultivated and diluted to achieve 1×10^5 CFU.mL⁻¹ in MHB. The EE13 at various concentrations of 1/4×MIC, 1/2×MIC, and 1×MIC were introduced to the bacterial suspension and incubated for various time intervals of 0-24 h at 37 °C. The aliquots of the cultured samples were analyzed using the spot plate technique on plate count agar (PCA) plates in triplicates. After incubating the plates at 37 °C for 24 h, enumeration was carried out and presented as log CFU.mL⁻¹.

4.3.5 The *in silico* peptide-membrane interaction

The PDB file of peptide EE13 was employed to determine the peptide-membrane interaction using the PMIPred server (<https://pmipred.fkt.physik.tu-dortmund.de>) (van Hilten et al., 2024). PMIPred was used to predict the free energy of membrane binding and classify the interaction of peptide and the membrane as non-binding, curvature sensing, or membrane binding.

The PDB file of the EE13 secondary structure predicted using PepFold3 was used to calculate peptide-membrane interactions using the PPM 3.0 server located at the Orientation of Proteins in Membranes (OPM) database (<http://opm.phar.umich.edu/server.php>) (Lomize, Pogozheva, Joo, Mosberg, & Lomize, 2012). The PPM 3.0 server was predicted the peptide arrangement in lipid bilayers by providing orientation parameters such as membrane penetration depth, tilt angle, and water-to-membrane transfer energy (ΔG_{transf}). The 3D-rendered images of the peptide were created by PyMoL v2.4.

4.3.6 Antibacterial mechanism

4.3.6.1 Membrane integrity

Disruption of the cell membrane was evaluated using a confocal laser scanning microscope (CLSM) method described by de Almeida et al. (2019) with minor modifications. *Staphylococcus aureus* ATCC 29213 cells were cultivated in TSB to a mid-log phase at 37 °C with a shaking speed of 120 rpm. Cells were collected by centrifugation at 5,000 × g for 5 min. Cell pellet were rinsed twice with 10 mM phosphate-buffered saline (PBS) 10 mM PBS and resuspended to an OD₆₀₀ at 0.2-0.3 in 10 mM PBS. The cells were treated with EE13 at 1/2×MIC and 1×MIC and incubated for 4 h at 37 °C. The cells without peptide was also prepared. Treated cells were collected and resuspended in 10 mM PBS. Propidium iodide (PI) at the final concentration of 10 µg.mL⁻¹ or SYTO-9 at 2.5 µg.mL⁻¹ was then added and incubated at

4 °C for 30 min in the dark. The treated bacterial cells were collected and rinsed with the same buffer solution. The cells without peptide were also stained with PI or SYTO-9. Subsequently, 10 µL cell suspension were embedded on a glass slide. The CLSM (Nikon 90i A1R, Nikon, Tokyo, Japan) was utilized for image observation. The excitation and emission wavelengths of SYTO9-stained cells are 488 and 530 nm, and those of PI-stained cells are 538 and 617 nm, respectively.

4.3.6.2 Localization of EE13 in bacterial cell

Cellular peptide localization was conducted as delivered by Ciociola et al. (2018) with minor modifications. Briefly, *Staphylococcus aureus* ATCC 29213 cells were seeded in TSB at 37 °C for 4-6 h to attain the mid-log phase. The cell pellets were harvested by centrifugation at 5,000 ×g for 5 min, rinsed twice, and resuspended in 10 mM phosphate-buffered saline (pH 7.2). Subsequently, the cell suspension was added 5-carboxyfluorescein-EE13 (5-FAM-EE13) at a final concentration of 1/2×MIC and 1×MIC and incubated at 37 °C for 4 h in the dark. Subsequently, the cell suspension was centrifuged, washed twice, and resuspended in 10 mM PBS. Untreated cells were also prepared. Propidium iodide (PI) at a final concentration of 10 µg.mL⁻¹ was added and incubated in the dark for 30 min at 4 °C. The bacterial cells were then analyzed with a confocal laser scanning microscope (Nikon 90i A1R, Nikon, Tokyo, Japan).

4.3.6.3 Cell morphology

The influence of peptide on bacterial cell morphology was evaluated using scanning electron microscopy (SEM) as described by Zhu et al. (2014). *Staphylococcus aureus* ATCC 29213 were cultured in TSB to a mid-log phase at 37 °C for 4-6 h. Cell pellets were collected by centrifugation at 5,000 ×g for 5 min, rinsed with 10 mM phosphate buffered saline (PBS), and resuspended to an OD₆₀₀ of 0.5. The peptide EE13 was applied at 1/2×MIC to the cell suspension and incubated at 37 °C for 4 h, alongside control cells without peptide. Following centrifugation and rinsing, cells were fixed with 2.5% glutaraldehyde (v/v) in 100 mM phosphate buffer (pH 7.2) at 4 °C for 24 h, then rinsed again. Post-fixation involved 1% osmium tetroxide for 2 h, followed by rinsed with distilled water. Cells were dehydrated through increasing acetone concentrations and finally prepared on conductive aluminium tape, coated with dual carbon and ultrathin gold, and observed using a field-emission SEM (FE-SEM) (Auriga-Carl Zeiss, Oberkochen, Germany) at 2-2.5 keV.

4.3.6.4 Changes of intracellular fingerprints

Synchrotron radiation under Fourier transform infrared spectromicroscopy (SR-FTIR) assay was used to examine the intracellular modifications caused by synthetic peptides. SR-FTIR was implemented as proposed by Tian et al. (2022) with a little adjustment. *Staphylococcus aureus* ATCC 29213 cells were grown in TSB at 37 °C for 4-6 h. The cell pellets were then harvested by centrifugation at 5,000 \times g for 5 min and resuspended in fresh TSB ($OD_{600}=0.2$). The EE13 was then added at a final concentration of $1/2 \times MIC$ and incubated at 37 °C for 4 h. The control was also prepared without peptide. Cell pellets were collected after incubation at 37 °C for 4 h. Pellets were rinsed twice using sterile 0.85% NaCl and thrice with sterile distilled water. One μ L of the culture suspension was spotted on a BaF₂ window. Samples were dehydrated at room temperature for 30 min in a biosafety cabinet (Esco, Horsham, PA, USA). Subsequently, they were dried in a vacuum desiccator to generate film before SR-FTIR measurement. The SR-FTIR experiment was conducted in a Beamline 4.1 of the Synchrotron Light Research Institute (Nakhon Ratchasima, Thailand) with a Vertex-70 spectrometer (Bruker Optics, Ettlingen, Germany) and a Hyperion-2000 microscope (Bruker Optics, Ettlingen, Germany). The SR-FTIR spectra were generated in the 4,000–800 cm^{-1} wavenumber region. Spectra were analyzed (cutting, smoothing, baseline correction, normalization, and averaging) by OPUS 7.5 software (Bruker Optics, Ettlingen, Germany). Spectra were smoothed by the Savitzky-Golay algorithm, then a second-order derivative of spectra by performing the Savitzky-Golay algorithm (17 smoothing points). They were then calculating for compensation of wavelength-dependent spectra effect using Extended Multiplicative Scatter Correction (EMSC) and further evaluated on principal component analysis (PCA), a multivariate statistical method at the Unscramble X 10.4 for Windows (Camo Analytics, Oslo, Norway).

4.3.6.5 Molecular docking

The crystallographic structures of nine receptors of *Staphylococcus aureus* were acquired from the Research Collaboratory for Structural Bioinformatics Protein Data Bank (RCSB PDB) (<https://www.rcsb.org>) (Berman et al., 2000) and selected for molecular docking. Membrane-bound transglycosylase (PDB ID: 3VMQ_B) (Huang et al., 2012), hydrolase AmiA (PDB ID: 4KNL_B) (Büttner, Zoll, Nega, Götz, & Stehle, 2014), D-alanine ligase (PDB ID: 7U9K_B) (Becker, Pederick, Dawes, Bruning, & Abell, 2023), amidase LtyH (PDB ID: 7TJ4_B) (Page, Skiba, Do, Kruse, & Walker, 2022), thymidylate kinase (PDB ID: 4GFD_B) (Keating et al., 2012), thymidylate synthase

(PDB ID: 4DQ1_B), DNA gyrase (PDB ID: 2XCT_B) (Bax et al., 2010), dihydrofolate reductase (PDB ID: 3SRQ) (Li et al., 2011), peptidoglycan D-acetyl transferase (PDB ID: 6WN9_B) (Jones, Sychantha, Howell, & Clarke, 2020) were selected as receptors. All receptor structures were cleaned by removing the water molecules using PyMOL v2.4.

The molecular docking simulation was executed on the CABSdock peptide-protein docking server (<https://biocomp.chem.uw.edu.pl/CABSdock/>) (Blaszczyk et al., 2016; Kurcinski, Jamroz, Blaszczyk, Kolinski, & Kmiecik, 2015). The docking results were projected in DimPlot of the LigPlot⁺ (Laskowski & Swindells, 2011) to highlight the EE13 and the receptors binding positions. For compare, another interaction graphics were created with the EMBL-EBI tool PDBsum (<http://www.ebi.ac.uk/thornton-srv/databases/pdbsum/Generate.html>) (Laskowski, 2009). The binding affinity (ΔG) and dissociation constant (Kd) values were predicted using the Prodigy (Protein binding energy prediction) server (<https://rascar.science.uu.nl/prodigy/>) (Honorato et al., 2021; Vangone & Bonvin, 2015; Xue, Rodrigues, Kastritis, Bonvin, & Vangone, 2016).

4.3.7 Hemolytic activity

The hemolytic capacity of EE13 was evaluated by following a modified technique of Wang et al. (2015). The experimental process was accepted by the Human Research Ethics Committee at Suranaree University of Technology (EC-6432) and conducted following ethical guidelines and regulations. In brief, one mL of fresh human red blood cells (hRBCs) was collected from a healthy person in a polycarbonate tube in the presence of heparin. The acquired hRBCs were centrifuged at 1,000 $\times g$ for 5 min at 4 °C and subsequently rinsed in PBS three times, followed by resuspending in PBS buffer (pH 7.2) and diluted to 1% (v/v) erythrocyte suspension. Subsequently, 50 μL of the hRBCs suspension was mixed with 50 μL of the peptide in PBS buffer (pH 7.2) at different concentrations. Samples were incubated at 37 °C for 1 h. After centrifugation at 1,000 $\times g$ for 5 min at 4 °C, the supernatant was carefully transferred to a 96-well microtiter plate, and hemoglobin acquisition was determined by observing the optical density at $\lambda=570$ nm (OD_{570}) using a microplate reader (Spectrostar® Nano, BMG Labtech, Ortenberg, Germany). Negative and positive controls were PBS buffer and 1% Triton X-100, respectively. Minimum hemolytic concentration (MHC) is the peptide required to achieve hemolysis of 10%. The hemolysis level was evaluated based on the following equation:

$$\% \text{ hemolysis} = \frac{\text{OD}_{\text{treated sample}} - \text{OD}_{\text{negative control}}}{\text{OD}_{\text{positive control}} - \text{OD}_{\text{negative control}}} \times 100$$

4.3.8 The effect of mild heat and peptide EE13 treatment on *S. aureus*

Mild heat treatment was followed Kennedy, Cronin, Piterina, & Wilkinson (2019). The most sensitive bacteria *Staphylococcus aureus* ATCC 29213 cells cultured in TSB at 37 °C for 24 h were suspended in 1 mM sterilized potassium phosphate-buffered saline. Cell suspensions with approximately 4 log CFU.mL⁻¹ were exposed to 40, 50, or 60 °C for 10 min in a water bath (Memmert, Büchenbach, Germany). Subsequently, samples were cooled immediately and inoculated to MHB containing EE13 at a final concentration of 0, 1/8×MIC (0.5 mM), 1/4×MIC (1.0 mM), and 1/2×MIC (2.0 mM). Samples were then incubated at 37 °C for 0, 4, and 8 h. The spot plate technique was used for enumeration of each incubation time on plate count agar (PCA) and incubated at 37 °C for 24 h, in triplicate. The selected combination treatments were then observed membrane integrity and morphological changes using the methods described above in 4.3.6.1 and 4.3.6.3.

4.3.9 Statistical analysis

All experiments were performed in triplicate, and the findings were expressed as mean ± standard deviation (SD). The statistical analyses was performed utilizing GraphPad Prism version 8 (GraphPad Software Inc., San Diego, CA, USA). One-way analysis of variance (ANOVA) and Tukey's multiple comparison range tests were carried out to determine significant differences ($p < 0.05$) between the mean values.

4.4 Results and discussion

4.4.1 Antibacterial activity of EE13

Eleven peptides were identified from CGMH fractionated by reverse-phase chromatography (Nurhartadi et al., 2024). Among the identified peptides, the peptide EAGGGEDDKKKVE (EE13) exhibited the most potent antibacterial capability (Table 4.1). It exhibited MIC of 4.0 mM against *S. aureus* ATCC 29213, *B. cereus* DMST 5040, and *S. Typhimurium* TISTR 292. Other peptides showed weak antibacterial activity with MIC > 4.0 mM.

Table 4.1 Minimum inhibitory concentration (MIC) of peptides obtained from CGMH on four different test bacteria

Peptide	Minimum Inhibitory Concentration (mM)			
	<i>Staphylococcus</i>	<i>Bacillus</i>	<i>Salmonella</i>	<i>Escherichia</i>
	<i>aureus</i>	<i>cereus</i>	Typhimurium	<i>coli</i>
	ATCC 29213	DMST 5040	TISTR 292	TISTR 780
EAGGGEDDKKKVE	4.0	4.0	4.0	>4.0
PTGAKVTKAAKKA	>4.0	>4.0	>4.0	>4.0
PTGAKVTKAAKA	>4.0	>4.0	>4.0	>4.0
KQVHPDTE	>4.0	>4.0	>4.0	>4.0
LKNGKKVE	>4.0	>4.0	>4.0	>4.0
APRPSSPHKA	>4.0	>4.0	>4.0	>4.0
PEPSKSAPAPKKLSSL	>4.0	>4.0	>4.0	>4.0
ERSNSSSGSGEQKEDQKE	>4.0	>4.0	>4.0	>4.0
KQQAAPPPKAKQ	>4.0	>4.0	>4.0	>4.0
EGVEEEQGGGGGQKSATA	>4.0	>4.0	>4.0	>4.0
PTGAKKGKHLKQ	>4.0	>4.0	>4.0	>4.0

Zhao et al. (2022) studied peptide MOp2 (HVLDTPLL) obtained from *Moringa oleifera* seed protein hydrolyzed by alkaline proteinase and found that it inhibited *S. aureus* growth with an MIC of 2.204 mM. Ghanbari & Ebrahimpour (2018) found the antibacterial activity of synthesized peptide derived from stonefish hydrolysates with bromelain with MIC at 2 mM against *Pseudomonas* sp., *P. aeruginosa*, *E. coli*, and *S. aureus*. The MIC of EE13 was estimated to be 0.54% (w/v), which should be in the range for application in food, providing a “natural” peptide derived from corn protein. The usage of antimicrobial compound in food need to be tailored in amount. For example, the maximum level of sodium benzoate in food is 0.1 %, as set by FDA (U. S. Food and Drug Administration, 2024). Notably, our peptide has a higher value when compared to sodium benzoate. Nevertheless, the potential use of peptide EE13 in food remains promising.

4.4.2 Characteristics of EE13

The peptide EE13 exhibits a molecular weight of 1361.41 Da and calculated pI of 4.16 with an anionic characteristic of -2 charges at pH 7. EE13 shows low hydrophobicity with a GRAVY index of -1.377 and hydrophobicity of -0.377, indicating its water-soluble characteristic (Table 4.2).

Table 4.2 Characteristics of peptide EE13

Peptide sequence	Theoretical (Measured MW ^a)	pI	GRAVY index	Charge	H ^b (μ H _{rel})
EAGGGEDDKKKVE	1361.43 (1361.41)	4.16	-1.377	-2	-0.377 (0.132)

^a Measured MW was determined by ESI-MS mass spectroscopy.

^b The mean hydrophobicity (H) and relative hydrophobic moment (μ H_{rel}) were calculated by HeliQuest analysis.

The primary structure of EE13 was illustrated by Pepdraw.com (Figure 4.1A). The 3D predicted structure of EE13 by Pepfold3 shows α -helical structure, which might be the preferred conformation in the amphiphilic environment (Figure 4.1B). The helical wheel projection of EE13 (Figure 4.1C) demonstrates the distribution of the residue and illustrates the amphiphilic interface of EE13.

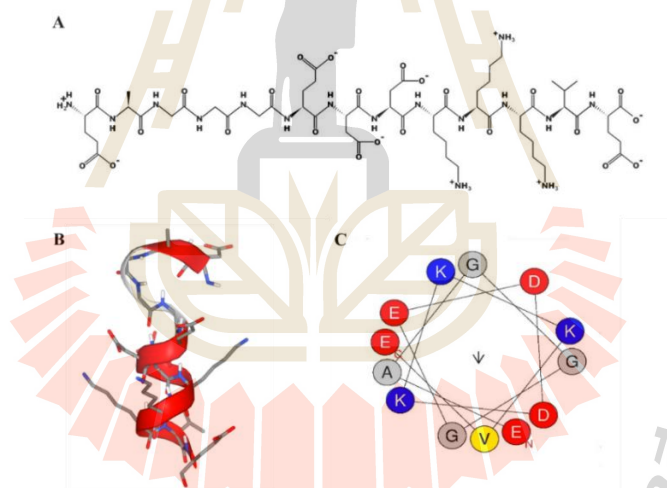


Figure 4.1 The primary structure visualization of the peptide EAGGGEDDKKKVE (EE13) using the program PEPDRAW (<http://pepdraw.com/>) (A) 3D Molecular prediction of EE13 obtained from Pepfold3 (<https://bioserv.rpbs.univ-paris-diderot.fr/services/PEP-FOLD3/>) (B) The helical wheel projection of EE13 obtained from HeliQuest (<http://heliquet.ipmc.cnrs.fr/cgi-bin/ComputParams.py>). Blue for positively charged residues (Lys) and red for negatively charged residues (Glu and Asp). Yellow for hydrophobic residues (Val) and grey for the neutral residues (Gly and Ala). The arrow featured the helical hydrophobic moment (C)

4.4.3 Peptide-bacterial membrane interaction model

The PMIpred prediction results show that peptide EE13 is unlikely to interact with the negatively charged membrane (e.g. POPC (1-palmitoyl-2-oleoyl-sn-glycero-3-phosphocholine) /POPG (1-Palmitoyl-2-oleoyl-sn-glycero-3-[phospho-rac-(1-glycerol)])), as illustrated in Figure 4.2A, with predicted $\Delta F_{sm}(R=50)$ of 10.571 kJ/mol. In addition, the PMIpred confirmed that EE13 was classified as a non-binder (predicted $\Delta\Delta F = -1.074$ kJ.mol⁻¹) with lack of hydrophobic/amphipathic character and unfavorable electrostatic interactions with the membrane (Figure 4.2B). van Hilten et al. (2024) categorized $\Delta\Delta F$ threshold as follows: $\Delta\Delta F > -6.4$ kJ.mol⁻¹ as non-binders, $-10.0 \leq \Delta\Delta F \leq -6.4$ kJ.mol⁻¹ as sensors, and $\Delta\Delta F < -10.0$ kJ.mol⁻¹ as binders.

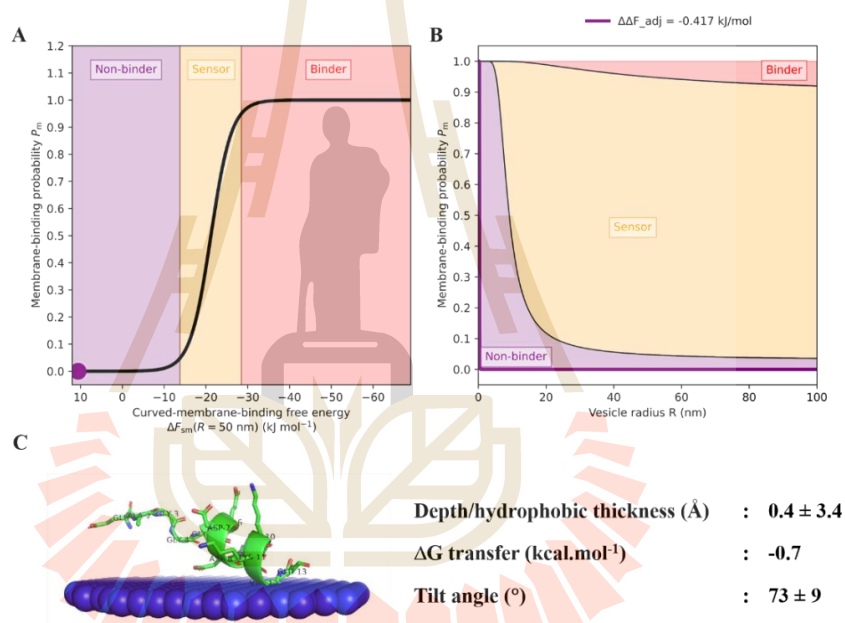


Figure 4.2 The prediction position of peptide EE13 on the non-binding → binding continuum. Predicted sensors of EE13 fall in the purple zone (A). The membrane-binding probability of peptide EE13 falls in the purple area using the PMIpred server (B). 3D model interaction between peptide EE13 and membrane using PPM 3.0 server (C)

EE13 is a negatively charged peptide (-2) that may not effectively interact with the membrane due to a lack of hydrophobic properties. Therefore, lack of hydrophobic character may lead to weaker interactions with the lipid bilayer, making EE13 positioned in non-binding areas (purple area).

Figure 4.2C illustrates a 3D model of the interaction of peptide EE13 with the bacterial membrane predicted using the PPM 3.0 server. The peptide EE13-membrane interaction has a tilt angle of $73 \pm 9^\circ$ and a penetration depth of $0.4 \pm 3.4 \text{ \AA}$, suggesting the minimal membrane interactions. A low ΔG value of $-0.7 \text{ kcal.mol}^{-1}$ for transferring EE13 from the aqueous solution to the membrane confirmed the weak affinity of EE13 on membrane interaction.

Peptide-membrane interactions are frequently attributed to electrostatic and hydrophobic forces. Anionic peptides, which are negatively charged, may exhibit different binding characteristics than cationic peptides, which are positively charged and interact more efficiently with a negatively charged membrane (Wimley, 2010). The *in silico* prediction result indicated that the anionic peptide EE13 might minimally interact with membranes. Therefore, these results were validated with the *in vitro* assay results in subsequent experiments.

4.4.4 Bacterial killing curve

In the absence of EE13, *S. aureus* exhibited a typical growth curve, exhibiting the lag, logarithmic, stationary, and death phases over 24 h (Figure 4.3). When bacterial cells were exposed to $1/8\times$ and $1/4\times$ MIC of EE13, the logarithmic growth phase was suspended for up to 2 h. while at $1/2\times$ MIC of EE13, it can be prolonged for up to 4 h. In contrast, following 6 h of peptide treatment at $1\times$ MIC, *S. aureus* growth was reduced by $1 \text{ log CFU.mL}^{-1}$. The growth of *S. aureus* then decreased significantly, becoming non-detectable after 12 h at $1\times$ MIC. Thus, the antimicrobial activities of peptide EE13 were dose- and time-dependent. Our result indicated that the bacteriostatic effect of peptide EE13 was observed at 2.0 mM ($1/2\times$ MIC), and the peptide acted as a bactericidal agent at 4.0 mM ($1\times$ MIC).

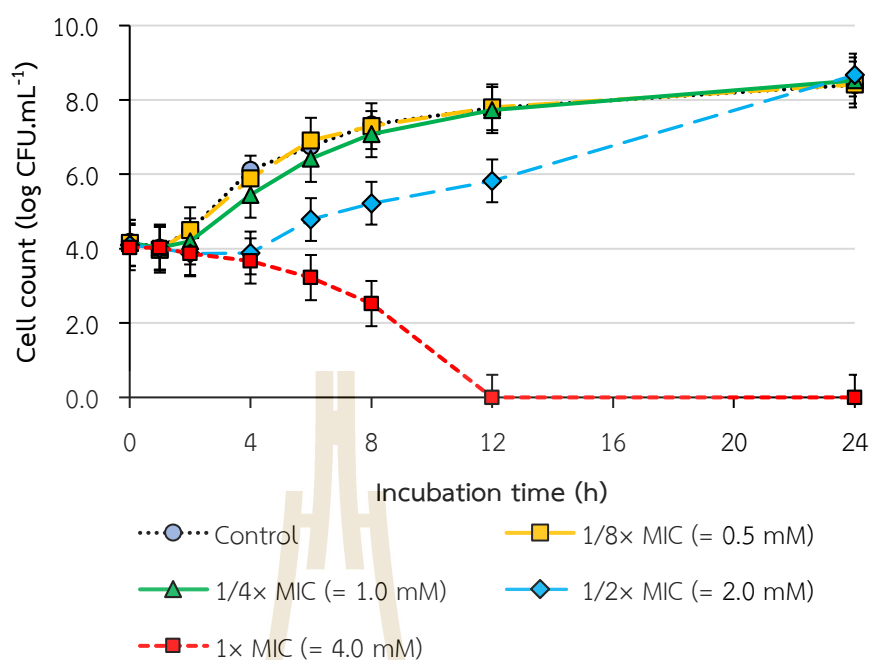


Figure 4.3 Killing curve of *Staphylococcus aureus* ATCC 29213 against EAGGGEDDKKKVE (EE13) at 1/8xMIC, 1/4xMIC, 1/2xMIC, and 1xMIC incubated at 37 °C, for 24 h. Data are given as Mean \pm SD ($n = 3$)

4.4.5 Antibacterial mechanism

4.4.5.1 Membrane integrity

As depicted in Figures 4.4 (A-C), the untreated cells (control) showed only green fluorescence of SYTO9, and red fluorescence of PI was not observed, indicating the presence of live cells with membrane integrity.

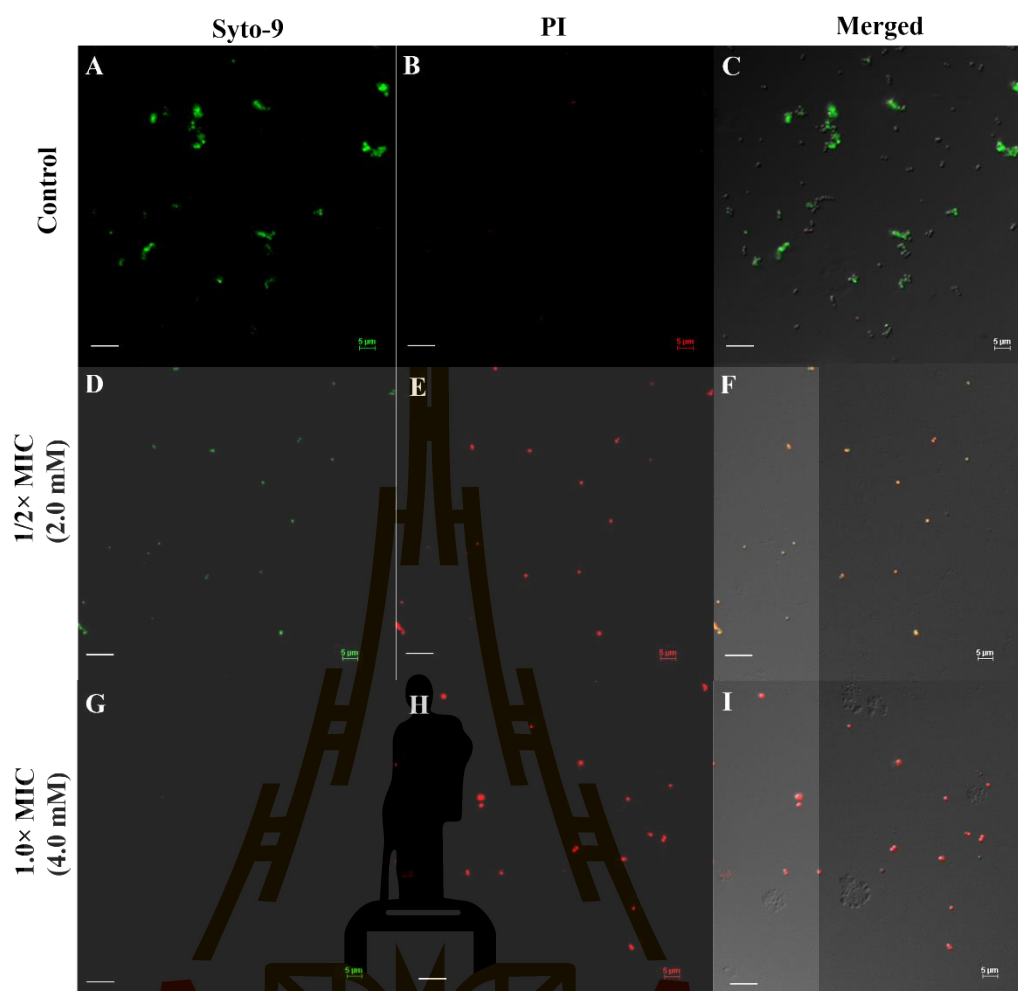


Figure 4.4 Confocal laser scanning micrographs of *Staphylococcus aureus* ATCC 29213 cells: (A-C) untreated cells (control), (D-F) cells exposed with EAGGGEDDKKKVE (EE13) at 1/2×MIC and (G-I) at 1×MIC. Cells were stained with SYTO-9 and propidium iodide (PI). The scale bar is 5 μ m.

In contrast, red fluorescence of PI was observed in *S. aureus* cells exposed to the EE13 at 1/2×MIC and 1×MIC for 4 h and appeared to increase with increasing concentrations. These results indicated that the cell envelopes of *S. aureus* were damaged and led to cell death, allowing PI to bind to nucleic acids. In addition, some cells exhibited only SYTO-9 fluorescence, suggesting that live cells were also present at both 1/2× and 1×MIC (Figures 4.4D-I). These findings confirmed that EE13 likely increases the membrane permeability.

4.4.5.2 Cell morphology

The control exhibited intact grape-like structure with smooth surface (Figure 4.5A). After the EE13 treatment at 1/2×MIC (2.0 mM), *S. aureus* cells

appeared slightly collapsed, and several pores were noticed on cell surfaces (Figure 4.5B). In addition, at 1×MIC (4.0 mM), irregular-shaped cell morphology with pores, severe cell collapse, and even cell lysis were observed (Figure 4.5C). These findings demonstrated that exposure to EE13 induced severe damage in *S. aureus* cells.

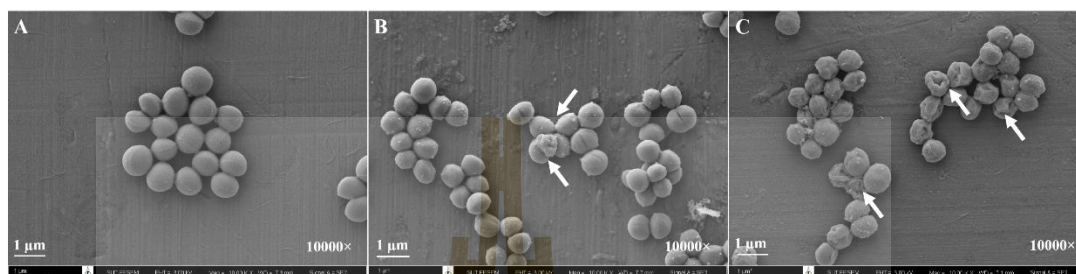


Figure 4.5 Scanning electron micrographs of (A) control of *Staphylococcus aureus* ATCC 29213 (B) *S. aureus* treated with peptide EAGGGEDDKKKVE (EE13) at 1/2×MIC (2.0 mM) incubated at 37 °C for 4 h. (C) *S. aureus* treated with EE13 at 1×MIC (4.0 mM) incubated at 37 °C for 4 h. Scale bars represent 1 μm. Magnification at 10,000×. White arrows indicate morphological changes.

The morphological changes of *S. aureus* observed in this study are similar to Zhao et al. (2022), whose reported MOp2 (HVLDTPLL), a novel anionic AMPs (-1) isolated from *Moringa oleifera* seed protein hydrolysates. They mentioned that this peptide at 1×MIC (2.204 mM) caused the *S. aureus* cells morphology to become rough, irregular, wrinkled, and abnormal. In addition, Dennison et al. (2006) reported the interaction of anionic peptide AP1 (GEQGALAQFGEWL) with the membrane lipid of *S. aureus* by developing an α -helical structure. Therefore, the peptide EE13 was suggested to have induced the morphological changes of *S. aureus* cells by interacting with the cell membrane.

4.4.5.3 SR-FTIR

FTIR spectra of bacterial cells can be categorized as follows: (1) 3000-2800 cm^{-1} for the amphiphilic membrane region, (2) 1700-1200 cm^{-1} for the protein and peptide region, with 1650 cm^{-1} for amide I, 1550 cm^{-1} for amide II, and 1260 cm^{-1} for amide III, (3) 1500-1200 cm^{-1} for the protein and fatty acid region, (4) 1200-900 cm^{-1} for the nucleic acid and polysaccharide region, and (5) 900-700 cm^{-1} for the fingerprint region (Lasch & Naumann, 2015).

Figure 4.6A shows the SR-FTIR spectra of all absorption regions, revealing the main functional groups of individual cell components.

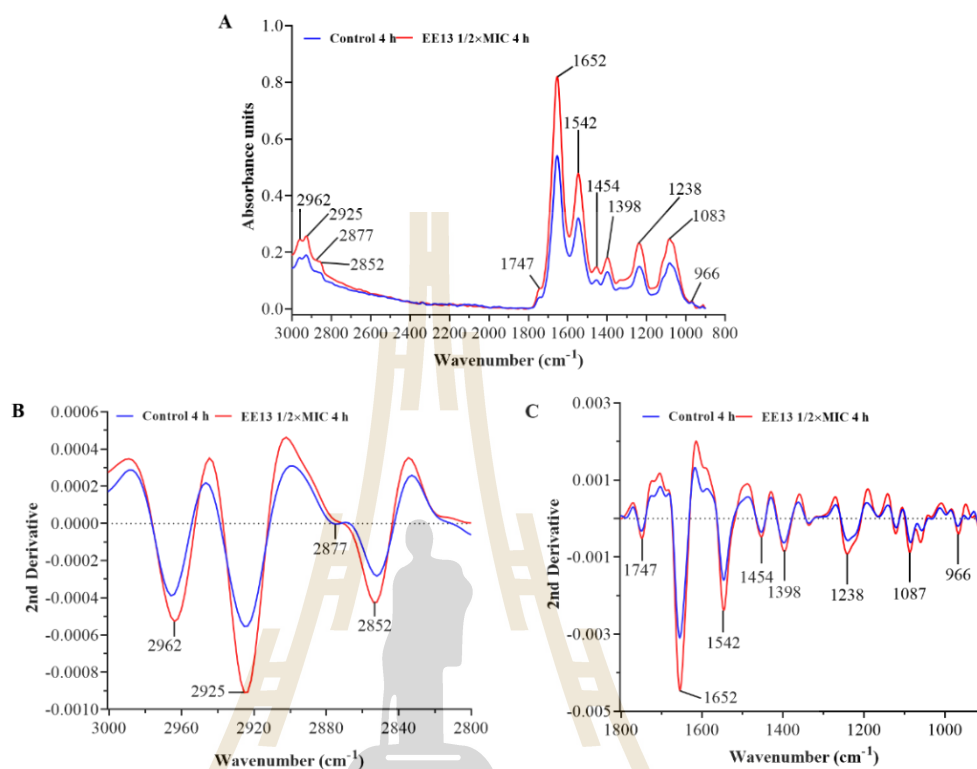


Figure 4.6 FTIR spectra of *Staphylococcus aureus* ATCC 29213 in the absence and presence of 1/2×MIC EAGGGEDDKKKVE (EE13), incubated at 37 °C for 4 h (A), 2nd derivative spectra of *S. aureus* control and subjected to EE13 at 1/2×MIC incubated at 37 °C for 4 h 3000–2800 cm⁻¹ (B), 2nd derivative spectra of *S. aureus* control and *S. aureus* exposed to EE13 at 1/2×MIC incubated at 37 °C for 4 h at region of 1800–900 cm⁻¹ (C). Three replicates of measurements were averaged from 210 spectra

The *S. aureus* cells treated with EE13 at 1/2×MIC (2.0 mM) incubated at 37 °C for 4 h have caused substantial shifts in the regions 2962, 2925, 2852, cm⁻¹ (Figure 4.6B) and 1756 cm⁻¹ (Figure 4.6C) associated with fatty acids compared to untreated cells. In addition, there were changes at 1652, and 1542 cm⁻¹ regions attributed with protein and amide II, respectively (Figure 4.6C) (Movasaghi et al., 2008). Moreover, changes at 1238 cm⁻¹, corresponding to the phosphate group (P=O) asymmetric stretching of phosphodiester in phospholipids and RNA (Davis & Mauer, 2010), and 1087 cm⁻¹ indicating a symmetric phosphate stretching in DNA, RNA, and phospholipids were observed (Yu & Irudayaraj, 2005). These observations suggested

alterations in *S. aureus* cells in the component of fatty acids, proteins, phospholipids, and nucleic acids upon treatment of EE13 at 1/2×MIC compared to untreated cells.

A substantial rupture in the cell membrane corresponded with a shift in 1398 cm^{-1} and 1454 cm^{-1} , which indicate the symmetrical stretching of COO^- groups of amino acids and/or fatty acids in the cell membrane as well as asymmetric deformation of CH_2 from lipids and fatty acids in the cell membrane (Movasaghi, Rehman, & Rehman, 2008). The rise of the spectra like amide I (1652 cm^{-1}), amide II (1542 cm^{-1}), proteins (1454 cm^{-1}), phosphate I (1398 cm^{-1}), and nucleic acid (1238 , 1087 , and 966 cm^{-1}) indicated changes of these intracellular components. These modifications are caused by alterations in cell membrane structure and nucleic acid released into the solvent (Yu & Irudayaraj, 2005). These findings described the most significant biomolecule alterations in the cell membrane, such as fatty acids and proteins substances, following nucleic acids, particularly DNA and RNA, after being treated with EE13 at 1/2×MIC for 4 h.

The 2D PCA score plot demonstrated that the spectra of the control group were distinctly clustered with 76% PC1 and 6% PC2 (Figure 4.7A). The high positive loading of PC1 at 2936 , 1604 , 1407 , and 1037 cm^{-1} were in agreement with the negative score plot observed in the control. In contrast, the high negative loading at 1698 , 1259 , and 1104 cm^{-1} corresponds with the positive score plot of *S. aureus* subjected to the EE13 (Figure 4.7B). These results implied alterations of intracellular components, particularly fatty acids (2965 , 2954 , and 2936 cm^{-1}), proteins (1677 , 1629 , and 1104 cm^{-1}), and nucleic acids (1104 cm^{-1}) after exposure to the EE13. These findings indicate that EE13 exerts its effect by disrupting the cell membrane of *S. aureus*, which affects the components of fatty acids, protein molecules in cells, and nucleic acids.

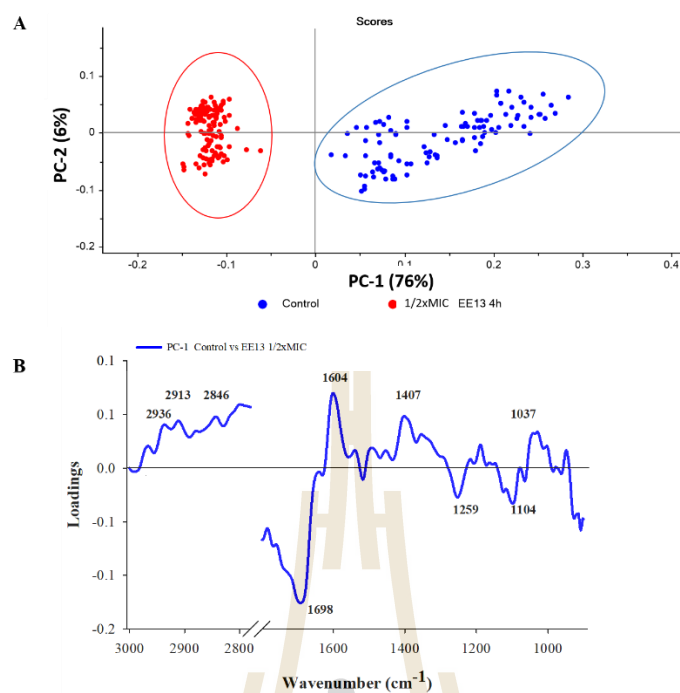


Figure 4.7 2D-PCA score plot (A) and loading plots (B) of whole spectrum data for *Staphylococcus aureus* ATCC 29213 treatment with EAGGGEDDKKKVE (EE13) at 1/2xMIC for 4 h

4.4.5.4 Molecular docking

Molecular docking simulations were conducted to identify the potential interactions between selected intracellular enzymes and EE13.

The lowest binding energy (ΔG) was demonstrated with the membrane-bound transglycosylase (PDB ID: 3VMQ_B), indicating the stronger binding affinity between the EE13 and the enzyme. Membrane-bound transglycosylase is a multidomain protein essential for cell wall synthesis in *S. aureus*. It is important for peptidoglycan synthesis, a key component of bacterial cell walls (Huang et al., 2012). The lowest dissociation constant (K_d) was also observed with this receptor. K_d represents a key measure of binding affinity in peptide-protein interactions. The lower the K_d , the tighter the interactions between the EE13 and the enzyme.

Table 4.3 Energy binding affinity (ΔG) and dissociation constant (K_d) of the interaction of EE13 with different receptors in *Staphylococcus aureus*

Receptor	Energy binding affinity (ΔG) (kcal.mol ⁻¹)	Dissociation constant (K_d) at 25 °C (M)
Membrane-bound transglycosylase (PDB ID: 3VMQ_B)	-10.6	1.8×10^{-8}
D-alanine-D-alanine ligase (PDB ID: 7U9K_B)	-10.1	4.2×10^{-8}
Amidase LtyH (PDB ID: 7TJ4_B)	-10.1	3.8×10^{-8}
Hydrolase AmiA (PDB ID: 4KNL_B)	-10.1	3.7×10^{-8}
Peptidoglycan D-Acetyl Transferase (PDB ID: 6WN9_B)	-6.9	8.3×10^{-6}
Thymidylate synthase (PDB ID: 4DQ1_B)	-10.3	2.9×10^{-8}
Thymidylate kinase (PDB ID: 4GFD_B)	-9.3	1.4×10^{-7}
DNA Gyrase (PDB ID: 2XCT_B)	-8.2	1.0×10^{-6}
Dihydrofolate reductase (PDB ID: 3SRQ)	-7.5	3.0×10^{-6}

The molecular docking complexes derived from CABSdock were employed to evaluate the amino acid residue interaction between peptide EE13 and the receptors. The DimPlot tool from LigPlot⁺ and the PDBsum tool of EMBL-EBI generated the two-dimensional interactions. Figure 4.8A presents the molecular docking of EE13 with membrane-bound transglycosylase (PDB ID: 3VMQ_B), which has the lowest binding energy of $-10.6 \text{ kcal.mol}^{-1}$. DimPlot (Figure 4.8B) and PDBsum (Figure 4.8C) demonstrate the interactions between the amino acid residues of EE13 and the amino acid residues of membrane-bound transglycosylase. Hydrogen bonds are formed between residues Gly3 of EE13 with Lys248 of the enzyme and Asp7 of EE13 with Ser221 of the enzyme (Figure. 4.8C). In addition, salt bridges were formed between residues Glu1 of EE13 with Arg117 of enzyme and Glu6 of EE13 with Arg241 of enzyme (Figure 4.8C). Moreover, there were several nonbonded interactions between EE13 and receptor 3VMQ_B. Nonbonded interaction in peptide-protein complex refers to a variety of non-covalent interactions that occur between peptides and proteins in the absence of the formation of chemical bonds. These interactions consist of van der Waals forces, electrostatic interactions, and hydrophobic effects (Atilgan, Turgut, & Atilgan, 2007). Huang et al. (2012) identified membrane-bound transglycosylase (PDB ID: 3VMQ) as a potential target for the development of antimicrobial agents. The role of

transglycosylase is to assemble the glycan backbone of peptidoglycan and facilitate its incorporation into the existing cell wall to maintain cell shape and integrity (Scheffers & Pinho, 2005). These results suggested that EE13 is preferentially bound to a membrane-bound transglycosylase (PDB ID: 3VMQ_B), which could lead to malfunction in cell membrane synthesis.

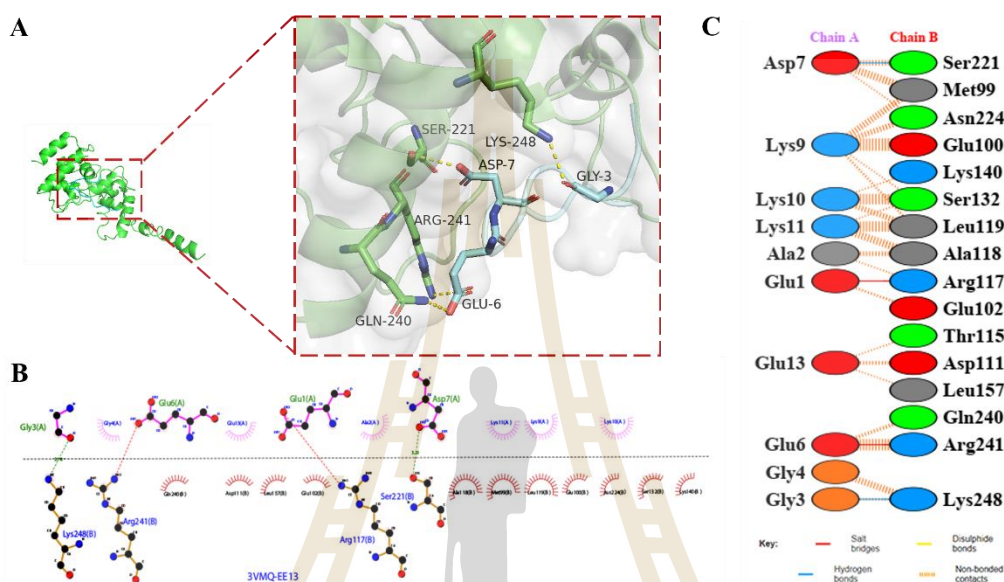


Figure 4.8 A docking illustration of the complex of membrane-bound transglycosylase (PDB ID: 3VMQ_B) and peptide EE13 (A) the binding site (B) the binding relationship between amino acid (C) interaction profile showed hydrogen bonds, salt bridges, and nonbonded interactions. The chain A is for EE13, and the chain B is for 3VMQ_B.

In addition, a low binding affinity energy of $10.1 \text{ kcal.mol}^{-1}$ was observed in D-alanine-D-alanine ligase (PDB ID: 7U9K_B, Table 4.4). D-alanine-D-alanine ligase represents an essential enzyme in the biosynthesis of the bacterial cell wall in *S. aureus* (Batson et al., 2017; Becker et al., 2023). The enzyme catalyzes the formation of D-alanine-D-alanine dipeptide, utilizing a two-step process. In the initial reaction, one mole of D-alanine and one mole of ATP act as substrates, while the second D-alanine is employed in the subsequent step (Liu et al., 2006). This dipeptide is important for the building block of peptidoglycan, the main structural component of bacterial cell walls. Figure 4.9A illustrates the interaction of EE13 and enzyme D-Ala-D-Ala ligase. The interaction between the EE13 and 7U9K_B was described by DimPlot (Figure 4.9B) and PDBsum (Figure 4.9C). A hydrogen bond was shown by residue Glu1 of EE13 and Trp49

of 7U9K (Figures 4.9B-C). No salt bridge was formed between the EE13 and the enzyme. In addition, there were several nonbonded interactions between residue EE13 and 7U9K_B. Based on molecular docking, EE13 displays a preference for interacting with enzymes involved in peptidoglycan synthesis.

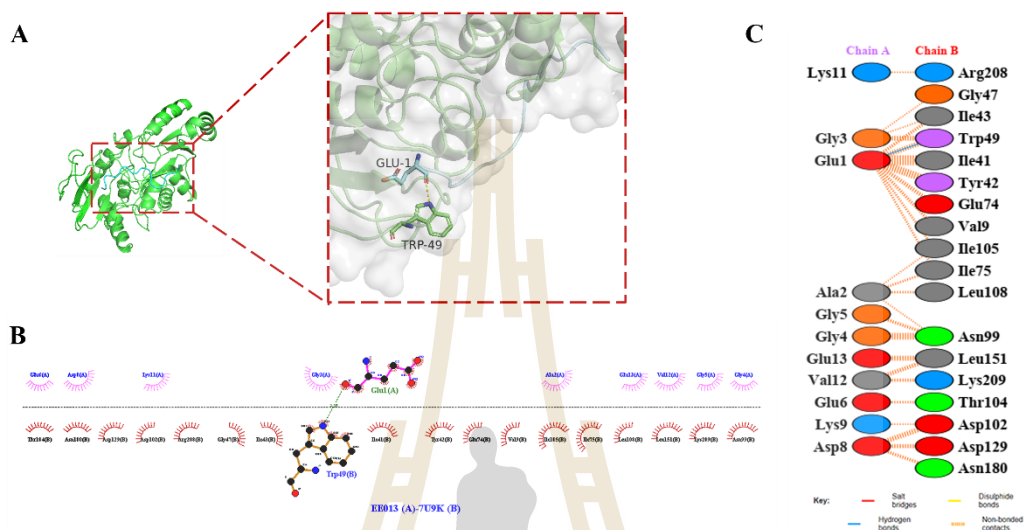


Figure 4.9 A docking illustration of the complex of d-alanine-d-alanine ligase (PDB ID: 7U9K_B) and peptide EE13 (A) the binding site (B) the binding relationship between amino acids (C) interaction profile showed hydrogen bond and nonbonded interactions. The chain A is for EE13 and the chain B is 7U9K_B.

The molecular docking studies indicate that enzymes involved in peptidoglycan biosynthesis could be the main target of EE13 peptide, resulting in discontinuity of the peptidoglycan synthesis as evidenced by membrane disruption shown in CLSM (Figure 4.4), morphological changes by SEM (Figure 4.5) and SR-FTIR (Figure 4.6).

4.4.6 Hemolytic activity

Synthetic peptides have to undergo hemolytic activity testing to ascertain their lack of toxicity to red blood cells (Robles-Loaiza et al., 2022). The EE13 was found to have no hemolytic effect at all concentrations tested. The EE13 at 1×MIC (4.0 mM) did not cause hemolysis (Figure 4.10). Hemolysis rate of EE13 in RBC samples was lower than 10%, which is considered as the maximum allowable hemolytic rate

(Greber, Dawgul, Kamysz, & Sawicki, 2017). The low hemolysis rate suggested that EE13 is safe for application in food industries.

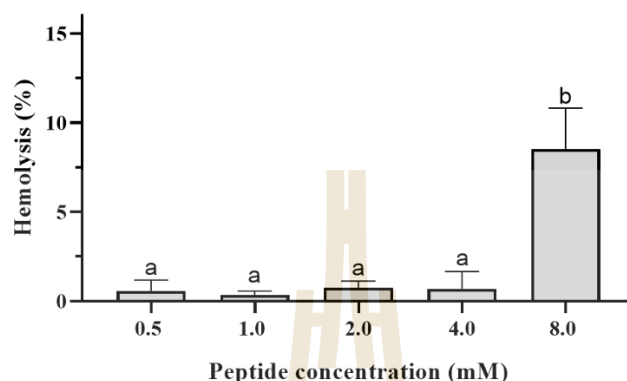


Figure 4.10 The hemolytic activity of the EAGGGEDDKKKVE (EE13) on human red blood cells.

Data are given as Mean \pm SD ($n = 3$)

4.4.7 The combined effect of mild heat and peptide EE13 treatment

To reduce the effective dose of EE13, the effect of combined mild heat and peptide was investigated. The combination of mild heat at 50 °C for 10 min with 2.0 mM EE13 (1/2xMIC) showed the most effective reduction of about 1 log CFU.mL⁻¹ (Figure 4.13). Cells that were not exposed to heat (25 °C) with added EE13 at 0.5 and 1.0 mM showed an increase in viable cell counts of 6.5 log CFU.mL⁻¹ to 7.2 log CFU.mL⁻¹ after 8 h (Figure 4.11), indicating ineffectiveness of EE13 at these concentrations. However, at 2.0 mM, a decrease in the cell number of about 0.6 log CFU.mL⁻¹ was observed after 8 h. This result indicated that EE13 at 2.0 mM slightly suppressed the growth of *S. aureus*.

Treatment at 40 °C for 10 min without peptide had no effect on growth inhibition of *S. aureus*, as a 7.3 log CFU.mL⁻¹ increase was observed (Figure. 4.11). The addition of EE13 at 1.0 and 2.0 mM showed a slight decrease of 6.5 and 6.0 log CFU.mL⁻¹, respectively, compared to the treatment without peptide.

At 50 °C for 10 min treatment alone, growth of *S. aureus* was still observed, with an approximately 7.2 log CFU.mL⁻¹ increase after 8 h. The addition of EE13 at 0.5 and 1.0 mM had no effect on growth inhibition. In contrast, when EE13 at 2.0 mM was added, a significant reduction of 4.5 log CFU.mL⁻¹ was observed compared

to the 50 °C without peptide group. This was likely due to cell damage caused by 50 °C for 10 min, facilitating damage to the cell membrane and further the peptide at 2.0 mM, intensifying the damage to the cell membrane and subsequently causing cell death. This is indicated by the cell count decrease from 5.5 log CFU.mL⁻¹ to 4.5 log CFU.mL⁻¹ after 8 h after peptide EE13 2.0 mM was added. In comparison to the variation in the combination of mild heat at a specific temperature and peptide concentration, it is evident that there is an increase in the number of cells. For instance, the combination of mild heat at 40 and 50 °C with peptide at 0.5 mM (1/8×MIC) caused a rise in cell counts from 6.5 log CFU.mL⁻¹ to 7.3 and 7.1 log CFU.mL⁻¹, respectively after incubated 8 h. This suggests that the *S. aureus* cells recovered from the cell injury condition caused by mild heat, and the peptide concentration was unsuitable for inhibiting the cell count.

In contrast, no cells were observed in the combined heat at 60 °C with peptide EE13 at 2.0 mM (1/2×MIC). These results suggested that cells experienced death in the combined thermal treatment at 60 °C, followed by the application of peptide at 2.0 mM. It should be mentioned that mild heat treatments at 40 and 50 °C without peptide had no effect on growth inhibition as about 7.2-7.4 log CFU.mL⁻¹ increase was observed after 8 h after the treatment. At 60 °C treatment without peptide, although about 2.8 log CFU.mL⁻¹ was noticed at the time after heat treatment, cell counts increased to 4.5-5 log CFU.mL⁻¹ after 8 h. This indicated that *S. aureus* cells at 60 °C for 10 min treatment experienced cell injury. These results suggest that combining mild heat at 50 °C for 10 min with peptide at 2.0 mM treatment was the best treatment for reducing the *S. aureus* cells (Figure 4.11).

These findings are consistent with the study of Ebrahimi, Csonka, & Alam, (2017), who reported the effect of mild heat shock at 50-55 °C for ≤12 min on the *S. Typhimurium* cell membrane, causing a small cytoplasmic leakage without cell lysis. In addition, Kennedy et al. (2019) mentioned that a mild heat effect between 50-60 °C for 10 min induced a slight permeability on the cell membrane of *S. aureus*. Ueckert, Ter Steeg, & Coote (1998) demonstrated the synergism of mild heat treatment (48 °C, 5 min) followed by the addition of nisin at a low concentration (0.1 µg.mL⁻¹) resulted in an increase in damaged cell membranes of *Lactobacillus plantarum* compared to either heat treatment alone.

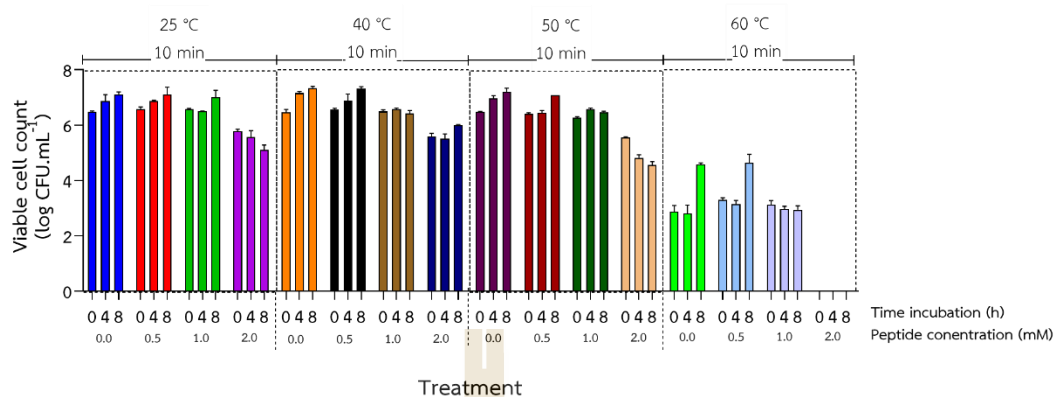


Figure 4.11 Effect of combined mild heat treatment and the peptide EAGGGEDDKKKVE (EE13) on the growth of *Staphylococcus aureus* ATCC 29213 cells after 0, 4, and 8 h incubation time

4.4.7.1 The combined effect on membrane integrity

The findings from the application of the most effective combination of mild heat (50 °C for 10 min) and peptide (1/2×MIC = 2.0 mM) were then elucidated through the examination of the membrane integrity and cell morphology of *S. aureus*.

CLSM images of the untreated *S. aureus* ATCC 29213 distinctly showed green fluorescence of SYTO-9, which indicated the integrity of cell membranes (Figure 4.12A). When cells were subjected to 50 °C for 10 min, the green color fluorescent of SYTO-9 was reduced in concomitant with an increase in red fluorescent of PI (Figure 4.12B). Cells exposed to only peptide 2 mM EE13 (2.0 mM) also showed an increased red fluorescence of PI (Figure 4.12C). These results indicated that a single treatment either mild heat (50 °C for 10 min) or the EE13 (1/2×MIC = 2.0 mM), was able to disrupt the cell membrane of *S. aureus* to a certain extent. With the combined treatment, it can be seen that the intensity of PI fluorescence did not increase significantly (Figure 4.12D). This may be due to *S. aureus* cells experiencing death due to the combination of mild heat and peptide EE13. So, it could not be captured by an increase in PI intensity. This observation revealed that the combined effect could result in a more extensive disruption of the membrane integrity of cells than that observed with the individual treatments. Furthermore, the application of mild heat treatment at 50 °C for 10 min on cells at an earlier stage can facilitate the entry of peptides with concentrations below its MIC (1/2×MIC=2.0 mM).

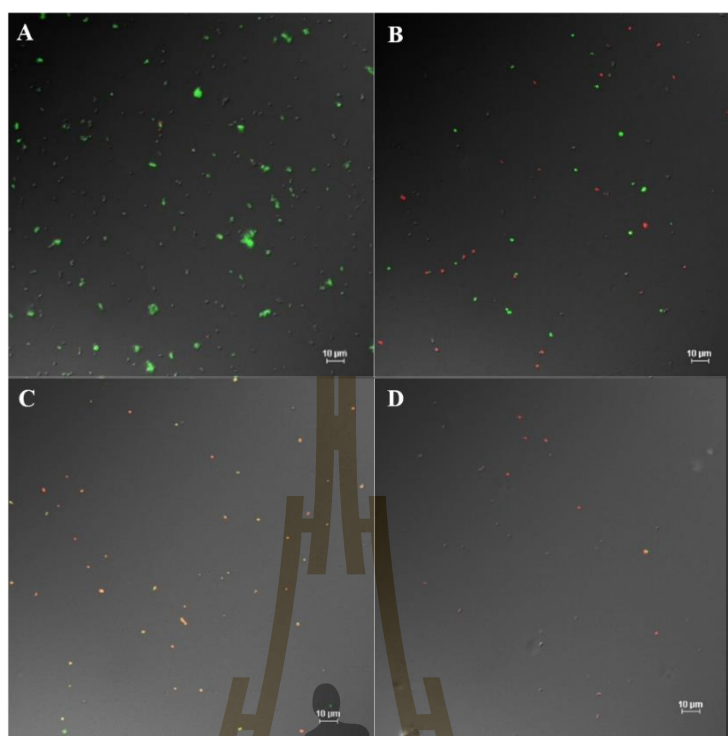


Figure 4.12 CLSM images of *Staphylococcus aureus* ATCC 29213 (A) untreated cells, (B) cells treated with mild heat temperature 50 °C for 10 min, (C) cells treated with EE13 at 1/2×MIC (2.0 mM), and (D) cells treated with the combination of mild heat temperature at 50 °C for 10 min and EE13 at 1/2×MIC (2.0 mM) incubated 37 °C, 4 h. Scale bar is 10 µm.

4.4.7.2 Localization of 5-carboxyfluorescein-EE13 in *S. aureus* cells

The CLSM image of the untreated *S. aureus* cells exhibited intact cells (Figure 4.13A). In contrast, cells treated with the EE13 labeled with 5-carboxyfluorescein (5-FAM) exhibited green fluorescence properties of FAM, while cells treated with PI displayed red fluorescence properties of PI (Figure 4.13B). FAM-EE13 would give green color if the peptide is permeable. Furthermore, cells treated with the combination of mild heat and FAM-peptide demonstrated an increasing number of cells exhibiting green fluorescent color (Figure 4.13C). These results indicate that the localization of peptide FAM-EE13 in *S. aureus* cells that experience sublethal injury due to mild heat previously seen more peptides interact with cell membranes that have been damaged.

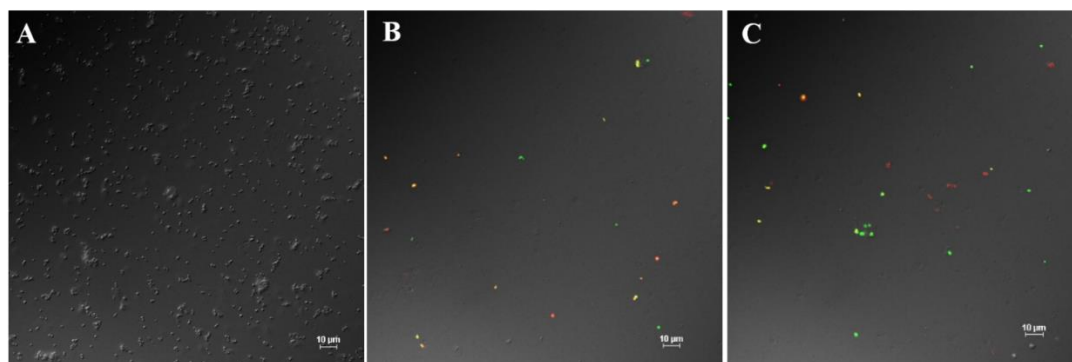


Figure 4.13 Localization of 5-carboxyfluorescein-EE13 in *Staphylococcus aureus* ATCC 29213 cells (A) untreated cells, (B) cells treated with 5-FAM-EE13 at 1/2xMIC (2.0 mM), and (C) cells treated with the combination of mild heat treatment at 50 °C for 10 min and 5-FAM-EE13 at 1/2xMIC (2.0 mM) incubated 37 °C for 4 h. Scale bar is 10 μm.

The EE13 labeled with FAM demonstrated that the peptide interacts with the cell membrane of *S. aureus*. This result was in line with Song et al. (2020), who demonstrated that KDFPGRR labeled with carboxyfluorescein (FAM), a peptide derived from cottonseed protein hydrolysate, interacts electrostatically with the cell membrane of *E. coli*. In addition, Rowe-Magnus, Kao, Prieto, Pu, & Kao (2019) reported that using the FAM-labeled cathelicidin analog could penetrate the *S. aureus* cell wall.

4.4.7.3 The combined effect on morphology changes of *S. aureus* cells

The morphological changes in *S. aureus* ATCC 29213 cells were induced by either mild heat or EE13 alone, and their combined treatments were observed (Figure 4.14). The untreated *S. aureus* ATCC 29213 cells appeared to have smooth cocci characteristics (Figure 4.14A). When a treatment of 50 °C for 10 min was applied, some dented cells, along with majority of typical cocci. This suggested that the impact of 50 °C on the *S. aureus* cells physical appearance. Morphological changes on the membrane surface were notable in cells treated with EE13 (Figure 4.14B and C), but no extensive damages to cell integrity. This could be due to the low concentration of the applied EE13. The combined treatment induced significant morphological changes of cell shrinkages and pore formation (Figure 4.14D). These results may suggest that both mild heat at 50 °C and peptide at low concentration alone have a minor effect on the morphological changes. On the other hand, the

combination of 50 °C and 1/2×MIC EE13 resulted in significant cell damage and disruption, indicating that mild heat may result in minor damage to the cell membrane, subsequently facilitating the penetration of the peptide into the cell membrane, resulting in cell death.

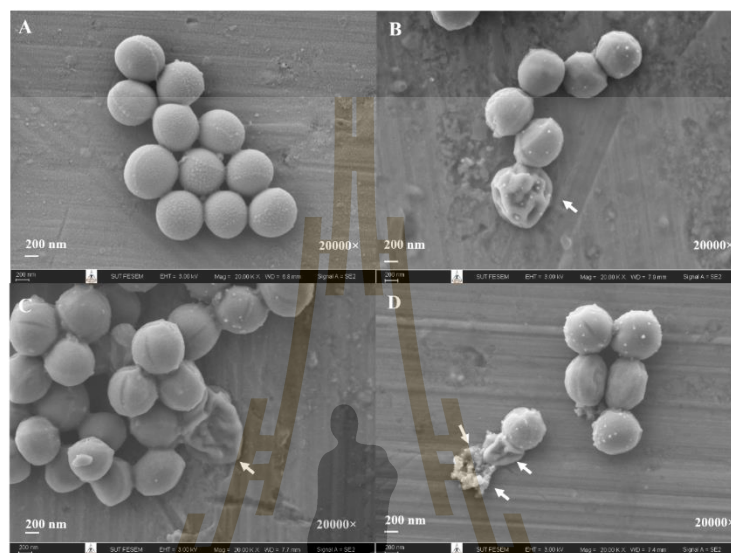


Figure 4.14 SEM images of *Staphylococcus aureus* ATCC 29213 cells subjected to various treatments: (A) Untreated cells (control), (B) cells treated with mild heat treatment at 50 °C for 10 min, (C) cells treated with EE13 at 1/2×MIC, and (D) cells treated with combined mild heat and followed by EE13 at 1/2×MIC treatment. The scale bar is 200 nm. White arrows indicate morphological changes.

4.5 Conclusion

The novel anionic EAGGGEDDKKKVE (EE13) peptide derived from CGM hydrolysate demonstrated the most potent antibacterial activity against *Staphylococcus aureus* ATCC 29213. EE13 caused a perforation in the membrane integrity of *S. aureus* cells. In addition, EE13 triggered morphological changes in *S. aureus* cells, including irregular shape with pore formation on the cell surface and cell lysis, leading to cell death. Moreover, SR-FTIR assay revealed alterations in cellular component of *S. aureus*, including fatty acids, proteins, and nucleic acids, when treated with EE13. Molecular docking studies revealed that EE13 has a strong binding affinity with membrane-bound transglycosylase, an essential enzymes for peptidoglycan synthesis in *S. aureus*. The EE13 was categorized as having low hemolytic activity below

8.0 mM. A synergistic effect was demonstrated by mild heat at 50 °C for 10 min, followed by 2.0 mM EE13 on *S. aureus* cells, resulting in membrane breakage in *S. aureus*. Therefore, this peptide could offer promising prospects for utilization in the food industries.

4.6 References

- Akbarian, M., Khani, A., Eghbalpour, S., & Uversky, V. N. (2022). Bioactive peptides: Synthesis, sources, applications, and proposed mechanisms of action. *International Journal of Molecular Sciences*, *23*(3), 1445.
- Atilgan, A. R., Turgut, D., & Atilgan, C. (2007). Screened nonbonded interactions in native proteins manipulate optimal paths for robust residue communication. *Biophysical Journal*, *92*(9), 3052–3062.
- Batson, S., De Chiara, C., Majce, V., Lloyd, A. J., Gobec, S., Rea, D., ... Roper, D. I. (2017). Inhibition of D-Ala:D-Ala ligase through a phosphorylated form of the antibiotic D-cycloserine. *Nature Communications*, *8*(1), 1–7.
- Bax, B. D., Chan, P. F., Eggleston, D. S., Fosberry, A., Gentry, D. R., Gorrec, F., ... Gwynn, M. N. (2010). Type IIA topoisomerase inhibition by a new class of antibacterial agents. *Nature*, *466*(7309), 935–940.
- Bechinger, B., & Gorr, S. U. (2017). Antimicrobial peptides: Mechanisms of action and resistance. *Journal of Dental Research*, *96*(3), 254–260.
- Becker, R., Pederick, J. L., Dawes, E. G., Bruning, J. B., & Abell, A. D. (2023). Structure-guided design and synthesis of ATP-competitive N-acyl-substituted sulfamide D-alanine-D-alanine ligase inhibitors. *Bioorganic and Medicinal Chemistry*, *96*, 117509.
- Benfield, A. H., & Henriques, S. T. (2020). Mode-of-action of antimicrobial peptides: Membrane disruption vs. intracellular mechanisms. *Frontiers in Medical Technology*, *2*, 610997.
- Berman, H. M., Westbrook, J., Feng, Z., Gililand, G., Bhat, T. N., Weissig, H., ... Bourne, P. E. (2000). The protein data bank. *Nucleic Acids Research*, *28*(1), 235–242.
- Błaszczuk, M., Kurcinski, M., Kouza, M., Wieteska, L., Debinski, A., Kolinski, A., & Kmiecik, S. (2016). Modeling of protein-peptide interactions using the CABS-dock web server for binding site search and flexible docking. *Methods*, *93*, 72–83.
- Büttner, F. M., Zoll, S., Nega, M., Götz, F., & Stehle, T. (2014). Structure-function analysis of *Staphylococcus aureus* amidase reveals the determinants of peptidoglycan recognition and cleavage. *Journal of Biological Chemistry*, *289*(16), 11083–11094.

- Ciociola, T., Giovati, L., Giovannelli, A., Conti, S., Castagnola, M., & Vitali, A. (2018). The activity of a mammalian proline-rich peptide against Gram-negative bacteria, including drug-resistant strains, relies on a nonmembranolytic mode of action. *Infection and Drug Resistance*, *11*, 969–979.
- Davis, R., & Mauer, L. (2010). Fourier transform infrared (FT-IR) spectroscopy: A rapid tool for detection and analysis of foodborne pathogenic bacteria. In Méndez-Vilas, A. (Ed.). *Current Research, Technology and Education Topics in Applied Microbiology and Microbial Biotechnology* (pp. 1582–1594). Badajoz: Formatex Research Center.
- de Almeida, N. R., Han, Y., Perez, J., Kirkpatrick, S., Wang, Y., & Sheridan, M. C. (2019). Design, synthesis, and nanostructure-dependent antibacterial activity of cationic peptide amphiphiles. *ACS Applied Materials and Interfaces*, *11*(3), 2790–2801.
- Dennison, S. R., Harris, F., Mura, M., & Phoenix, D. A. (2018). An atlas of anionic antimicrobial peptides from amphibians. *Current Protein & Peptide Science*, *19*(8), 823–838.
- Dennison, S. R., Howe, J., Morton, L. H. G., Brandenburg, K., Harris, F., & Phoenix, D. A. (2006). Interactions of an anionic antimicrobial peptide with *Staphylococcus aureus* membranes. *Biochemical and Biophysical Research Communications*, *347*(4), 1006–1010.
- Ebrahimi, A., Csonka, L. N., & Alam, M. A. (2017). Analyzing thermal stability of cell membrane of *Salmonella* using time-multiplexed impedance sensing. *Biophysical Journal*, *114*(3), 609–618.
- Gasteiger, E., Hoogland, C., Gattiker, A., Duvaud, S., Wilkins, M. R., Appel, R. D., & Bairoch, A. (2005). Protein identification and analysis tools on the ExPASy server. In Walker, J. M. (Ed.). *The Proteomics Protocols Handbook* (pp. 571–608). Totowa: Humana Press-Springer Science.
- Gautier, R., Douguet, D., Antonny, B., & Drin, G. (2008). HELIQUEST: A web server to screen sequences with specific α -helical properties. *Bioinformatics*, *24*(18), 2101–2102.
- Ghanbari, R., & Ebrahimpour, A. (2018). Separation and identification of bromelain-generated antibacterial peptides from *Actinopyga lecanora*. *Food Science and Biotechnology*, *27*(2), 591–598.
- Giaccone, D., Revello-Chion, A., Galassi, L., Bianchi, P., Battelli, G., Coppa, M., ... Borreani, G. (2016). Effect of milk thermisation and farming system on cheese sensory profile and fatty acid composition. *International Dairy Journal*, *59*, 10–19.
- Greber, K. E., Dawgul, M., Kamysz, W., & Sawicki, W. (2017). Cationic net charge and counter ion type as antimicrobial activity determinant factors of short

- lipopeptides. *Frontiers in Microbiology*, *8*, 123.
- Honorato, R. V., Koukos, P. I., Jiménez-García, B., Tsaregorodtsev, A., Verlato, M., Giachetti, A., ... Bonvin, A. M. J. J. (2021). Structural biology in the clouds: The WeNMR-EOSC ecosystem. *Frontiers in Molecular Biosciences*, *8*, 729513.
- Huang, C. Y., Shih, H. W., Lin, L. Y., Tien, Y. W., Cheng, T. J. R., Cheng, W. C., .. Ma, C. (2012). Crystal structure of *Staphylococcus aureus* transglycosylase in complex with a lipid II analog and elucidation of peptidoglycan synthesis mechanism. *Proceedings of the National Academy of Sciences of the United States of America*, *109*(17), 6496–6501.
- Jones, C. S., Sychantha, D., Lynne Howell, P., & Clarke, A. J. (2020). Structural basis for the O-acetyltransferase function of the extracytoplasmic domain of OatA from *Staphylococcus aureus*. *Journal of Biological Chemistry*, *295*(24), 8204–8213.
- Keating, T. A., Newman, J. V., Olivier, N. B., Otterson, L. G., Andrews, B., Boriack-Sjodin, P. A., ... Martínez-Botella, G. (2012). In vivo validation of thymidylate kinase (TMK) with a rationally designed, selective antibacterial compound. *ACS Chemical Biology*, *7*(11), 1866–1872.
- Kennedy, D., Cronin, U. P., Piterina, A., & Wilkinson, M. G. (2019). Heat and chemical treatments affect the viability, morphology, and physiology of *Staphylococcus aureus* and its subsequent antibody labeling for flow cytometric analysis. *Applied and Environmental Microbiology*, *85*(17), 1–15.
- Kurcinski, M., Jamroz, M., Blaszczyk, M., Kolinski, A., & Kmiecik, S. (2015). CABS-dock web server for the flexible docking of peptides to proteins without prior knowledge of the binding site. *Nucleic Acids Research*, *43*(W1), W419–W424.
- Lamiable, A., Thevenet, P., Rey, J., Vavrusa, M., Derreumaux, P., & Tuffery, P. (2016). PEP-FOLD3: Faster denovo structure prediction for linear peptides in solution and in complex. *Nucleic Acids Research*, *44*(1), W449–W454.
- Lasch, P., & Naumann, D. (2015). Infrared spectroscopy in microbiology. In *Encyclopedia of Analytical Chemistry* (pp. 1–32). Hoboken, NJ: John Wiley & Sons, Inc.
- Laskowski, R. A. (2009). PDBsum new things. *Nucleic Acids Research*, *37*(Suppl_1), D355–D359.
- Laskowski, R. A., & Swindells, M. B. (2011). LigPlot+: Multiple ligand-protein interaction diagrams for drug discovery. *Journal of Chemical Information and Modeling*, *51*(10), 2778–2786.
- Li, X., Hilgers, M., Cunningham, M., Chen, Z., Trzoss, M., Zhang, J., ... Finn, J. (2011). Structure-based design of new DHFR-based antibacterial agents: 7-aryl-2,4-diaminoquinazolines. *Bioorganic and Medicinal Chemistry Letters*, *21*(18), 5171–5176.

- Lima, R. C., de Carvalho, A. P. A., Vieira, C. P., Moreira, R. V., & Conte-Junior, C. A. (2021). Green and healthier alternatives to chemical additives as cheese preservative: Natural antimicrobials in active nanopackaging/coatings. *Polymers*, *13*(16), 2675.
- Liu, S., Chang, J. S., Herberg, J. T., Hornig, M. M., Tomich, P. K., Lin, A. H., & Marotti, K. R. (2006). Allosteric inhibition of *Staphylococcus aureus* D-alanine:D-alanine ligase revealed by crystallographic studies. *Proceedings of the National Academy of Sciences of the United States of America*, *103*(41), 15178–15183.
- Lomize, M. A., Pogozheva, I. D., Joo, H., Mosberg, H. I., & Lomize, A. L. (2012). OPM database and PPM web server: Resources for positioning of proteins in membranes. *Nucleic Acids Research*, *40*(D1), 370–376.
- López-Malo, A., Barreto-Valdivieso, J., Palou, E., & Martín, F. S. (2007). *Aspergillus flavus* growth response to cinnamon extract and sodium benzoate mixtures. *Food Control*, *18*(11), 1358–1362.
- Ma, B., Guo, Y., Fu, X., & Jin, Y. (2020). Identification and antimicrobial mechanisms of a novel peptide derived from egg white ovotransferrin hydrolysates. *LWT - Food Science and Technology*, *131*, 109720.
- McMahon, M. A. S., Xu, J., Moore, J. E., Blair, I. S., & McDowell, D. A. (2007). Environmental stress and antibiotic resistance in food-related pathogens. *Applied and Environmental Microbiology*, *73*(1), 211–217.
- Movasaghi, Z., Rehman, S., & Rehman, I. U. (2008). Fourier transform infrared (FTIR) spectroscopy of biological tissues. *Applied Spectroscopy Reviews*, *43*(2), 134–179.
- Nurhartadi, E., Rodtong, S., Thumanu, K., Park, S. H., Aluko, R. E., & Yongsawatdigul, J. (2024). Antibacterial activity of enzymatic corn gluten meal hydrolysate and ability to inhibit *Staphylococcus aureus* in ultra-high temperature processed milk. *Manuscript Submitted for Publication*.
- Page, J. E., Skiba, M. A., Do, T., Kruse, A. C., & Walker, S. (2022). Metal cofactor stabilization by a partner protein is a widespread strategy employed for amidase activation. *Proceedings of the National Academy of Sciences of the United States of America*, *119*(26), 1–10.
- Robles-Loaiza, A. A., Pinos-Tamayo, E. A., Mendes, B., Ortega-Pila, J. A., Proaño-Bolaños, C., Plisson, F., ... Almeida, J. R. (2022). Traditional and computational screening of non-toxic peptides and approaches to improving selectivity. *Pharmaceuticals*, *15*(3), 323.
- Rowe-Magnus, D. A., Kao, A. Y., Prieto, A. C., Pu, M., & Kao, C. (2019). Cathelicidin peptides restrict bacterial growth via membrane perturbation and induction of reactive oxygen species. *MBio*, *10*(5), 1–19.

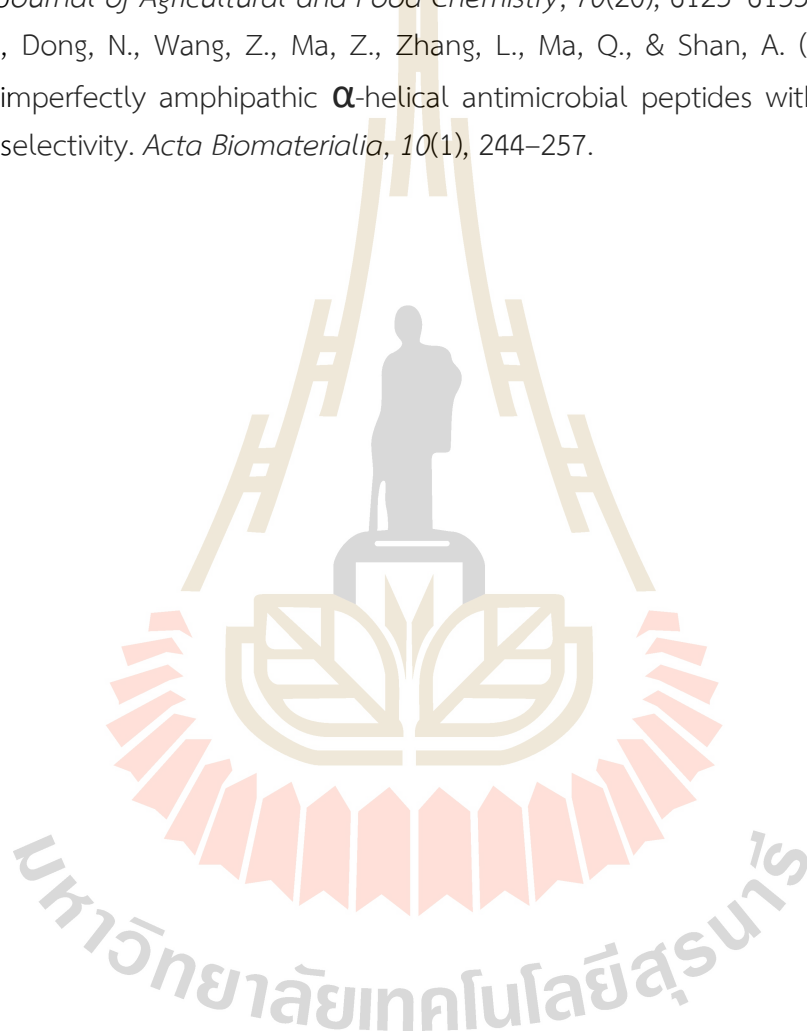
- Scheffers, D.-J., & Pinho, M. G. (2005). Bacterial cell wall synthesis: New insights from localization studies. *Microbiology and Molecular Biology Reviews*, 69(4), 585–607.
- Song, W., Kong, X., Hua, Y., Chen, Y., Zhang, C., & Chen, Y. (2020). Identification of antibacterial peptides generated from enzymatic hydrolysis of cottonseed proteins. *LWT - Food Science and Technology*, 125, 109199.
- Straus, S. K., & Hancock, R. E. W. (2006). Mode of action of the new antibiotic for Gram-positive pathogens daptomycin: Comparison with cationic antimicrobial peptides and lipopeptides. *Biochimica et Biophysica Acta - Biomembranes*, 1758(9), 1215–1223.
- Tian, F., Rodtong, S., Thumanu, K., Hua, Y., Roytrakul, S., & Yongsawatdigul, J. (2022). Molecular insights into the mode of action of antibacterial peptides derived from chicken plasma hydrolysates. *Foods*, 11(22), 3564.
- U. S. Food and Drug Administration. (2024). *CFR-Code of Federal Regulations Title 21*. Retrieved from <https://www.accessdata.fda.gov/scripts/cdrh/cfdocs/cfcfr/cfrsearch.cfm?fr=184.1733>
- Ueckert, J. E., Ter Steeg, P. F., & Coote, P. J. (1998). Synergistic antibacterial action of heat in combination with nisin and magainin II amide. *Journal of Applied Microbiology*, 85(3), 487–494.
- van Hilten, N., Verwei, N., Methorst, J., Nase, C., Bernatavicius, A., & Risselada, H. J. (2024). PMLpred: a physics-informed web server for quantitative protein-membrane interaction prediction. *Bioinformatics*, 40(2), 1–10.
- Vangone, A., & Bonvin, A. M. J. J. (2015). Contacts-based prediction of binding affinity in protein–protein complexes. *ELife*, 4, e07454.
- Wang, J., Chou, S., Xu, L., Zhu, X., Dong, N., Shan, A., & Chen, Z. (2015). High specific selectivity and membrane-active mechanism of the synthetic centrosymmetric α -helical peptides with Gly-Gly pairs. *Scientific Reports*, 5, 15963.
- Wiegand, I., Hilpert, K., & Hancock, R. E. W. (2008). Agar and broth dilution methods to determine the minimal inhibitory concentration (MIC) of antimicrobial substances. *Nature Protocols*, 3(2), 163–175.
- Wimley, W. (2010). Describing the mechanism of antimicrobial peptide action with the interfacial activity model. *ASC Chemical Biology*, 5(10), 905–917.
- Wuytack, E. Y., Phuong, L. D. T., Aertsen, A., Reyns, K. M. F., Marquenie, D., De Ketelaere, B., ... Michiels, C. W. (2003). Comparison of sublethal injury induced in *Salmonella enterica* serovar Typhimurium by heat and by different nonthermal treatments. *Journal of Food Protection*, 66(1), 31–37.
- Xue, L. C., Rodrigues, J. P., Kastiris, P. L., Bonvin, A. M., & Vangone, A. (2016). PRODIGY:

A web server for predicting the binding affinity of protein-protein complexes. *Bioinformatics*, 32(23), 3676–3678.

Yu, C., & Irudayaraj, J. (2005). Spectroscopic characterization of microorganisms by Fourier transform infrared microspectroscopy. *Biopolymers*, 77(6), 368–377.

Zhao, Q., He, L., Wang, X., Ding, X., Li, L., Tian, Y., & Huang, A. (2022). Characterization of a novel antimicrobial peptide isolated from *Moringa oleifera* seed protein hydrolysates and its membrane damaging effects on *Staphylococcus aureus*. *Journal of Agricultural and Food Chemistry*, 70(20), 6123–6133.

Zhu, X., Dong, N., Wang, Z., Ma, Z., Zhang, L., Ma, Q., & Shan, A. (2014). Design of imperfectly amphipathic α -helical antimicrobial peptides with enhanced cell selectivity. *Acta Biomaterialia*, 10(1), 244–257.



CHAPTER V

MODIFICATION AND MECHANISM OF ACTION OF PEPTIDE DERIVED FROM CORN GLUTEN MEAL HYDROLYSATE

5.1 Abstract

The current study aims to modify a peptide from corn gluten meal hydrolysate and explain its action on the susceptible *Salmonella* Typhimurium TISTR 292. Results showed that the structural modification of peptide PTGAKVTKAAKKA (PA13), which has a minimum inhibition concentration (MIC) of >4 mM to RLLRKVTKLWKKF (RF135), resulted in enhancing antibacterial activity with the MIC of 4.0 μ M against *S. Typhimurium* TISTR 292. The *S. Typhimurium* killing curve revealed that RF135 at 1/2xMIC indicated a bacteriostatic effect at 1 h exposure, at 1xMIC causing a bactericidal effect after 2 h, except for 2xMIC and 4xMIC, causing a bactericidal effect within 1 h. RF135 disrupted the membrane integrity of *S. Typhimurium* at 1xMIC for 2 h, indicated by the increase in red fluorescence intensity of propidium iodide. Localization of 5-FAM-labeled-RF135 revealed that the peptide interacted to *S. Typhimurium* cell membrane as observed by the green fluorescence. The increase in OD₂₆₀ indicated nucleic acid release from *S. Typhimurium* induced by RF135 at 1xMIC. Scanning electron microscopy (SEM) showed morphological alterations of the *S. Typhimurium* cells after being incubated with RF135 at 1/2xMIC and 1xMIC for 2 h. The pore formation, dents on the surface, and irregular shape of the peptide-treated cells were observed. The ultrastructure alteration of *S. Typhimurium* cells, including membrane cell leakage, cell swelling, and cytoplasmic leakage, was observed under transmission electron microscope after being treated with RF135 at 1xMIC and 2xMIC for 2 h. The RF135 at 1xMIC caused changes on fatty acids, proteins, and nucleic acids of *S. Typhimurium* cells as monitored by Synchrotron radiation-based Fourier transform infrared spectroscopy. The molecular docking suggested that RF135 strongly interacted with ArnD deformylase in the outer membrane of *S. Typhimurium*. The hemolysis assay showed low hemolysis up to a concentration of 512 μ M, which implies the safety of RF135. The structure modification of PA13 to RF135 resulted in an increase in the characteristics of molecular mass, pI, hydrophobicity, hydrophobic moment, and net

charge. The findings suggest that the structure alteration of peptides obtained from CGM hydrolysis could contribute to developing antibacterial peptides and potential applications in the food and pharmaceutical industries.

Keywords: Antibacterial peptide, disruption, mechanism of action, membrane integrity, peptide modification

5.2 Introduction

The overuse and misuse of antibiotics lead to an increase in antimicrobial resistance (AMR) problems. Bacterial AMR caused an estimated 1.27 million global deaths in 2019, contributing to 4.95 million overall (Murray et al., 2022). Antibiotic-resistant bacteria can be spread to humans in several forms, such as through contaminated food and water (Manyi-Loh, Mamphweli, Meyer, & Okoh, 2018).

Bacteria can become resistant to antibiotics through a variety of mechanisms, such as the production of enzymes that degrade and inactivate antibiotics, changes to antibiotic-binding ribosomal proteins, reduction of porins in the cell membrane, activation of antibiotics via efflux pumps, overproduction of dihydrofolate reductase; development of alternative metabolic pathways; and enzyme-mediated modification or inactivation of antibiotics (Reygaert, 2018; Zhang & Cheng, 2022). Growing evidence points on antimicrobial peptides (AMPs) as an effective strategy in the fight against antibiotic misuse. Various species, including microbes, plants, and mammals, naturally create AMPs to defend multiple microorganisms, including bacteria, fungi, and viruses (Huan, Kong, Mou, & Yi, 2020; Moretta et al., 2021). Contrary to antibiotics, AMPs have complex modes of action that involve intracellular processes and disruption of cell membranes (Benfield & Henriques, 2020). Therefore, the potential development of AMPs is highly significant as an alternative strategy to counteract antibiotic abuse.

The effectiveness of AMPs against microorganisms is influenced by a variety of properties. These include peptide length, net charge, hydrophobicity, specific structural features like α -helices, stability under different conditions, cellular impact, and their roles in biological processes (Huan et al., 2020; Zhang et al., 2023). Thus, understanding these characteristics is essential for obtaining insights into innate defenses, advancing infection treatments, and innovating new therapies for bacterial infection.

Peptide modification is a technique that has the potential to significantly enhance the antibacterial activity of AMPs. Various modifications have been sought to strengthen the efficacy of AMPs. These methods include designing hybrid peptides, creating self-assembled AMPs, increasing positive charges, coupling with antibiotics, lipidation, conjugating with metal-organic compounds, targeted alterations, amino acid substitutions, cyclic peptides development, microparticles, polymer formation, and applying nanotechnological changes (Han, Zhang, Lai, & Zhang, 2021; Tan et al., 2021). Modification of amino acid sequence might effectively enhance the peptides ability to combat bacteria (Mwangi, Kamau, Thuku, & Lai, 2023). The amino acid substitution technique can increase its stability, membrane interaction, amphiphaticity, specificity, and potential combination with other agents (Almeida et al., 2022; Chegini, Nikokar, Tabarzad, Faezi, & Mahboubi, 2019). Moreover, the substitution of amino acids can substantially increase peptide antimicrobial potency, primarily by increasing their binding to the bacterial membrane via hydrophobic amino acids (Huan et al., 2020). In addition, D-amino acid substitution can enhance membrane disruption and stabilize peptide structure (Hong, Oh, & Lee, 1999). Thereby, substituting amino acids can significantly transform peptide conformation, improving their ability to engage with and interfere the bacterial cell membrane integrity (Lu et al., 2020; Saint Jean et al., 2018).

In our former study, antibacterial activity testing was conducted on 11 peptides identified from corn gluten meal hydrolysate fraction. From the test, it was found that peptide PTGAKVTKAAKKA (PA13), which had a net charge of +4, its antibacterial activity was observed at more than 4000 μM against all bacteria tested. Peptide PA13 is a component of the parent peptide elongation factor 1-alpha of *Zea mays* (447 aa, MW 49,094 Da) at residue numbers 433 to 446 (Nurhartadi, Rodtong, Thumanu, & Yongsawatdigul, 2024b; Nurhartadi et al., 2024a). Therefore, PA13 was selected for the peptide structure modification study.

In this research, an authentic peptide obtained from corn gluten meal hydrolysate was modified to yield greater antimicrobial activity. Mechanisms of action on the most sensitive test bacterium were also investigated.

5.3 Materials and methods

5.3.1 Materials

Tryptic soy broth (TSB), Mueller-Hinton broth (MHB), microbiological agar, and plate count agar (PCA) were purchased from HiMedia™ (Mumbai, India). Sodium

chloride was purchased from RCI Labscan Ltd (Bangkok, Thailand). Propidium iodide and SYTO-9 were obtained from ThermoFisher Scientific™ (Waltham, MA, USA). Glutaraldehyde and osmium tetroxide were purchased from Electron Microscopy Sciences (Hatfield, PA, USA). Unless otherwise specified, all chemicals utilized in this research were of analytical grade.

5.3.2 Bacterial cultures

In this study, four Gram-positive bacteria, *Staphylococcus aureus* ATCC 29213, *Listeria monocytogenes* DMST 17303, *Bacillus cereus* DMST 5040, methicillin-resistant *S. aureus* ATCC 20652, and two Gram-negative bacteria, *Escherichia coli* TISTR 780, *Salmonella* Typhimurium TISTR 292 were employed as test microorganisms. All bacteria were maintained in a 20% glycerol solution and stored at -20 °C. Before use, the bacteria were cultured in trypticase soy broth (TSB) incubated at 37 °C for 24 h and subsequently streaked on tryptic soy agar (TSA) and incubated at 37 °C for 18-24 h to collect a single colony of the pure culture.

5.3.3 Peptide modification

PTGAKVTKAAKKA (PA13) was identified from the P1 fraction peptide derived from peptic-hydrolyze corn gluten meal and revealed that it did not exhibit antibacterial activity against all tested bacteria. Furthermore, RLLRKVTKLWKKF (RF135) was designed using PA13 peptide arrangement by replacing Pro (P¹) with Arg (R), Thr (T²) with Leu (L), Gly (G³) with Leu (L), Ala (A⁴) with Arg (R), Ala (A⁹) with Leu (L), Ala (A¹⁰) with Trp (W), and Ala (A¹³) with Phe (F) as depicted in Figure 5.1.

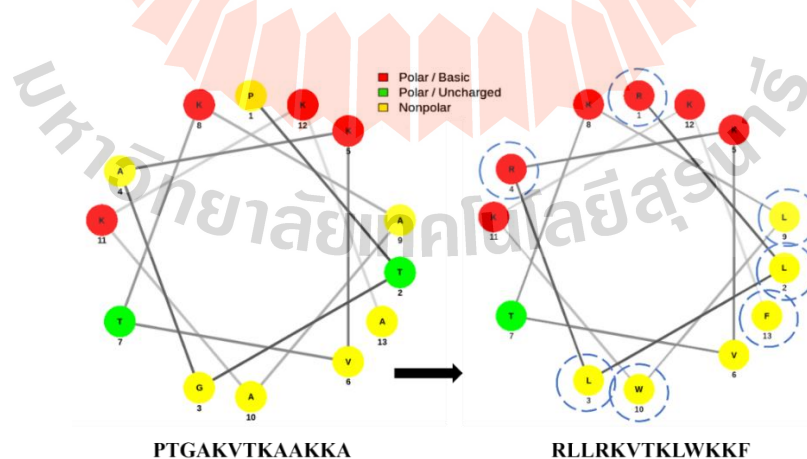


Figure 5.1 Structural modification of PA13 to RF135 using NetWheels. (<http://lbqp.unb.br/NetWheels/>)

5.3.4 Peptide synthesis

PTGAKVTKAAKKA (PA13) and its analog RLLRKVTKLWKKF (RF135) were synthesized using Fmoc chemistry at GL Biochem Ltd. (Shanghai, China). The crude peptides were refined and evaluated using RP-HPLC and ESI-MS to verify the purity which should be higher than 98%. Peptides were dissolved in sterile deionized water to make up a stock concentration of 1,000 μM and stored at $-20\text{ }^{\circ}\text{C}$.

5.3.5 Peptide informatic analysis

The peptide properties, including physical and chemical attributes, were explored using the ExPASy Bioinformatics Resource Portal (<http://www.expasy.org/tools/>). The net charge, hydrophobicity, and hydrophobic moment were generated using the HeliQuest (<http://heliquet.ipmc.cnrs.fr/cgi-bin/ComputParams.py>). The peptide 3D structures were determined by a novel computational framework, PEP-FOLD3 (<https://mobyle2.rpbs.univ-paris-diderot.fr/cgi-bin/portal.py#forms::PEP-FOLD3>).

The prediction of antibacterial activity of the original peptide PA13 and modified peptide RF135 were performed using the following databases: CAMPR3 (Collection of Antimicrobial Peptides, <http://www.camp3.bicnirrh.res.in/>) (Waghu, Barai, Gurung, & Idicula-Thomas, 2016) and AntiBP3 (Prediction server for Antibacterial peptides in Protein sequences, <https://webs.iitd.edu.in/raghava/antibp3/>) (Bajjiya, Choudhury, Dhall, & Raghava, 2024). The sequences of original and modified peptides were used to predict AMPs. The peptide sequences were transformed into FASTA format, which was recognized by all software.

5.3.6 Prediction and modeling of peptide-membrane interaction

The PDB files of the original peptide PA13 and modified peptide RF135 were employed to determine the peptide-membrane interaction using the PMIPred server (<http://pmipred.fkt.physik.tu-dortmund.de>) (van Hilten et al., 2024). PMIPred is used to predict the free energy of membrane binding and classify the interaction of peptide and microbial membrane as non-binding, curvature sensing, or membrane binding.

In addition, to provide comprehensive prediction analysis, the PDB files of peptide PA13 and RF135 secondary structure predicted using PEP-FOLD3 were used to calculate peptide-membrane interactions using the PPM 3.0 server (https://opm.phar.umich.edu/ppm_server3_cgopm) (Lomize, Todd, & Pogozheva, 2022). The PPM server predicted the peptide arrangement in lipid bilayers by providing

orientation parameters such as membrane penetration depth, tilt angle, and water-to-membrane transfer energy. The 3D-rendered images of the peptide were created by PyMol v2.4.

5.3.7 Antibacterial activity

5.3.7.1 Minimum inhibitory concentration (MIC)

The original peptide PA13 and its analog RF135 were tested for antibacterial activity using the broth microdilution technique in a sterile 96-well microtiter plate (Thermo Fisher Scientific™ Nunc™, Jiangsu, P.R.China) based on Wiegand, Hilpert, & Hancock (2008) with slight modifications. Each bacterial culture grown on TSA at 37 °C for 24 h was used. The culture population was adjusted to an OD₆₀₀ of 0.085-0.100 (0.5 McFarland scale) in sterile 0.85% NaCl solution using a spectrophotometer 7315 (Jenway, Stone, Staffordshire, UK). After a 10-fold dilution with the final concentration of approximately 5×10⁵ CFU.mL⁻¹ in 0.85% NaCl, 50 μL of MHB-containing bacterium were added with 50 μL of peptide in a sterilized 96-well microplate. Kanamycin of 0.01 mg.mL⁻¹ was applied as a positive control. The minimum inhibitory concentration (MIC) was visually determined as the synthetic peptide with the lowest concentration that exhibited inhibition on the tested bacterial growth by assessing the turbidity at 600 nm (OD₆₀₀) using a microplate reader (Spectrostar® Nano, BMG Labtech, Ortenberg, Germany).

5.3.7.2 Bacterial-killing curve

The bacterial-killing curve of the modified peptide RF135 was evaluated by testing against the most sensitive test bacterium. A mid-logarithmic phase of the bacterium was cultivated and used to prepare a cell suspension with sterile 0.85% NaCl to achieve an OD₆₀₀ ≈ 0.085-0.100. Subsequently, the cell suspension in 0.85% NaCl was diluted with 10-fold serial dilution to achieve a concentration level of at least 1×10⁵ CFU.mL⁻¹ in MHB. Modified RF135 peptide at 1/2x, 1x, 2x, and 4xMIC were introduced to the bacterial suspension and incubated for various time intervals (0, 1, 2, 4, 6, 12, and 24 h) at 37 °C, then aliquots of the bacteria were analyzed using spot plate technique on plate count agar (PCA) plates in triplicates. After incubating the plates at 37 °C for 18-24 h, colonies of the bacterium were counted as log CFU.mL⁻¹.

5.3.8 Antibacterial mechanism

5.3.8.1 Membrane integrity

The modified peptide RF135 induced alterations to the cell envelope of bacteria were observed under a confocal laser scanning microscope (CLSM) as described by de Almeida et al. (2019) with minor adjustments. The most sensitive bacterial cells were cultivated in TSB to a mid-logarithmic phase at 37 °C with a shaking speed of 120 rpm, harvested, and rinsed twice by centrifugation $5,000 \times g$ for 5 min, then resuspended to an OD_{600} at 0.2-0.3 in 10 mM phosphate-buffered saline (PBS). Propidium iodide (PI) and SYTO-9 were used to stain dead and live cells. The cells suspension was added with the modified peptide RF135 at 1/2x, 1x, and 2xMIC and without peptide (control) and incubated at 37 °C for 2 h. The treated bacterial cells were then rinsed twice and resuspended in 10 mM PBS, PI at the final concentration of $10 \mu\text{g.mL}^{-1}$ or SYTO-9 at $2.5 \mu\text{g.mL}^{-1}$ were added, and incubated at 4 °C for 30 min in the dark. The treated bacterial cells were collected and rinsed using the same buffer solution. The bacterial cells without peptide were stained with PI or SYTO-9 as a negative control. Subsequently, 10 μL of bacterial suspension were embedded on a glass slide and observed under the CLSM (Nikon 90i A1R, Nikon, Tokyo, Japan). The excitation and emission wavelengths of SYTO9-stained cells are 488 and 530 nm, and those of PI-stained cells are 538 and 617 nm, respectively.

5.3.8.2 FAM-labeled peptide localization

The most sensitive bacterial cells in the mid-logarithmic phase were collected by centrifugation at $5,000 \times g$ for 5 min. The cell pellets were rinsed twice with 0.1 mol.L^{-1} phosphate-buffered saline (PBS, pH 7.2) and resuspended in PBS until the $OD_{600} \approx 0.3$. Labeling of the modified peptide RF135 conjugated with 5-carboxyfluorescein (5-FAM) was accomplished as previously described (Song et al., 2020). Briefly, the FAM-labeled peptide at a final concentration of 1/2xMIC and 1xMIC were prepared with bacterial suspension and incubated at 37 °C for 2 h in the dark. Untreated sample was also prepared. Propidium iodide (PI) at a final concentration $10 \mu\text{g.mL}^{-1}$ was added to the suspension. The bacterial suspension was then incubated at 4 °C for 30 min in the dark and centrifuged at $5,000 \times g$ for 5 min. Cell pellets were resuspended in 10 mmol.L^{-1} PBS (pH 7.2). The bacterial suspension (10 μL) was transferred into glass slide and observed by a confocal fluorescence microscope (Nikon 90i A1R, Nikon, Tokyo, Japan) equipped with an objective lens (40x). The excitation and

emission wavelength of SYTO9-stained cells are 488 and 530 nm. Those of PI-stained cells are 538 and 617 nm.

5.3.8.3 Nucleic acid leakage

The DNA/RNA loss of bacterial cells treated with the modified peptide RF135 was performed according to Carson, Mee, & Riley (2002) protocol with some modifications. Briefly, 100 μ L of bacterial suspension were added with the peptide RF135 at concentrations of 1/2xMIC and 1xMIC and incubated at 37 °C for 6 h. Samples were collected at various intervals and filtered with a 0.22- μ m syringe filter. The presence of DNA and RNA was measured with a NanoDrop™ 2000c spectrophotometer (Thermo Scientific, Waltham, MA, USA) at OD₂₆₀.

5.3.8.4 Cell morphology changes

The impact of modified peptide RF135 on morphological alterations of the most sensitive bacteria was assessed by scanning electron microscopy (SEM), as previously described by Zhu et al. (2014). The logarithmic phase bacterial cells were cultivated in TSB at 37 °C for 4-6 h. Subsequently, the cell pellets were collected by centrifugation at 5,000 \times g for 10 min, rinsed twice with 10 mM phosphate buffered saline (PBS), and resuspended to OD₆₀₀ of 0.5. The modified peptide RF135 was applied at 1/2x and 1xMIC to the cell suspension and incubated at 37 °C for 2 h. Untreated cells were also prepared as a control. Subsequently, cell pellets were collected by centrifugation at 5,000 \times g for 5 min and rinsed twice with 10 mM PBS. Cells were initially exposed to 2.5% glutaraldehyde (v/v) in 100 mM phosphate buffer pH 7.2 and incubated at 4 °C for 24 h. Subsequently, cells were rinsed twice in 100 mM PB. The second fixation was performed using 1% osmium tetroxide (w/v) for 2 h at ambient temperature in a fume hood, then rinsing twice in distilled water. Subsequently, cells were dehydrated in serially ascending acetone concentrations of 20, 40, 60, 80, and 100% with incubation intervals of 15 min. Finally, specimens were spotted on conductive aluminium tape, placed on an SEM sample stub, applied dual carbon and ultrathin gold coating, and observed images with a field-emission scanning electron microscopy (FE-SEM) (Auriga-Carl Zeiss, Oberkochen, Germany) at 2-2.5 keV electron energy.

5.3.8.5 Ultrastructural alteration

Transmission electron microscopy (TEM) specimens were prepared after the dehydration step, as mentioned in SEM sample preparation, and the

specimens were further infiltrated with epoxy resin in graded acetone (1:3, 1:1, 3:1) (Zhu et al., 2014). The specimens with 100% epoxy resin were polymerized at 60 °C for 24 h and ultrathin sectioned to a 70-90 nm thickness using an ultramicrotome with a diamond knife, post-stained with 2% (w/v) uranyl acetate and 0.25% (w/v) lead citrate within each staining being incubated for 15 min at room temperature, then observed under FE-TEM (Talos F200X, ThermoFisher Scientific, Waltham, MA, USA) with 120 keV electron energy.

5.3.8.6 Biochemical intracellular changes

The intracellular modifications induced by the modified peptide RF135 were evaluated using synchrotron radiation based on Fourier transform infrared spectromicroscopy (SR-FTIR) as described by Pimchan, Tian, Thumanu, Rodtong, & Yongsawatdigul (2023) with slight modifications. The mid-logarithmic of *Salmonella* Typhimurium TISTR 292 cells were collected by spun at 5,000 ×g for 5 min and resuspended in fresh TSB to get OD₆₀₀ = 0.2, added with the peptide RF135 at 1×MIC and kept at 37 °C for 2 h. Untreated cells were used as control. Cell pellets were collected after incubation at 37 °C for 2 h. Cell pellets were rinsed twice using sterile 0.85% NaCl and thrice with sterile distilled water. One µL of the cell suspension was dropped on a barium fluoride (BaF₂) window. Samples were dehydrated at room temperature for 30 min under laminar flow. Subsequently, they were dried in a vacuum desiccator to generate film before SR-FTIR measurement. SR-FTIR assay with a Vertex-70 spectrometer (Bruker Optics, Ettlingen, Germany) equipped with a Hyperion-2000 microscope (Bruker Optics, Ettlingen, Germany) in Beamline 4.1 (BL4.1) of the Synchrotron Light Research Institute (Nakhon Ratchasima, Thailand). The wave number of SR-FTIR spectra were generated in the 4,000–800 cm⁻¹. Spectra analysis used OPUS version 7.5 software (Bruker Optics, Ettlingen, Germany). Spectra pre-processing consists of atmospheric compensation, smoothing, normalization, baseline correction, and averaging. Smoothing spectra applied with 3 polynomial order and 17 smoothing points of Savitzky-Golay algorithm. Then compensation of wavelength-dependent spectra effect using Extended Multiplicative Scatter Correction (EMSC) were calculated. Principal component analysis (PCA), a multivariate statistical method, was evaluated using the Unscramble X 10.4 for Windows (Camo Analytics, Oslo, Norway).

5.3.9 Molecular docking

The crystallographic structures of six receptors of *Salmonella* Typhimurium were obtained from the Research Collaboratory for Structural

Bioinformatics Protein Data Bank (RCSB PDB) (<https://www.rcsb.org>) (Berman et al., 2000) and selected to study the modified peptide RF135 molecular docking. dTDP-6-deoxy-L-lyxo-4-hexulose reductase (PDB ID: 7TJ4_B) (Blankenfeldt et al., 2002), FaBG enzyme (PDB ID: 6T5X_B) (Vella et al., 2021), transcription factor SlyA (PDB ID: 3QPT) (Dolan, Duguid, & He, 2011), DNA gyrase (PDB ID: 5ZTJ) (Sachdeva et al., 2020), dihydrofolate reductase (PDB ID: 8T0J) (Muñoz-Escudero et al., 2023), glycoside hydrolase (PDB ID: 4GVF_B) (Bacik, Whitworth, Stubbs, Vocadlo, & Mark, 2012) were selected as receptors. The structure of all receptors were cleaned by removing the water molecules using PyMOL v2.4.

The molecular docking simulation was developed on the CABS-dock peptide-protein docking server (<https://biocomp.chem.uw.edu.pl/CABSdock/>) (Blaszczyk et al., 2016; Kurcinski, Jamroz, Blaszczyk, Kolinski, & Kmiecik, 2015). The docking results were depicted in DimPlot of the LigPlot⁺ (Laskowski & Swindells, 2011) to designate the binding position of RF135 and the receptors. For conformity, other interaction graphics were constructed on the EMBL-EBI tool PDBsum (<http://www.ebi.ac.uk/thornton-srv/databases/pdbsum/Generate.html>) (Laskowski, 2009). The binding affinity (ΔG) and dissociation constant (Kd) values were predicted using the Prodigy (Protein binding energy prediction) server (<https://rascar.science.uu.nl/prodigy/>) (Honorato et al., 2021; Vangone & Bonvin, 2015; Xue, Rodrigues, Kastritis, Bonvin, & Vangone, 2016). It should be understood that molecular docking is only intended to simulate peptide-protein interactions.

5.3.10 Hemolysis activity

To conduct the hemolysis study experiment using human red blood cells originated from a healthy volunteer, the study protocol was prepared and submitted to be certified by the Human Research Ethics Committee of the Suranaree University of Technology (EC-64-32). The experimental process was conducted following ethical guidelines and regulations. The hemolytic capacity of RF135 was determined by adopting a modified technique of Wang et al. (2015). In brief, one mL of a fresh human red blood cells (RBCs) was collected from healthy volunteer in polycarbonate tube in the presence of heparin. The acquired RBCs were separated by centrifuge at 1,000 $\times g$ for 5 min at 4 °C and subsequently rinsed in PBS three times, followed by resuspension in PBS buffer pH 7.2 and diluted to 1% (v/v) erythrocyte suspension. Subsequently, 50 μL of the hRBCs suspension was added with 50 μL of peptide in PBS buffer pH 7.2 at varying concentrations. Samples were incubated at 37

°C for 1 h. Following centrifugation at 1,000 ×g for 5 min at 4 °C, the supernatant was gently collected in a fresh 96-well plate. The hemoglobin acquisition was determined by observing the absorbance at 570 nm (OD₅₇₀) with a microplate reader (Spectrostar® Nano, BMG Labtech, Ortenberg, Germany). PBS buffer and 1% Triton X-100 were utilized as negative and positive controls, respectively. The hemolysis percentage was measured as follows:

$$\% \text{ Hemolysis} = \frac{\text{OD}_{\text{peptide+hRBC}} - \text{OD}_{\text{PBS+hRBC}}}{\text{OD}_{\text{Triton X-100+hRBC}} - \text{OD}_{\text{PBS+hRBC}}} \times 100\%$$

5.3.11 Statistical analysis

Every analysis carried out in three separate trials and the results were stated as mean ± standard deviation (SD). Statistical analyses carried out using GraphPad Prism version 8 for Windows (GraphPad Software, Boston, MA, USA). One-way ANOVA was used, accompanied by Tukey's multiple comparison range test. The significant differences were regarded at $p < 0.05$.

5.4 Results and discussion

5.4.1 Peptide design and characterization

Table 5.1 summarizes the physicochemical properties of the parent peptide (PA13) and its modified peptide RLLRKVTKLWKKF (RF135). The modified peptide displays higher molecular mass, hydrophobicity, hydrophobic moment, and net charges, which may affect their solubility and stability, in addition to their interaction with the bacterial membrane.

The theoretical isoelectric points (pI) of RF135 was higher than PA13. The increase in pI indicates the modifications have increased the overall positive charge. The hydrophobicity and hydrophobic moment of RF135 was higher than PA13. The increasing hydrophobicity and hydrophobic moment suggest more significant potential for membrane interaction, enhanced biological activity, and improved stability.

Yin, Edwards, Li, Yip, & Deber (2012) reported that hydrophobicity is a crucial component of the antimicrobial activity of cationic AMPs. Hydrophobicity enables cationic AMPs to penetrate bacterial cell membranes, disrupting their integrity. The hydrophobic region of cationic AMPs facilitates interaction with the hydrophobic core of bacterial membranes. Additionally, the balance of hydrophobicity and cationic

charge is vital for the activity of cationic AMPs. Cationic AMPs need a threshold level of hydrophobicity to interact with cell membranes, as excessive hydrophobicity could lead to toxicity.

PA13 and RF135 are classified as cationic peptides but different in their net charges, with PA13 being +4 and RF135 being +6 (Table 5.1). The increased net charge is due to the introduction of two Arg (R) residues into the peptide sequence. Increasing the net charge of modified peptide enhances its antimicrobial activity against a broad spectrum of bacteria, including Gram-positive and Gram-negative (Jiang et al., 2008). However, Jiang et al. (2008) also noted that increasing the net charge of AMPs enhances hemolytic activity, which is the ability of the peptide to lyse human red blood cells.

Table 5.1 Physicochemical properties comparison between PA13 and RF135 peptides

Peptide sequence	Residues	pI ^a	Molecular mass Theoretical ^a / Observed ^b (Da)	Hydrophobicity ^c <H>	Hydrophobic moment ^c <μH>	Net Charge ^c (pH 7)
PTGAKVTKAAKKA (PA13)	13	10.48	1270.54/ 1270.52	-0.020	0.287	+4
RLLRKVTKLWKKF (RF135)	13	12.03	1716.19/ 1716.16	0.357	0.908	+6

^a Determined by the compute_pi algorithm (http://web.expasy.org/compute_pi/);

^b Determined by ESI-MS mass spectroscopy

^c Determined by the Heliquist server (<http://heliquist.ipmc.cnrs.fr/>)

Figure 5.2 shows a schematic drawing of the PA13 and RF135 structures using the Pepdraw program. RF135 are derivatives of PA13, which is done by replacing P¹ with R, T² with L, G³ with L, A⁴ with R, A⁹ with L, A¹⁰ with W, and A¹³ with F. The 2D illustration of PepDraw reveals a notable distinction in the amino acid composition between PA13 and RF135. Villaró-Cos & Lafarga (2023) reported that using PepDraw can facilitate the visualization of peptides, which is fundamental to understanding the interaction and function of biological systems.

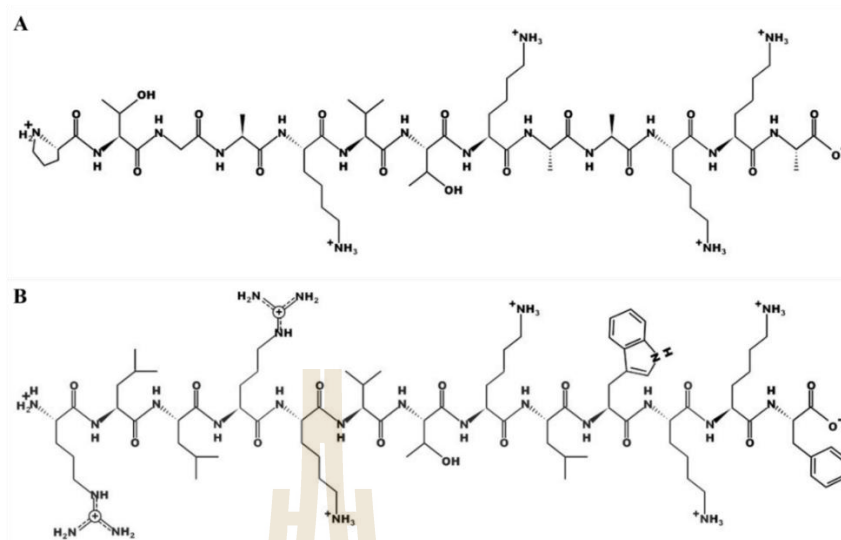


Figure 5.2 Schematic representation of the peptide (A) PA13, (B) RF135, using the program PepDraw (<http://pepdraw.com/>)

The 3D structure prediction of PA13 and RF135 was generated using the PEP-FOLD3 server. As illustrated in Figures 5.3A and 5.3B, it is evident that there are significant distinctions between the 3D structural characteristics of PA13 and RF135. Lamiable et al. (2016) reported that PEP-FOLD3 is capable of predicting the 3D structure of a peptide solely based on its amino acid sequence without the need for experimental structural data.

A diagram illustrating the helical wheel projection of the two peptides (PA13 and RF135) created with the HeliQuest web server is presented in Figures 5.3 C-D. The modified RF135 peptide was synthesized by replacing some amino acid residues with Arg (R), Leu (L), Trp (W), and Phe (F) residues to the parent PA13 structure. The amino acid replacement process begins at the N-terminal end, with Pro (P^1) replaced by Arg (R), Thr (T^2) by Leu (L), Gly (G^3) by Leu (L), and Ala (A^4) by Arg (R). In addition, the sequence of Lys (K), Val (V), Thr (T), and Lys (K) was unaltered. Subsequently, Ala (A^9) was replaced with Leu (L) and Ala (A^{10}) with Trp (W). Then, two remaining Lys (K) were not replaced. Finally, the last amino acid is Ala (A^{13}), substituted with Phe (F).

Therefore, by replacing hydrophilic amino acids with hydrophobic amino acids, the overall hydrophobicity of the peptide was increased, which might enhance antibacterial activity, resulting in an increased affinity for and disruption of the bacterial membrane. Furthermore, the replacement of amino acids $P1$ and $A4$ with R, respectively, results in an increase in the net charge from +4 to +6. The increasing net charge also enhances the antibacterial activity of the modified peptide RF135.

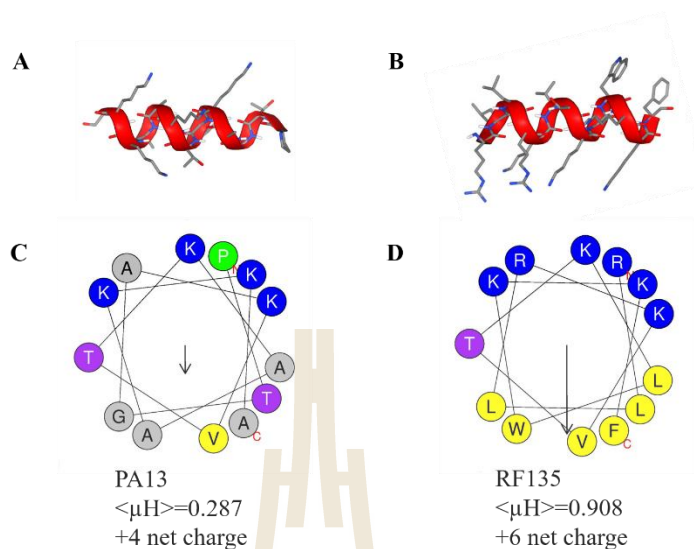


Figure 5.3 The 3D prediction structure of (A) PA13 and (B) RF135; the projection of the helical wheels (C) PA13 and (D) RF135. The images were compiled with <http://heliquet.ipmc.cnrs.fr/cgi-bin/ComputParams.py>. The hydrophobic moment and net charge are displayed. Residues with a positive charged colored in blue; hydrophobic residues are colored yellow; uncharged residues colored in grey, green, and purple. The N and C terminal amino acids are recognized by the small red letters. The arrow denotes the hydrophobic moment.

5.4.2 Prediction of antibacterial activity

The development of a web-based prediction tool for antimicrobial peptides would facilitate the accelerated discovery of new antimicrobial compounds (Wang, Vaisman, & van Hoek, 2022). The parent peptide PA13 and modified peptide RF135 were subjected to analysis using two AMP prediction web tools, CAMPr3 and AntiBP3, which employ distinct prediction models to assess the antimicrobial potential (Table 5.2).

The CAMPr3 prediction results indicate that the original PA13 and the modified RF135 peptides are classified as antimicrobial peptides (AMPs). The principal approach of the CAMPr3 software in predicting AMPs is based on the sequence, structure, and signature of peptides (Waghu et al., 2016). Similarly, the antiBP3 assay results indicate that both peptides are AMPs. The principles of AntiBP3 in predicting

AMPs involve a hybrid approach that combines several techniques to improve prediction accuracy (Bajiya et al., 2024).

Table 5.2 Comparison classification prediction as antimicrobial peptides (AMPs) for the original and modified peptides using CAMPr3 and AntiBP3.

No.			PA13	RF135
Peptide Sequence			PTGAKVTKAAKKA	RLLRKVTKLWKKF
CAMP3	Support Vector Machine		0.791	0.998
	Random Forest		0.4595	0.972
	Artificial Neural Network		AMP	AMP
AntiBP3	Gram + ABP	Random Forest	0.62	0.82
		Forest	AMP	AMP
	Gram - ABP	Extra Tree	0.69	0.79
			AMP	AMP
	Gram variable ABP	Support Vector	0.69	0.97
		AMP	AMP	

Meher, Sahu, Saini, & Rao (2017) reported that developing efficient computational tools is essential to identifying the most promising AMPs candidates before *in vitro* experimentation. Additionally, Ramazi, Mohammadi, Allahverdi, Khalili, & Abdolmaleki (2022) argued that online peptide AMPs prediction tools represent a convenient and efficient method for predicting AMPs that does not necessitate the use of extensive computational resources or expertise. Therefore, the advantages of machine learning facilitate the discovery and design of novel AMPs, which is crucial in combating multidrug-resistant pathogenic bacteria.

5.4.3 Prediction of peptide-membrane interaction model

5.4.3.1 Prediction using PMIPred web server

The prediction results from the PMIPred web server indicated that the original peptide PA13 demonstrated a slight interaction with the neutral membrane, such as 1-palmitoyl-2-oleoyl-sn-glycero-3-phosphocholine (POPC). It was indicated by the prediction position of PA13 nearly into the sensor (orange zone) or predicted sensing domains regions, which refer to the region of its structure that is predicted to be involved in interacting with the membrane (predicted $\Delta F_{sm}(R=50)$: -12.553 kJ/mol) (Figure 5.4A). In addition, the PMIPred results showed that PA13 as a

peptide interacting with the membrane in the orange zone due to the physicochemical properties, including hydrophobicity (-0.02) and hydrophobic moment (0.287) character and positively net charged (+4) might have interactions with the membrane. Moreover, PA13 possessed the predicted curvature-sensing free energy ($\Delta\Delta F_{L24}$) was $-6.092 \text{ kJ}\cdot\text{mol}^{-1}$. This result indicates that the $\Delta\Delta F_{L24}$ mutation stabilizes the peptide, increasing its ability to bind to membranes. This prediction result suggests the role of PA13 in curvature sensing or other membrane-interaction processes. In contrast, the PMIPred result of RF135 (Figure 5.4B) showed this peptide could bind with the neutral membrane (POPC), which was indicated by the position in the red region or membrane-binding domains (predicted $\Delta F_{sm}(R=50)$: $-70.702 \text{ kJ}\cdot\text{mol}^{-1}$). In addition, RF135 is classified as a membrane-binding peptide based on the predicted membrane-binding energy (predicted $\Delta\Delta F_{L24}$: $-20.362 \text{ kJ}\cdot\text{mol}^{-1}$). This PMIPred prediction indicates that modifying peptide PA13 to RF135 may change the physicochemical properties when interacting with the model membrane. This change may be attributed to transitioning from curvature membrane sensing to membrane binding.

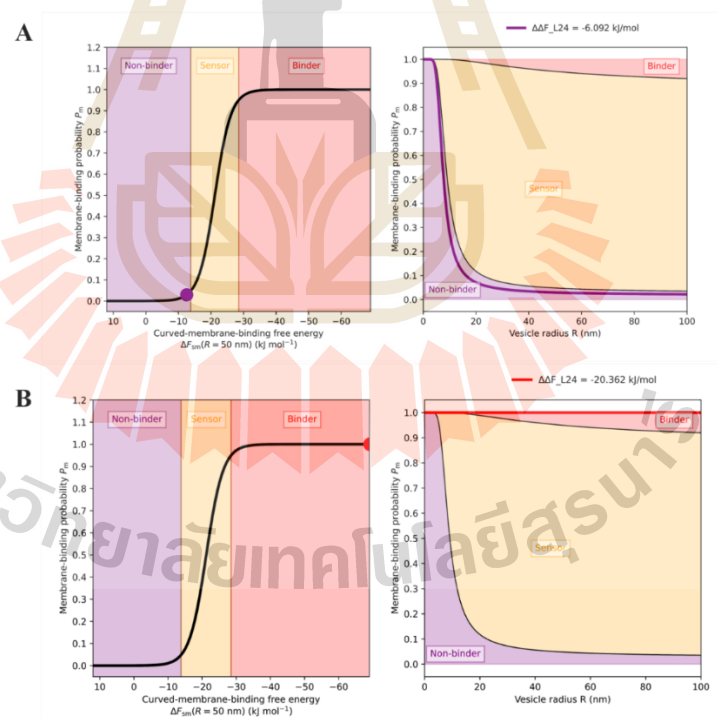


Figure 5.4 Prediction of peptide (A) PA13 on the neutral membrane (e.g., 1-palmitoyl-2-oleoyl-sn-glycero-3-phosphocholine (POPC)) (B) RF135 on the neutral membrane (e.g., 1-palmitoyl-2-oleoyl-sn-glycero-3-phosphocholine (POPC))

Similar results were also obtained in the interaction between PA13 and the negatively charged membrane model (e.g., 1-palmitoyl-2-oleoyl-sn-glycero-3-phosphocholine/palmitoyl oleoyl phosphatidyl glycerol (POPC/POPG)), which was used to predict the results. Figure 5.5A shows that PA13 is categorized as a curvature-sensing membrane peptide with energy binding prediction (predicted $\Delta F_{sm}(R=50)$) of $-27.711 \text{ kJ.mol}^{-1}$. In addition, the predicted adjusted change in free energy (predicted $\Delta\Delta F_{adj}$) was $-9.812 \text{ kJ.mol}^{-1}$. In contrast, the interaction between RF135 and the negatively charged membrane model (Figure 5.5B) was categorized as a membrane-binding peptide with an energy-binding prediction (predicted $\Delta F_{sm}(R=50)$) of $-93.439 \text{ kJ.mol}^{-1}$. Moreover, the adjusted free energy change (predicted $\Delta\Delta F_{adj}$) was $-25.942 \text{ kJ.mol}^{-1}$. These results indicate that the modified peptide RF135, due to greater hydrophobicity, exhibits higher binding energy in the two membrane models than the original peptide PA13.

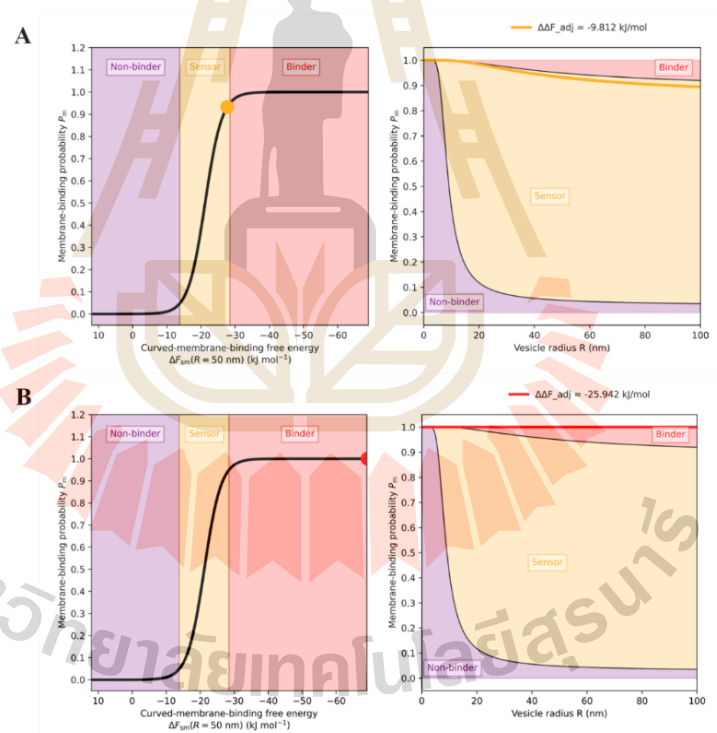


Figure 5.5 Prediction of membrane-peptide interaction (A) PA13 on the negatively charged membrane (e.g. 1-palmitoyl-2-oleoyl-sn-glycero-3-phosphocholine/ palmitoyl oleoyl phosphatidyl glycerol (POPC/POPG)) (B) RF135 on the negatively charged membrane (e.g. 1-palmitoyl-2-oleoyl-sn-glycero-3-phosphocholine/ palmitoyl oleoyl phosphatidyl glycerol (POPC/POPG))

5.4.3.2 Prediction using PPM 3.0 web server

The 3D model of the interaction of native peptide PA13 and modified peptide RF135 with membranes, generated by the Orientations of Proteins in Membranes (OPM) with PPM 3.0 web server, is shown in Figures 5.6A-B. Interaction between the original peptide PA13-membrane has a tilt angle of $77 \pm 7^\circ$, a penetration depth of $2.2 \pm 1.0 \text{ \AA}$, and water-to-membrane transfer Energy ($\Delta G_{\text{transfer}}$) of $-4.2 \text{ kcal.mol}^{-1}$. In contrast, the modified peptide RF135 -membrane has a tilt angle of $90 \pm 6^\circ$, penetration depth of $6.5 \pm 0.9 \text{ \AA}$, and water-to-membrane transfer energy ($\Delta G_{\text{transfer}}$) of $-12.3 \text{ kcal.mol}^{-1}$. The result indicated that modified peptide RF135 might exhibit a more robust interaction with the membrane than PA13 due to its more considerable net charge value and greater hydrophobicity. In addition, analysis of the PPM 3.0 prediction results reveals that when the transfer energy from the aqueous environment to the membrane is reduced, the tilt angle and penetration depth increase compared to PA13.

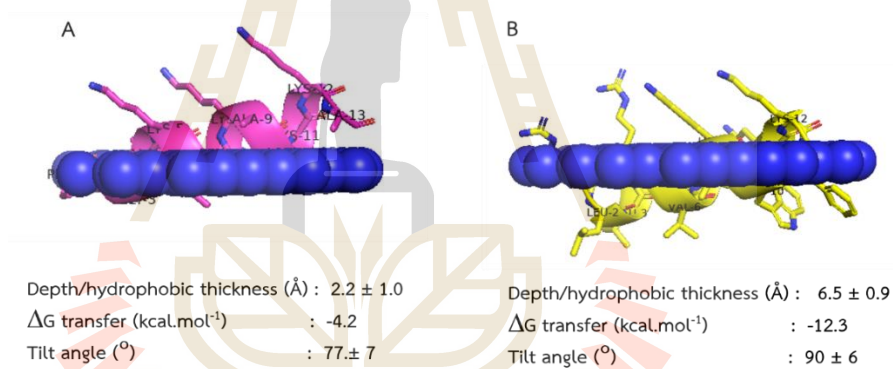


Figure 5.6 The 3D structure obtained from PEP-FOLD3 was utilized to model bacterial membrane interactions through a PPM 3.0 server: (A) PA13, (B) RF135.

5.4.4 Antibacterial activity

5.4.4.1 Minimum inhibitory concentration (MIC)

The minimum inhibitory concentration (MIC) of PA13 and RF135 against Gram-positive and Gram-negative bacteria was determined using the microbroth dilution method described by Wiegand et al. (2008).

In Table 5.3, Gram-positive and Gram-negative bacterial strains were susceptible to RF135 at $2 \mu\text{M}$ to $128 \mu\text{M}$, respectively. Modifying the parent peptide PA13 to RF135 resulted in increasing higher growth inhibition. For instance, MIC

value for RF135 on *S. aureus*, *B. cereus*, *E. coli*, and *S. Typhimurium* were 128, 2, 8, and 4 μM , respectively. The results indicated that increase hydrophobicity and charges of peptides appeared to increase inhibition capacity.

Sosiangdi et al.(2023) reported modification on peptide QAIHNEKVQAHGKKVL (QL17) derived from pepsin hydrolyzed hemoglobin from *Crocodylus siamensis*. First, they removed Q (Gln) and A (Ala) residues in the N-terminus and got a new sequence IL15 (IIHNEKVQAHGKKVL). Next, they performed some modification on IL15 and found IL15.3 (IKHWKKVWKHAKKVL) exhibited the strongest antimicrobial activity with MIC values at a range of 4-14 $\mu\text{g.mL}^{-1}$ against *E. coli*, *K. pneumoniae*, *P. aeruginosa*, *S. aureus*, *B. subtilis*, and *S. epidermidis*.

Table 5.3 The minimum inhibitory concentration (MIC) of PA13 and RF135 was calculated from the microbroth dilution assay (μM) of the test bacteria.

Peptide sequence	Code	Gram-positive		Gram-negative	
		<i>Staphylococcus aureus</i> ATCC 29213 (μM)	<i>Bacillus cereus</i> DMST 5040 (μM)	<i>Escherichia coli</i> TISTR 780 (μM)	<i>Salmonella Typhimurium</i> TISTR 292 (μM)
PTGAKVTKA AKKA	PA13	>4000	>4000	>4000	>4000
RLLRKVTKL WKKF	RF135	128	2	8	4

5.4.4.2 Bacterial killing curve

In the absence of RF135, *S. Typhimurium* cells showed a typical growth curve, exhibiting lag, logarithmic, stationary, and death phases during 24 h (Figure 5.7). There was a slight decline in the number of cells from 4.4 log CFU.mL⁻¹ to 2.2 log CFU.mL⁻¹ within 2 h at 1/2xMIC (2.0 μM). However, there was a notable increase in cell number to 5.0 log CFU.mL⁻¹ and a further increase to 8.6 log CFU.mL⁻¹ at 24 h.

At 1xMIC (4.0 μM), The RF135 reduced cells from 4.5 log CFU.mL⁻¹ to 2.5 log CFU.mL⁻¹ for 2 h and continued to decrease to undetectable levels after 4 h. The growth of *S. Typhimurium* cells was significantly decreased after 1 h at

concentrations of 2×MIC (8.0 μM) and 4×MIC (16.0 μM), with a reduction in the cell counts from 4.5 log CFU.mL⁻¹ and 4.2 log CFU.mL⁻¹ to undetectable levels, respectively. The antimicrobial activities of RF135 were dose- and time-dependent. The findings demonstrate the bacteriostatic effect of RF135 was observed at 2.0 μM for 1 h. Meanwhile, RF135 was termed as a bactericidal agent at 8.0 μM after 1 h of incubation. The assay results indicate that adding a modified peptide to the cell suspension resulted in a distinct inhibition compared to untreated cells.

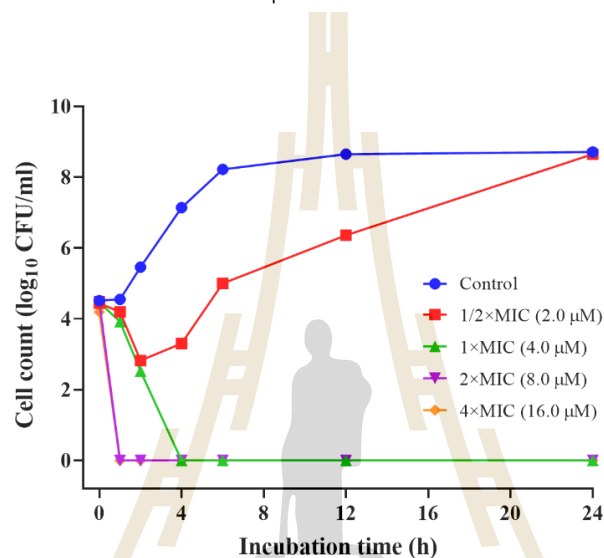


Figure 5.7 Bacterial-killing curve of RF135 against *Salmonella* Typhimurium TISTR 292 at 1/2×MIC, 1×MIC, 2×MIC, and 4×MIC incubate at 37 °C for 24 h. Data are given as Mean \pm SD ($n = 3$)

5.4.5 Antibacterial mechanism

5.4.5.1 Membrane integrity

The disintegration of cell membrane integrity of *Salmonella* Typhimurium TISTR 292 was observed using confocal laser scanning microscopy after staining with propidium iodide (PI) and SYTO-9. As depicted in Figure 5.8A, The untreated cells showed green fluorescence after staining with SYTO-9, and red fluorescence of PI was not observed (Figure 5.8A), indicating live cells with membrane integrity.

In contrast, after exposure to RF135 at 1/2×MIC and 1×MIC for 2 h, red fluorescence was observed and appeared to increase with higher concentrations of peptides (Figure 5.8B). Once the cell membrane is leaked, PI can enter the cell and interact with DNA, increasing red fluorescence intensity, as observed using CLSM (Boix-Lemonche, Lekka, & Skerlavaj, 2020). This result indicates that the cell envelopes of *S. Typhimurium* were damaged. In addition, some cells exhibited only

SYTO-9 fluorescence, suggesting that live cells remained in the presence of RF135 at 1/2x and 1xMIC (Figure 5.8C). These results revealed that RF135 could increase the membrane permeability and disrupt the membrane integrity.

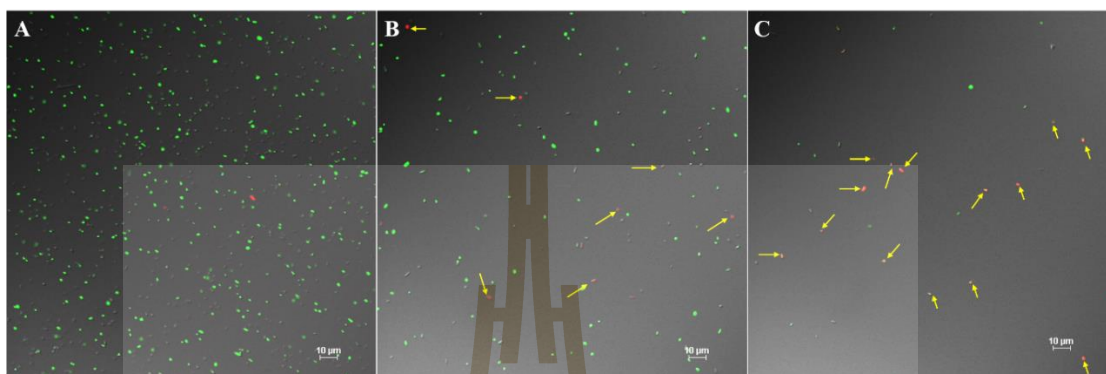


Figure 5.8 Confocal laser scanning micrographs of untreated *Salmonella* Typhimurium TISTR 292 (A), *S. Typhimurium* was exposed to the RF135 at 1/2xMIC (B), and *S. Typhimurium* exposed to RF135 at 1xMIC and stained with SYTO-9 and propidium iodide (PI). The scale bar is 10 µm. The yellow arrows indicate dead cells.

5.4.5.2 Labeled 5-FAM-RF135 localization

As illustrated in Figure 5.12, the modified peptide RF135 labeled with 5-carboxyfluorescein (5-FAM) could have ionic interaction with the negatively charged cell membrane of *S. Typhimurium*. It can be observed that the untreated cells show no fluorescence color (Figure 5.9A). In contrast, *S. Typhimurium* cells treated with increased concentrations of RF135 labeled with 5-FAM increased the intensity of green fluorescence emitted by this dye (Figures 5.9 B-C). Red fluorescence by PI (propidium iodide) indicates cell membrane disruption by peptide RF135, and PI passes through the membrane cell to bind with the DNA of cells. Ciociola et al. (2018) reported that the use of 5-FAM labeling could assist in the localization of proline-rich antimicrobial peptides (PrAMPs) within the cells of Gram-negative bacteria, including *Escherichia coli* and *Pseudomonas aeruginosa*. In addition, Song et al. (2020) also described that the peptide KDFPGRR labeled with FAM and added with PI exhibited the interacting localization of peptide in the *E. coli* membrane cell.

The findings suggest that the modified peptide RF135 can cause disruption of the cell membrane by ionic interaction with the negative charge of the cell membrane and penetration into *S. Typhimurium* cells.

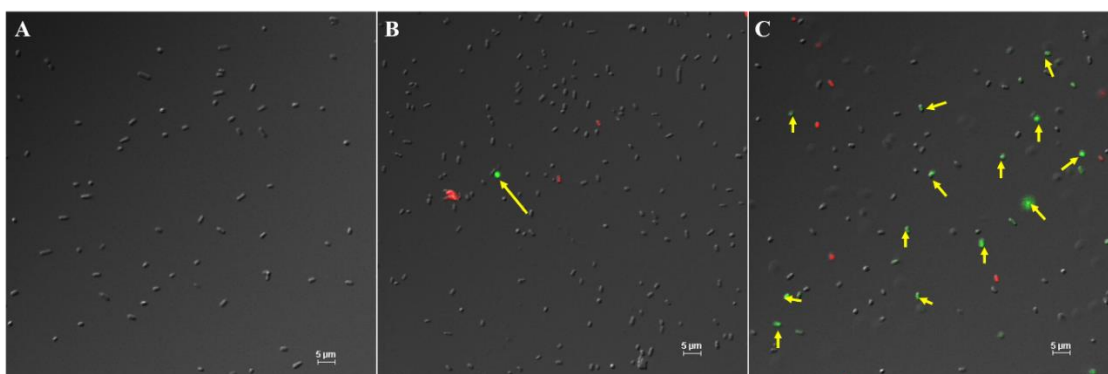


Figure 5.9 Confocal laser scanning micrographs of untreated *Salmonella Typhimurium* TISTR 292 (A), *S. Typhimurium* was exposed to the 5-FAM-RF135 at 1/2xMIC (B), and *S. Typhimurium* exposed to 5-FAM-RF135 at 1xMIC and stained with propidium iodide (PI) (C). The scale bar is 5 μm. 5-FAM, 5-carboxyfluorescein. The yellow arrow indicates that the peptide inside the cells.

5.4.5.3 Nucleic acid leakage

Figure 5.10 demonstrates that untreated *Salmonella Typhimurium* TISTR 292 cells exhibited an OD_{260nm} values that were consistently lower than cells that received peptide treatment at either 1xMIC (4.0 μM) or 2xMIC (8.0 μM) during incubated at 37 °C for 360 min.

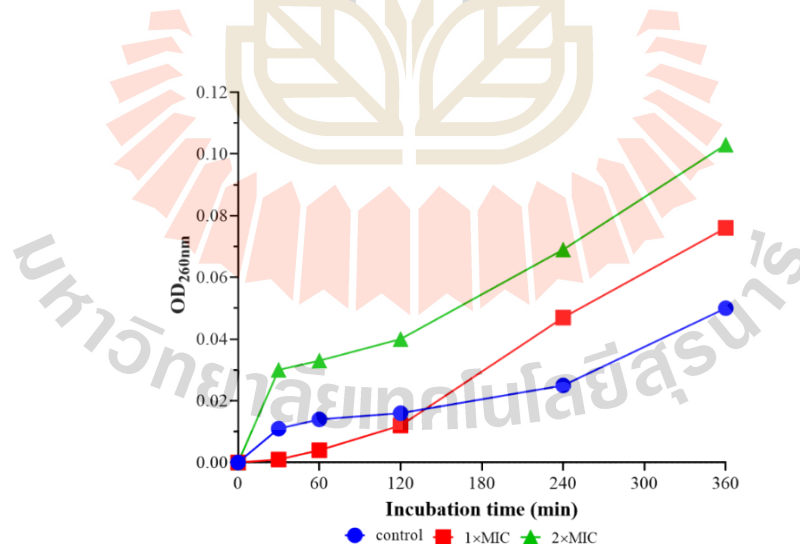


Figure 5.10 The leakage of nucleic acid from *Salmonella Typhimurium* TISTR 292 cells treated with RF135 at 1xMIC and 2xMIC compared to the untreated cells incubated at 37 °C for 6 h. Data are given as Mean ± SD ($n = 3$)

This indicated integrity of the bacterial cell membrane. Zhao et al. (2022) reported that MOp2 (HVLDTPLL), a novel peptide isolated from *Moringa oleifera* seed protein hydrolysate, induced DNA release of *Staphylococcus aureus* cells. Therefore, an increase in OD₂₆₀ value suggested the release of DNA from *S. Typhimurium* cells due to the pore formation on the surface of the cell membrane caused by the modified peptide RF135.

5.4.5.4 Scanning electron microscopy (SEM)

The control without peptide treatment exhibited intact cell structure, smooth surface morphology, and regular shape characteristics (Figure 5.11A). Following treatment with RF135 at 1/2×MIC, *S. Typhimurium* cells appeared slightly collapsed, with several pores noticed and dents on the cell surface (Figure 5.11B). Furthermore, the morphology of *S. Typhimurium* cells after being subjected to RF135 at 1×MIC for 2 h exhibited deeper craters, enlarged pores in the envelope, rough surface, and an increasingly irregular cell shape that led to cell lysis. (Figure 5.11C). The morphological changes observed in *S. Typhimurium* cells after being induced with RF135 were found to be significantly different from those observed in the control cells. These findings suggested that the modified peptide RF135 has a membranolytic action, resulting in morphological alterations in *S. Typhimurium*. *Salmonella* cells exposed to [K4K15]CZS-1 (α -helical cationic AMPs) also showed surface roughness, membrane roughness, cell lysis, pore formation, and surface indentation (Bermúdez-Puga et al., 2023)

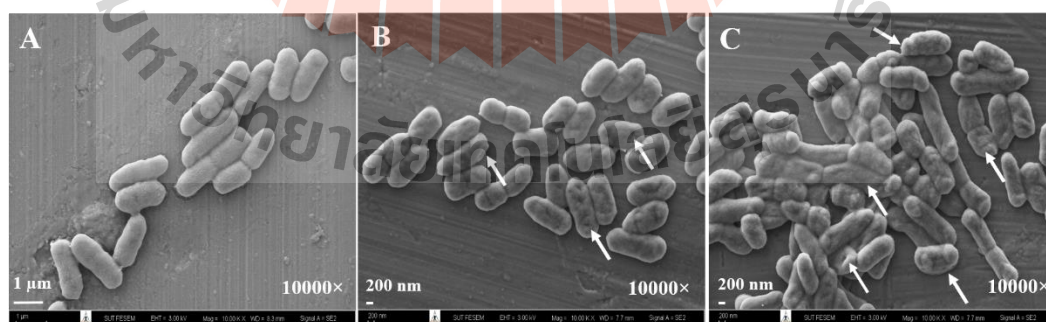


Figure 5.11 Scanning electron micrographs of (A) untreated *Salmonella Typhimurium* TISTR 292 cells (B) *S. Typhimurium* cells exposure with RF135 at 1/2×MIC and (C) cells treated with 1×MIC for 2 h. Scale bars represent 1 μ m (A) and 200 nm (B, C).

5.4.5.5 Transmission electron microscopy (TEM)

The effects of modified peptide RF135 on alterations in the ultrastructure of *Salmonella* Typhimurium were observed with transmission electron microscopy (TEM). Untreated *S. Typhimurium* cells displayed intact membrane structure and uniform intracellular composition (Figure 5.12A).

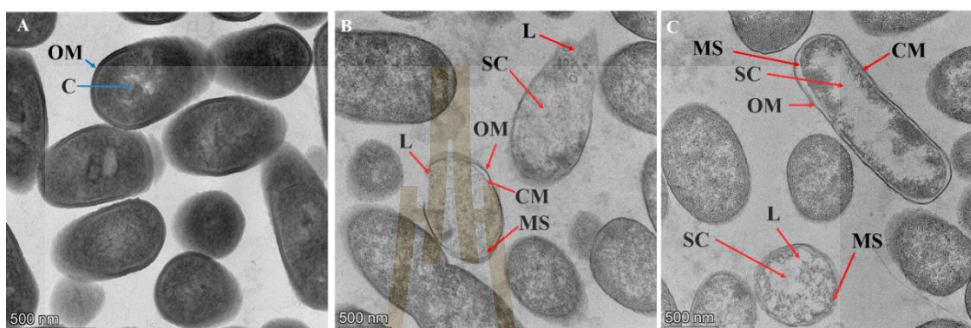


Figure 5.12 Transmission electron micrographs of (A) untreated *S. Typhimurium* TISTR 292 cells (B) *S. Typhimurium* cells exposure with RF135 at 1×MIC and (C) 2×MIC for 2 h. Scale bars represent 500 nm. C, cytoplasm; CM, cytoplasmic membrane; OM, outer membrane; L, leakage of cytoplasm; MS, membrane separation; SC, sparse cytoplasm

In contrast, the induction of RF135 at 1× and 2×MIC in *S. Typhimurium* resulted in the appearance of several ultrastructural changes, including condensed cytoplasmic content, cell membrane damage, and changes in membrane integrity (Figures 12B-C). TEM images demonstrate the presence of cellular damage of *S. Typhimurium* after being induced with a modified peptide, including cell membrane disruption, cell swelling, and change or cytoplasmic leakage.

5.4.5.6 SR-FTIR

SR-FTIR spectroscopy is a highly effective instrument for elucidating the molecular interactions and structural alterations, including vibrational information that occur during the interaction between AMPs and bacterial cells (Hornemann et al., 2022). Naumann, Helm, & Labischinski (1991) classified the range spectral of bacterial absorption in FTIR into five groups. The first range of 3000-2800 cm^{-1} is associated with the vibrations of functional groups of fatty acids (lipids). The second range of 1700-1500 cm^{-1} is related to the vibrations of amide I and amide II bands (proteins and peptides). The third was range of 1500-1200 cm^{-1} is corresponded

with proteins, fatty acids and phosphate-carrying compounds. The fourth was range of 1200-900 cm^{-1} is linked with absorption bands of carbohydrates present within the cell wall (polysaccharides). And the last was range of 900-700 cm^{-1} is connected with specific spectral patterns (fingerprint region). Figure 5.13A presents the average of the original SR-FTIR spectra of untreated *Salmonella* Typhimurium TISTR 292 and treated cells exposed with modified peptide RF135 at 1×MIC incubated at 37 °C for 2 h at wavenumbers of 3000-900 cm^{-1} .

The 2nd derivative spectra of SR-FTIR showed significant absorptions in the regions corresponding to lipids, proteins, and nucleic acids, which reveals the main functional groups of the cells undergoing changes caused by peptide RF135 at 1×MIC, as depicted in Figures 5.13B-C.

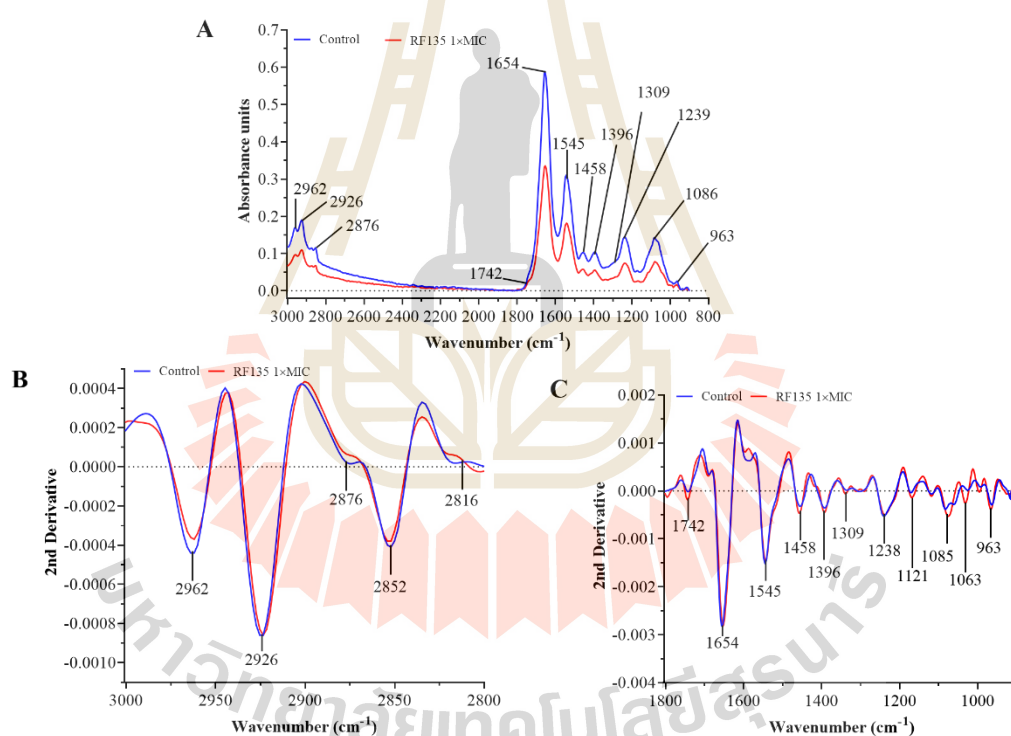


Figure 5.13 The average of original SR-FTIR spectra of untreated *Salmonella* Typhimurium TISTR 292 cells and cells exposed to RF135 at 1×MIC at 37 °C for 2 h in the wavenumber range of 3000-900 cm^{-1} (A); 2nd derivative spectra of untreated *S.* Typhimurium cells and cells exposed to RF135 at 1×MIC at 37 °C for 2 h in the wavenumber range 3000-2800 cm^{-1} (B); 2nd derivative spectra of untreated *S.* Typhimurium cells and cells exposed to RF135 at 1×MIC at 37 °C for 2 h in the wavenumber range 1800-900 cm^{-1} (C). Three sets of measurements were averaged.

Salmonella Typhimurium cells exhibited considerable alterations after 2 h exposure to RF135 at 1×MIC compared with untreated cells. The most substantial shift occurred in fatty acids structures which at the absorptions of bands 2962, 2926, 2876, 2852 (Figure 5.13B) and 1740 cm^{-1} (Figure 5.13C), respectively. The alteration that occurs in each band is related to C-H asymmetric stretching vibrations of CH_3 group (2962 cm^{-1}), C-H asymmetric stretching vibration of CH_2 , CH_3 (2926 cm^{-1}), C-H symmetric stretching vibration of CH_2 and CH_3 (2876 cm^{-1}), symmetric stretching vibration of CH_2 (2852 cm^{-1}), and C=O stretching vibration of ester functional group of fatty acids and triglycerides (1740 cm^{-1}) (Movasaghi, Rehman, & Rehman, 2008; Yu & Irudayaraj, 2005).

In addition, the effect of modified peptide RF135 at 1×MIC on *S. Typhimurium* cells leads to a moderately strong absorption at wavenumbers 1085, 1063, and 963 cm^{-1} , respectively (Figure 5.13C), which corresponds to modifications such as symmetric PO_2^- stretching in the phosphodiester backbone of nucleic acid (1085 cm^{-1}), C-O stretching vibration of nucleic acid (1063 cm^{-1}), and C-C, C-O stretching vibration of deoxyribose of nucleic acid (963 cm^{-1}) (Movasaghi et al., 2008).

A substantial rupture in the cell membrane was observed through shifts in two absorption bands at 1396 cm^{-1} and 1458 cm^{-1} (Figure 5.13C), with the latter corresponding to the symmetrical stretching of COO groups of amino acids and/or fatty acids in the cell membrane as well as asymmetric deformation of CH_2 from lipids and fatty acids in the cell membrane (Movasaghi et al., 2008). These modifications are caused by alterations in membrane structure and nucleic acid released into the solvent. These findings described the most significant biomolecule alteration in the lipids and protein substances following phosphodiester in nucleic acids, particularly DNA and RNA, after being exposed to RF135 at 1×MIC for 2 h.

The 2D-PCA score plot displayed that the spectra of *S. Typhimurium* cells treated with modified peptide RF135 at 1×MIC for 2 h and untreated cells could be distinguished grouped differentially within 49% PC-1 and 17% PC-2, respectively (Figure 5.14A). These differences appear to be linked to alterations in the *S. Typhimurium* molecular structures, particularly in fatty acids (2962, 2926, 2876, 2852, and 1740 cm^{-1}) and the heterogeneous region that defines the cell membrane and DNA/nucleic acids (1082, 1063, and 963 cm^{-1}) (Figures 5.13 B-C). The high positive loading plot of PC-1 observed at 2938, 1594, 1249, 1106, and 1059 cm^{-1} , respectively, indicated distinct functional groups of *S. Typhimurium* cells treated RF135. The high

negative loading of PC-1 at 1744, 1565, and 996 cm^{-1} , respectively, were characteristics of the control group (Figure 5.14B). These differences were appeared to be linked to alterations in the *S. Typhimurium* molecular structures, particularly in lipids/fatty acids (2938 and 1744 cm^{-1}), proteins (1594, 1565, 1249, 1106 cm^{-1}), and nucleic acids (1059 and 996 cm^{-1}).

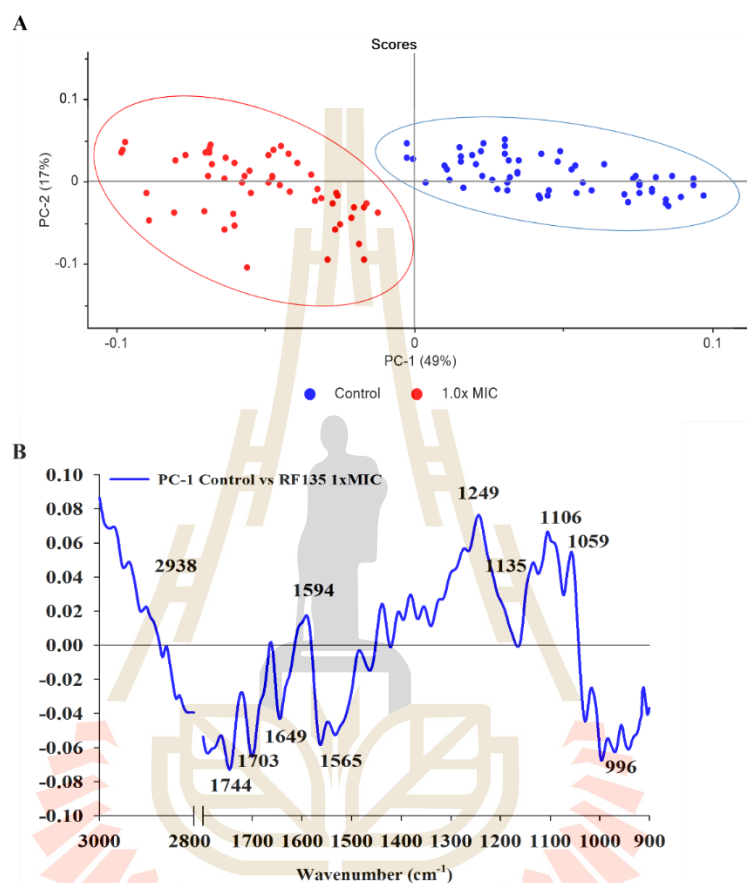


Figure 5.14 PCA analysis of SR-FTIR spectra of *Salmonella* Typhimurium TISTR 292 control and cells treated with RLLRKVTKLWKKF (RF135) incubated at 37 °C for 2 h. (A) 2D-PCA score plot; (B) PCA loading plot of PC-1.

5.4.6 Molecular docking study

The Prodigy server measured predictions of the energy binding affinity (ΔG) and dissociation constant (K_d) for the engagement of modified peptide RF135 with various receptors on *S. Typhimurium*, as presented in Table 5.4.

Lower energy binding conformations indicate higher binding affinities observed in peptide-proteins interactions. In addition, the peptide-protein complex interaction are also marked with the dissociation constant (K_d). A lower K_d value suggests a more robust binding and higher affinity between the peptide and protein.

Moreover, a lower K_d is associated with increased stability within the peptide-protein complex (Zhao & Grigoryan, 2023).

Table 5.4 Predicted energy binding affinity (ΔG) and dissociation constant (K_d) results in the interplay of modified peptide RF135 with several different receptors in *Salmonella Typhimurium* with the Prodigy server.

Receptor	Energy binding affinity (ΔG) (kcal mol ⁻¹)	Dissociation constant (K_d) at 25 °C (M)
ArnD deformylase (PDB ID: 8T0J)	-10.3	3.0×10^{-8}
3-oxoacyl-[acyl-carrier-protein] reductase (PDB ID: 6T5X_B)	-10.1	4.2×10^{-8}
apo-dTDP-6-deoxy-L-lyxo-4-hexulose reductase (PDB ID: 1KBZ)	-9.8	6.3×10^{-8}
Transcription factor SlyA (PDB ID: 3QPT)	-9.7	7.9×10^{-8}
Glycoside hydrolase (PDB ID: 4GVF_B)	-9.3	1.5×10^{-7}
DNA gyrase (PDB ID: 5ZTJ)	-7.5	2.9×10^{-6}

Table 5.4 illustrates the results of the Prodigy prediction for the energy binding affinity (ΔG) and dissociation constant (K_d) of the association between modified peptide RF135 and various receptors of *S. Typhimurium*. The analysis underscores that RF135 demonstrates the most robust interaction with the ArnD deformylase receptor (PDB ID: 8T0J), which displays the lowest ΔG value among the assessed receptors. Muñoz-Escudero et al.(2023) described the role of ArnD deformylase in the alteration of lipid A with 4-amino-4-deoxy-L-arabinose (Ara4N) in *S. Typhimurium*, as this modification might provide resistance to cationic AMPs and polymyxin antibiotics in Gram-negative bacteria.

After conducting CABS-dock analysis, the docking complexes of peptide-protein were scrutinized to investigate the interactions among the amino acid residues of the RF135 and its corresponding receptor. Utilizing the DimPlot tool from LigPlot⁺ and the PDBsum tool of EMBL-EBI, the interactions were visually represented in 2D illustration using the PDB file generated from the CABS-dock analysis. The diagram in Figure 5.15A demonstrates the interrelationship between the modified peptide RF135 and ArnD deformylase receptor, displaying a binding energy (ΔG) of $-10.3 \text{ kcal.mol}^{-1}$ and

modified peptide RF135 may potentially disrupt the lipid A portion of the outer membrane of *S. Typhimurium* through interaction with ArnD deformylase (8T0J).

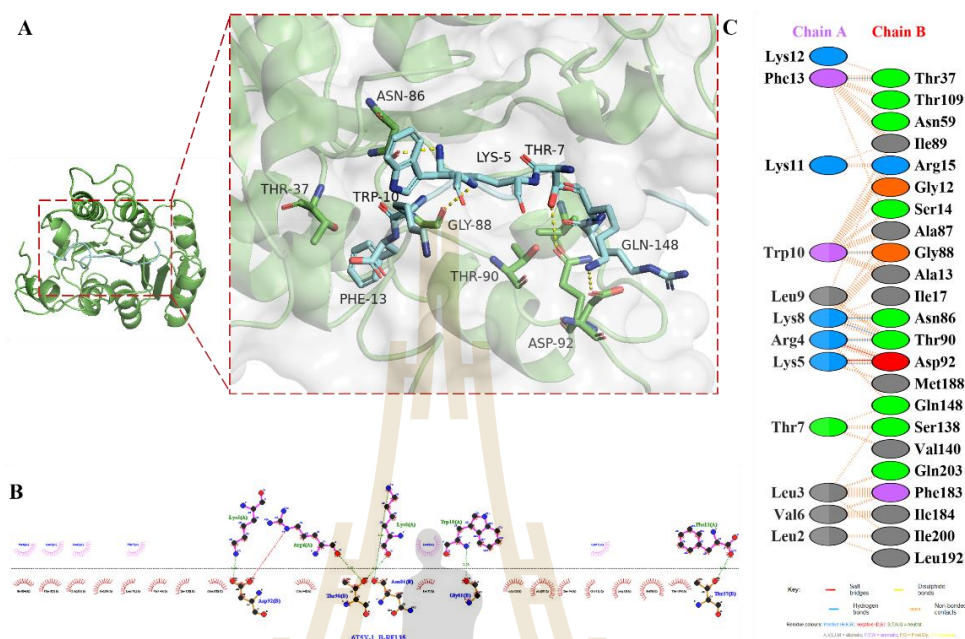


Figure 5.16 A docking illustration of the complex of 6T5X_B and peptide RF135 (A) the interface for binding (B) the binding interaction of residues amino acid (C) the visualization of interactions indicated the presence of hydrogen bonds, salt bridges, and non-bonded interactions. The chain A is for RF135 and the chain B is for 6T5X_B.

Figure 5.16A depicts the molecular docking of RF135 and 3-oxoacyl-[acyl-carrier-protein] reductase of *S. Typhimurium*. FabG (3-oxoacyl-[acyl-carrier-protein] reductase) plays a crucial role on the fatty acid synthesis pathway by catalyzing NADPH as a cofactor in the transformation of β -ketoacyl-ACP substrates to β -hydroxyacyl-ACP products. This enzyme is essential for the fatty acids elongation, which is necessary for synthesizing various lipids and other cellular components (Vella et al., 2021). Six hydrogen bonds were shown by residue Phe13-Thr37, Trp10-Gly88, Lys8-Asn86, Lys8-Thr90, Arg4-Thr90, and Lys5-Asp92 (Figure 5.16C). Residue Lys5-Asp92 and Arg4-Asp92 exhibited salt bridge interactions. In addition, there were several non-bonded interactions between residue RF135 and 6T5X_B. This finding indicated that RF135 likely interacted with enzymes involved in fatty acid synthesis.

Molecular docking also suggested the involvement of RF135 with the enzymes ArnD deformylase and with 3-oxoacyl [acyl-carrier-protein] reductase related

to outer membrane biosynthesis. This would lead to perturbation of fatty acid bilayer formation, as evidenced by membrane disruption assay by CLSM, morphological alteration by SEM, ultrastructural alteration by TEM, and biochemical composition alteration by SR-FTIR.

5.4.7 Hemolytic activity

The modified peptide RF135 did not cause lysis at any concentration from the lowest of 1.0 μM to the highest of 512 μM , as illustrated in Figure 5.17. In addition, the degree of hemolysis of the modified peptide RF135 on RBC samples remained below the 10% minimum hemolytic concentration (MHC) (Greber, Dawgul, Kamysz, & Sawicki, 2017). The modified peptide RF135 indicated no hemolytic activity even at the highest concentration of 512 μM while retaining high antibacterial activity, as evidenced by its MIC value. The low hemolysis rate indicates the modified peptide is harmless and has no hemolyzing properties. Our findings are aligned with a recent study by Islam et al. (2023), who observed the modified peptides derived from cationic AMPs amphibia with a net charge of +5 and +6 exhibited almost no hemolytic activity while maintaining high antibacterial activity. In addition, Zhao et al. (2021) reported the structural modification of L-Arg and L-Lys with D-Arg and D-Lys in OM19R (VDKPPYLPRPRPIRRPGGR-NH₂) to OM19D (VDkPPYLPRPrPrPIrrPGGr-NH₂) showed hemolytic rate lower than 10% (1-512 $\mu\text{g}\cdot\text{mL}^{-1}$) against rabbit red blood cells. Therefore, RF135 could be safe for applications in the healthcare or food industries.

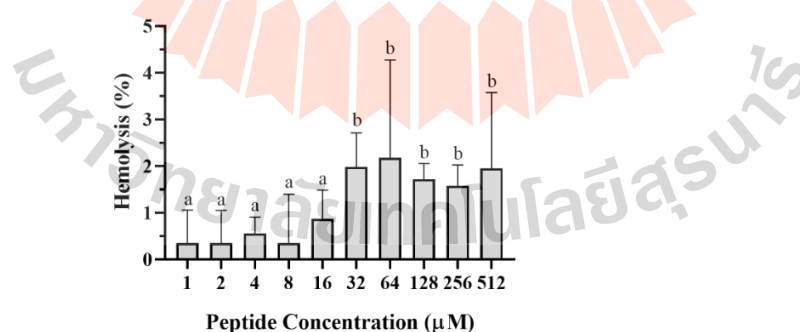


Figure 5.17 The hemolytic activity of the peptide RF135 on human red blood cells. Data are given as Mean \pm SD ($n = 3$).

5.5 Conclusions

Modification of amino acids of the parent peptide PTGAKVTKAAKKA (PA13) identified in the P1 fraction derived from CGMH resulted in RLLRKVTKLWKKF (RF135) which showed enhanced antibacterial activity. The RF135 demonstrated a thousand times increase in antibacterial activity with a MIC of 4.0 μM against *Salmonella* Typhimurium TISTR 292. In addition, the modified peptide RF135 caused disruption to the integrity of the outer membrane of *S. Typhimurium*. The RF135 effect on *S. Typhimurium* was characterized by the morphological and ultrastructural alterations in the cell membrane, including pores formation, dents on the surface, irregular shapes, and cytoplasmic leakages, ultimately resulting in cell death. The SR-FTIR demonstrated the intracellular composition of fatty acids, and nucleic acids of *S. Typhimurium* exhibited alterations upon treatment with RF135 at 1 \times MIC after incubating at 37 °C for 2 h. Molecular docking showed that RF135 likely intervene with synthesis of the outer membrane of *S. Typhimurium*. The hemolytic assay result indicated that RF135 exhibited low hemolytic activity, implying its safety for possible use in the food and healthcare industry. The findings demonstrate that structural modification can be employed to develop an antibacterial peptide based on corn gluten meal hydrolysate.

5.6 References

- Almeida, J. R., Mendes, B., Lancellotti, M., Franchi, G. C., Passos, Ó., Ramos, M. J., ... da Silva, S. L. (2022). Lessons from a single amino acid substitution: Anticancer and antibacterial properties of two phospholipase A2-derived peptides. *Current Issues in Molecular Biology*, 44(1), 46–62.
- Bacik, J. P., Whitworth, G. E., Stubbs, K. A., Vocadlo, D. J., & Mark, B. L. (2012). Active site plasticity within the glycoside hydrolase NagZ underlies a dynamic mechanism of substrate distortion. *Chemistry and Biology*, 19(11), 1471–1482.
- Bajjiya, N., Choudhury, S., Dhall, A., & Raghava, G. P. S. (2024). AntiBP3: A method for predicting antibacterial peptides against Gram-positive/negative/variable bacteria. *Antibiotics*, 13(2), 168.
- Berman, H. M., Westbrook, J., Feng, Z., Gililand, G., Bhat, T. N., Weissig, H., ... P. E. (2000). The protein data bank. *Nucleic Acids Research*, 28(1), 235–242.
- Bermúdez-Puga, S., Dias, M., Freire de Oliveira, T., Mendonça, C. M. N., Yokomizo de Almeida, S. R., Rozas, E. E., ... Oliveira, R. P. de S. (2023). Dual antibacterial mechanism of [K4K15]CZS-1 against *Salmonella* Typhimurium: A membrane active and intracellular-targeting antimicrobial peptide. *Frontiers in Microbiology*,

14, 1320154.

- Blankenfeldt, W., Kerr, I. D., Giraud, M. F., McMiken, H. J., Leonard, G., Whitfield, C., ... Naismith, J. H. (2002). Variation on a theme of SDR: dTDP-6-deoxy-L-lyxo-4-hexulose reductase (RmlD) shows a new Mg²⁺-dependent dimerization mode. *Structure*, *10*(6), 773–786.
- Blaszczyk, M., Kurcinski, M., Kouza, M., Wieteska, L., Debinski, A., Kolinski, A., & Kmiecik, S. (2016). Modeling of protein-peptide interactions using the CABS-dock web server for binding site search and flexible docking. *Methods*, *93*, 72–83.
- Boix-Lemonche, G., Lekka, M., & Skerlavaj, B. (2020). A rapid fluorescence-based microplate assay to investigate the interaction of membrane active antimicrobial peptides with whole Gram-positive bacteria. *Antibiotics*, *9*(2), 92.
- Carson, C. F., Mee, B. J., & Riley, T. V. (2002). Mechanism of action of Melaleuca alternifolia (tea tree) oil on *Staphylococcus aureus* determined by time-kill, lysis, leakage, and salt tolerance assays and electron microscopy. *Antimicrobial Agents and Chemotherapy*, *46*(6), 1914–1920.
- Chegini, P. P., Nikokar, I., Tabarzad, M., Faezi, S., & Mahboubi, A. (2019). Effect of amino acid substitutions on biological activity of antimicrobial peptide: Design, recombinant production, and biological activity. *Iranian Journal of Pharmaceutical Research*, *18*(Suppl1), 157–168.
- Ciociola, T., Giovati, L., Giovannelli, A., Conti, S., Castagnola, M., & Vitali, A. (2018). The activity of a mammalian proline-rich peptide against Gram-negative bacteria, including drug-resistant strains, relies on a nonmembranolytic mode of action. *Infection and Drug Resistance*, *11*, 969–979.
- de Almeida, N. R., Han, Y., Perez, J., Kirkpatrick, S., Wang, Y., & Sheridan, M. C. (2019). Design, synthesis, and nanostructure-dependent antibacterial activity of cationic peptide amphiphiles. *ACS Applied Materials and Interfaces*, *11*(3), 2790–2801.
- Dolan, K. T., Duguid, E. M., & He, C. (2011). Crystal structures of SlyA protein, a master virulence regulator of *Salmonella*, in free and DNA-bound states. *Journal of Biological Chemistry*, *286*(25), 22178–22185.
- Greber, K. E., Dawgul, M., Kamysz, W., & Sawicki, W. (2017). Cationic net charge and counter ion type as antimicrobial activity determinant factors of short lipopeptides. *Frontiers in Microbiology*, *8*, 123.
- Han, Y., Zhang, M., Lai, R., & Zhang, Z. (2021). Chemical modifications to increase the therapeutic potential of antimicrobial peptides. *Peptides*, *146*, 170666.
- Hong, S. Y., Oh, J. E., & Lee, K. H. (1999). Effect of D-amino acid substitution on the stability, the secondary structure, and the activity of membrane-active peptide. *Biochemical Pharmacology*, *58*(11), 1775–1780.

- Honorato, R. V., Koukos, P. I., Jiménez-García, B., Tsaregorodtsev, A., Verlato, M., Giachetti, A., ... Bonvin, A. M. J. J. (2021). Structural biology in the clouds: The WeNMR-EOSC ecosystem. *Frontiers in Molecular Biosciences*, *8*, 729513.
- Hornemann, A., Eichert, D. M., Hoehl, A., Tiersch, B., Ulm, G., Ryadnov, M. G., & Beckhoff, B. (2022). Investigating membrane-mediated antimicrobial peptide interactions with synchrotron radiation Far-infrared spectroscopy. *ChemPhysChem*, *23*(4), e202100815.
- Huan, Y., Kong, Q., Mou, H., & Yi, H. (2020). Antimicrobial peptides: Classification, design, application and research progress in multiple fields. *Frontiers in Microbiology*, *11*, 582779.
- Islam, M. M., Asif, F., Zaman, S. U., Arnab, M. K. H., Rahman, M. M., & Hasan, M. (2023). Effect of charge on the antimicrobial activity of alpha-helical amphibian antimicrobial peptide. *Current Research in Microbial Sciences*, *4*, 100182.
- Jiang, Z., Vasil, A. I., Hale, J. D., Hancock, R. E. W., Vasil, M. L., & Hodges, R. S. (2008). Effects of net charge and the number of positively charged residues on the biological activity of amphipathic α -helical cationic antimicrobial peptides. *Biopolymers*, *90*(3), 369–383.
- Kurcinski, M., Jamroz, M., Blaszczyk, M., Kolinski, A., & Kmiecik, S. (2015). CABS-dock web server for the flexible docking of peptides to proteins without prior knowledge of the binding site. *Nucleic Acids Research*, *43*(W1), W419–W424.
- Lamiable, A., Thevenet, P., Rey, J., Vavrusa, M., Derreumaux, P., & Tuffery, P. (2016). PEP-FOLD3: Faster denovo structure prediction for linear peptides in solution and in complex. *Nucleic Acids Research*, *44*(1), W449–W454.
- Laskowski, R. A. (2009). PDBsum new things. *Nucleic Acids Research*, *37*(Suppl_1), D355–D359.
- Laskowski, R. A., & Swindells, M. B. (2011). LigPlot+: Multiple ligand-protein interaction diagrams for drug discovery. *Journal of Chemical Information and Modeling*, *51*(10), 2778–2786.
- Lomize, A. L., Todd, S. C., & Pogozheva, I. D. (2022). Spatial arrangement of proteins in planar and curved membranes by PPM 3.0. *Protein Science*, *31*(1), 209–220.
- Lu, J., Xu, H., Xia, J., Ma, J., Xu, J., Li, Y., & Feng, J. (2020). D- and unnatural amino acid substituted antimicrobial peptides with improved proteolytic resistance and their proteolytic degradation characteristics. *Frontiers in Microbiology*, *11*, 563030.
- Manyi-Loh, C., Mamphweli, S., Meyer, E., & Okoh, A. (2018). Antibiotic use in agriculture and its consequential resistance in environmental sources: Potential public health implications. *Molecules*, *23*(4), 795.

- Meher, P. K., Sahu, T. K., Saini, V., & Rao, A. R. (2017). Predicting antimicrobial peptides with improved accuracy by incorporating the compositional, physico-chemical and structural features into Chou's general PseAAC. *Scientific Reports*, 7, 42362.
- Movasaghi, Z., Rehman, S., & Rehman, I. U. (2008). Fourier transform infrared (FTIR) spectroscopy of biological tissues. *Applied Spectroscopy Reviews*, 43(2), 134–179.
- Muñoz-Escudero, D., Breazeale, S. D., Lee, M., Guan, Z., Raetz, C. R. H., & Sousa, M. C. (2023). Structure and function of ArnD. A deformylase essential for lipid A modification with 4-Amino-4-deoxy-L-arabinose and polymyxin resistance. *Biochemistry*, 62(20), 2970–2981.
- Murray, C. J., Ikuta, K. S., Sharara, F., Swetschinski, L., Robles Aguilar, G., Gray, A., ... Naghavi, M. (2022). Global burden of bacterial antimicrobial resistance in 2019: A systematic analysis. *The Lancet*, 399(10325), 629–655.
- Mwangi, J., Kamau, P. M., Thuku, R. C., & Lai, R. (2023). Design methods for antimicrobial peptides with improved performance. *Zoological Research*, 44(6), 1095–1114.
- Naumann, D., Helm, D., & Labischinski, H. (1991). Microbiological characterizations by FT-IR spectroscopy. *Nature*, 351, 81–82.
- Nurhartadi, E., Rodtong, S., Thumanu, K., Park, S. H., Aluko, R. E., & Yongsawatdigul, J. (2024). Antibacterial activity of enzymatic corn gluten meal hydrolysate and ability to inhibit *Staphylococcus aureus* in ultra-high temperature processed milk. *Manuscript Submitted for Publication*.
- Nurhartadi, E., Rodtong, S., Thumanu, K., & Yongsawatdigul, J. (2024). Antibacterial activity and potential application of a novel anionic antibacterial peptide derived from corn gluten meal hydrolysate. *Manuscript in Preparation*.
- Pimchan, T., Tian, F., Thumanu, K., Rodtong, S., & Yongsawatdigul, J. (2023). Isolation, identification, and mode of action of antibacterial peptides derived from egg yolk hydrolysate. *Poultry Science*, 102(7), 102695.
- Ramazi, S., Mohammadi, N., Allahverdi, A., Khalili, E., & Abdolmaleki, P. (2022). A review on antimicrobial peptides databases and the computational tools. *Database*, 2022, baac011.
- Sachdeva, E., Kaur, G., Tiwari, P., Gupta, D., Singh, T. P., Ethayathulla, A. S., & Kaur, P. (2020). The pivot point arginines identified in the β -pinwheel structure of C-terminal domain from *Salmonella typhi* DNA gyrase A subunit. *Scientific Reports*, 10(1), 1–11.
- Saint Jean, K. D., Henderson, K. D., Chrom, C. L., Abiuso, L. E., Renn, L. M., & Caputo, G. A. (2018). Effects of hydrophobic amino acid substitutions on antimicrobial peptide behavior. *Probiotics and Antimicrobial Proteins*, 10(3), 408–419.

- Song, W., Kong, X., Hua, Y., Chen, Y., Zhang, C., & Chen, Y. (2020). Identification of antibacterial peptides generated from enzymatic hydrolysis of cottonseed proteins. *LWT - Food Science and Technology*, *125*, 109199.
- Sosiangdi, S., Taemaitree, L., Tankrathok, A., Daduang, S., Boonlue, S., Klaynongsruang, S., & Jangpromma, N. (2023). Rational design and characterization of cell-selective antimicrobial peptides based on a bioactive peptide from *Crocodylus siamensis* hemoglobin. *Scientific Reports*, *13*(1), 1–15.
- Tan, R., Wang, M., Xu, H., Qin, L., Wang, J., Cui, P., & Ru, S. (2021). Improving the activity of antimicrobial peptides against aquatic pathogen bacteria by amino acid substitutions and changing the ratio of hydrophobic residues. *Frontiers in Microbiology*, *12*, 773076.
- van Hilten, N., Verwei, N., Methorst, J., Nase, C., Bernatavicius, A., & Risselada, H. J. (2024). PMLpred: a physics-informed web server for quantitative protein-membrane interaction prediction. *Bioinformatics*, *40*(2), 1–10.
- Vangone, A., & Bonvin, A. M. J. J. (2015). Contacts-based prediction of binding affinity in protein–protein complexes. *ELife*, *4*, e07454.
- Vella, P., Rudraraju, R. S., Lundbäck, T., Axelsson, H., Almqvist, H., Vallin, M., ... Schnell, R. (2021). A FabG inhibitor targeting an allosteric binding site inhibits several orthologs from Gram-negative ESKAPE pathogens. *Bioorganic and Medicinal Chemistry*, *30*, 115898.
- Villaró-Cos, S., & Lafarga, T. (2023). Online tools to support teaching and training activities in chemical engineering: enzymatic proteolysis. *Frontiers in Education*, *8*, 1290287.
- Waghu, F. H., Barai, R. S., Gurung, P., & Idicula-Thomas, S. (2016). CAMPR3: A database on sequences, structures and signatures of antimicrobial peptides. *Nucleic Acids Research*, *44*(D1), D1094–D1097.
- Wang, G., Vaisman, I. I., & van Hoek, M. L. (2022). Machine learning prediction of antimicrobial peptides. *Methods in Molecular Biology*, *2405*, 1–37.
- Wang, J., Chou, S., Xu, L., Zhu, X., Dong, N., Shan, A., & Chen, Z. (2015). High specific selectivity and membrane-active mechanism of the synthetic centrosymmetric α -helical peptides with Gly-Gly pairs. *Scientific Reports*, *5*, 15963.
- Wiegand, I., Hilpert, K., & Hancock, R. E. W. (2008). Agar and broth dilution methods to determine the minimal inhibitory concentration (MIC) of antimicrobial substances. *Nature Protocols*, *3*(2), 163–175.
- Xue, L. C., Rodrigues, J. P., Kastiris, P. L., Bonvin, A. M., & Vangone, A. (2016). PRODIGY: A web server for predicting the binding affinity of protein-protein complexes. *Bioinformatics*, *32*(23), 3676–3678.

- Yin, L. M., Edwards, M. A., Li, J., Yip, C. M., & Deber, C. M. (2012). Roles of hydrophobicity and charge distribution of cationic antimicrobial peptides in peptide-membrane interactions. *Journal of Biological Chemistry*, 287(10), 7738–7745.
- Yu, C., & Irudayaraj, J. (2005). Spectroscopic characterization of microorganisms by Fourier transform infrared microspectroscopy. *Biopolymers*, 77(6), 368–377.
- Zhang, Y., Meng, Z., Li, S., Liu, T., Song, J., Li, J., & Zhang, X. (2023). Two antimicrobial peptides derived from *Bacillus* and their properties. *Molecules*, 28(23), 7899.
- Zhao, Q., He, L., Wang, X., Ding, X., Li, L., Tian, Y., & Huang, A. (2022). Characterization of a novel antimicrobial peptide isolated from *Moringa oleifera* seed protein hydrolysates and its membrane damaging effects on *Staphylococcus aureus*. *Journal of Agricultural and Food Chemistry*, 70(20), 6123–6133.
- Zhao, X., Zhang, M., Muhammad, I., Cui, Q., Zhang, H., Jia, Y., ... Ma, H. (2021). An antibacterial peptide with high resistance to trypsin obtained by substituting D-amino acids for trypsin cleavage sites. *Antibiotics*, 10(12), 1465.
- Zhao, Y., & Grigoryan, G. (2023). Multiplex measurement of protein-peptide dissociation constants using dialysis and mass spectrometry. *Protein Science*, 32(4), e4607.
- Zhu, X., Dong, N., Wang, Z., Ma, Z., Zhang, L., Ma, Q., & Shan, A. (2014). Design of imperfectly amphipathic α -helical antimicrobial peptides with enhanced cell selectivity. *Acta Biomaterialia*, 10(1), 244–257.



CHAPTER VI

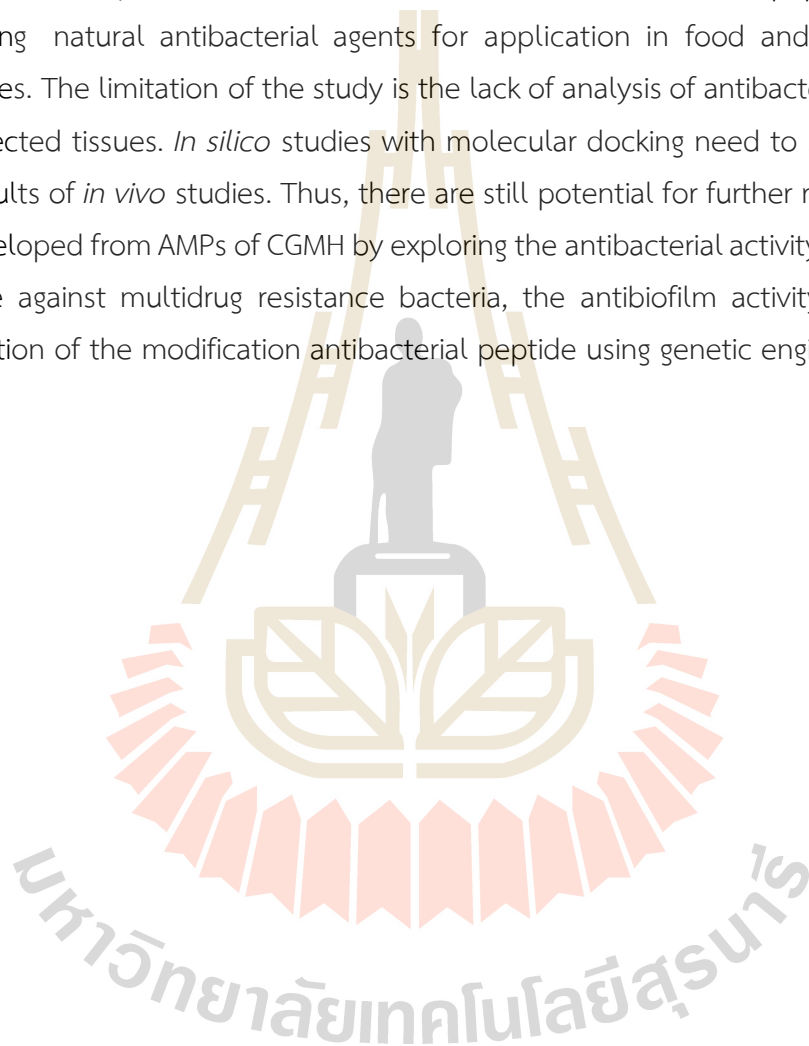
SUMMARY

Corn gluten meal hydrolysate (CGMH) prepared by pepsin hydrolysis demonstrated a potential source of antibacterial peptides. The P1 fraction of CGMH isolated by reverse-phase chromatography showed the strongest antibacterial activity at 1 mM against *Staphylococcus aureus* ATCC 29213 when tested with *S. aureus*, *B. cereus*, *S. Typhimurium*, *E. coli*, methicillin-resistant *S. aureus*. The mechanism of action of the P1 peptides fraction disrupts the *S. aureus* cell membrane as observed by confocal laser scanning microscopy (CLSM), morphological change with scanning electron microscopy (SEM), ultrastructure alteration with transmission electron microscopy (TEM), and changes intracellular components by synchrotron radiation-Fourier transmission infra-red (SR-FTIR). The P1 fraction inhibited *S. aureus* growth in ultra-high temperature (UHT) milk at 8 mM. Six cationic and five anionic peptides have been identified from the P1 fraction that might have contributed to the antibacterial activity. This finding implies that antibacterial peptides could be obtained from CGMH.

One anionic peptide, EAGGGEDDKKVE, identified from the P1 fraction, demonstrated potential antibacterial activity against *Staphylococcus aureus* ATCC 29213 at MIC of 4 mM after testing against *S. aureus*, *B. cereus*, *S. Typhimurium*, *E. coli*. The mode of action of EAGGGEDDKKVE is to perturb the cell membrane of *S. aureus*, as observed by confocal laser scanning microscopy (CLSM), scanning electron microscopy (SEM), and synchrotron radiation-Fourier transmission infra-red (SR-FTIR). Molecular docking analysis showed that EAGGGEDDKKVE might bind strongly to the membrane-bound transglycosylase enzyme. A synergistic effect of mild heat treatment at 50 °C for 10 min and EAGGGEDDKKVE at 2 mM was demonstrated to inhibit *S. aureus* growth. Therefore, the use of concentrations below the MIC of the peptide may increase cell injury when combined with mild heat treatment. This finding implies that the anionic peptide's antibacterial potency derived from CGMH inhibits bacterial growth.

Furthermore, the peptide RLLRKVTKLWKKF was a structural modification peptide from PTGAKVTKAAKKA, a cationic peptide identified from the P1 fraction of

CGMH. The modified peptide exhibits antibacterial activity against *Salmonella* Typhimurium TISTR 292 at a MIC of 4 μ M. The RLLRKVTKLWKKF causes perturbation on the *S. Typhimurium* cell membrane, as observed by CLSM, SEM, TEM, and SR-FTIR. A molecular docking study revealed that RLLRKVTKLWKKF bound firmly to ArnD deformylase enzyme. Therefore, structural modification of the peptide could enhance the antibacterial activity of the original peptide derived from CGMH. These findings could potentially increase the utilization of CGMH, and these peptides might be promising natural antibacterial agents for application in food and pharmaceutical industries. The limitation of the study is the lack of analysis of antibacterial peptides on the infected tissues. *In silico* studies with molecular docking need to be confirmed by the results of *in vivo* studies. Thus, there are still potential for further research that can be developed from AMPs of CGMH by exploring the antibacterial activity of the modified peptide against multidrug resistance bacteria, the antibiofilm activity of CGMH, and production of the modification antibacterial peptide using genetic engineering.



APPENDIX

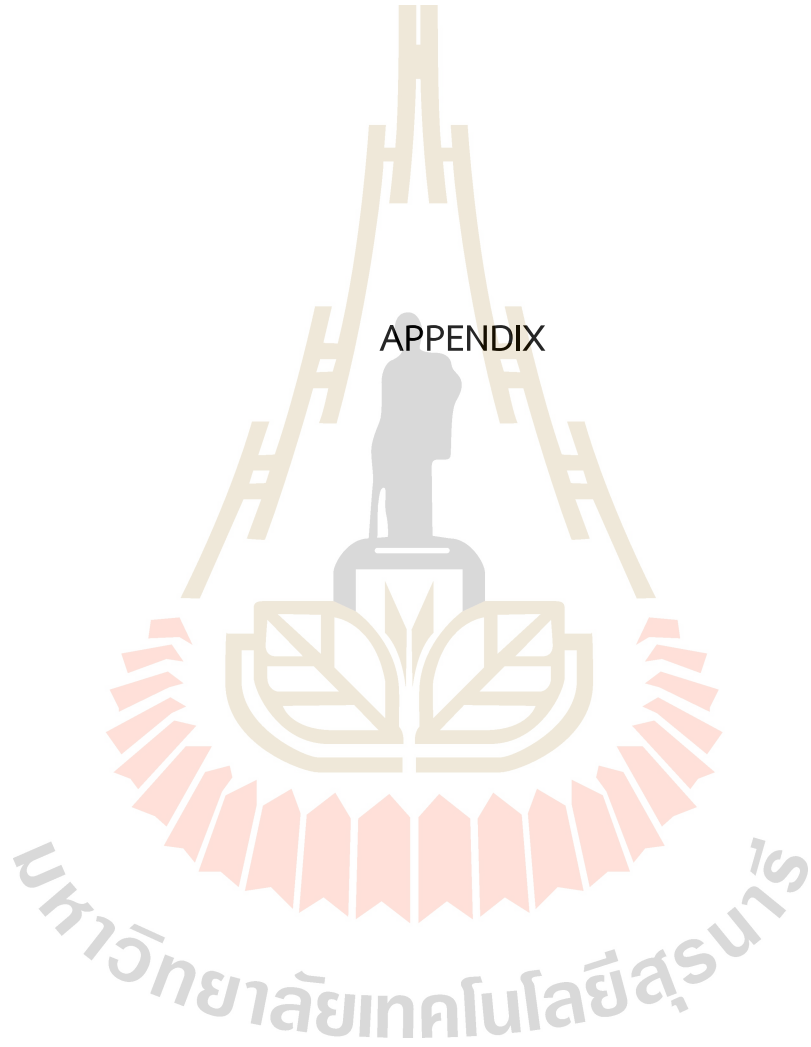
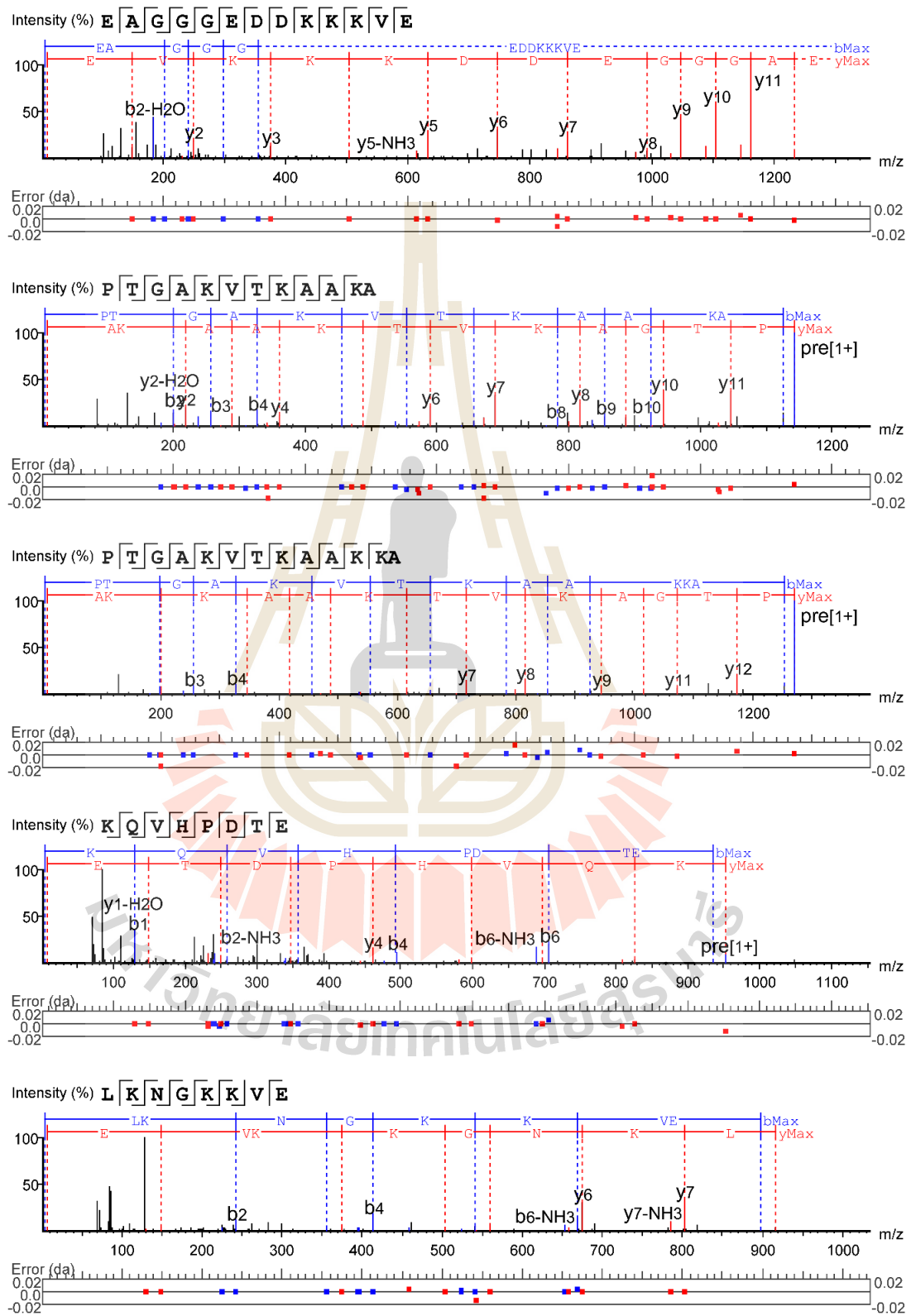
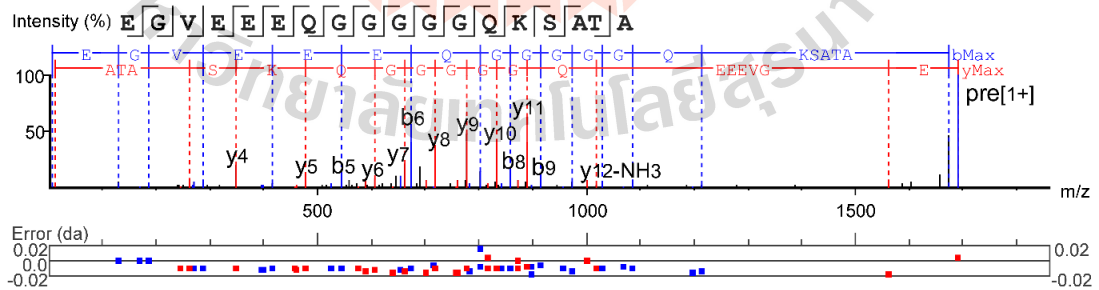
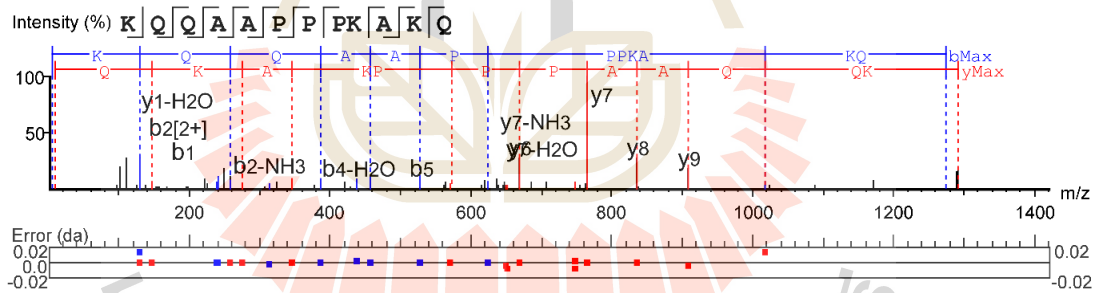
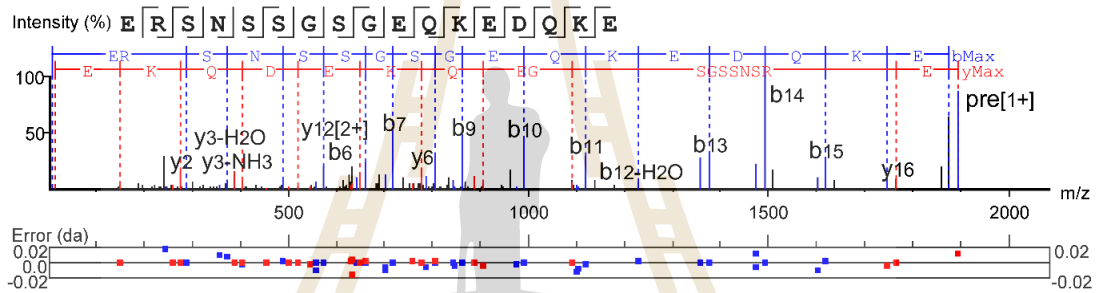
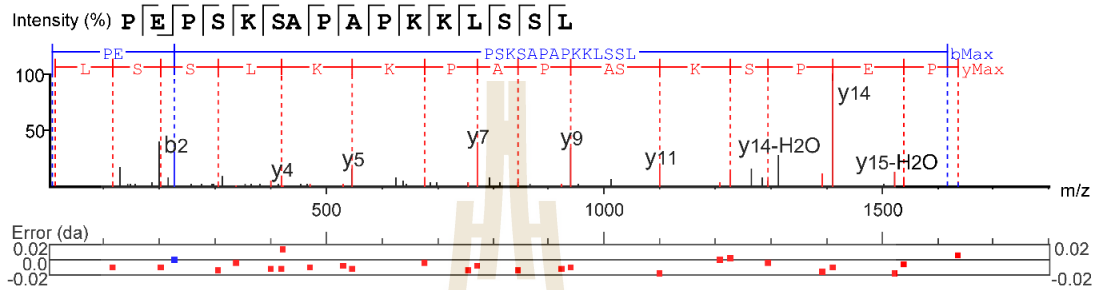
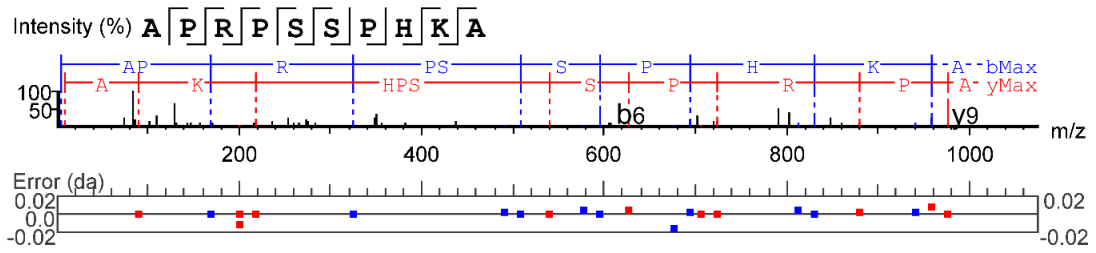


Figure S1 De novo sequencing MS/MS spectra of 11 identified peptides derived from CGM-H





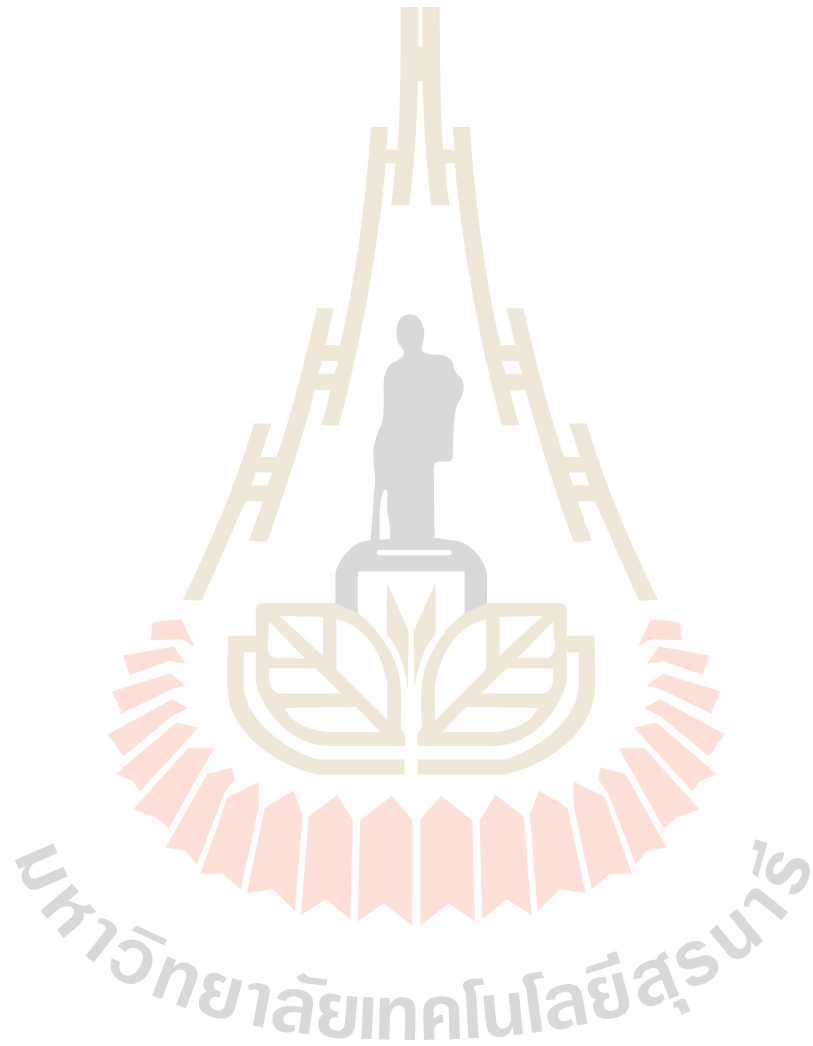
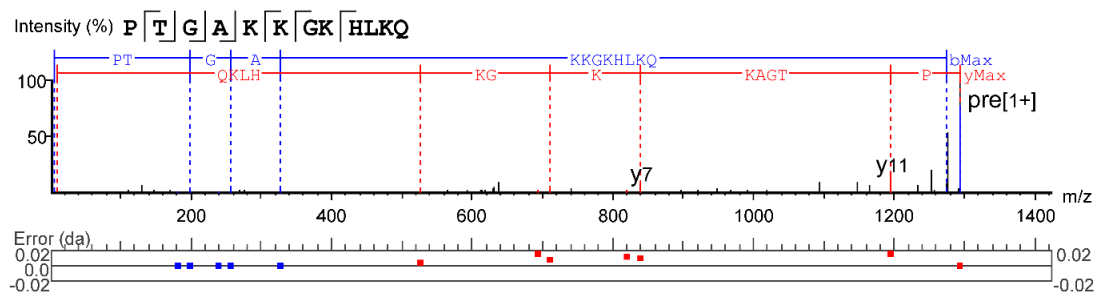


Figure S2 Characterization of EAGGGEDDKKKVE (EE13): (A) HPLC of EE13; (B) Electrospray ionization mass spectrometer of EE13.

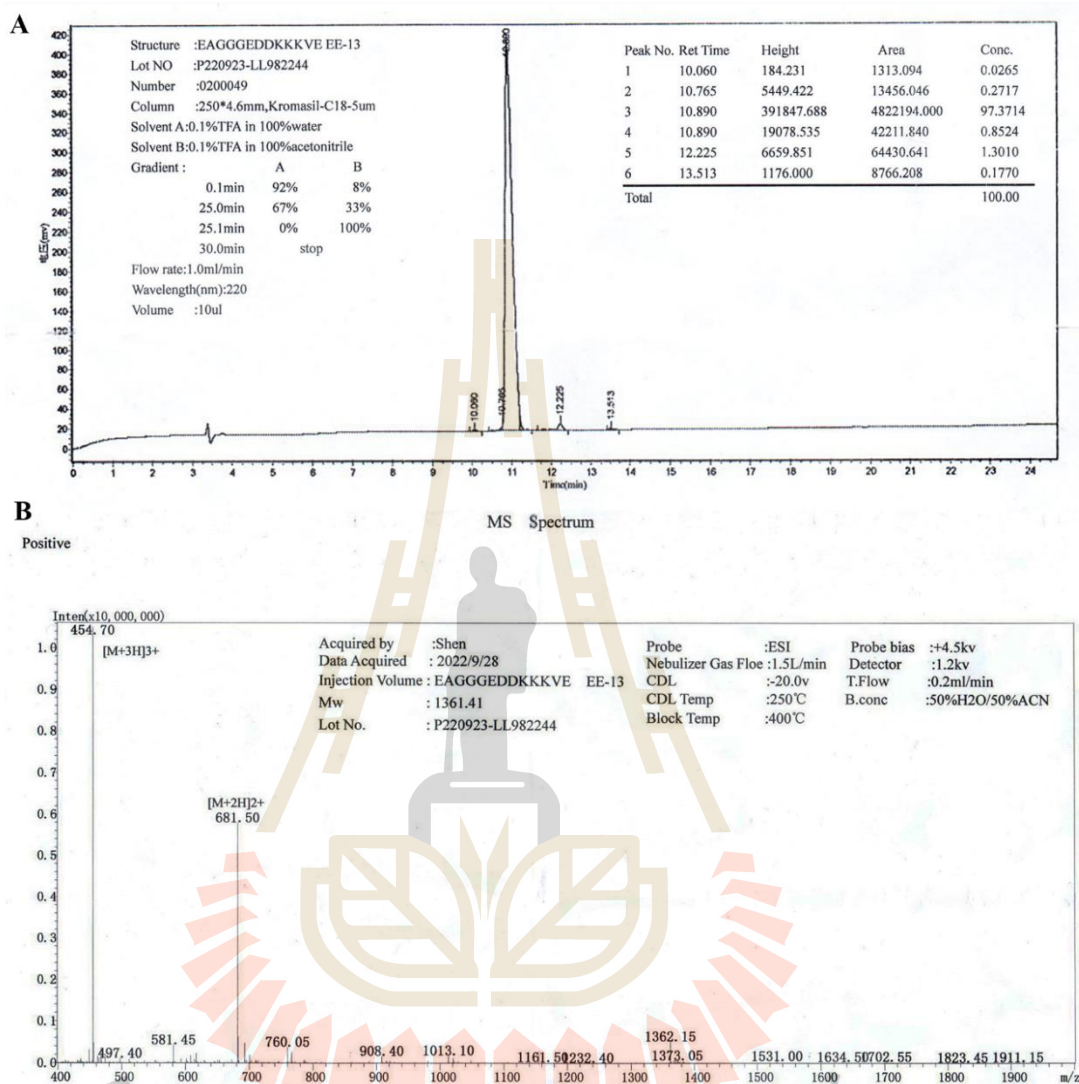
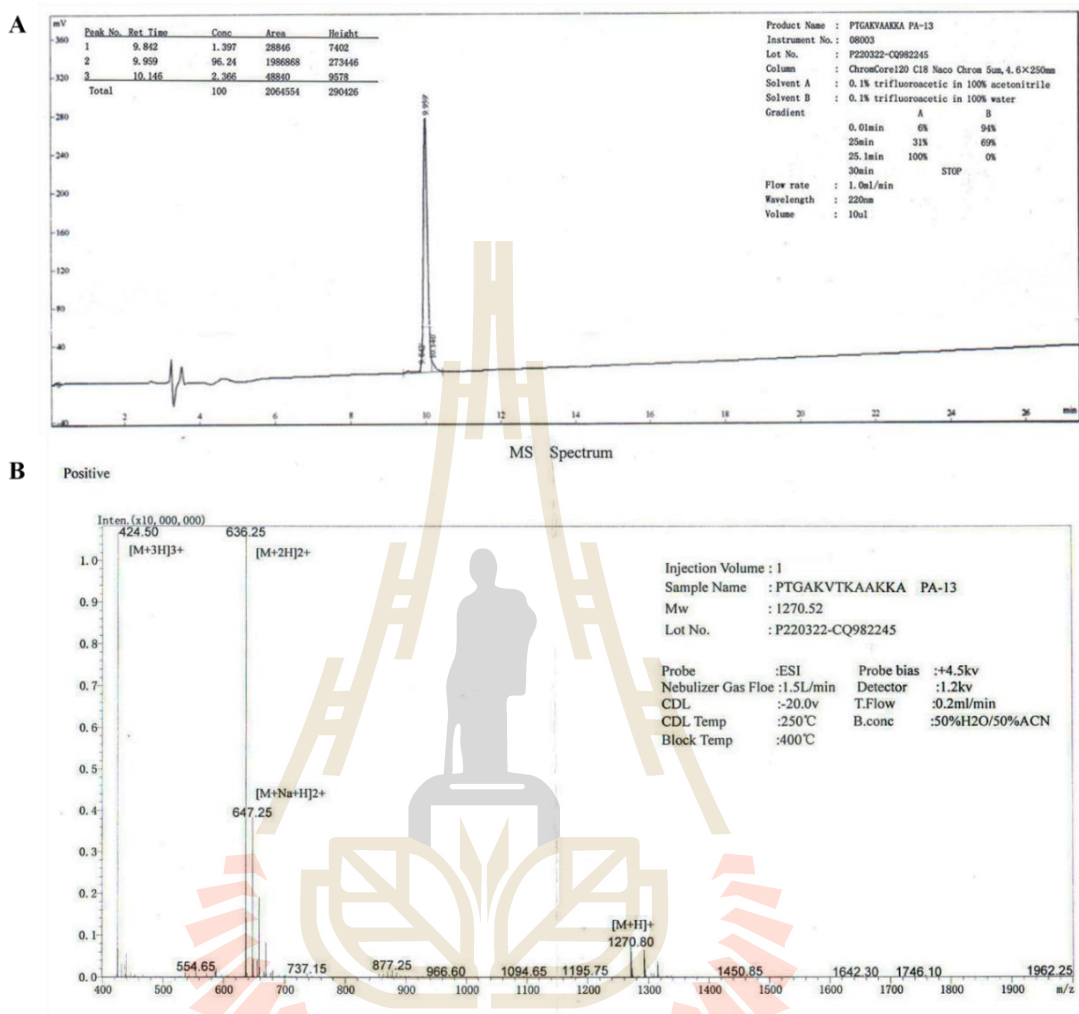
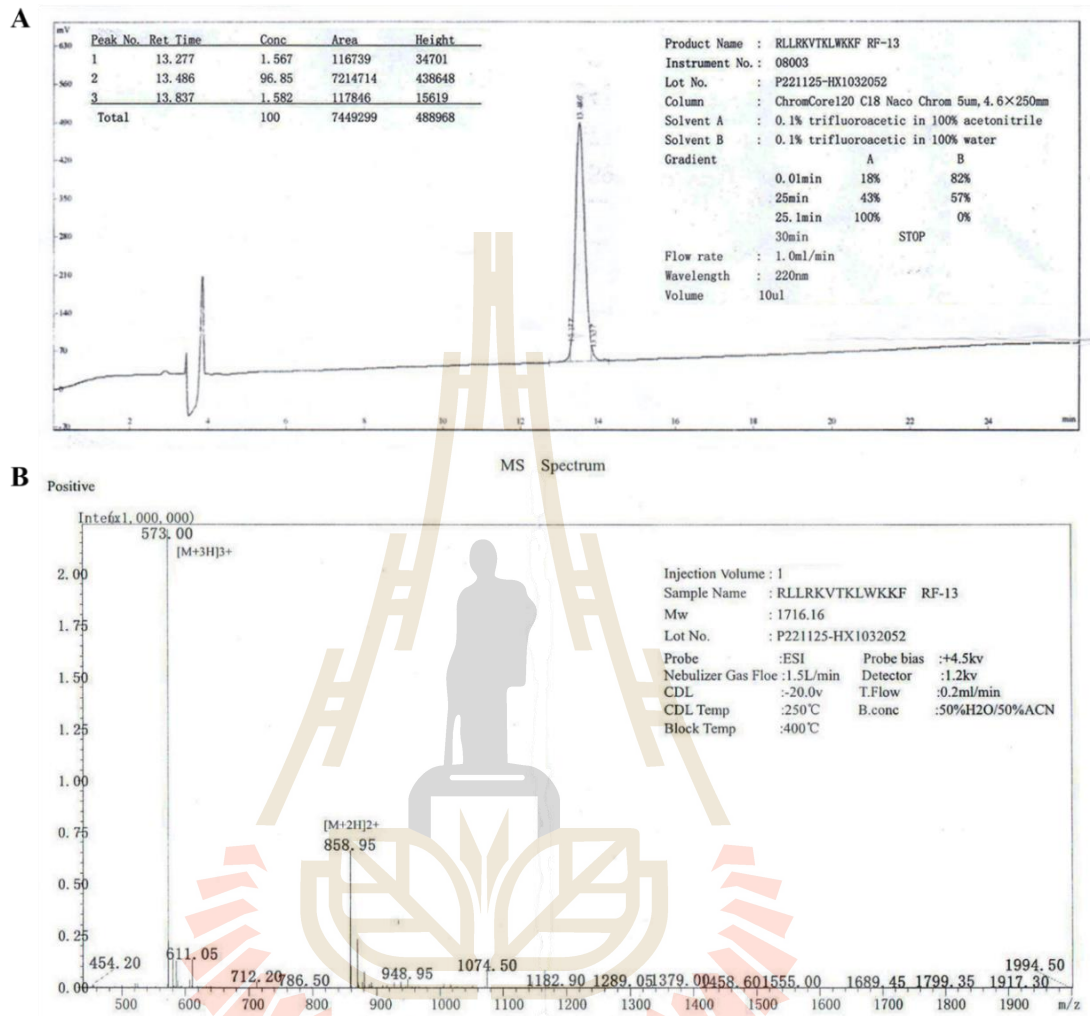


Figure S3 Characterization of PTGAKVTKAAKKA (PA13): (A) HPLC of PA13; (B) Electrospray ionization mass spectrometer of PA13.



มหาวิทยาลัยเทคโนโลยีสุรนารี

Figure S4 Characterization of RLLRKVTKLWKKF (RF135) (A) HPLC of RF135; (B) Electrospray ionization mass spectrometer of RF135



มหาวิทยาลัยเทคโนโลยีสุรนารี

Figure S5 Abstract entitled “Antibacterial activity and mode of action of PLLAKVTKLWKKF, a novel modified peptide derived from corn gluten meal on *Bacillus cereus* DMST 5040” presented at Food Innovation Asia Conference 2024, Bangkok, Thailand.



DB-0128

The 26th Food Innovation Asia Conference 2024: Food Innovation: Trends, Impacts and Solutions for a Sustainable Future 13-14 June 2024, BITEC, Bangkok, THAILAND

Antibacterial Activity and Mode of Action of PLLAKVTKLWKKF, a Novel Modified Peptide Derived from Corn Gluten Meal on *Bacillus cereus* DMST5040

E. Nurhartadi^{1,2}, S. Rodtong³, K. Thumanu⁴, and J. Yongsawatdigul^{1*}

¹School of Food Technology, Institute of Agricultural Technology, Suranaree University of Technology, Nakhon Ratchasima, Thailand; ²Department of Food Science and Technology, Universitas Sebelas Maret, Surakarta, Indonesia; ³School of Preclinical Sciences, Institute of Science, Suranaree University of Technology, Nakhon Ratchasima, Thailand; ⁴Synchrotron Light Research Institute (Public Organization), Nakhon Ratchasima, Thailand, *E-mail: jirawat@sut.ac.th

Abstract

PTGAKVTKAAKKA (PA13) is a peptide identified from corn gluten meal hydrolysate, which exhibited no antibacterial activity. The structure of PA13 was, thus, modified to PLLAKVTKLWKKF (PF13), and its antibacterial activity of PF13 was elucidated along with its mode of action. Minimum inhibitory concentration (MIC) was determined using the micro-broth dilution method. The membrane integrity was evaluated by propidium iodide (PI) and SYTO-9 staining observed by confocal laser scanning microscopy (CLSM). The altered cell morphology was observed by scanning electron microscopy (SEM). The changes in cellular composition were investigated using Synchrotron radiation-based Fourier transform infrared (SR-FTIR) microspectroscopy. The DNA leakage was quantified by monitoring absorbance at 260 nm. The PF13 showed antibacterial activity toward *Bacillus cereus* DMST5040, *Salmonella Typhimurium* TISTR292, *Escherichia coli* TISTR780, *Listeria monocytogenes* DMST17303 and *Staphylococcus aureus* ATCC29213 with MIC value of 2, 16, 32, 128, and 4000 μM , respectively. The CLSM image demonstrated that PF13 induced disruption of the *B. cereus* membrane integrity at $1 \times \text{MIC}$ (2 μM) when incubated at 37°C for 2 h, as indicated by fluorescence signals of PI. DNA leakage also increased with prolonged incubation time with PF13 at 2 μM . The SEM images revealed that PF13 at 2 μM induced morphological alterations in the *B. cereus* cells, including the formation of the pores, dents on the cell surface, and irregular cell shape followed by cell lysis after incubated at 37°C for 2 h compared to the untreated cells. The PF13 treatment also led to alterations in cellular components, including lipids, fatty acid esters, proteins, and nucleic acids, as observed by SR-FTIR. The hemolysis test on PF13 demonstrated no hemolytic on red blood cells up to 512 μM , indicating its safety. These findings shed lights on the development of antimicrobial peptides based on structural modification.

Keywords: antibacterial peptide, modified peptide, corn gluten meal, *Bacillus cereus*, minimum inhibitory concentration

Figure S6 Manuscript entitled “Antibacterial activity of enzymatic corn gluten meal hydrolysate and ability to inhibit *Staphylococcus aureus* in ultra-high temperature processed milk” under reviewed at Food Control (Q1, IF=5.6)

The figure displays two screenshots from a computer screen. The top screenshot shows the Editorial Manager (EM) interface for a user named Edhi Nurhartadi. The page title is "Submissions Being Processed for Author". It features a table with one submission entry:

Action	Manuscript Number	Title	Authorship	Initial Date Submitted	Status Date	Current Status
Action Links	FOODCONT-D-24-03026	Antibacterial activity of enzymatic corn gluten meal hydrolysate and ability to inhibit <i>Staphylococcus aureus</i> in ultra-high temperature processed milk	Other Author	2024-07-12 10:41:30.803	2024-09-05 01:46:26.377	Required Reviews Completed

The bottom screenshot shows the Elsevier Author Hub interface for the same manuscript. The title is "Antibacterial activity of enzymatic corn gluten meal hydrolysate and ability to inhibit *Staphylococcus aureus* in ultra-high temperature processed milk". A blue box indicates "Required Reviews Complete" with a last review activity on 5th September 2024. The journal is Food Control, and the corresponding author is Jirawat Yongswatdigul. The first author is Edhi Nurhartadi, and the submission date is 12th July 2024. The manuscript number is FOODCONT-D-24-03026.

BIOGRAPHY

Edhi Nurhartadi was born on June 15, 1976, in Yogyakarta, Indonesia. In 1999, he received a bachelor's degree in Food Science and Technology from Gadjah Mada University Yogyakarta, Indonesia. In 2005, he completed his master's degree in Food Science and Technology at Gadjah Mada University, Yogyakarta, Indonesia. He has been employed as a lecturer at the Department of Food Technology and Science, Faculty of Agriculture, Sebelas Maret University, Surakarta, Indonesia, since 2010. In 2019, he continued to pursue the Doctor of Philosophy degree in Food Technology at Suranaree University of Technology, Nakhon Ratchasima, Thailand. His research works are being prepared into three manuscripts for publication. The first manuscript is entitled "Antibacterial activity of enzymatic corn gluten meal hydrolysate and ability to inhibit *Staphylococcus aureus* in ultra-high temperature processed milk." The second manuscript is entitled "Antibacterial activity and potential application of a novel anionic antibacterial peptide derived from corn gluten meal hydrolysate." The last manuscript is entitled "Modification and mechanism of action of peptide derived from corn gluten meal hydrolysate." He achieved the first position in the graduate student oral presentation competition at the Food Innovation Asia Conference 2024 in Bangkok, Thailand.

มหาวิทยาลัยเทคโนโลยีสุรนารี